



National Library
of Canada

Bibliothèque nationale
du Canada

Canadian Theses Service

Service des thèses canadiennes

Ottawa, Canada
K1A 0N4

NOTICE

The quality of this microform is heavily dependent upon the quality of the original thesis submitted for microfilming. Every effort has been made to ensure the highest quality of reproduction possible.

If pages are missing, contact the university which granted the degree.

Some pages may have indistinct print especially if the original pages were typed with a poor typewriter ribbon or if the university sent us an inferior photocopy.

Previously copyrighted materials (journal articles, published tests, etc.) are not filmed.

Reproduction in full or in part of this microform is governed by the Canadian Copyright Act, R.S.C. 1970, c. C-30.

AVIS

La qualité de cette microforme dépend grandement de la qualité de la thèse soumise au microfilmage. Nous avons tout fait pour assurer une qualité supérieure de reproduction.

S'il manque des pages, veuillez communiquer avec l'université qui a conféré le grade.

La qualité d'impression de certaines pages peut laisser à désirer, surtout si les pages originales ont été dactylographiées à l'aide d'un ruban usé ou si l'université nous a fait parvenir une photocopie de qualité inférieure.

Les documents qui font déjà l'objet d'un droit d'auteur (articles de revue, tests publiés, etc.) ne sont pas microfilmés.

La reproduction, même partielle, de cette microforme est soumise à la Loi canadienne sur le droit d'auteur, SRC 1970, c. C-30.

The University of Alberta

Numerical Modelling of Frazil Ice Growth

by

Ravi Sharma

A thesis
submitted to the Faculty of Graduate Studies and Research
in partial fulfilment of the requirements for the degree of
M.Sc.

Department of Mechanical Engineering

Edmonton, Alberta

Fall, 1988

Permission has been granted to the National Library of Canada to microfilm this thesis and to lend or sell copies of the film.

The author (copyright owner) has reserved other publication rights, and neither the thesis nor extensive extracts from it may be printed or otherwise reproduced without his/her written permission.

L'autorisation a été accordée à la Bibliothèque nationale du Canada de microfilmer cette thèse et de prêter ou de vendre des exemplaires du film.

L'auteur (titulaire du droit d'auteur) se réserve les autres droits de publication; ni la thèse ni de longs extraits de celle-ci ne doivent être imprimés ou autrement reproduits sans son autorisation écrite.

ISBN 0-315-45684-1

The University of Alberta
Release Form

Name of Author: Ravi Sharma
Title of Thesis: Numerical Modelling of Frazil Ice Growth
Degree: M.Sc.
Year this degree granted: Fall 1988

Permission is hereby granted to The University of Alberta Library to reproduce single copies of this thesis and to lend or sell such copies for private, scholarly, or scientific research purposes only.

The author reserves other publication rights, and neither the thesis nor extensive tracts from it may be printed or otherwise reproduced without the author's written consent.

..... Ravi Sharma

(Student's signature)

Ravi Sharma
3226-105A St.

Edmonton, Alberta
T6J 3A6

Date : September 22, 1988

The University of Alberta
Faculty of Graduate Studies and Research

The undersigned certify that they have read, and recommend to the Faculty of
Graduate Studies and Research for acceptance, a thesis entitled

Numerical Modelling of Frazil Ice Growth

submitted by

Ravi Sharma

in partial fulfilment of the requirements for the degree of

M.Sc..

Jan Hunt
.....

(Supervisor)

Ally Lipsitt
.....

Mark A.
.....

.....

.....

Date : *Sept. 30, 1988*

Abstract

This work is primarily concerned with the numerical investigation of frazil ice crystal growth in a supercooled body of water. The major aspect of this study focuses on the application of the "Boundary Fitted Coordinate" method for the solution of crystal growth problems and explores the validity of the solution obtained in a quiescent melt of infinite extent. Of particular importance in this study is the examination of c-axis growth rates of the ice particle. Earlier investigators have almost always assumed that growth perpendicular to the basal plane can be ignored because it is significantly smaller in comparison to the a-axis growth rate. The results of this study however indicate that although crystal thickening rates at moderate supercooling values may be small, the net effect over a sufficiently large time span is indeed significant so that ignoring it would lead to an overestimate of radial growth rates.

The influence of fluid turbulence on crystal growth is considered by employing the concept of a thin stagnant film of fluid surrounding the crystal. The major outcome is increased heat transfer rates to the surrounding liquid region. Comparison of growth rates which are calculated on using this method were found to be considerably larger than results from a previous study using empirical heat transfer data. This difference of growth rate magnitudes demonstrates the presence of existing flaws in the more traditional methods of calculation. An important outcome of this study is the need for more rigorous experimental work together with a more precise measurement of turbulence parameters.

Acknowledgements

I wish to thank my supervisor, Dr. Tom Forest, for his guidance and support throughout the course of this work.

I also wish to express my gratitude for the financial support provided me during the course of this research by the University of Alberta Department of Mechanical Engineering and the Natural Sciences and Engineering Research Council (NSERC).

Finally, I dedicate this thesis to my parents whom I could not begin to thank.

Contents

Abstract	iv
Acknowledgements	vi
Nomenclature	xvi
Chapter 1	
INTRODUCTION	1
1.1 BACKGROUND AND LITERATURE REVIEW	4
1.1.1 FORMATION AND GROWTH OF FRAZIL ICE IN BODIES OF WATER	4
1.1.2 GROWTH AND MORPHOLOGY OF FRAZIL ICE CRYSTALS	11
1.2 ANALYTICAL AND NUMERICAL INVESTIGATIONS OF ICE GROWTH	25
1.2.1 THEORETICAL INVESTIGATIONS	27
1.2.2 NUMERICAL STUDIES OF ICE GROWTH FROM THE MELT	34
Chapter 2	
MATHEMATICAL FORMULATION AND METHOD OF SOLUTION	42
2.1 PHYSICAL MODEL AND ASSUMPTIONS	42

2.2	GOVERNING EQUATIONS AND BOUNDARY CONDITIONS . . .	46
2.3	NONDIMENSIONALIZATION	48
2.4	NUMERICAL METHODOLOGY	53
2.4.1	BOUNDARY FITTED CURVILINEAR COORDINATE SYSTEMS	54
2.4.2	MATHEMATICAL DEVELOPMENT	59
2.4.3	APPLICATION TO THE FRAZIL GROWTH PROBLEM . . .	62
2.4.4	DISCRETIZATION OF EQUATIONS AND METHOD OF SOLUTION	65

Chapter 3

	GROWTH OF A FRAZIL ICE CRYSTAL IN A SUPERCOOLED MELT	70
3.1	GROWTH IN THE a-AXIS DIRECTION IN A QUIESCENT SUPERCOOLED MELT	70
3.1.1	COMPARISON OF THE NUMERICAL AND ANALYTICAL SOLUTION	71
3.1.2	TRANSIENT GROWTH OF A DISC CRYSTAL	95
3.2	GROWTH OF A DISC CRYSTAL WITH THICKENING IN A QUIESCENT SUPERCOOLED MELT	101
3.2.1	QUASI-STEADY STATE c-AXIS GROWTH MODEL RESULTS	103

Chapter 4

	GROWTH OF FRAZIL CRYSTALS IN A TURBULENT FLUID	120
--	---	------------

4.1	EFFECT OF FLUID TURBULENCE ON CRYSTAL GROWTH . . .	120
4.2	GROWTH OF FRAZIL IN TURBULENT FLUID	127
4.2.1	CRYSTAL GROWTH BASED ON EMPIRICAL HEAT TRANSFER DATA	127
4.2.2	STAGNANT LAYER MODEL	138
4.3	RESPONSE OF FRAZIL CRYSTAL GROWTH TO APPLIED COOLING RATES	154
4.4	SUMMARY	169
5 CONCLUSIONS		171
References		175
Appendix A		
	DERIVATION OF THE SURFACE NUCLEATION GROWTH MODEL	184
Appendix B		
	SUMMARY OF DERIVATIVE TRANSFORMATIONS	188
B.1	FINITE DIFFERENCE APPROXIMATIONS IN THE TRANSFORMED PLANE	190
Appendix C		
	PROPERTIES OF WATER AND ICE	193

List of Tables

1.1	Values used for constants for empirical surface nucleation growth models	18
3.1	Locations of the outer boundary for the disc crystal	75
3.2	Comparison of analytical and numerical values of centerline growth rate and basal plane temperature at $(0, h/2)$	87
3.3	Variation in the growth rate along the disc edge for the identical conductivity case	92

List of Figures

1.1	Freezing process for water (from Knight [44])	5
1.2	Sequence of events during formation of frazil	10
1.3	Water temperature during occurrence of frazil	10
1.4	A unit cell of an ice crystal (from Kallungal [41])	13
1.5	Comparison of surface nucleation growth kinetics models. Simpson's results are a function of ΔT	16
1.6	Temperature variation near the tip of a growing ice crystal	19
1.7	The two principal radii of curvature for a frazil ice crystal. The crystal is considered flat edged when R_2 is very large ($R_2 \rightarrow \infty$)	21
1.8	Variation of the system free energy with crystal size for a frazil ice disc	22
1.9	Variation of the critical radius at various supercoolings for a flat edged disc crystal	23
1.10	Growth sequence of a disc crystal (from Arakawa [3]). Note the morphological instability at the large disc diameters.	26
1.11	Comparison of analytical growth models and previous experimental results at $\Delta T = 0.15^\circ C$	32
1.12	Experimental growth measurements of frazil crystal growth rates by Bukina [12]. The quantity V represents the mean flow velocity	33
1.13	Solution domain employed by Bonnerot and Jamet	38
1.14	Solution domain and boundary conditions for shape preserving dendrite (From Singh [69])	39
2.1	Model frazil ice crystal	43
2.2	Solution region considered for the frazil growth problem and boundary conditions	51
2.3	Transformation from physical to computational domain (a) Real Domain (b) Computational Domain	56

2.4	Numerical solution procedure for general crystal growth problem . . .	68
3.1	Example of a grid mesh required for the frazil growth problem. The mesh is concentrated near the location of the edge interface. The interface is located at $r = 1$ and $z = 0.033$	79
3.2	Comparison between analytical and numerical solution for $R = 50\mu m$ and $h/2 = 5\mu m$	81
3.3	Comparison between analytical and numerical solution for $R = 200\mu m$ and $h/2 = 5\mu m$	82
3.4	Comparison between analytical and numerical solution for $R = 400\mu m$ and $h/2 = 5\mu m$	83
3.5	Comparison between analytical and numerical solution near the edge interface for $h/2R = 0.10$	84
3.6	Comparison between analytical and numerical solution near the edge interface for $h/2R = 0.0125$	85
3.7	Normalized temperature contours for an ice disc of aspect ratio 0.20 ($k_i = k_s$)	88
3.8	Normalized temperature contours for an ice disc of aspect ratio 0.20 (dual conductivity case)	90
3.9	Normalized temperature contours for an ice disc of aspect ratio 0.05 (dual conductivity case)	91
3.10	a-axis growth rates for $\Delta T = 0.05^\circ C$ and three constant values of disc thickness	93
3.11	a-axis growth rates for $\Delta T = 0.10^\circ C$ and three constant values of disc thickness	94
3.12	Transient growth rates for ice discs of various thicknesses exposed to water with $\Delta T = 0.05^\circ C$	98
3.13	The radius-time behaviour for ice discs of various thicknesses exposed to water with $\Delta T = 0.05^\circ C$	99
3.14	The radius-time behaviour for an ice disc $50\mu m$ thick	100

3.15	c-axis growth rates for ice discs at various supercoolings with initially $R = 30\mu m$ and $h/2 = 10\mu m$. Note that the c-axis growth rate is virtually nonexistent for $\Delta T = 0.05^\circ C$ and therefore cannot be differentiated from the horizontal axis of the graph	105
3.16	Dimensionless temperature at the center of the basal plane ($r = 0, z = h/2$) for several values of ΔT	107
3.17	a-axis growth rates for ice discs at various supercoolings with initially $R = 30\mu m$ and $h/2 = 10\mu m$	108
3.18	Increase in radius of a frazil ice disc for various supercoolings	110
3.19	Increase in thickness of a frazil ice disc for various supercoolings	111
3.20	a-axis growth rates of frazil crystals of different initial thicknesses and $\Delta T = 0.08^\circ C$	113
3.21	a-axis growth rates of frazil crystals of different initial thicknesses and $\Delta T = 0.10^\circ C$	114
3.22	c-axis growth rates of frazil crystals for different initial thicknesses and $\Delta T = 0.08^\circ C$	115
3.23	a-axis growth rates of frazil crystals for different initial thicknesses and $\Delta T = 0.10^\circ C$	116
3.24	Temperature at the basal plane ($r = 0, z = h/2$) for different initial thicknesses and $\Delta T = 0.08^\circ C$	117
3.25	Temperature at the basal plane ($r = 0, z = h/2$) for different initial thicknesses and $\Delta T = 0.10^\circ C$	118
4.1	Schematic representation of the turbulence energy cascade	123
4.2	Turbulence energy spectra exhibited by many common turbulent flows	124
4.3	Nondimensional heat transfer correlation based on a turbulent Nusselt number (from Daly [18])	130
4.4	Ratio of heat transfer coefficient from the disc edge and the face (from Wadia [76])	131
4.5	a-axis growth rate calculated from Daly's model for $\Delta T = 0.05^\circ C$. Initial values of R and $h/2$ are $30\mu m$ and $10\mu m$ respectively. The label "INFINITE" corresponds to the quiescent fluid of infinite extent.	134

4.6	a-axis growth rate calculated from Daly's model for $\Delta T = 0.10$ °C. Initial values of R and $h/2$ are $30\mu m$ and $10\mu m$ respectively. The label "INFINITE" corresponds to the quiescent fluid of infinite extent.	135
4.7	c-axis growth rate calculated from Daly's model for $\Delta T = 0.05$ °C. Initial values of R and $h/2$ are $30\mu m$ and $10\mu m$ respectively. The c-axis growth rate for the infinite quiescent fluid is very low and represented by the horizontal axis of the graph.	136
4.8	c-axis growth rate calculated from Daly's model for $\Delta T = 0.10$ °C. Initial values of R and $h/2$ are $30\mu m$ and $10\mu m$ respectively. The label "INFINITE" corresponds to the quiescent fluid of infinite extent.	137
4.9	a-axis growth rates for stagnant layer model with $\Delta T = 0.05$ °C. Initial values of R and $h/2$ taken as $30\mu m$ and $10\mu m$ respectively. The label "INFINITE" corresponds to the quiescent fluid of infinite extent.	141
4.10	a-axis growth rates for stagnant layer model with $\Delta T = 0.10$ °C. Initial values of R and $h/2$ taken as $30\mu m$ and $10\mu m$ respectively. The label "INFINITE" corresponds to the quiescent fluid of infinite extent.	142
4.11	c-Axis growth rates for stagnant layer model with $\Delta T = 0.05$ °C. Initial values of R and $h/2$ taken as $30\mu m$ and $10\mu m$ respectively. The c-axis growth rate for the infinite quiescent fluid is very low and represented by the horizontal axis of the graph.	143
4.12	c-axis growth rates for stagnant layer model with $\Delta T = 0.10$ °C. Initial values of R and $h/2$ taken as $30\mu m$ and $10\mu m$ respectively. The label "INFINITE" corresponds to the quiescent fluid of infinite extent.	144
4.13	Maximum dimensionless basal plane undercooling as a function of crystal radius for $\Delta T = 0.05$ °C. The initial crystal radius is $30\mu m$ and $h/2 = 10\mu m$. The label "INFINITE" corresponds to the quiescent fluid of infinite extent.	146
4.14	Maximum dimensionless basal plane undercooling as a function of crystal radius for $\Delta T = 0.10$ °C. The initial crystal radius is $30\mu m$ and $h/2 = 10\mu m$. The label "INFINITE" corresponds to the quiescent fluid of infinite extent.	147
4.15	Comparison of the aspect ratios of ice discs as a function of disc radius between the stagnant layer model and Daly's model. The supercooling is $\Delta T = 0.10$ °C with $F = 30\mu m$ and $h/2 = 10\mu m$ initially.	149

4.16	Variation of the average edge Nusselt number for an ice disc of initial radius $30\mu m$ and $h/2 = 10\mu m$ and an overall supercooling of $0.10^\circ C$. The label "INFINITE" corresponds to the quiescent fluid of infinite extent.	152
4.17	Variation of the average Nusselt number along the basal plane for an ice disc of initial radius $30\mu m$ and $h/2 = 10\mu m$ and an overall supercooling of $0.10^\circ C$. The label "INFINITE" corresponds to the quiescent fluid of infinite extent.	153
4.18	Effect of different rates of cooling on the overall supercooling ΔT for the stagnant layer model with $\delta = 100\mu m$	157
4.19	Effect of a cooling rate of $-0.00106^\circ C/s$ on the overall supercooling ΔT . The results for the stagnant layer model are shown for several values of δ and the result from Daly's model for $\eta_k = 160\mu m$ is included.	159
4.20	Comparison of nucleation supercooling ΔT_n attained for different rates of cooling. Stagnant layer model is shown for varying values of δ and Daly's model is for the same dissipation scale as Carstens' data	161
4.21	Comparison of maximum supercooling ΔT_{max} attained for different rates of cooling. Stagnant layer model is shown for varying values of δ and Daly's model is for the same dissipation scale as Carstens data	162
4.22	Disc radius at the maximum supercooling for several cooling rates predicted by the stagnant layer model	164
4.23	Disc radius at the maximum supercooling for several cooling rates predicted by Daly's model	165
4.24	Aspect ratio of ice discs at the maximum supercooling for several cooling rates predicted by the stagnant layer model	166
4.25	Aspect ratio of ice discs at the maximum supercooling for several cooling rates predicted by Daly's model	167
A.1	Portion Of Basal Plane Surface Containing Monolayer	185

Nomenclature

A	area
A_S	effective area for heat transfer to the surroundings
$A(\lambda)$	parameter defined by Equation (3.5)
C	constant defined after Equation (1.21)
C_p	specific heat
d	defined in Equations (1.15) and (1.16)
Ec	Eckert number
ΔF	Helmholtz potential
$g(x, y)$	defined after Equation (1.21)
h	thickness of frazil ice disc
h_a	heat transfer coefficient to surroundings
\bar{h}	average heat transfer coefficient
$H(x)$	Heaviside step function
l	length scale of large scale turbulent eddies
l_c	characteristic length scale
k	thermal conductivity

k_a	thermal conductivity of air
k_b	Boltzman constant
l	length scale of large scale turbulent eddies
l_c	characteristic length scale
L	latent heat of fusion
n	direction of unit normal vector
m_i	mass of ice phase
m_w	mass of liquid phase
N	number of moles
Nu_T	turbulent Nusselt number
$P(\xi, \eta)$	function defined by Equation (2.59)
Pe	Peclet number
Pr	Prandtl number
\bar{q}	average heat flux
$q_0(x)$	toroidal intergral of order zero
$Q(\xi, \eta)$	function defined by Equation (2.60)
Q_G	latent heat energy liberated to the water
Q_L	heat losses to the surroundings

Q_s	thermal energy stored in the water
r, z	radial and axial coordinate directions
\bar{r}, \bar{z}	nondimensional radial and axial coordinate directions
R	radius of frazil ice disc
R_{cr}	critical radius of frazil crystal defined by Equation (1.12)
R_g	universal gas constant
R_o	initial radius of ice disc
R_1	primary radius of curvature
R_2	secondary radius of curvature
R_∞	location of outer boundary in the radial direction
s	molar entropy
Ste	Stefan number
t	time
t_e	time at which equilibrium temperature occurs
t_{max}	time at which maximum supercooling occurs
t_n	time at which nucleation temperature occurs
t_r	time at which residual supercooling occurs
T	temperature

T_A	average temperature of the surroundings
T_e	thermodynamic equilibrium temperature at a curved interface
T_i	interfacial temperature
T_m	melting temperature of ice
T_n	nucleation temperature
T_r	residual temperature
T_w	temperature of water frazil immersed in
T_∞	bulk liquid temperature
ΔT	overall temperature difference
ΔT_{max}	maximum supercooling
ΔT_c	temperature depression due to capillarity effects
ΔT_h	temperature depression due to thermal resistance
ΔT_k	temperature depression due to interfacial kinetics
ΔT_n	nucleation supercooling
ΔT_o	initial liquid supercooling
\bar{u}	velocity distribution
$\bar{\bar{u}}$	nondimensional velocity distribution
u_s	rms value of velocity fluctuations

U_c	characteristic velocity of liquid
v_n	normal velocity of growing interface
V	mean flow velocity
V_a	growth rate parallel to the a-axis
V_c	growth rate parallel to the c-axis
V_r	radial growth rate
V_z	axial growth rate
V_n	normal velocity
V_w	volume of water
Z_∞	location of outer boundary in the axial direction

Subscripts

a	air
c	effects due to curvature
h	effects due to heat dissipation
$init$	initial
k	effects due to interfacial kinetics
l	liquid phase region
r, z	differentiation with respect to the corresponding variables

s solid phase region

B basal Plane of crystal

E edge of crystal

T Total

ξ, η differentiation with respect to the corresponding variables

Superscripts

α iteration number

$+$ liquid portion of solid-liquid interface

$-$ solid portion of solid-liquid interface

1 defined in Figure A.1

2 defined in Figure A.1

l defined in Figure A.1

Greek

α thermal diffusivity

α_p parameter defined in Equation (1.1)

α_T free stream turbulence intensity

ζ, β, γ parameters defined after Equation (2.44)

- β_s parameter defined in Equation (4.8)
- γ_{sl} surface energy of ice-water interface
- Γ_g surface adsorption coefficient
- ξ, η computational plane coordinates
- η_k Kolmogorov length scale
- λ parameter defined in Equation (3.8)
- λ_o step height of embryo on basal plane
- ν kinematic viscosity
- μ dynamic viscosity
- μ_p chemical potential
- μ_1 constant defined after Equation (1.3)
- μ_2 constant defined after Equation (1.3)
- ϵ rate of turbulence energy dissipation
- ρ density
- τ nondimensional time
- θ nondimensional temperature
- δ stagnant layer thickness
- δ_g magnitude of grid spacing in real plane

- Δ_ϵ grid spacing in the computational plane
- Δ_n grid spacing in the computational plane
- φ wavenumber
- κ Constant defined after Equation (A.12)
- σ Constant defined after Equation (2.2)
- ϵ fraction of total binding energy of an atom

Chapter 1

INTRODUCTION

Generally in a quiescent body of water, both the supercooling and hence the ice formation take place on its surface and consequently result in a more or less continuous ice cover. The presence of turbulence, on the other hand, leads to a thick supercooled layer in which ice may form. Due to the mixing and agitation of the water surface, the creation of a monolithic ice sheet on the water surface is prevented. Instead, the existing ice crystals are brought down to lower layers where they can grow and interact with each other. This interaction forms the basis of additional frazil production and is probably the most significant factor responsible for the commonly observed large accumulation of ice crystals. Frazil ice is almost always formed in turbulent, supercooled bodies of water and appears as fine spicule, plate or discoid crystals distributed throughout the volume of water. Under certain conditions, these crystals can stick to underwater objects such as vegetation along the river bottom and to each other, thereby, becoming either ice floes on the water surface or anchor ice on the river basin. The nucleation and growth of frazil ice crystals in northern rivers and lakes has a tremendous negative impact on man's activities in cold climate regions. The adverse engineering problems associated with frazil include the blockage of water supply intakes, hydroelectric plant intakes and of irrigation and water supply canals. Frazil ice is also responsible for the formation of ice jams which can block an entire river cross-section and often causes extensive flood damage during the spring thaw period.

Although frazil causes considerable damage every year in regions in the northern hemisphere, the amount of information available about it is usually quite general and limited in scope. Existing research has been fragmentary and has concentrated

primarily on describing the nucleation, formation and subsequent production of frazil ice crystals through observations in the field and limited experimentation in the laboratory. Although this research is quite useful and acts as a helpful base for additional work by itself, it leaves huge gaps and lacks significant detail so that several important questions still remained unanswered. The rather slow development of theoretical and numerical work for the realistic prediction and modelling of frazil growth phenomenon is mainly due to this lack of quantitative experimental analysis.

Previous analytical studies on the growth rates of frazil ice crystals have generally made several simplifying assumptions, which have resulted in inaccurate growth rates and crystal size predictions. Two such assumptions in particular have been to neglect the growth rate of the ice crystal in the c-axis direction and to treat the ice crystal as an isothermal particle. Usually at the low supercoolings associated with frazil growth, c-axis growth rates may indeed appear to be negligible in quiescent water. However, this may not necessarily be true in turbulent, supercooled bodies of water. Although the c-axis growth rate is generally considerably smaller than the a-axis growth rate of the crystal by an order of magnitude and appears to be insignificant, it may still have some effect on the radial extent of the crystal over a period of time. The effects of turbulence have also not been effectively incorporated into available analytical solutions of frazil growth problems.

Factors such as these form the motivation to develop an improved model to predict the growth behaviour of frazil ice crystals under more realistic conditions. In this thesis, we first develop the background physics and mathematics needed to describe the growth behaviour of a frazil ice crystal in a quiescent body of water. This is later extended to include the qualitative effects of turbulence. The validity of these results is then verified by comparing them with available empirical methods. In order to effectively employ this technique for the prediction of frazil growth behaviour and

to apply it to existing frazil ice interaction models, the calculated results must be verified more rigorously with further experimentation. An outline of the development of this thesis proceeds in the following order.

The remainder of this chapter presents background material for crystal growth processes and reviews the available literature on frazil ice and crystallization mechanisms. A literature review of available analytical solutions related to frazil crystals is also presented, including a brief review of recent numerical developments in ice growth problems.

Chapter 2 deals with the governing equations and boundary conditions describing the growth of a frazil ice crystal. Simplifications due to geometrical and physical assumptions are made in order to reduce some of the complexities in the equations. Later, the "Boundary Fitted Coordinates" scheme together with its application to the solution of the frazil growth problem is described in some detail.

In Chapter 3, the growth of a frazil ice crystal submerged in a quiescent liquid is examined. The validity of the numerical scheme is verified by comparing it with an analytical solution for a simplified case. In addition, the justification of a quasi-steady state growth assumption is investigated. Finally, the traditional assumption of negligible c-axis growth rates are examined along with its effect on the radial growth of the crystal.

Growth of a frazil crystal suspended in a turbulent, supercooled fluid is examined in Chapter 4. It is known that the major effect of turbulence results in increased heat transfer rates to the liquid phase. This fact can effectively be incorporated into the model developed in Chapter 4 by assuming that the entire volume of fluid (in which the crystal is suspended) is well mixed and hence, at a uniform temperature, except for a thin conductive layer surrounding the crystal. By increasing or decreasing the conductive thickness layer, the level of turbulence can be respectively decreased

or increased. These results obtained are verified by comparison with an existing simplified frazil growth model which is based on empirical turbulent heat transfer data. The correctness of the results is further checked by modelling the growth behaviour of a collection of crystals subject to the typical icing trends exhibited during the initiation and development of frazil in bodies of water and comparing sizes predicted with existing experimental and field data.

Conclusions and recommendations for additional studies are outlined in the final chapter. In particular, the need for more rigorous experimental work consistent with parameters used in the numerical study is emphasized. Also, more detailed studies on the effects of turbulence intensity and its correlation with the conductivity layer thickness are needed. Thus, frazil growth rates under more realistic conditions can be determined for use in a frazil crystal dynamics model [18] which can then be used for more comprehensive studies in river icing and hydrology problems.

1.1 BACKGROUND AND LITERATURE REVIEW

1.1.1 FORMATION AND GROWTH OF FRAZIL ICE IN BODIES OF WATER

Nucleation is the initiation of the transformation of an unstable phase to a more stable one. When liquid water is lowered below its freezing point, it becomes thermodynamically metastable and will begin to change phase when the temperature is lowered below a certain value known as the nucleation temperature. Figure 1.1 schematically illustrates the freezing process. Sensible heat is removed from the liquid until it is cooled past its melting point T_m to its nucleation temperature T_n . At this point, transition to the solid phase begins. The process occurring between states A and B, and between states B and C is called crystal growth and

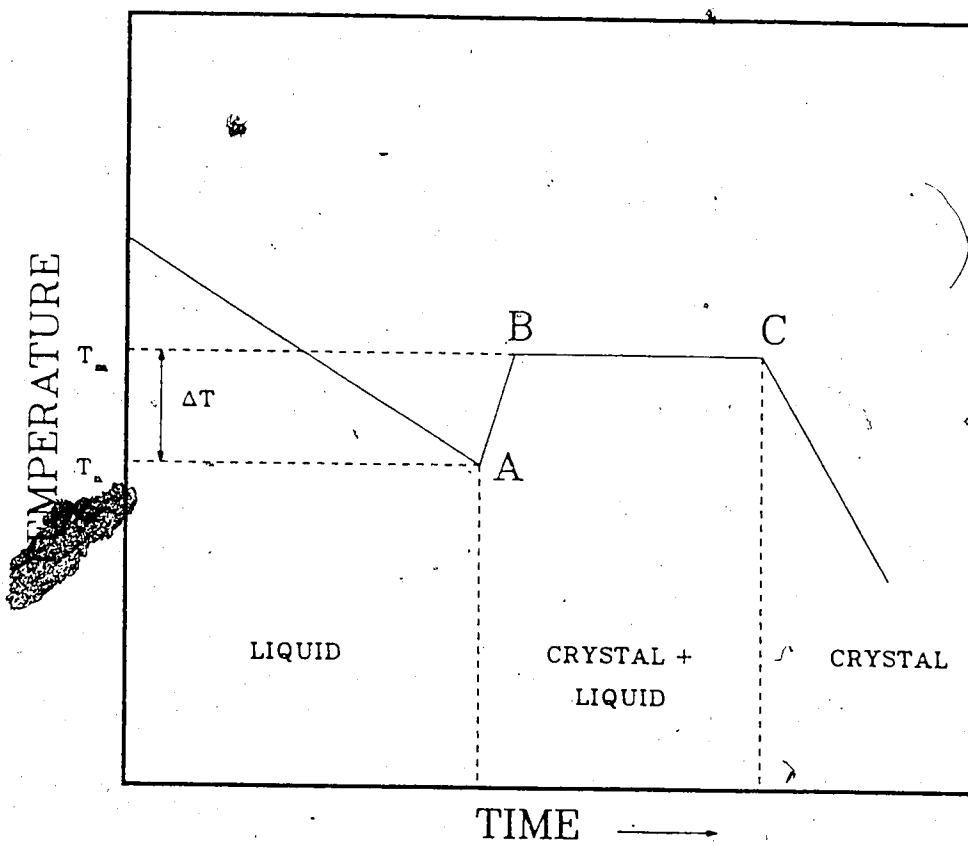


Figure 1.1: Freezing process for water (from Knight [44])

is characterized by the latent heat release resulting from the phase transition. The temperature of the liquid water below its melting temperature is termed supercooling or undercooling. All liquids require supercooling before solidification can take place. For pure water, Hobbs [36] reports a supercooling of $40\text{ }^{\circ}\text{C}$ for freezing to occur (homogeneous nucleation). The presence of impurities in the liquid acts to lower the supercooling required for nucleation (heterogeneous nucleation).

Frazil ice crystals are almost always formed in slightly supercooled, turbulent bodies of water. Explaining the source of initial frazil crystals has been the object of several research investigations. Normally, frazil crystals have been observed where the supercooling of the water has been less than $0.05\text{ }^{\circ}\text{C}$ [60]. Consequently, the homogeneous nucleation of ice particles is not physically possible. Altberg [1] and Devik [20] proposed that initial ice nuclei formed by spontaneous heterogeneous nucleation. However, examination of the nucleation temperatures of water with various organic and inorganic materials present indicate that a minimum supercooling of $1.3\text{ }^{\circ}\text{C}$ is required [75].

Michel [54] suggested that spontaneous heterogeneous nucleation occurs in a thin layer of highly supercooled water on the surface. This excess supercooling was thought to occur due to an enhanced heat loss into the atmosphere along the water surface. Later, this theory was refuted by Osterkamp [61] who showed that the water surface temperature supercooling was well above the nucleation temperatures of any impurities present. Hanley [32] presented a thermodynamical argument proving that the only material capable of providing nucleation sites for subsequent frazil growth at supercoolings of the order $0.05\text{ }^{\circ}\text{C}$ is ice itself. Thus it can be concluded that initial seed crystals are required for the initiation and production of frazil ice crystals. The obvious question is how the water surface is seeded.

Osterkamp [61] proposed that highly supercooled ice crystals in the cold

atmosphere, resulting from ice fog, water spray, or snow, rain down upon the water surface providing the initial ice nuclei required for frazil ice to form and grow. Alternatively, Tsang [75] suggested that highly cooled dust particles in the cold atmosphere fall to the water surface and cool the water in immediate contact with them to a degree where heterogeneous nucleation of ice particles is possible. Both these processes described above are referred to as atmospheric seeding and appear to adequately explain the presence of initial ice nuclei at relatively low water supercoolings. The number of seed crystals deposited on the water surface undoubtedly influence ensuing frazil production and is highly dependent on the atmospheric meteorological conditions. The relation between these two parameters however has not been studied in great detail.

The necessity of seed crystals for frazil ice production is further supported by observations in turbulence jars or industrial crystallizers. Mueller [57] conducted experiments for frazil ice formation in a turbulence jar with the level of supercooling ranging between 0.05°C and 0.30°C . His experiments revealed that regardless of the degree of supercooling, the turbulence intensity or the presence of foreign materials in the water, no frazil ice formed unless the water was seeded with initial ice nuclei. Other experimental studies conducted by Garbabedian and Strickland-Constable [29] and Ettema et al. [21] report similar results.

Osterkamp [60] notes that although the turbulence intensity does not affect initial nucleation of frazil crystals, the enhanced heat transfer it provides strongly affects the growth rates of the individual crystals. Also, collision breeding of ice crystals is greatly enhanced by the presence of turbulence. As initially deposited ice nuclei grow on the water surface, they are transported to lower depths by water agitation arising from the flow turbulence. Formation of a monolithic ice layer on the water surface is prevented by the water turbulence. The subsequent growth and interaction

then leads to collisions between the larger crystals and produces extremely small bits and fragments which act as additional ice nuclei. This process, known as secondary nucleation, was stated by Daley [18] "to be the single most important mechanism for frazil production in lakes, rivers and industrial crystallizers".

Garbabedian and Strickland-Constable [29] conducted experiments to check the effect of secondary nucleation for enhancing crystal production. Their experimental apparatus consisted of a chunk of ice contained in an enclosed jar filled with supercooled water. The fluid was stirred at various rates by a motor driven impeller to generate turbulence. They concluded from their studies that in the stirred pure liquid, the collision of the large ice crystal with the vessel walls resulted in high rates of nucleation. They also observed that higher rates of stirring led to a larger number of ice nuclei being formed. Experimental studies by Ettema et al. [21] yielded similar results. Their experimental apparatus consisted of a vessel containing water which could be supercooled and maintained at a constant temperature by means of cooling coils. Turbulence in the jar was generated by means of an oscillating grid whose oscillation frequency ranged from 15 cycles/second to 110 cycles/second. The study revealed that although higher turbulence intensities result in higher frazil production, the rate of frazil production was more pronounced for lower water supercoolings. Thus secondary nucleation rates were found to depend on the three factors— turbulence level, crystal size distribution and the degree of supercooling.

The importance of secondary nucleation in frazil ice production has also been observed in the field. The sequence of events during frazil ice formation in the fast flowing turbulent body of water, the Niagara river, are described in detail by Arden and Wigle [6] and illustrated schematically in Figure 1.2. Frazil formation occurred in the river during cold clear nights when the atmospheric meteorological conditions were sufficient to dissipate the heat content stored in the river. Arden and Wigle

reported frazil nucleation on the water surface when the mean temperature of the river was $+0.03\text{ }^{\circ}\text{C}$. Crystals on the surface were observed to grow as the river was further cooled to a temperature of $-0.05\text{ }^{\circ}\text{C}$ and eventually were submerged to lower depths by the turbulent eddies. Cooling of the river progressed from the surface to the bottom and during a period of about one hour they reported that the top 2 m to 3 m of the river became supercooled while the remaining depth of 5 m to 7 m remained slightly above freezing. During this period frazil was observed only in the top supercooled layer. Frazil was reported to exist at all depths as the entire river eventually became supercooled. The majority of the ice crystals observed during this sequence were disc shaped with very few irregular shaped crystals. The high frazil production rates developed into "a driving snow storm such as can be seen through the headlight beams of a moving automobile at night" when viewed under a light source [6]. Crystals colliding into each other eventually sintered together and agglomerated into ice flocs which eventually floated to the surface and formed large floes of slush ice.

The corresponding water temperature behaviour during frazil formation has been studied by Michel [55] and Carstens [15]. A typical sequence of water temperatures leading to and during frazil formation is shown in Figure 1.3. The water is cooled by heat loss to the cold ambient surroundings causing the temperature to drop linearly to a value just slightly below the equilibrium temperature T_e . At a temperature a few hundredths of a degree below the freezing temperature T_n , small ice particles, invisible unless magnified, can be detected. These particles grow larger in size and interact producing additional crystals as explained before. This increased production however results in a decreased cooling rate of the water. When the water reaches its maximum supercooling ΔT_{max} , the temperature slowly increases due to the latent heat release from the multitude of growing crystals. This temperature rise in the

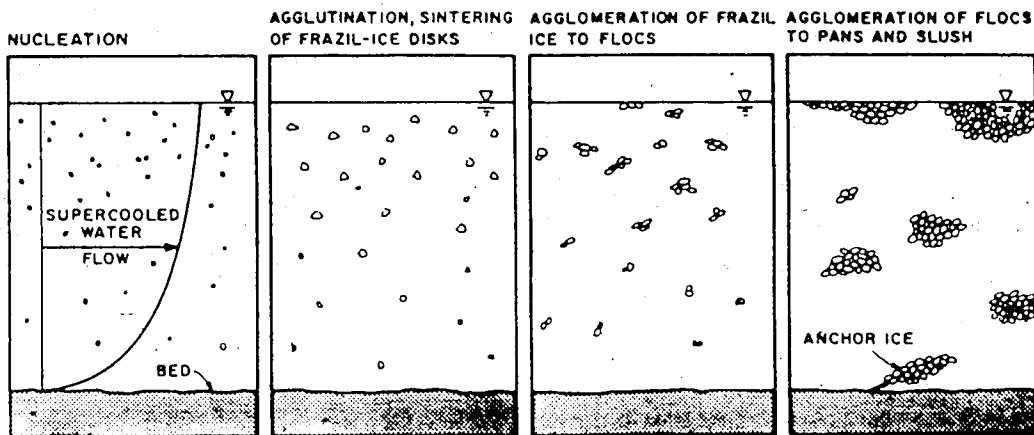


Figure 1.2: Sequence of events during formation of frazil

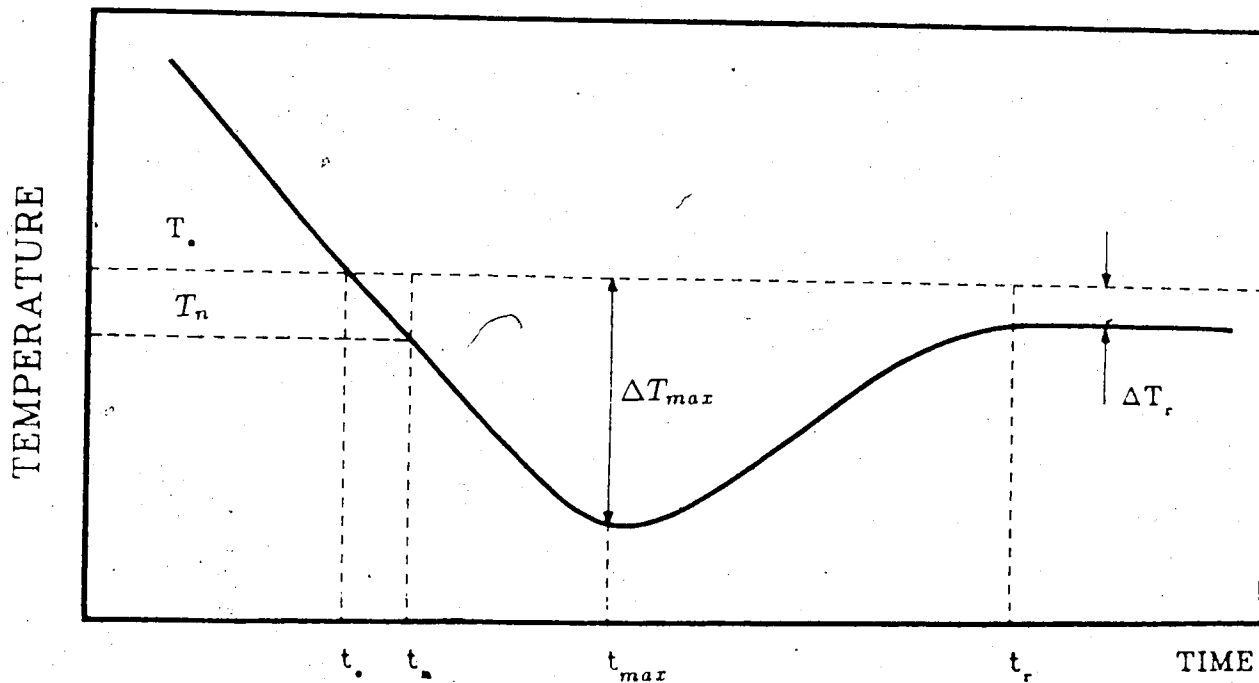


Figure 1.3: Water temperature during occurrence of frazil

water continues until a heat balance between the latent heat released by the growing crystals is balanced by the heat loss from the water surface. At this point, the water temperature asymptotically approaches a constant temperature T_r , termed the residual supercooling. The value of T_r was found to depend on the hydrometeorological conditions under which frazil is formed. The values T_n , T_{max} and T_r for natural lakes and rivers have not been well documented as it is difficult to measure under variable field conditions. Hanley [32], Carstens [15] and Michel [55] noted however that the maximum supercooling could be as low as $0.10\text{ }^\circ\text{C}$ and frazil ice nucleation was observed to occur at a supercooling not less than $0.02\text{ }^\circ\text{C}$.

An excellent review of frazil and anchor ice formations in northern lakes and rivers is given by Tsang [75]. He provides a thorough, concise description of nucleation mechanisms, sources of heat loss from the perspective of an overall thermal energy balance of natural bodies of water. Also contained in this manuscript are several cases of hydraulic problems associated with frazil and anchor ice growth.

1.1.2 GROWTH AND MORPHOLOGY OF FRAZIL ICE CRYSTALS

An understanding of crystal growth mechanisms and ice morphology is important in the study of frazil evolution in turbulent bodies of water. The major role of crystal growth mechanisms is to influence the morphology of ice particles, their resulting size and ultimately their number concentration. Once the water has been seeded, as described in the previous section, the rate at which new crystals form depends strongly on the number of available crystals and their respective sizes. In order to understand the dependence of these parameters on crystal growth rates, we shall examine the growth mechanisms of frazil ice crystals and discuss their influence on ice morphology.

An ice crystal immersed in a pure supercooled melt will grow only if the difference in free energy between the liquid and solid phase is positive and increases with distance from the solid-liquid interface. The two principal factors which control the growth rates of ice crystals are the rate of transport of latent heat from the growing surface and the rate of atomic deposition on the solid phase. The magnitude of these two parameters depends on the major driving force, the overall temperature difference ΔT . A frazil ice crystal has two distinct growth mechanisms which give rise to the commonly observed disc like morphology. Growth in the radial and axial directions is dictated by two different growth mechanisms. Experimental observations have shown that radial growth proceeds much more rapidly than axial growth since the thickness to diameter ratio is reported to be approximately 0.02 [61]. Before proceeding further in discussing the characteristics of frazil growth mechanisms, it is first necessary to introduce some terminology associated with crystal growth and briefly discuss the physics of crystallization.

The two principal growth directions observed in ice crystal growth arise due to the atomic rearrangement of a water molecule during solidification and its subsequent bonding with adjacent molecules. A unit cell of an ice crystal is hexagonal in shape, as shown in Figure 1.4, from which its two principal growth directions are readily seen. The hexagonal axis of the cell is referred to as the c-axis and the three axes (120° from each other) perpendicular to it are termed the a-axes. The top surface of the hexagonal prism is referred to as the basal plane, which is perpendicular to the c-axis. The existence of these two major growth directions can be verified from the optical properties of an ice crystal. The unit ice cell consists of twelve oxygen atoms bonded to each other with hydrogen atoms in which the oxygen atoms lie in layers. The hydrogen atoms, on the other hand, are alternatively raised and lowered. Also, water molecules in adjacent layers have the hydrogen atoms orientated in opposing

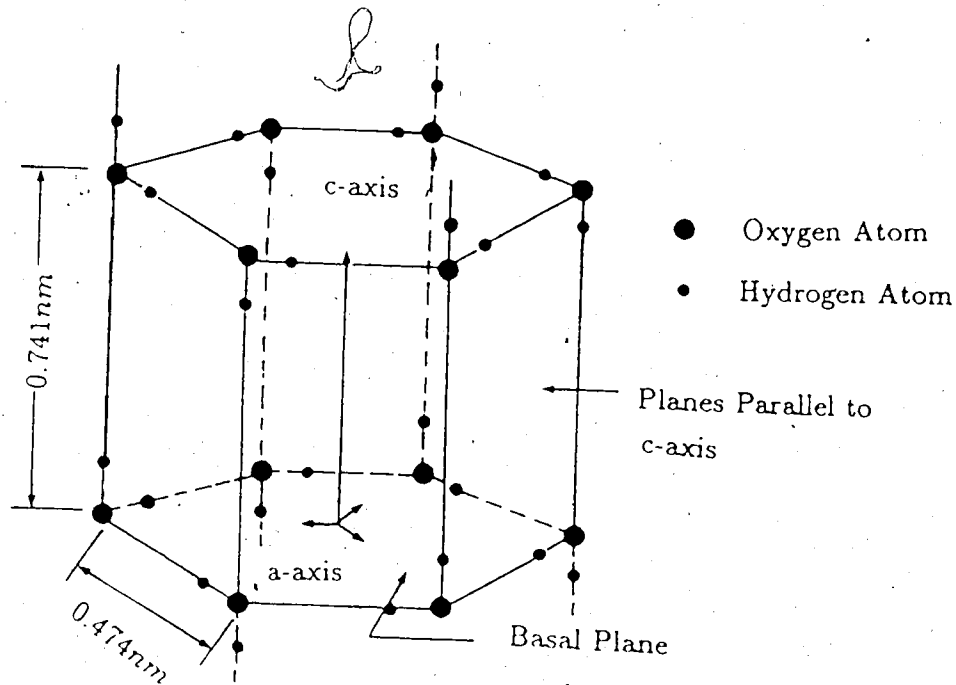


Figure 1.4: A unit cell of an ice crystal (from Kallungal [41])

directions resulting in the shared hydrogen atoms to be closer to one oxygen atom than the other. For growth of the crystal to occur in the c-axis direction, six hydrogen-oxygen bonds are required compared to four in each of the a-axis directions. Since crystal growth is more likely to proceed where the fewest number of molecular bonds are required for a stable arrangement, growth in the a-axis direction will proceed at a more rapid rate compared with the c-axis direction.

A theory characterizing the roughness of a solid-liquid interface was proposed by Jackson [38], [39] based on the minimum free energy condition of the system. He defines the parameter α_p , given by

$$\alpha_p = \frac{\epsilon L}{R_g T_m} \quad (1.1)$$

where ϵ is the fraction of the total binding energy of an atom that can be associated

with an atomic layer parallel to the face under consideration and R_g is the universal gas constant. Jackson concluded that a crystal face for which $\alpha_p > 2$ will be smooth while the one with $\alpha_p < 2$ will correspond to rough crystal face. The kinetics for a smooth crystal face are more likely to be so slow that it will control the crystal growth rate so that the crystal will grow with large, flat faces in a stepwise fashion. Conversely, for atomically rough crystal faces, the kinetics are rapid enough so that the surface grows in a smooth, continuous manner indicating that some factors at the macroscopic level actually limit the growth rate. Fujioka [28] has shown that the values of α_p for ice in the a- and c-axes directions are 0.88 and 2.64 respectively. Therefore for frazil ice crystals, the interface in the radial direction is rough and parallel to the a-axis. This implies that growth in this direction is very rapid and dominated by macroscopic factors such as heat diffusion. The crystal surface perpendicular to the c-axis is smooth and therefore growth proceeds very slowly indicating that it is controlled by the interfacial kinetics.

Growth mechanisms important for frazil ice crystal growth fall into two major categories described below:

Continuous Growth: A solid-liquid crystal interface may be rough at a molecular scale due to certain conditions. Water molecules can then easily attach themselves at random sites on the rough surface quite rapidly, resulting in a continuous growth normal to the surface. The rate at which the surface grows is postulated to be of the form

$$V_n = \mu_1 \Delta T \quad (1.2)$$

where μ_1 is a constant.

Surface Nucleation: A perfectly smooth crystal surface grows by the consecutive nucleation of thin monolayers spreading across the flat crystal face. For growth

to occur, a stable island must be nucleated on the growing surface (Figure 1.9) which spreads across covering the crystal face instantaneously. The general form for this growth mechanism can be shown to be

$$V_n = \mu_1 e^{\mu_2/\Delta T_k} \quad (1.3)$$

where V_n is the growth velocity of the surface, μ_1 and μ_2 are constants, and ΔT_k is the interfacial supercooling.

The interface kinetics for a frazil ice crystal are of type 1 in the a-axis direction and of type 2 in the c-axis direction. In the literature, both these growth mechanisms have been investigated theoretically and experimentally resulting in a large accumulation of references. Many of these studies however, arose as a consequence of desalination research where more emphasis was placed on the effect of dissolved impurities upon growth in the two principal directions rather than upon a detailed analysis of the growth mechanism itself. Several studies have been conducted for the measurement and prediction of a-axis and c-axis growth rates. Most notable are the works of Hillig [35], Sperry [53] and Simpson [68]. Hillig and Sperry grew ice crystals orientated in the c-axis direction inside capillary tubes. The capillary tubes were cooled by being immersed in a cooled bath. Simpson, on the other hand measured growth rates of free, unconfined crystals. Hillig's (H(1) in Figure 1.5) and Sperry's results are similar at supercoolings less than 0.05 °C as seen in Figure 1.5. For higher values of supercooling, Hillig's relation gives significantly higher c-axis growth rates than does Sperry's. This is due to Hillig's failure to "consider the heat transfer resistance of the cooling water boundary layer on the outside wall of the capillary tube" [53] in the heat dissipation analysis to determine the true interface temperature. Consequently, Hillig's relation as a function of the actual interface supercooling differs from Sperry's relation which accounts for these additional thermal resistances. It is

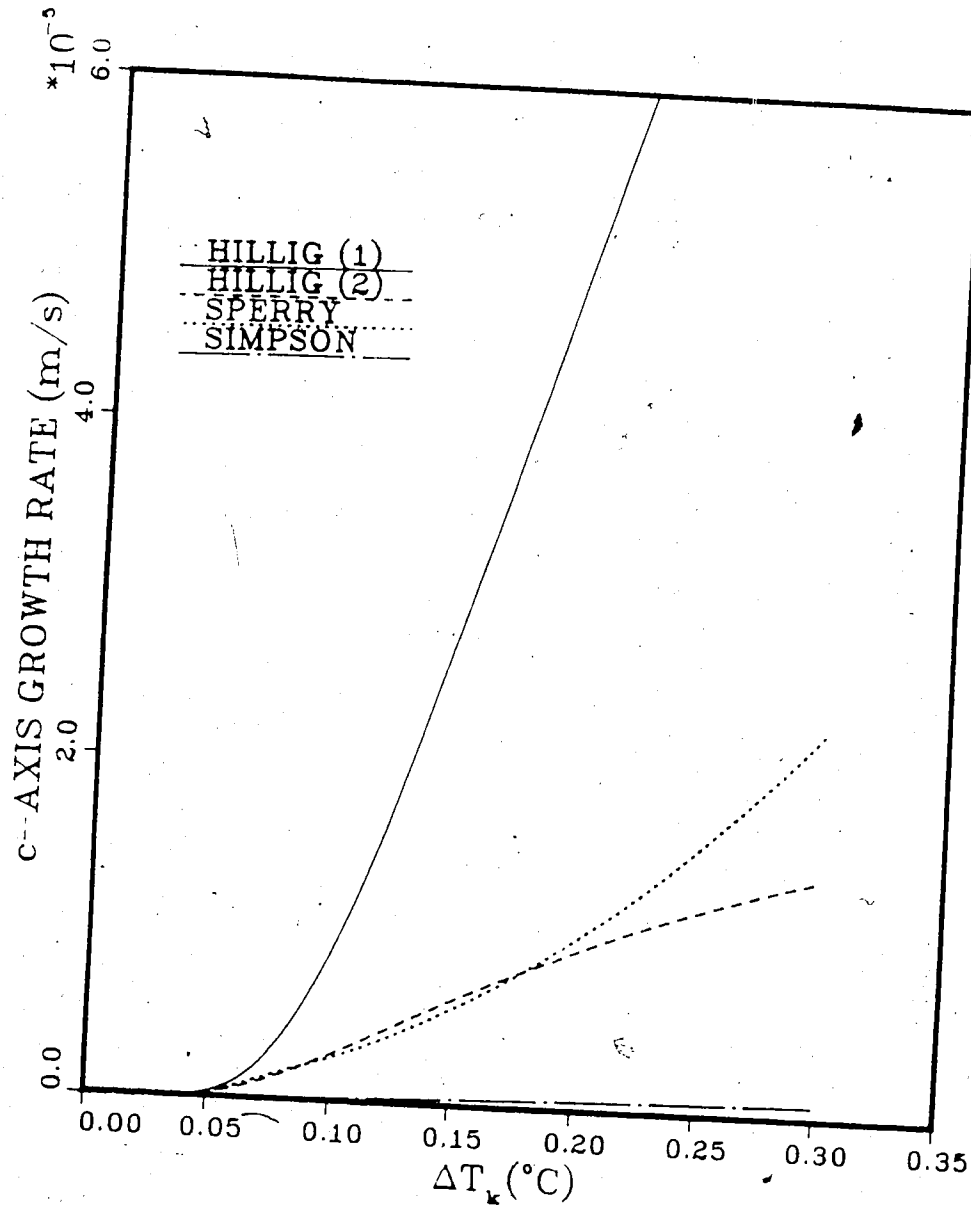


Figure 1.5: Comparison of surface nucleation growth kinetics models. Simpson's results are a function of ΔT

noteworthy to mention that Hillig's experimental results, which are a function of the overall supercooling ΔT , are almost identical to Sperry's results when the interface temperature correction has been taken into account. Therefore, we may use Hillig's experimentally obtained coefficients (H(2)) in the surface nucleation model (1.3) to estimate c-axis growth rates for crystals when ΔT_k is less than 0.20°C in place of Sperry's relation which is in a form not suitable for numerical implementation. A comparison of Simpson's results with those of Hillig and Sperry shows that the unconfined growth rates are approximately of an order of magnitude lower than those of the confined growth cases. Despite the lack of agreement between the two techniques, both indicate that growth perpendicular to the basal plane proceeds by surface nucleation. It can be shown that the rate of growth by two dimensional surface nucleation (see Appendix A for derivation of this expression and definition of the symbols) is given by

$$V_c = \kappa A \lambda_o e^{-\Delta F_{max}/3k_b T} \quad (1.4)$$

The semi-empirical relations for c-axis growth determined by Hillig, Sperry and Simpson are given in Table 1.1.

Growth rates parallel to the basal plane have been measured by several investigators such as Fletcher [23] Hobbs [36], Kallungal [42] and Fernandez [22]. They report growth rates described by the relation

$$V_a = A(\Delta T)^m \quad (1.5)$$

where the value of m is approximately unity for a continuous growth mechanism. However the coefficient m was found to vary between 1.3 to 2.2 indicating that another type of growth mechanism was dominant. Nevertheless, they concluded that the interface kinetics in the a-axis direction are very rapid and did not limit the growth rate. Instead, growth is controlled by the rate of latent heat dissipation from

REFERENCE	GROWTH MODEL	μ_1	μ_2
HILLIG (1)	$V_c = \mu_1 e^{-\mu_2/\Delta T_k}$	3.0×10^{-5}	0.35
HILLIG (2)	$V_c = \mu_1 e^{-\mu_2/\Delta T}$	3.2×10^{-5}	0.246
SPERRY	$V_c = \mu_1 \Delta T_k^{\mu_2}$	1.024×10^6 ($\Delta T_k \leq 0.0629 \text{ } ^\circ\text{C}$)	2.0
		2.524×10^{-4} ($\Delta T_k \geq 0.0629 \text{ } ^\circ\text{C}$)	10.0
SIMPSON	$V_c = \mu_1 e^{-\mu_2/\Delta T}$	1.734×10^{-6}	0.234

Table 1.1: Values used for constants for empirical surface nucleation growth models

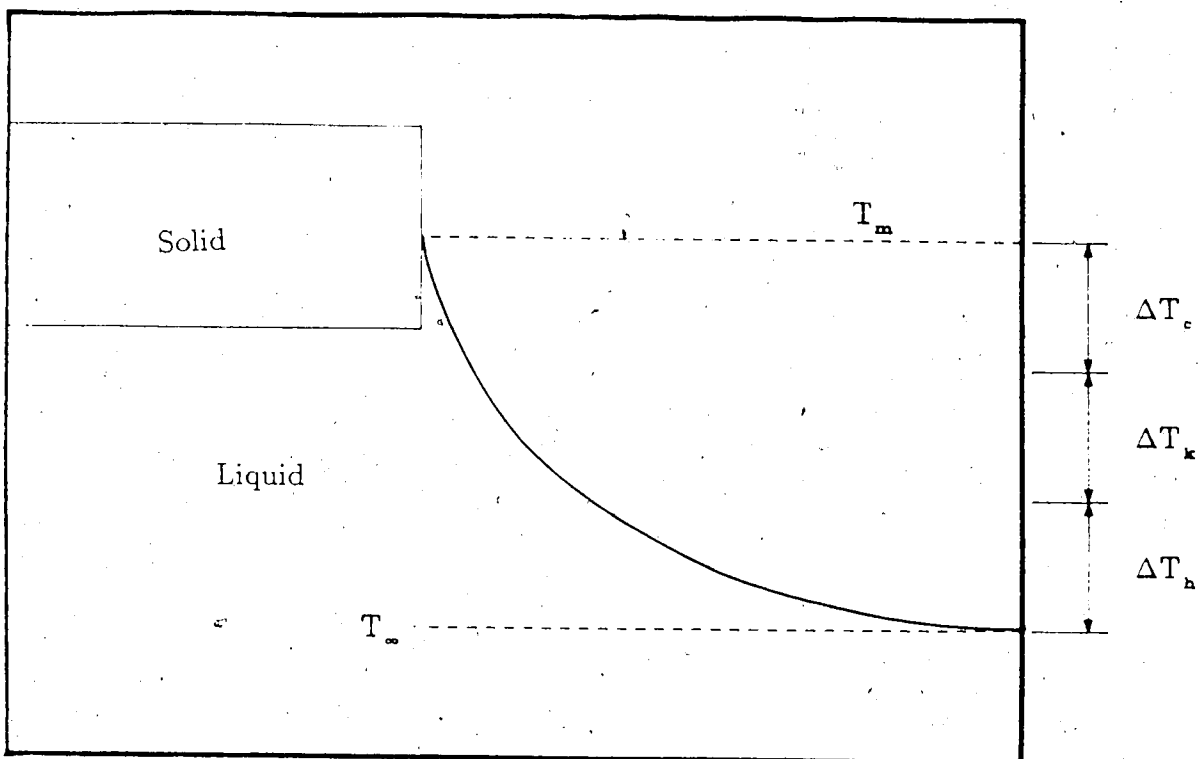


Figure 1.6: Temperature variation near the tip of a growing ice crystal

the interface. The rate of latent heat transfer itself can be affected by several factors such as the temperature difference, the interface curvature, turbulence intensity in the liquid and the presence of impurities in the liquid.

The major driving force for crystal growth in a supercooled melt is the overall supercooling ΔT given by

$$\Delta T = T_m - T_\infty \quad (1.6)$$

where T_m is the melting temperature of the pure liquid and T_∞ is the mean bulk temperature of the liquid far from the growing surface. Figure 1.6 shows the variation typically found in the supercooled liquid into which the crystal is growing. For pure water, the total supercooling ΔT is made up of three distinct temperature differences

$$\Delta T = \Delta T_c + \Delta T_k + \Delta T_h \quad (1.7)$$

where

$$\Delta T_c = T_m - T_e \quad (1.8)$$

$$\Delta T_k = T_e - T_i \quad (1.9)$$

$$\Delta T_h = T_i - T_\infty \quad (1.10)$$

Each of these temperature differences is used up by the three resistances to crystal growth. The first of these resistances is due to the interface curvature which acts to decrease the thermodynamic equilibrium temperature T_m . The second is a result of the intrinsic kinetics (rate of atomic deposition) which depresses the crystal surface temperature from T_e to T_i . The magnitude of this undercooling (ΔT_k) depends on the growth mechanism of the crystal. The remaining portion of the total driving force is used up for the transfer of heat away from the crystal face.

The temperature required to overcome the resistance to surface curvature is given by the Gibbs-Thompson relation

$$\Delta T_c = T_m - T_e = \frac{\gamma_{sl} T_m}{\rho_s L} \left(\frac{1}{R_1} + \frac{1}{R_2} \right) \quad (1.11)$$

where γ_{sl} is the ice-water surface free energy, ρ_s is the density of ice and L is the latent heat of fusion. The quantities R_1 and R_2 are the principal radii at any point on the interface (see Figure 1.7). Frazil ice crystal interfaces in the a-axis direction are generally assumed to be flat (ie. $R_2 \rightarrow \infty$) so that $1/R_2$ can be neglected. It can be seen from Equation (1.11) that the resistance due to curvature will be quite large, for very small crystal sizes, resulting in no growth or possibly melting. The size at which this will occur is termed the critical radius (R_{cr}) and can be shown to be

$$R_{cr} = \frac{\gamma_{sl} T_m}{\rho_s L \Delta T} \quad (1.12)$$

Figure 1.8 shows the variation of the Helmholtz free energy as function of the crystal radius. The crystal will only grow for sizes greater than R_{cr} since a maximum value

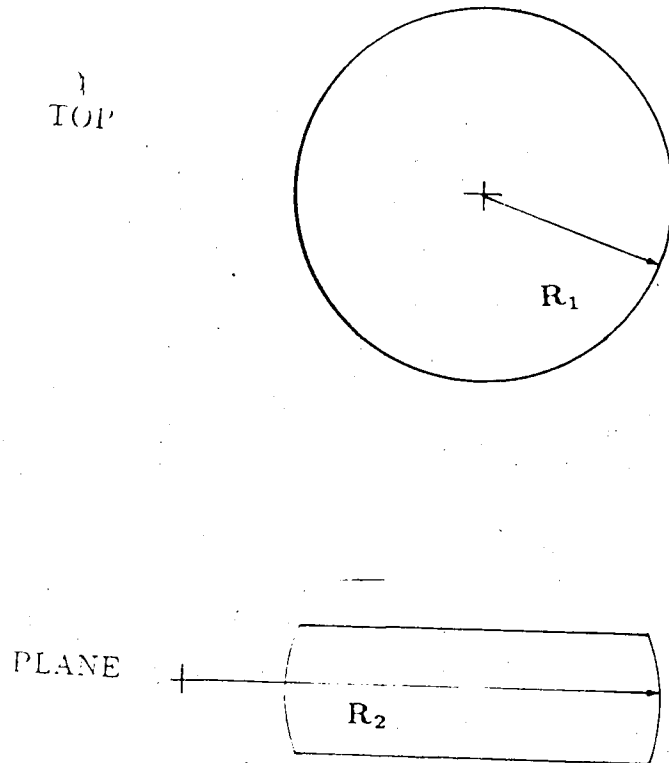


Figure 1.7: The two principal radii of curvature for a frazil ice crystal. The crystal is considered flat edged when R_2 is very large ($R_2 \rightarrow \infty$)

occurs at $r = R_{cr}$ indicating an unstable equilibrium. The dependence of R_{cr} on the supercooling ΔT is shown in Figure 1.9. As the supercooling increases, the minimum crystal radius required for growth correspondingly decreases. Consequently at relatively low supercoolings, larger ice particles are required for sustained growth compared to high supercoolings. The influence of dissolved impurities in the melt has the effect of depressing the freezing temperature of water and can be incorporated into the expression for R_{cr} and ΔT_c but will not be considered in the course of this study. The temperature difference ΔT_k is the reduction in the crystal surface temperature due to its growth kinetics. The magnitude of ΔT_k depends on the type of growth mechanism along a crystal face. This in turn depends on the orientation of the a-

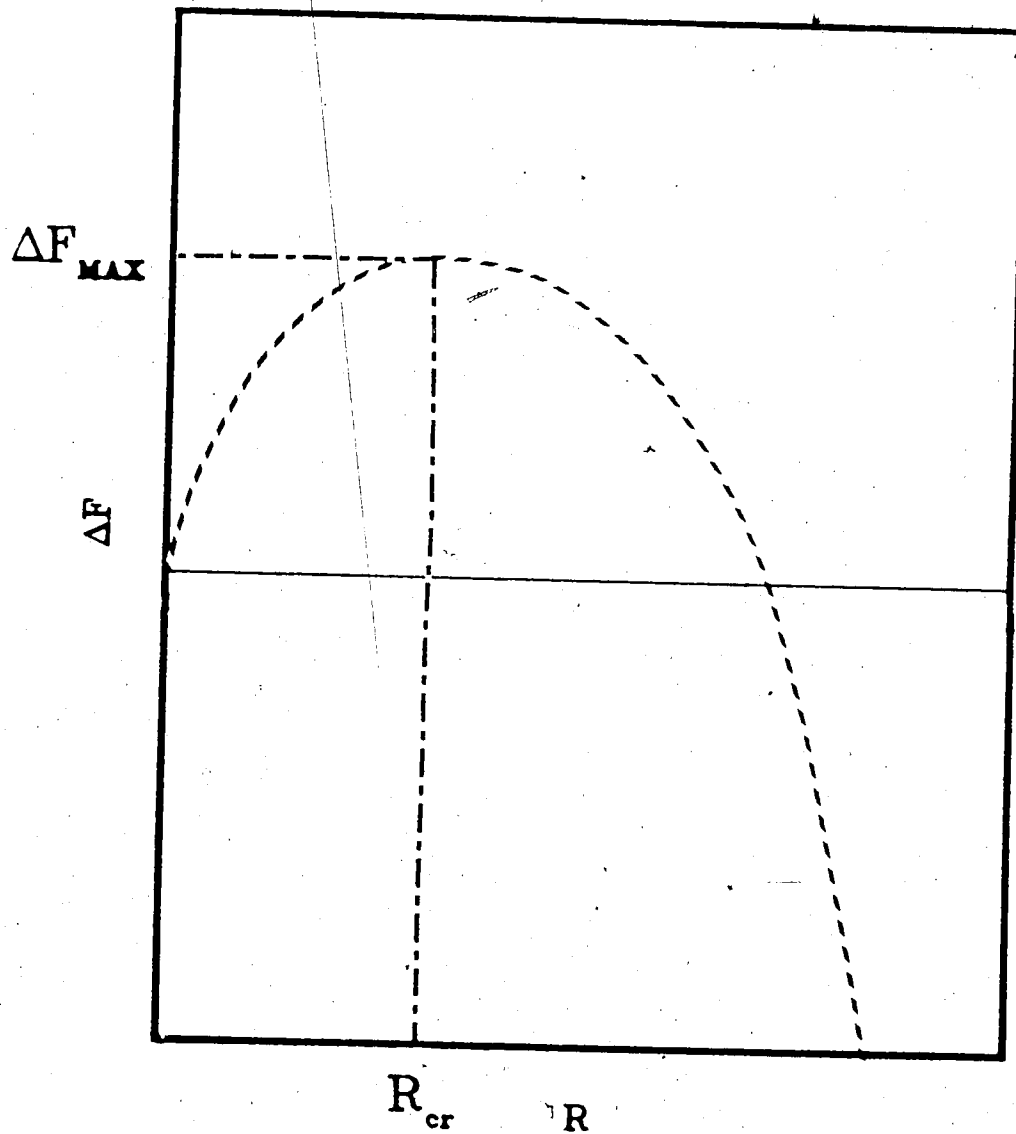


Figure 1.8: Variation of the system free energy with crystal size for a frazil ice disc

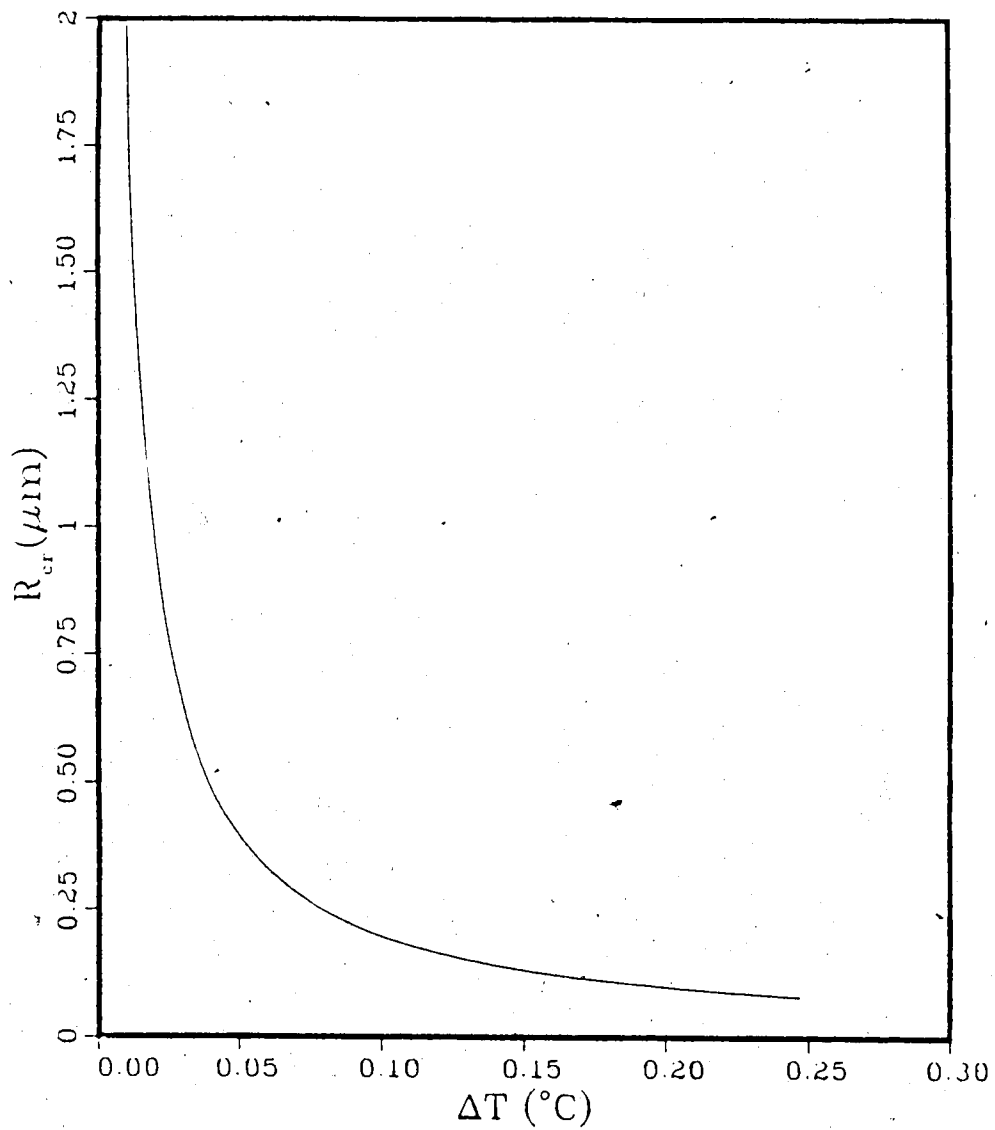


Figure 1.9: Variation of the critical radius at various supercoolings for a flat edged disc crystal

and c-axes.

The dominant shape of ice crystals observed in bodies of water such as lakes, rivers and industrial crystallizers is disc shaped. Ice crystals appear in natural lakes and rivers in an assortment of shapes and sizes ranging from spicules and discs to multi-branched dendrites. Field observations by several investigators indicate that the most common frazil ice morphology is disc-shaped and that in natural water bodies ice nuclei resulting from initial seeding or secondary nucleation eventually evolve into the disc shape regardless of the initial geometry. Arden and Wigle [6] report that crystal shapes at the onset of frazil production are irregular "like thin pieces of broken glass" and gradually assume a discoid shape after a period of a few hours. These ice crystals continue to grow as discs until they reach a certain size after which the disc boundary becomes jagged and irregular eventually developing into dendritic growth at the edges. The fact that a disc morphology is observed, supports the idea that the disc shape is a result of the strong anisotropy in interfacial growth kinetics. This fact is supported by the observation that the low levels of supercooling (usually $\Delta T \leq 0.15 \text{ }^\circ\text{C}$ [60]) normally associated with frazil growth lead to c-axis growth rates which are approximately an order of magnitude lower than a- axis growth rates.

The shape of an ice crystal and its size greatly influence the heat transfer characteristics from the crystal. This in turn has an important effect on the resulting growth rate. The factors causing this seem to be due to an interaction of the heat transfer requirements of the crystal and its interface kinetics. This can be thought of in the following manner. As the crystal grows larger in size, the rate of latent heat released along its phase boundary increases. In order to better dissipate this heat energy, the crystal boundary edge develops protuberances and becomes tapered and irregular to better dissipate the increased latent heat. Tsang [75] writes that when the number of nuclei are large and the ambient water temperature is relatively warm, the

rate of heat dissipation by each crystal is low and the crystals can continue growing as discoids. However, at a high degree of supercooling and with a low number of initial nuclei, the rate of heat dissipation by each crystal will be high resulting in a spicule or needle shape in order to better diffuse the high rate of latent heat liberated. The spicule shape essentially yields a higher surface area to volume ratio as compared to the discoid shape.

Morphological instability limits the maximum diameter of frazil crystals to about 8 mm. Osterkamp [60] reports that frazil crystals maintain their disc form for diameters up to 5 mm with diameter to thickness ratios from 5 to 100. Other studies [57] report frazil crystal diameters on the average of 1 mm with maximum thicknesses of approximately one third the diameter. A classical experiment exhibiting the growth behaviour of ice discs growing in slightly supercooled water was conducted by Arakawa [4]. He introduced small ice particles approximately 0.01 mm in diameter into the bottom of a container containing water supercooled to -0.30°C . On rising to the surface, the crystals assumed a disc morphology and continued growing as discs until they reached diameters ranging from 0.50 mm to 3.0 mm. The thicknesses of the discs were estimated to be between 0.005 mm and 0.60 mm. Upon reaching a critical size, (different from the thermodynamical critical size R_{cr}) the crystal morphology became unstable and began to develop a jagged irregular disc perimeter. Figure 1.10 pictorially depicts Arakawa's visual observations.

1.2 ANALYTICAL AND NUMERICAL INVESTIGATIONS OF ICE GROWTH

Although a great deal of experimental work on the nucleation and evolution of ice crystals has been done and the growth mechanisms involved have been investigated,

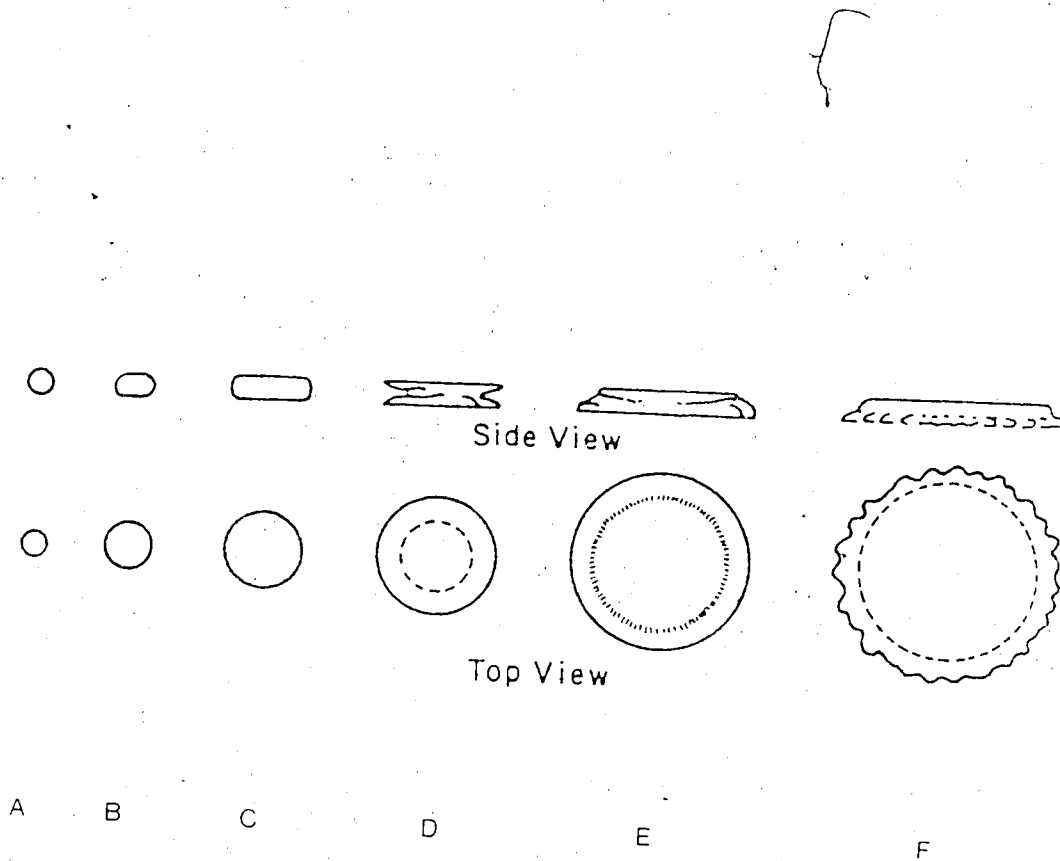


Figure 1.10: Growth sequence of a disc crystal (from Arakawa [3]). Note the morphological instability at the large disc diameters.

very little work is available on the theoretical study of frazil ice crystal growth. Limited theoretical models for the growth of disc shaped crystals have been developed by a small number of individuals and will be discussed in this section. Some numerical studies on ice growth problems will also be reviewed. The main purpose here is to evaluate the methodology and relative simplicity of popular numerical schemes for application to this particular research. The literature reported will be divided into two categories. The first section will report previous theoretical studies related to frazil crystal growth and the second section will investigate numerical studies of ice growth problems.

1.2.1 THEORETICAL INVESTIGATIONS

The theoretical determination of ice crystal growth rates falls into the general classification of "phase change" or "Stefan problems". The primary difficulty involved in determining an analytical solution is the nonlinear boundary condition at the solid-liquid interface. This nonlinearity arises from the unknown position of the moving interface. Therefore, it is usually necessary to make simplifying assumptions in order to obtain a solution. Theoretical studies for determining the growth rates of disc crystals were conducted by Mason, Williamson, Avignon and Fujioka. In order to obtain a solution, all these studies involved making some simplifying assumptions.

Mason [50] developed a simplified mathematical model for an ice disc growing in a supercooled, quiescent liquid of infinite extent. He assumed that the thermal conductivity of ice was infinite and that the disc was of infinitesimal thickness. By virtue of these assumptions, it is implied that the ice disc is entirely isothermal and that the temperature varies only in the liquid region. The resulting growth rate of

the disc in the radial direction was determined to be

$$\frac{dR}{dt} = \frac{4k_l}{\pi h L} \Delta T \quad (1.13)$$

(where k_l is the thermal conductivity of the supercooled water and L is the latent heat of fusion) by assuming that the total heat produced at the edge interface was released at the upper and lower basal plane surfaces. Also, for this part of the calculation only a finite thickness h is assigned to the disc.

Williamson [77] determined an expression for the growth rate of an unperturbed ice disc which arose indirectly, as a consequence of his studies on the stability of ice discs. Williamson assumed that the disc would grow like a spherical particle. His justification for this was that growth in the c -axis direction would prevent the radial growth of the disc resulting in a spherical temperature distribution around the disc. The edgewise growth rate was then calculated to be

$$\frac{dR}{dt} = \frac{k_l}{LR} \Delta T \quad (1.14)$$

which is much smaller than actual growth rates and those obtained from Mason's model.

Like Williamson, Avignon's [7] growth rates for ice discs also arose as a result of his model for the morphological stability of a disc shaped nucleus. His model is based on the analysis of the two dimensional growth of a nucleus attached to a substrate. He assumes that heat transfer by convection occurs between a thin infinitesimal layer on the basal plane of the disc and the air above it. Heat conduction only, occurred in this thin layer where the temperature distribution in the layer above the solid phase was satisfied by

$$\nabla^2 T_s = \frac{k_a T_s - T_o}{d k_s h} \quad (1.15)$$

and in the layer above the liquid phase by

$$\nabla^2 T_l = \frac{k_a}{d} \frac{T_l - T_o}{k_l h} \quad (1.16)$$

where T_o is the temperature of the ambient air and k_a is its thermal conductivity; h is the thickness of the disc and d is the thickness of the conductivity layer. The temperature gradient in the direction perpendicular to the water surface was assumed to be negligibly small. Thus, all the heat released at the growing edge was diffused through this thin layer and the calculated temperature distribution in the layer was a function of the radial position only. As Avignon did not derive the growth rate of an unperturbed ice disc, Fujioka [28] solved Equation (1.15) and (1.16) above and determined an expression for the unperturbed growth rate given by

$$\frac{dR}{dt} = \frac{\Delta T}{L} \left(1 - \frac{R_{cr}}{R}\right) \left(\mu_s \frac{I_1(X_s)}{I_0(X_s)} + \mu_l \frac{K_1(X_s)}{K_0(X_s)}\right) \quad (1.17)$$

where

$$\mu_{s,l} = \sqrt{\frac{k_{s,l} k_a}{hd}}$$

and

$$x_{s,l} = \sqrt{\frac{k_a}{k_{s,l}} \frac{r}{\sqrt{hd}}}$$

$$X_{s,l} = \sqrt{\frac{k_a}{k_{s,l}} \frac{R}{\sqrt{hd}}}$$

R_{cr} is the critical radius of nucleation and the functions I_0 , I_1 , K_0 and K_1 are modified Bessel functions of order 0 and 1 respectively. For large values of thermal conductivity of the air such that k_a is much larger than k_s , and by the further assumption that the conductivity of the solid layer is approximately four times the conductivity of the liquid layer, the expression for the growth rate simplifies to

$$\frac{dR}{dt} = \frac{3\Delta T}{L} \sqrt{\frac{k_l k_a}{hd}} \quad (1.18)$$

Unlike Williamson and Avignon, Fujioka and Sekerka [27] developed a model to determine the unperturbed growth of a disc shaped crystal. They considered growth of a submerged disc in a quiescent, undercooled bath and assumed that growth in the c-axis direction was small enough to be considered negligible. Hence, the disc remained a finite constant thickness h . Also, they assumed that the temperature field was not explicitly a function of time; thus a quasi-steady state approximation was used. Their justification for this was that since the growth rate of the crystal edge is so small (on the order of 10^{-6} m/s), the change in position of the solid liquid interface over a short discrete time step would be negligible. It should be noted that this assumption would be valid when the crystal is relatively large in size and the growth rate is quite small. The applicability of the quasi-steady state approximation will be examined in more detail in the next chapter.

Fujioka and Sekerka further assumed that the thermal conductivity remained constant and was equal to that of water for the entire solution domain. The growth rate of the disc at its centerline was determined to be

$$\frac{dR}{dt} = \frac{\pi k}{LR} \frac{\Delta T}{q_0[h/2R]} \left(1 - \frac{R_{cr}}{R}\right) \quad (1.19)$$

where R is the disc radius and $q_0(z)$ is the toroidal integral of order zero. For disc radii much larger than disc thickness (ie. $R \gg h$), the expression for growth rate can be simplified to be

$$\frac{dR}{dt} = \frac{2\pi k}{Lh} \frac{\Delta T}{\ln[16eR/h]} \quad (1.20)$$

A comparison of the growth rates of disc shaped ice crystals obtained by Fujioka and Sekerka with the previous models at a supercooling of 0.15°C is shown in Figure 1.11. Also shown in this plot are the experimentally observed growth rates for ice discs in a quiescent fluid obtained by Kumai and Itigaki [47] and Fujioka [28]. The growth rates of frazil crystals submerged in a mean flow of various magnitudes,

measured by Bukina [12] are shown in Figure 1.12. It is clearly seen from Figure 1.11 that the predicted growth results of Williamson are significantly lower than those obtained by Mason or Fujioka and Sekerka. None of the analytical results appear to compare well with the experimental results. This is undoubtedly due to the assumptions made in determining the temperature distribution. The result of Williamson's incorrect assumption that the ice disc grows as a spherical shaped particle is demonstrated by the low growth rates calculated. It should be noted that the growth rates observed by Kumai and Itigaki are for floating discs of undetermined thickness. Therefore, it is probably not valid to compare them with the other results. Fujioka's experimental results appear more realistic since the trend of the data is similar to the calculated model results, although the thickness of the crystal is not precisely known. Fujioka and Sekerka initially attributed this difference to additional heat loss mechanisms not accounted for in their model, although no specific sources were mentioned. Later Fujioka [28] developed a model which takes into account the difference in thermal conductivities between water and ice. The growth rate determined from this model is also shown in Figure 1.11. A comparison of these two results shows that underestimating the thermal conductivity of the ice phase yields a faster reduction in the crystal growth rate.

Fujioka also solved for the growth rate of an ice disc which included growth in the c-axis direction. The major drawback to this solution was the assumption that the solid and liquid thermal conductivities were identical. Solutions were obtained for the two cases of thickening with latent heat as a significant factor and thickening of the disc with negligible latent heat release from the basal plane. From these results he concluded that the thickening process of a frazil crystal appears to slow down the radial growth rate. The latent heat release from the basal plane was found to be negligible in comparison to the disc edge. However, it was noted that it was sufficiently

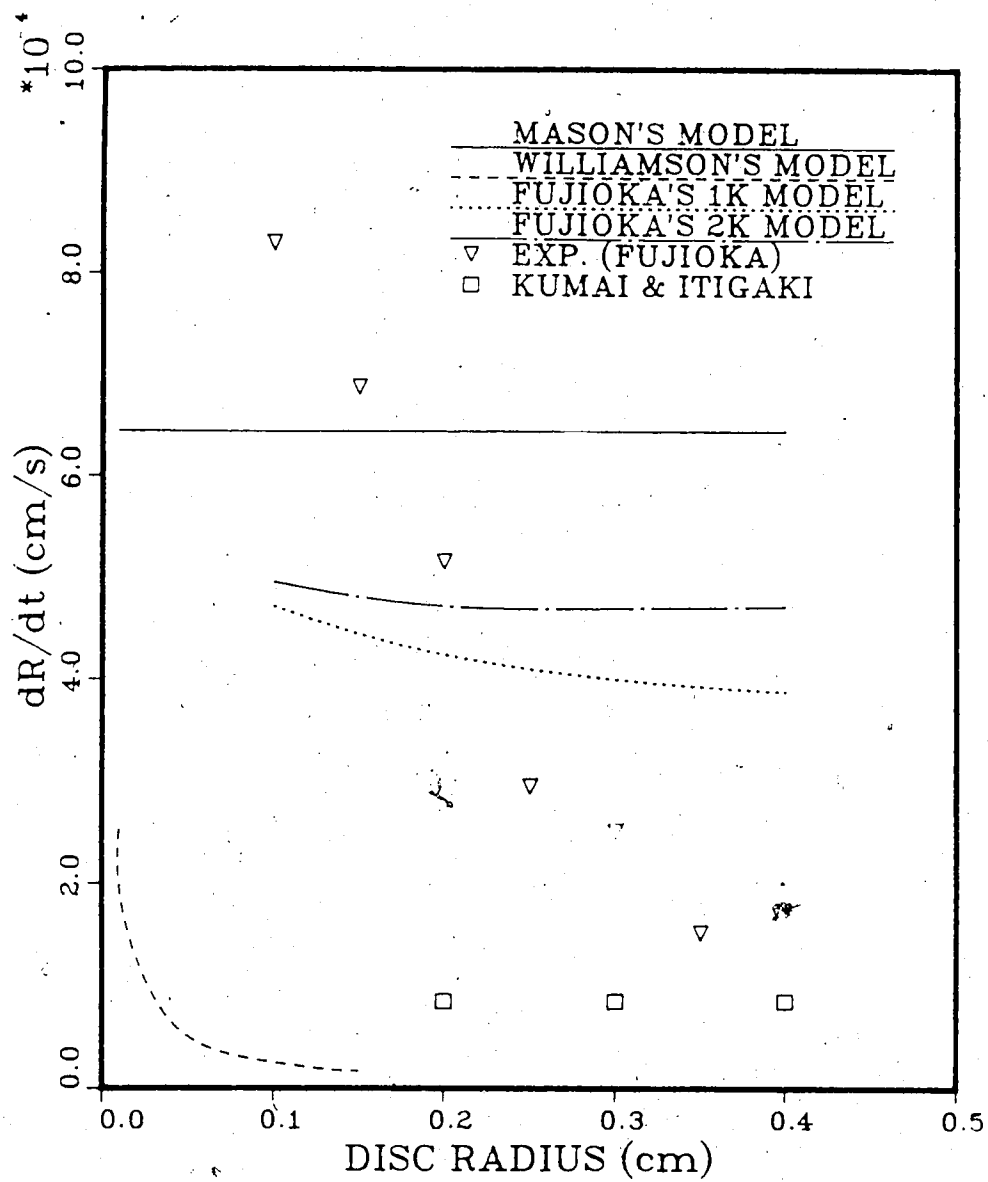


Figure 1.11: Comparison of analytical growth models and previous experimental results at $\Delta T = 0.15$ °C

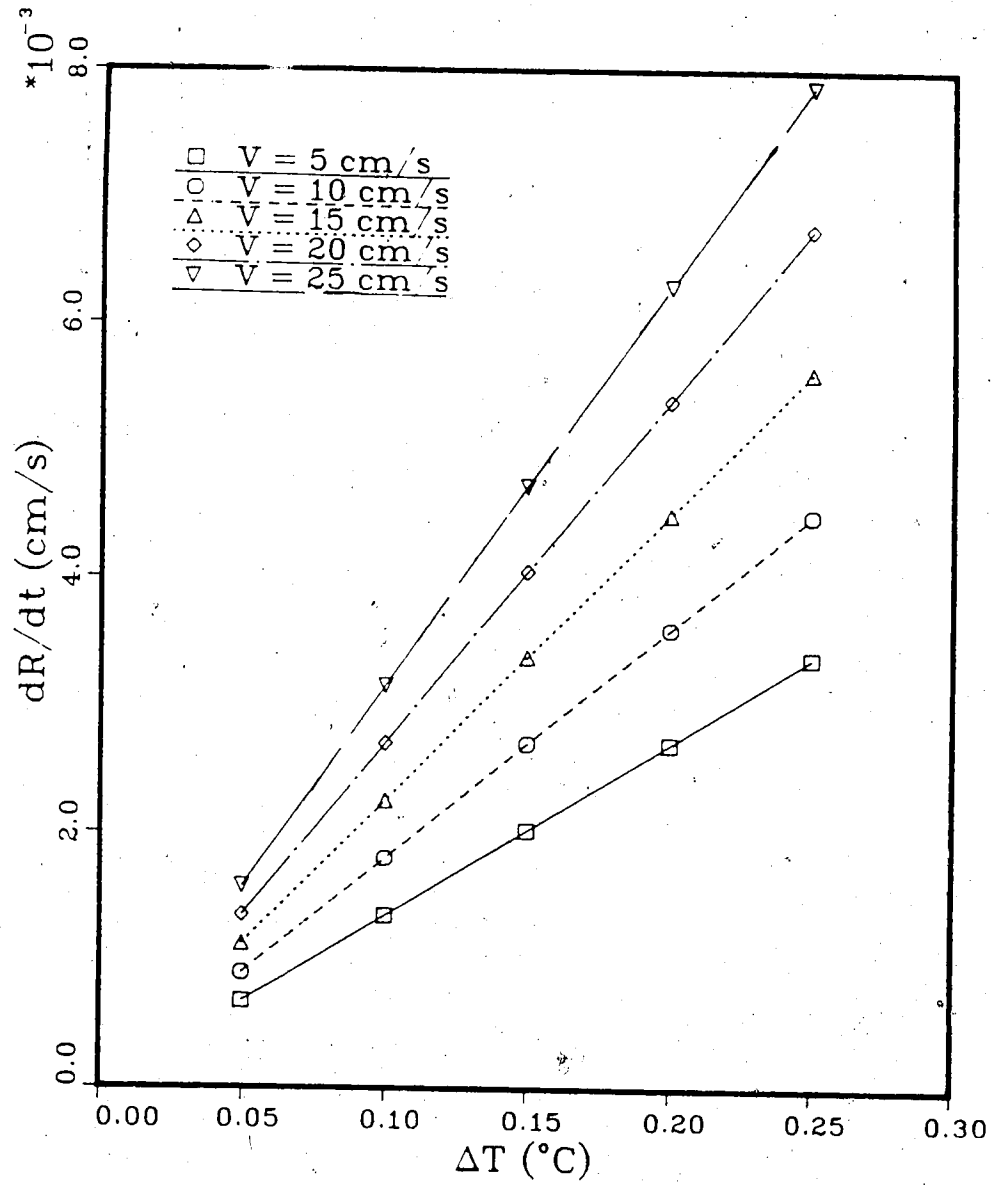


Figure 1.12: Experimental growth measurements of frazil crystal growth rates by Bukina [12]. The quantity V represents the mean flow velocity.

large to retard the thickening rate of the crystal. The expressions describing the temperature field for these two cases were complicated integral-differential equations which had to be evaluated numerically. If additional complexities such as a variable thermal conductivity, or a complicated crystal geometry were considered, this would undoubtedly result in additional difficulties in obtaining a solution. As a result, it is of significant importance to develop a convenient numerical scheme for solving crystal growth problems.

1.2.2 NUMERICAL STUDIES OF ICE GROWTH FROM THE MELT

Analytical solutions for multidimensional ice growth problems are difficult to obtain without simplifying the problem. The solution, if available, is of a complex form making the evaluation of the expression difficult. The assumptions needed to obtain solutions are often unrealistic and the analytic expression for the solution can be evaluated only by numerical approximations. Singh [69] appropriately states that "analytical techniques for crystal growth problems have reached the limit of their usefulness".

The most popular numerical techniques for solving ice growth problems are front tracking methods where the governing equations, subject to some boundary conditions, are solved using either the finite element method or the finite difference method. In this section, we describe the numerical schemes along with their major advantages and disadvantages. Although this review of the numerical literature is by no means comprehensive, the research surveyed provides a wide cross-section of the popular numerical schemes of solving ice growth problems.

Various methods have been proposed for the numerical solution of phase transition problems. They primarily differ in the way that heat transfer on the phase boundary

is modeled. If a heat flux balance is conducted on the phase boundary, then an expression explicitly containing the solid-liquid interface position enters the problem formulation which then must be determined prior to determining the temperature distribution. This leads to what are termed front tracking methods. Popular numerical strategies for solving ice growth problems have traditionally used front tracking methods in which the phase front evolves smoothly in space and time. The other method, known as a fixed domain method, involves absorbing the heat flux conditions on the solid-liquid interface into the governing heat conduction equations which are then solved on the fixed domain. The resulting nonlinear equations are then solved numerically using a finite difference discretization or by the finite element technique or by the numeric solution of a variational inequality. The position of the phase boundary is determined after solving for the temperature distribution and then tracing the contour given by $T(r, z) = T_i$, where T_i is the known interface temperature value. The major advantage of this method is that complicated interface geometries can be handled with relative ease. But freezing point reductions due to curvature cannot be included since the interface temperature T_i must be known in order to determine the phase boundary position. Another disadvantage of this method is that it has been found to be less accurate than the front tracking methods [52].

The major difficulties associated with front tracking methods have resulted from the deficiencies in the discretized grid domain. Older numerical work is based on finite difference approximations defined on a fixed rectangular grid mesh. Consequently, the solid-liquid interface boundary will not always coincide with the grid lines requiring cumbersome two dimensional interpolation between grid mesh points. Also, a large number of nodes, closely spaced together, is required for an accurate determination of the growth rate of the phase boundary. This is because the temperature gradients at the solid-liquid interface are very high and estimating them accurately requires a

large concentration of nodes near the vicinity of the phase boundary. This unnecessary resolution of the grid in regions far from the interface where the temperature gradient is relatively small can result in time consuming computer runs. Similar difficulties arise when the finite element method is implemented on a stationary fixed grid.

The recent use of adaptive or deforming grids has helped overcome the difficulties encountered when using fixed grids. Here, the phase boundary is always coincident with a grid line and its shape is sufficiently defined since more nodes can be concentrated along the interface without unnecessarily refining the rest of the mesh. One of the earlier works using an adaptive grid was due to Bonnerot and Jamet [10]. They used the finite element method for the solution of a two dimensional freezing problem. The problem consisted of a growing solid mass of ice as shown in Figure 1.13. The temperature distribution in the solid satisfied the heat conduction equation

$$\frac{\partial^2 T}{\partial x^2} + \frac{\partial^2 T}{\partial y^2} = \frac{1}{\alpha} \frac{\partial T}{\partial t} \quad (1.21)$$

subject to the boundary conditions

$$T(x, y, 0) = T_{init}$$

$$T(x, y, t) = g(x, y) \quad \text{on } S_1$$

$$\frac{\partial T}{\partial n} = 0 \quad \text{on } S_2$$

$$T(s(t), t) = 0 \quad \text{on } S(t)$$

$$\frac{dS}{dt} = -C \frac{\partial T}{\partial n}$$

where T_{init} and C are constants and derivatives with respect to n represent derivatives normal to the surface (see Figure 1.13 when referring to application of the boundary conditions) Bonnerot and Jamet discretized the domain with 200 three node triangles resulting in 600 nodes. The phase boundary was approximated by a polygonal line

whose vertices coincide with the triangularization nodes. A new mesh was determined at each time step as the boundary moved forward. Nodes were not highly concentrated near the moving boundary. Moreover, since the domain was expanding with each time step, triangles which had vertices on the free boundary became much larger than the interior triangles resulting in a poor approximation of the temperature gradient and hence of the nodal velocity. They further noted that the use of higher order quadrilateral elements or isoparametric elements made application of their procedure conceptually more difficult as well as computationally more time consuming.

Singh [69] modeled the growth rate of a needle shaped dendritic crystal growing in a supercooled melt of infinite extent. He modeled the dendrite geometry as a paraboloid of revolution and assumed the interface shape would remain similar for all time (ie. shape preserving). This assumption allowed the time dependence in the heat conduction equation to be eliminated by considering a coordinate system originating from the dendrite tip. As a result, the governing equation in the solid and liquid regions become

$$\frac{\partial^2 T}{\partial r^2} + \frac{1}{r} \frac{\partial T}{\partial r} + \frac{\partial^2 T}{\partial z^2} + \frac{V_n}{\alpha} \frac{\partial T}{\partial r} = 0 \quad (1.22)$$

where V_n is the rate of growth of the phase boundary. Figure 1.14 shows the solution domain and corresponding boundary conditions. The domain was divided into 400 cubic triangular elements with nodes more densely packed near the interface. The infinite boundary for the liquid phase was approximated by a finite boundary such that the temperature gradient was sufficiently close to zero. This was found to occur at a distance of $20R$ in the z direction and $40R$ in the r direction where R is the characteristic length. It was assumed that the growth process was diffusion controlled thereby ignoring the interface kinetics. The interface temperature varied due to curvature effects in accordance with the Gibbs-Thompson relation. The curvature at the phase boundary was approximated by fitting a cubic spline through the nodes

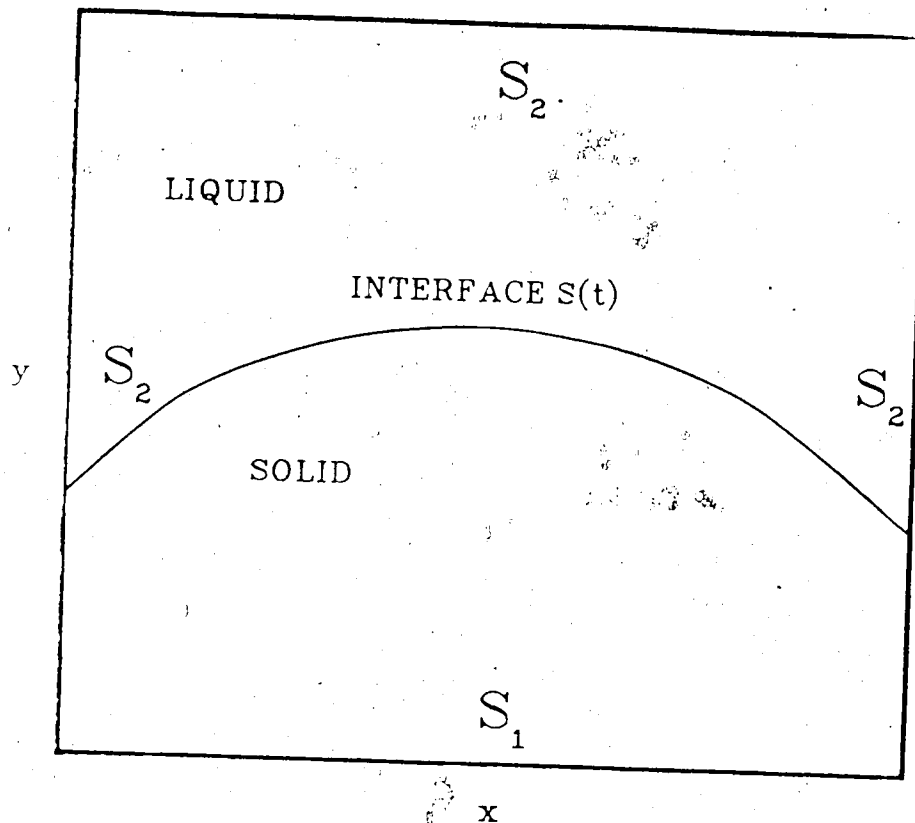


Figure 1.13: Solution domain employed by Bonnerot and Jamet

comprising it. The accuracy of the method was verified by calculating growth rates for spheres and cylinders and comparing them with available analytical solutions.

For problems where the shape does not repeat, the above formulation would be cumbersome and a deforming grid would be necessary. O'Neill and Lynch [59] developed a finite element method with a moving coordinate system for solving ice growth problems. They applied their scheme for the simple one dimensional case with heat conduction into the solid phase only and with a constant interface temperature. They noted that their formulation became significantly more complicated when extended to more realistic multidimensional cases. Also, the concept of a moving grid introduced an additional term for the time derivative of temperature which essentially was the velocity of each node.

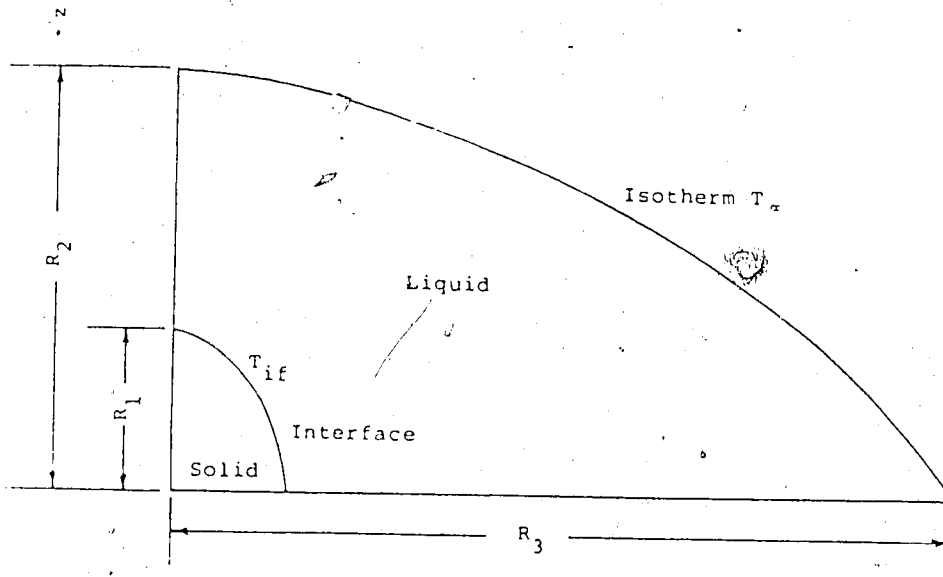


Figure 1.14: Solution domain and boundary conditions for shape preserving dendrite (From Singh [69])

Sullivan [71] extended the method of O'Neill and Lynch to study the stability of planar growth restricted to two dimensions. He discretized the domain with linear triangular elements and employed adaptive grid strategies for mesh motion and control. The solution domain was discretized with 20 proportionally spaced elements in the liquid phase and 4 similarly spaced elements in the solid phase. The immediate neighbourhood near the phase front was more refined and consisted of 44 equally spaced elements in both the solid and liquid regions. Sullivan also included the effects of interfacial kinetics in his problem formulation. His use of moving elements added a mesh advection term to the governing equations as shown below

$$\alpha \nabla^2 T + V_n \frac{\partial T}{\partial n} = \frac{\partial T}{\partial t} \quad (1.23)$$

where V_n is the rate of growth rate of the interface. This equation was then solved iteratively with the interfacial energy balance equation. Neglecting the mesh advection term results in a temperature distribution that is not heat conserving.

Sullivan noted that the mesh must retain a topology suitable for computation at each time step (ie. the triangular elements cannot be grossly deformed). Sullivan found that node deployment introduced an additional complication. Consideration of several methods led him to a scheme where internal node deployment was handled by considering the mesh to be a solid body that deformed elastically. Thus the equations of elasticity for plane stress were used to determine the mesh deformation at each time step. This rather cumbersome formulation was used with considerable accuracy to model growth profiles of dendrites.

An efficient yet simple moving coordinate method was employed to simulate an arbitrary shaped solid melting in a circular cylinder by Rieger et al [63]. This technique, commonly referred to as "Boundary Fitted Coordinates" was first developed by Thompson et al [73] for the solution of partial differential equations on arbitrary shaped domains. Rieger et al solved the energy equation in the liquid phase and the conduction equation in the solid phase by numerically mapping the real domain to a rectangular computational grid consisting of 600 nodes. Time steps were quite small but were increased when the process was conduction dominated. The governing equations were discretized using a finite difference formulation and were solved implicitly subject to the given boundary conditions. We feel that this method is versatile and simple for the solution of crystal growth problems with nonlinear boundary conditions. It will be described in more detail in the following chapter.

To summarize, analytical solutions for problems simulating more realistic crystal growth conditions are difficult to obtain and are often not possible. Further difficulties arise when the expression for the solution is in a form that requires numerical approximations. Therefore, it is more advantageous to solve numerically the governing partial differential equations with the accompanying boundary conditions. Numerical formulations employing front tracking methods have been fairly popular in the past

and are best suited for applications to crystal growth problems including the effects of interface kinetics and boundary curvature. In particular, methods utilizing moving or deforming coordinates are ideally suited to this formulation and offer enhanced accuracy and stability without extra computational effort compared to fixed grid methods. We feel that implementation of the finite element method utilizing moving coordinates is far more complicated compared to the "Boundary Fitted Coordinate" (BFC) scheme. The BFC method offers the advantages of the finite element method with the simplicity of finite differences. The application of this method to frazil crystal growth problems will be described in detail in the next chapter.

Chapter 2

MATHEMATICAL FORMULATION AND METHOD OF SOLUTION

In this chapter, the mathematical formulation for the growth of a frazil ice crystal is presented. The first portion deals with a description of the governing equations and boundary conditions implied by the physics of the problem. The second portion discusses the assumptions made in the general equations and their implications. The last section of this chapter is concerned with the discussion of the numerical technique selected for solving the frazil crystal growth problem and the methodology followed. Also, a brief description of some other popular techniques for solving moving boundary problems is presented and the merits of the method used in this study are outlined.

2.1 PHYSICAL MODEL AND ASSUMPTIONS

This study is concerned with the modelling of frazil ice crystal growth rates in slightly supercooled water. Models for predicting the growth rates of ice crystals are based on a description of the heat transport process and its physical constraints such as crystal morphology, interface curvature and the surrounding fluid velocity and temperature distribution. Previous experimental and theoretical investigations, discussed in Chapter 1, have provided some important data on the nucleation, growth and morphology of ice crystals submerged in supercooled waters. These results provide the basis for the development of a justifiable physical model.

Consider the idealized situation shown in Figure 2.1 which shows a single frazil crystal immersed in a volume of supercooled liquid water of infinite extent. The solid-liquid system is maintained at a constant pressure and is bounded by an

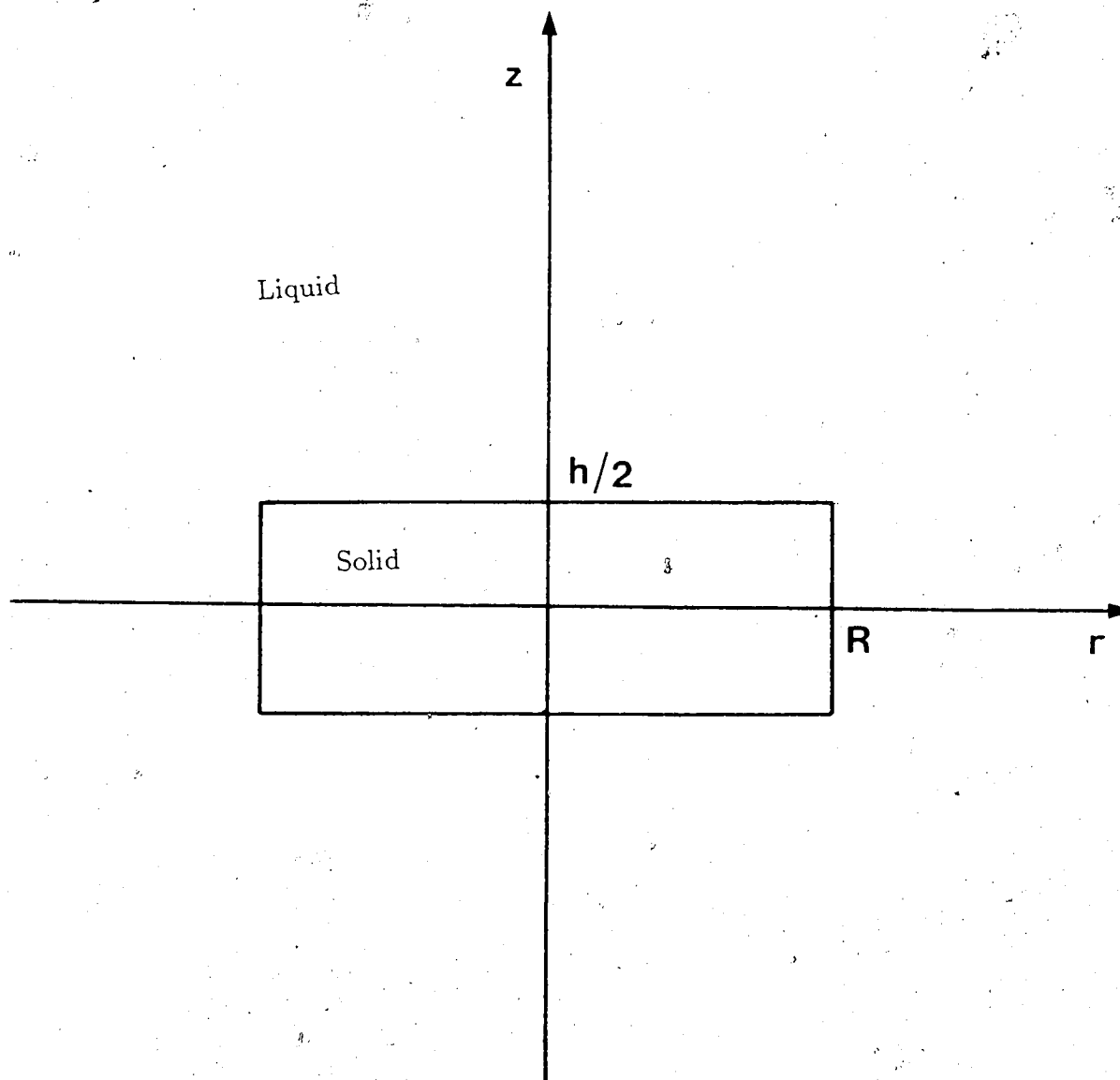


Figure 2.1: Model frazil ice crystal

isothermal, impermeable wall. It is assumed that both the liquid water and ice are pure, homogeneous and isotropic with no dissolved solutes present in either phase. Most experimental data and field observations have reported that the typical water supercooling rarely exceeds $0.10\text{ }^{\circ}\text{C}$ during the course of frazil production. In fact, the initial stages of frazil nucleation and growth usually require a supercooling less than $0.05\text{ }^{\circ}\text{C}$. Thus, the model crystal is assumed to be disc shaped since the commonly observed ice crystal morphology at supercoolings less than $0.13\text{ }^{\circ}\text{C}$ is that of discoids and thin platlets [78]. Provided the disc remains symmetrical (true for crystals less than 3 mm in diameter), this assumption implies that the temperature distribution in the solid-liquid region only varies in the radial and axial directions and can be assumed to be axisymmetric.

The shape of the edge interface is of particular importance since its curvature determines the temperature variation along the interface. Researchers such as Takawa [4] and Osterkamp [61] had made some observations on the shape of the edge interface (in the a -axis direction) of disc-shaped crystals by visual inspection. The general conclusion from these limited observations was that the interface shape was flat in the center portion with curved portions joining the face and edge of the crystal. More recently Knight [45] has shown that the corners between a - and c -axes are sharp and not rounded as previously indicated. The major consequence of this assumption is that the edge interface of the model crystal will be at a constant temperature and will only be a function of the disc radius as indicated by Equation (1.4). Thus as the crystal radius increases, the freezing point depression along the edge also decreases and approaches the thermodynamic freezing point T_m .

Since it is assumed that the liquid phase is free of dissolved solutes, the thermodynamic freezing temperature T_m can be taken to be $0\text{ }^{\circ}\text{C}$ and the freezing point depression along the crystal interface will only be caused by the surface

curvature. We also assume that thermal properties such as conductivity, density, specific heat and viscosity are constant within each phase. The values of these properties change from those of the ice to those of water in a stepwise manner at the solid-liquid interface.

Convective heat transfer (due to the displacement of the liquid ahead of the growing interface arising from the different densities of the ice and water phases) is ignored due to its negligible effect. As the crystal grows larger due to the freezing process, a conservation of mass at the interface shows that the liquid is displaced ahead of the crystal with a normal velocity V_n given by

$$V_n = \left(\frac{\rho_l - \rho_s}{\rho_s} \right) v_n \quad (2.1)$$

where v_n is the normal velocity of the growing interface and ρ_s and ρ_l are the densities of the solid and liquid phases respectively. Chambre [16] has shown that when the ratio,

$$\sigma = \left(\frac{\rho_l - \rho_s}{\rho_s} \right) \ll 1 \quad (2.2)$$

the temperature distribution is not affected by this fluid displacement. Since $\sigma < 0.10$ for ice/water systems, the effect of this displacement convection can be justifiably neglected from the model.

Natural convection at the growing tip of an ice crystal was shown to be an important factor for the growth of dendrites in a large, enclosed volume of water at supercoolings of 1 °C and greater [62]. The dominant heat transfer mechanism for the growth of dendrites in small quantities of water is conduction. Gilpin [31] had shown that the influence of natural convection was only important for a matrix of dendritic crystals growing in an enclosed volume of supercooled water. Natural convective effects at low supercoolings (normally associated with frazil morphologies for freely suspended ice crystals) is negligible and its effects can be ignored. It should

also be noted that forced convection arising from relative motion between the crystal and liquid would be of greater magnitude than natural convective effects and hence would have a more dominating influence in the latent heat dissipation.

2.2 GOVERNING EQUATIONS AND BOUNDARY CONDITIONS

In this section, the general governing equations and boundary conditions describing the temperature distribution for the ice-water region and the growth rates of the crystal are presented. These governing equations are later simplified through an order of magnitude analysis conducted in section 2.2.

For the single disc shaped crystal of Figure 2.1 growing in a supercooled liquid of infinite extent, the temperature distribution at any time t can be obtained by solving the heat conduction equation in the solid phase

$$\nabla^2 T_s = \frac{1}{\alpha_s} \frac{\partial T_s}{\partial t} \quad (2.3)$$

where the subscript, s refers a property to the solid phase and the energy equation in the liquid region

$$\frac{\partial T_l}{\partial t} + \vec{u} \cdot \nabla T_l = \alpha_l \nabla^2 T_l + \frac{\mu}{\rho_l C_{pl}} (\nabla \cdot \vec{u})^2 \quad (2.4)$$

where the subscript, l refers a property to the liquid phase. The quantities α_s and α_l are the thermal diffusivities of the solid and liquid phases respectively. The quantity \vec{u} represents the fluid velocity distribution near the vicinity of the ice disc. The rate at which the disc grows in the radial direction, V_r is determined from an energy balance along the edge of the disc given by

$$\rho_s L V_r = \left(k_s \frac{\partial T_s}{\partial r} \Big|_{r=R^-} - k_l \frac{\partial T_l}{\partial r} \Big|_{r=R^+} \right) \quad (2.5)$$

where ρ_s is the density of the solid phase and R^+ and R^- represent the liquid and solid regions in the vicinity of the edge interface. Similarly, the thickening rate V_z is obtained by an energy balance along the basal plane of the disc which yields

$$\rho_s L V_z = \left(k_s \frac{\partial T_s}{\partial z} \Big|_{z=\frac{h}{2}^-} - k_l \frac{\partial T_l}{\partial z} \Big|_{z=\frac{h}{2}^+} \right) \quad (2.6)$$

where $h/2^+$ and $h/2^-$ represent the liquid and solid regions in the vicinity of the basal plane. Inclusion of the interfacial kinetics for disc-thickening results in the additional condition

$$V_z = f(\Delta T_k) \quad (2.7)$$

where $f(\Delta T_k)$ is one of the expressions given in Table 1.1. In addition to these, the temperature along the edge of the disc is

$$T(R, z) = T_m - \Delta T_c, \quad 0 \leq z < \frac{h}{2} \quad (2.8)$$

where ΔT_c is defined as in Equation (1.14). Two additional interfacial conditions are required in order to maintain a continuity in the temperature distribution in the solid and liquid phases. Along the edge of the crystal, this additional condition is

$$T_s(R, z) = T_l(R, z), \quad \text{for } z = \pm \frac{h}{2} \quad (2.9)$$

and along the basal plane, it is

$$T_s(r, \frac{h}{2}) = T_l(r, \frac{h}{2}), \quad \text{for } 0 \leq r < R. \quad (2.10)$$

Also, the fluid far away from the growing disc surfaces is well mixed and the temperature has a constant value, i.e.

$$T_l = T_\infty, \quad \text{as } r \rightarrow \infty, z \rightarrow \infty \quad (2.11)$$

where T_∞ is the bulk fluid temperature.

The above equations and boundary conditions completely formulate a frazil crystal growth problem.

2.3 NONDIMENSIONALIZATION

It is convenient to normalize Equations (2.4) through (2.9) by choosing the following dimensionless parameters

$$\bar{r} = \frac{r}{l_c} \quad (2.12)$$

$$\bar{z} = \frac{z}{l_c} \quad (2.13)$$

$$\theta_s = \frac{T_s - T_\infty}{T_m - T_\infty} \quad (2.14)$$

$$\theta_l = \frac{T_l - T_\infty}{T_m - T_\infty} \quad (2.15)$$

$$\tau = \frac{\alpha_s t}{l_c^2} \quad (2.16)$$

$$\bar{u} = \frac{u}{U_c} \quad (2.17)$$

$$\bar{V}_r = \frac{t V_r}{l_c} \quad (2.18)$$

$$\bar{V}_z = \frac{t V_z}{l_c} \quad (2.19)$$

where l_c and U_c are the characteristic length and velocity scales respectively. After the governing equations have been normalized, the dimensionless parameters defined above will no longer be written with a bar over top for convenience.

Substitution of the parameters (2.12) to (2.19) into Equations (2.3) and (2.4) yields

$$\nabla^2 \theta_s = \frac{\partial \theta_s}{\partial \tau} \quad (2.20)$$

and

$$\frac{\alpha_s}{\alpha_l} \frac{\partial \theta_l}{\partial \tau} + Pe \bar{u} \cdot \nabla \theta_l = \nabla^2 \theta_l + Pr Ec (\nabla \cdot \bar{u})^2 \quad (2.21)$$

where Pr , Ec , and Pe are the Prandtl, Eckert and Peclet numbers defined as

$$Pr = \frac{\mu}{\rho_l C_{p_l}} \quad (2.22)$$

$$Ec = \frac{\rho_l U_c^2}{C_{p_l}(T_m - T_\infty)} \quad (2.23)$$

$$Pe = \frac{U_c l_c}{\alpha_l} \quad (2.24)$$

The interfacial energy balances (2.5) and (2.6) along the disc edge and face become

$$\bar{V}_r = Ste \left(\left. \frac{\partial \theta_s}{\partial \bar{r}} \right|_{\bar{r}=\frac{R}{l_c}} - \frac{k_l}{k_s} \left. \frac{\partial \theta_l}{\partial \bar{r}} \right|_{\bar{r}=\frac{R}{l_c}} \right) \quad (2.25)$$

and

$$\bar{V}_z = Ste \left(\left. \frac{\partial \theta_s}{\partial \bar{z}} \right|_{\bar{z}=\frac{h}{2l_c}} - \frac{k_l}{k_s} \left. \frac{\partial \theta_l}{\partial \bar{z}} \right|_{\bar{z}=\frac{h}{2l_c}} \right) \quad (2.26)$$

where Ste is the Stefan number defined as

$$Ste = \frac{C_{p_s}(T_m - T_\infty)}{L} \quad (2.27)$$

Finally, the boundary conditions (2.11) and (2.9) can be expressed in normalized form as

$$\theta_s(R/l_c, \bar{z}) = \theta_l(R/l_c, \bar{z}) = \theta_c \quad (2.28)$$

where

$$\theta_c = \left(1 - \frac{R_{cr}}{R} \right)$$

and

$$\theta_l(\bar{r}, \bar{z}) = 0 \quad ; \quad \text{as } \bar{r} \rightarrow \infty \text{ and } \bar{z} \rightarrow \infty \quad (2.29)$$

Before proceeding further, the problem can be simplified by eliminating terms which are small in magnitude relative to each other. Also, it is necessary to quantify the values to be used for the characteristic scales in the normalized forms above. Rather than determining these values from an order of magnitude analysis, these

terms will be chosen according to experimental observations. This way, there is some basis for neglecting terms which appear insignificant. The obvious choice for the characteristic length scale is to choose it to be the critical radius of the ice crystal as defined in Equation (1.5). The characteristic fluid velocity scale U_c is chosen to be the mean relative solid-liquid velocity rather than the mean flow velocity. This is because frazil ice crystals are often formed in bodies of water where there is no mean flow as in industrial crystallizers or lakes. Also, even in fast flowing rivers, ice particles do not experience the effects of the mean free stream velocity since they are entrained in the flowing water. Frazil ice particles are however subject to inertial and gravitational forces which result in the crystals rising to the water surface. Daly [18] has shown that the terminal rise velocity of suspended ice particles due to gravity are of the order of 1 cm/s. He also states that this value may be an overestimate of the actual rise velocities of frazil ice crystals since turbulence acts to counter the upward motion. Therefore taking $U_c = 1$ cm/s, it can be seen that $Pe \ll 1$ and hence the convective term in Equation (2.21) can be neglected. Inserting the value for U_c into the expression for the Eckert number, we see that at these low velocities and temperature differences, the viscous dissipation term can also be neglected. These additional simplifications allow the heat transfer mechanism in the liquid phase to be modelled as conduction. Also, from the symmetry of the geometry and the temperature distribution, only the top right hand portion of the disc section need be considered as shown in Figure 2.2.

Then to obtain a complete temperature distribution and determine the crystal growth rates, we need to solve the following partial differential equations for the regions shown in Figure 2.2:

1. In the solid region

$$\nabla^2 \theta_s = \frac{\partial \theta_s}{\partial \tau} \quad (2.30)$$

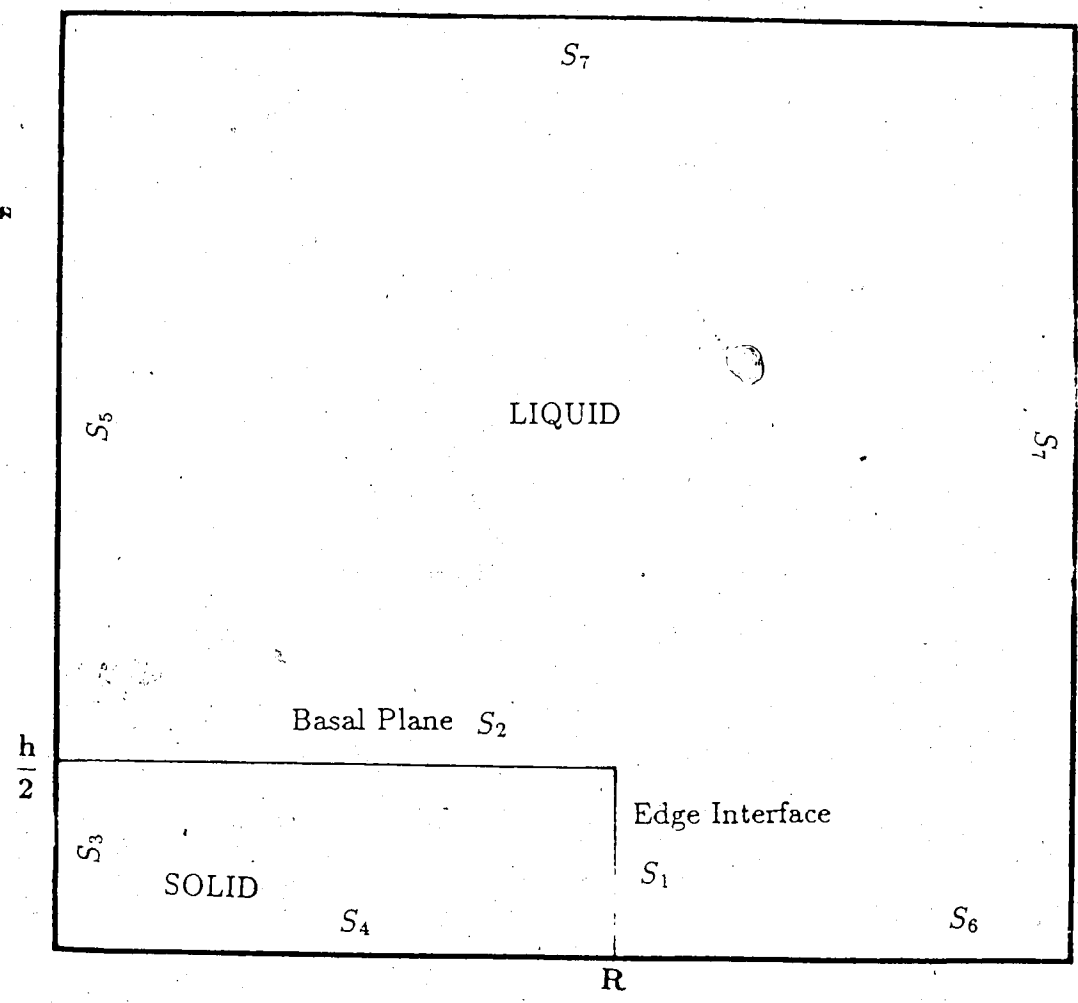


Figure 2.2: Solution region considered for the frazil growth problem and boundary conditions

subject to the boundary conditions

$$\theta_s = \theta_c \quad \text{on} \quad S_1 \quad (2.31)$$

$$\theta_s = \theta_k \quad \text{on} \quad S_2 \quad (2.32)$$

$$\frac{\partial \theta_s}{\partial \bar{r}} = 0 \quad \text{on} \quad S_3 \quad (2.33)$$

$$\frac{\partial \theta_s}{\partial \bar{z}} = 0 \quad \text{on} \quad S_4 \quad (2.34)$$

where θ_c and θ_k are dimensionless undercoolings due to the Gibb's-Thompson effect (curvature) and interface kinetics respectively.

2. In the liquid region

$$\nabla^2 \theta_l = \frac{\alpha_l}{\alpha_s} \frac{\partial \theta_l}{\partial \tau} \quad (2.35)$$

subject to the boundary conditions

$$\theta_l = \theta_c \quad \text{on} \quad S_1 \quad (2.36)$$

$$\theta_l = \theta_k \quad \text{on} \quad S_2 \quad (2.37)$$

$$\frac{\partial \theta_l}{\partial \bar{r}} = 0 \quad \text{on} \quad S_3 \quad (2.38)$$

$$\frac{\partial \theta_l}{\partial \bar{z}} = 0 \quad \text{on} \quad S_6 \quad (2.39)$$

$$\theta_l = 0 \quad \text{on} \quad S_7 \quad (2.40)$$

The heat balance conditions at the interface are given by

$$\bar{V}_r = Ste \left(\frac{\partial \theta_s}{\partial \bar{r}} \Big|_{\bar{r}=\frac{R}{l_c^-}} - \frac{k_l}{k_s} \frac{\partial \theta_l}{\partial \bar{r}} \Big|_{\bar{r}=\frac{R}{l_c^+}} \right) \quad (2.41)$$

on S_1 and

$$\bar{V}_z = Ste \left(\frac{\partial \theta_s}{\partial \bar{z}} \Big|_{\bar{z}=\frac{h}{2l_c^-}} - \frac{k_l}{k_s} \frac{\partial \theta_l}{\partial \bar{z}} \Big|_{\bar{z}=\frac{h}{2l_c^+}} \right) \quad (2.42)$$

on S_2 . The interface kinetics condition on S_2 is given by

$$\bar{V}_z = f(\theta_k) \quad (2.13)$$

To summarize, the growth of a frazil ice crystal entrained in a flowing body of water can be modelled as an ice disc suspended in a quiescent slightly supercooled volume of water. Thus, the latent heat dissipation mechanism from the growing surface of the crystal can be reduced to transient heat conduction in both the solid and liquid phases. It should be noted that in the analysis so far, the effects of turbulence in the fluid have been ignored. This is partly due to the fact that few studies have been done to understand the turbulence properties of bodies of water in which frazil crystals are formed. Also, modelling crystal growth rates in a quiescent fluid is not only a reasonable approximation but also forms the basis for making comparisons with actual measurements and for making later models which will incorporate the effects of turbulence.

Fujioka [28] modelled the growth of an ice disc assuming that transient effects were negligible. His rationale for this was that at the relatively low supercoolings of the surrounding water, transient effects should damp out very quickly and hence the transient term was neglected in the model. The validity of this assumption will be checked in the following chapter. However at this point, a relatively simple but efficient method for solving the governing system of equations in a moving boundary domain will be described.

2.4 NUMERICAL METHODOLOGY

Several popular numerical and semi-analytical methods for the solution of crystal growth problems were described in the last section of the previous chapter. Features

required in a scheme for modelling frazil growth rates include (a) applicability to non-uniform domains, (b) concentration of nodal points in regions of high gradients, (c) tracking of moving fronts without increased computational difficulty, (d) application to various geometries and boundary conditions with little modification to the computer source code, and (e) good reliable accuracy with a minimum of formulation and computational effort. The two most popular numerical methods that have been previously used for solving moving boundary problems are the finite difference method and the finite element method (see [8], [37] and [67] for a detailed description of the finite element method).

The finite element method provides many of the desired features but with the disadvantages of a complex formulation and implementation. For this study, it was desired to use a method which retains the advantages offered by the finite element method but with the simplicity and ease of implementation of finite differences. This method referred to as "Boundary Fitted Coordinates" (BFC for brevity) was developed by Thompson et al [73] for the solution of partial differential equations in irregularly shaped or deforming regions. An overview of the method is given in the next section followed by a detailed description of coordinate transformation and numerical mesh generation.

2.4.1 BOUNDARY FITTED CURVILINEAR COORDINATE SYSTEMS

The following discussion and the subsequent development of the equations will be restricted to two dimensions although in principle it can be extended to three dimensions. It should be noted that the general equations and constraints to be developed can be simplified considerably if the solution domain is classified in terms of regular, simple coordinate systems. The major advantage of using BFC for such

regions is its ability in handling nonuniformly spaced grids.

The underlying concept of boundary fitted coordinates is to solve the governing partial differential equations along with its boundary conditions on a region with a simple, regular geometry, where regular geometry means regions that can be easily described in standard coordinate systems (examples of such standard coordinate systems are cartesian, cylindrical or spherical systems). This is accomplished by mapping (or transforming) the real physical domain and the governing equations and boundary conditions to a simple computational domain. This makes the governing equations and their constraints more complex in form; however, the solution domain is a simple rectangular or polar region where application of the boundary conditions becomes much simpler. Such a coordinate transformation is shown schematically in Figure 2.3 where the two phase irregularly shaped region is mapped to a rectangle with vertices A , B , C and D . In addition, the accuracy of a numerical solution for a system of parabolic or elliptic partial differential equations is highly dependent on an accurate representation of its boundary conditions. The boundary conditions usually dominate the character of the solution; hence an inaccurate representation of the boundary position and geometry result in numerical errors in precisely the region of greatest sensitivity. These errors are then magnified and propagate to interior grid points in the solution domain. One can often choose a cylindrical coordinate system if the region is circular or elliptical coordinates if the geometry of the region is elliptical. If the region is irregular, Thompson [73] and others ([17], [33], [56] and [64]) suggested developing a natural coordinate system for the region of interest that fits its boundaries exactly. They state that in principle, one can develop the natural coordinates for any given boundary profile that is not fitted by standard coordinate systems. The traditional finite difference approach was to interpolate the position of the boundary between mesh points. Such methods can result in large

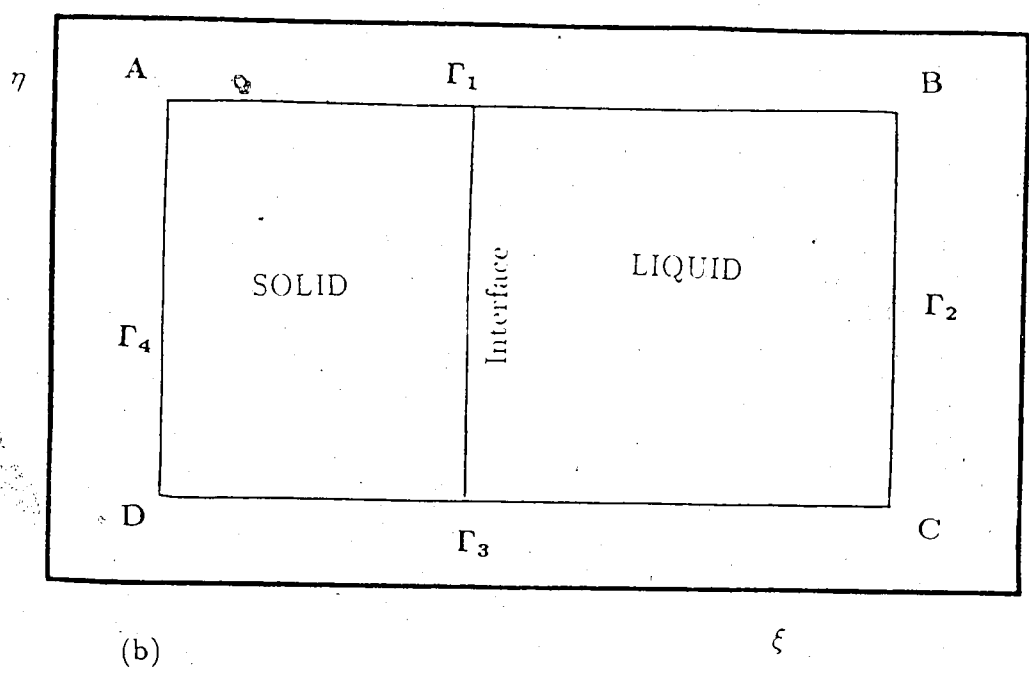
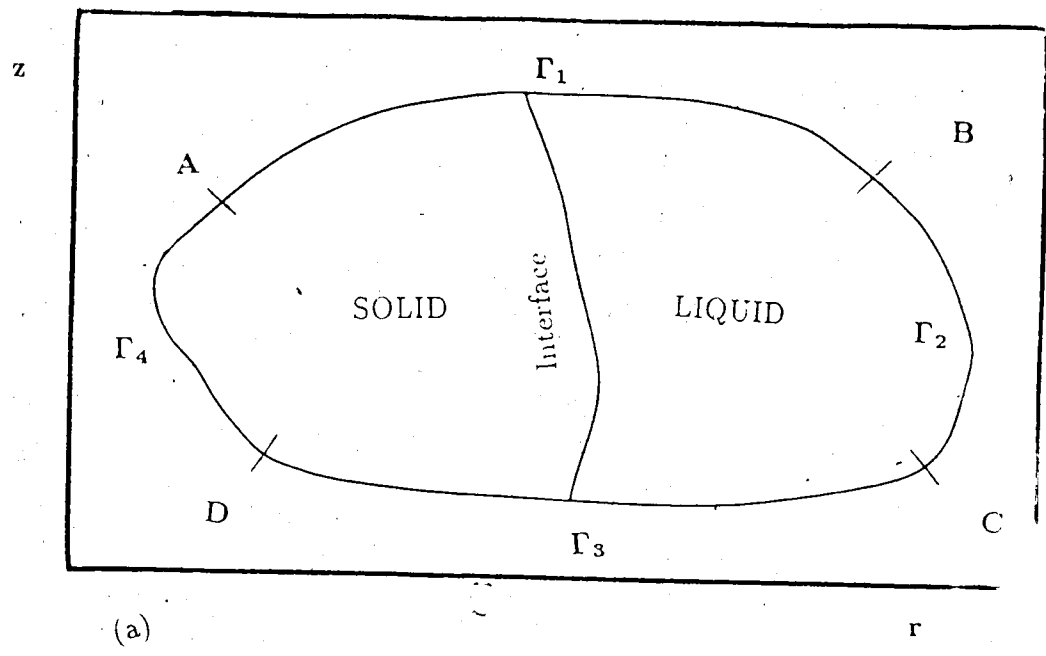


Figure 2.3: Transformation from physical to computational domain (a) Real Domain (b) Computational Domain

sources of error particularly if the variation of the dependent variable is high near the boundary.

Consider the region shown in Figure 2.3 bounded by Γ_1 , Γ_2 and Γ_3 on which a partial differential equation of the parabolic type is to be solved. The equation is given by

$$L(\phi) = f(r, z, t) \quad (2.44)$$

where L is linear differential operator and f is a function of the coordinates r , z , and the time t . The region is divided into two subdomains, which represent the solid and liquid phase. These two phases are separated by the interface Γ_4 which deforms with time. Boundary conditions along Γ_1 , Γ_2 and Γ_3 are of the Dirichlet and Neumann type and the condition along Γ_4 determines the rate at which this boundary moves. The natural coordinates for this bounded region are given by $\eta(r, z)$, which runs parallel to the lines Γ_1 and Γ_4 , and $\xi(r, z)$ which is made to be orthogonal to η . This condition of orthogonality is not necessary but assuming it to be so, greatly simplifies the analysis. In general though, it is possible to determine an orthogonal set of natural coordinates in most cases.

The region D is the rectangular region shown in Figure 2.3 in the (ξ, η) coordinate system. By a suitable transformation, the Equation (2.44) and its boundary conditions can be transformed to the simpler coordinate system. Solution of the governing equation in the (ξ, η) coordinate system, referred to as the computational domain, results in a simplified difference approximation. Also, the computational space remains constant for all time since changes to the physical domain geometry are taken into account in the transformation of coordinates. Coordinate lines can be concentrated in areas of high gradients since a suitable transformation will always yield a computational domain with constant grid spacing. Ultimately, the solution of Equation (2.44) will be determined as a function of the computational coordinates.

This can easily be expressed as a function of the physical coordinates since the relation between the physical and the computational coordinates has already been established.

The major difficulty involved in the above procedure is to determine the relationship between the physical coordinates and the computational coordinates (ie. to develop suitable mapping functions). Anderson et al [2] classify techniques for grid generation (coordinate transformation) into the three main categories:

1. Complex variable methods.
2. Algebraic methods.
3. Differential equation methods.

Any of the above procedures is valid if it leads to an acceptable grid. One of the most highly developed techniques for generating acceptable grids is the differential equation method. Winslow [79] suggested the use of elliptic equations for generating a system of natural coordinates. Thompson et al and others ([73], [33], [56] and [64]) have worked extensively on the use of Laplace and Poisson equations for the generation of grids. The application of such families of equations for grid generation is best understood with an analogy with heat conduction.

If we consider the example of steady state heat conduction, then the solution of Laplace's equation with Dirichlet boundary conditions will result in smooth and continuous isotherms which are nonintersecting. If these isotherms were used as grid lines, they would yield the desirable properties of continuity and uniqueness. Another feature useful in grid generation is the ability to concentrate grid points in regions of high gradients. Considering again the heat conduction analogy, we see that inclusion of a source term in the heat conduction problem would act to increase the concentration of isotherms in the vicinity of the source. Applying this concept to grid

generation, concentration of the grid lines can be achieved at any desired location on the mesh by incorporating suitable source terms in the mesh generation equations. In this manner, Poisson type equations could be used to generate grids and control the placement and concentration of coordinate lines.

The mapping of coordinates according to the method of Thompson consists of specifying the desired grid points (r, z) on the boundary of the physical domain. The interior distribution of grid points can be determined by solving the system of equations

$$\begin{aligned}\xi_{rr} + \xi_{zz} &= P(\xi, \eta) \\ \eta_{rr} + \eta_{zz} &= Q(\xi, \eta)\end{aligned}\quad (2.45)$$

where P and Q are terms for controlling the coordinate point spacing in the interior of the region and the subscripts denote differentiation with respect to the subscripted variable. The solution of these two equations in the uniform rectangular region is made possible by interchanging the roles of the dependent and independent variables.

2.4.2 MATHEMATICAL DEVELOPMENT

Consider again the regions shown in Figure 2.3. The general transformation from the physical region to the transformed region is given by the vector valued function

$$\begin{bmatrix} \xi \\ \eta \end{bmatrix} = \begin{bmatrix} \xi(r, z) \\ \eta(r, z) \end{bmatrix} \quad (2.46)$$

The inverse function of the above transform is written as

$$\begin{bmatrix} r \\ z \end{bmatrix} = \begin{bmatrix} r(\xi, \eta) \\ z(\xi, \eta) \end{bmatrix} \quad (2.47)$$

The Jacobian matrix of the transformation (2.46) is

$$[J_1] = \begin{bmatrix} \xi_r & \xi_z \\ \eta_r & \eta_z \end{bmatrix} \quad (2.48)$$

and similarly, the Jacobian matrix of the inverse transformation (2.46) is

$$[J_2] = \begin{bmatrix} r_\xi & r_\eta \\ z_\xi & z_\eta \end{bmatrix} \quad (2.49)$$

The matrices $[J_1]$ and $[J_2]$ are related to each other as indicated by

$$[J_1][J_2] = [I] \quad (2.50)$$

where $[I]$ is the identity matrix. The determinant of the matrix $[J_2]$ (equivalently the Jacobian) is then

$$J = r_\xi z_\eta - r_\eta z_\xi \quad (2.51)$$

Then, from (2.50), the following relations can be determined

$$\begin{aligned} \xi_r &= z_\eta / J \\ \xi_z &= -r_\eta / J \\ \eta_r &= -z_\xi / J \\ \eta_z &= r_\xi / J \end{aligned} \quad (2.52)$$

Partial derivatives of a function $f(r, z)$, which is some sufficiently differentiable function of r and z , are transformed using the relations

$$\frac{\partial f}{\partial r} = \frac{\partial(f, z) / \partial(\xi, \eta)}{\partial(r, z) / \partial(\xi, \eta)} = \frac{(z_\eta f_\xi - z_\xi f_\eta)}{J} \quad (2.53)$$

and

$$\frac{\partial f}{\partial z} = \frac{\partial(r, f) / \partial(\xi, \eta)}{\partial(r, z) / \partial(\xi, \eta)} = \frac{(-r_\eta f_\xi + r_\xi f_\eta)}{J} \quad (2.54)$$

Higher order derivatives are obtained by the repeated application of (2.53) and (2.54).

Derivatives with respect to time remain unchanged, unless the region is deforming or the boundary is moving (i.e. $df(r, z)/dt = df(\xi, \eta)/dt$). A moving boundary or boundaries in the region introduces an additional term to the time derivative which accounts for the change in position of the coordinate points within the region as it

deforms. In this case, the independent variables r and z are now functions of time and the dependent variable f can be expressed in the following manner

$$f(r, z, t) = f(r(t), z(t), t) \quad (2.55)$$

Differentiating the above expression with respect to time yields

$$\frac{\partial f}{\partial t} = \frac{\partial f}{\partial r} \frac{dr}{dt} + \frac{\partial f}{\partial z} \frac{dz}{dt} \quad (2.56)$$

Using Equation (2.56) and Equation (2.52) to Equation (2.54), this can be rewritten in the more useful form as

$$\left. \frac{\partial f}{\partial t} \right|_{r,z} = \left. \frac{\partial f}{\partial t} \right|_{\xi,\eta} - \frac{(f_{\xi} z_{\eta} - f_{\eta} z_{\xi})}{J} \left(\frac{dr}{dt} \right) + \frac{(f_{\xi} r_{\eta} - f_{\eta} r_{\xi})}{J} \left(\frac{dz}{dt} \right) \quad (2.57)$$

where dr/dt and dz/dt are the velocity of a moving grid node. Details of the mathematical verification of the above relations including a comprehensive set of transformed derivatives and operators is contained in Appendix B.

Sufficient conditions for the existence of the transformation described above are given by the inverse function theorem [46]. In particular, if the component functions of (2.46) are continuously differentiable at a point, say (a, b) , and the Jacobian matrix (2.48) is nonsingular at (a, b) , then there exists a disk N_o about (a, b) such that the inverse function (2.47) exists and (2.49) holds for all $[r, z]$ in N_o . It can be seen that the inverse function theorem only guarantees existence in a local manner. Thus, functions of (2.46) are sought which possess even more desirable properties than those required by the inverse function theorem.

The basic approach of the present transformation is to let the component functions of (2.46) be solutions of a system of elliptic partial differential equations with Dirichlet boundary conditions. Since harmonic functions have continuous derivatives of all orders and obey a maximum principle (which states that the maximum and minimum

values of the function must occur on the boundaries of the region D), the best choice for the functions $\xi(r, z)$ and $\eta(r, z)$ would be either harmonic, subharmonic, or superharmonic. Subharmonic and superharmonic functions also obey the maximum principle, although it is not as strong a condition as it is for harmonic functions. Hence, subharmonic and superharmonic functions are also continuously differentiable. Since no extrema occur within the region D , the first derivatives of the function will not simultaneously vanish within D and hence, the Jacobian will not be zero due to the presence of an extremum. Further, the maximum principle guarantees uniqueness of the coordinate functions $\xi(r, z)$ and $\eta(r, z)$ [48] and thus ensures that no overlapping of the boundaries will occur. A more general and rigorous discussion of the mathematical properties of the transformation is given in [51].

2.4.3 APPLICATION TO THE FRAZIL GROWTH PROBLEM

Consider the region shown in Figure 2.3 representing the upper right hand quadrant of a frazil disk submerged in a supercooled liquid. Since it is desired to perform all numerical computations on the uniform, transformed plane, the dependent and independent variables are interchanged through application of the relations established in the previous section. As a result, the grid generation equations (2.45) are transformed to yield the coupled system

$$\begin{aligned} \zeta r_{\xi\xi} + 2\beta r_{\xi\eta} - \gamma r_{\eta\eta} &= -J^2(P r_{\xi} + Q r_{\eta}) \\ \zeta z_{\xi\xi} + 2\beta z_{\xi\eta} - \gamma z_{\eta\eta} &= -J^2(P z_{\xi} + Q z_{\eta}) \end{aligned} \quad (2.58)$$

where

$$\begin{aligned} \zeta &= r_{\eta}^2 + z_{\eta}^2 \\ \beta &= r_{\xi} r_{\eta} + z_{\xi} z_{\eta} \\ \gamma &= r_{\xi}^2 + z_{\xi}^2 \end{aligned}$$

and J is given by Equation (2.51) The governing equations and boundary conditions are transformed to the computational (ξ, η) plane using Equations (2.53) to (2.57) and become

$$\begin{aligned} \zeta \theta_{\xi\xi}^s + 2\beta \theta_{\xi\eta}^s - \gamma \theta_{\eta\eta}^s + -J^2(P r_\xi + Q r_\eta) &= J^2 \theta_\tau^s - J\Psi \\ \zeta \theta_{\xi\xi}^l + 2\beta \theta_{\xi\eta}^l - \gamma \theta_{\eta\eta}^l + -J^2(P z_\xi + Q z_\eta) &= J^2 \alpha_s / \alpha_l \theta_\tau^l - J \alpha_s / \alpha_l \Psi \end{aligned} \quad (2.59)$$

where

$$\Psi = (z_\eta \theta_\xi - z_\xi \theta_\eta) R_\tau + (r_\xi \theta_\eta - r_\eta \theta_\xi) h_\tau$$

and subject to the conditions

$$R_\tau = Ste \left[\left(\frac{z_\eta \theta_\xi - z_\xi \theta_\eta}{J} \right)_s - \frac{k_l}{k_s} \left(\frac{z_\eta \theta_\xi - z_\xi \theta_\eta}{J} \right)_l \right]$$

$$\mu_1 e^{\mu_2 \theta_k} = Ste \left[\left(\frac{r_\xi \theta_\eta - r_\eta \theta_\xi}{J} \right)_s - \frac{k_l}{k_s} \left(\frac{r_\xi \theta_\eta - r_\eta \theta_\xi}{J} \right)_l \right]$$

$$(r_\xi \theta_\eta - r_\eta \theta_\xi) = 0 \text{ for } \xi = 0$$

$$(z_\eta \theta_\xi - z_\xi \theta_\eta) = 0 \text{ for } \eta = 0$$

The other boundary conditions are the same as before.

The functions P and Q are included if the grid spacing is to be nonuniform or certain mesh properties such as grid orthogonality are required, otherwise they may be taken to be zero. Thompson et al [73] suggest that the choice of the source terms $P(\xi, \eta)$ and $Q(\xi, \eta)$ be comprised of sums of terms of decaying exponential functions. These functions provide the means for concentrating grid lines at desired locations in the region. In addition, they can be used as weighting functions to yield orthogonal grids where none was possible otherwise. Choosing the functions P and Q in this manner however, is a trial and error procedure with each successful choice being limited only to a particular grid.

A more consistent method for choosing P and Q was developed by Thomas and Middlecoff [72]. This method is particularly useful for obtaining orthogonal grids when the region boundary is specified by a nonuniform distribution of grid points.

The form which they suggest for the source terms P and Q are

$$P = \phi(\xi, \eta)(\xi^2_r + \xi^2_z) \quad (2.60)$$

and

$$Q = \psi(\xi, \eta)(\eta^2_r + \eta^2_z) \quad (2.61)$$

where $\phi(\xi, \eta)$ and $\psi(\xi, \eta)$ are functions yet to be specified. Substituting these forms for P and Q into Equations (2.59) results in

$$\zeta(r_{\xi\xi} + \phi r_{\xi}) - 2\beta r_{\xi\eta} + \gamma(r_{\eta\eta} + \psi r_{\eta}) = 0 \quad (2.62)$$

$$\zeta(z_{\xi\xi} + \phi z_{\xi}) - 2\beta z_{\xi\eta} + \gamma(z_{\eta\eta} + \psi z_{\eta}) = 0 \quad (2.63)$$

They then develop a set of equations which define the parameters ϕ and ψ and can be obtained from Equations (2.62) and (2.63) above by imposing two a priori constraints on the local slope and curvature of the coordinate curves transverse to the boundary. These constraints are that the transverse coordinate curves be locally straight and orthogonal to the boundary.

Eliminating ψ in Equation (2.62) and Equation (2.63) yields a single equation which can be written as

$$\zeta[z_{\eta}(r_{\xi\xi} + \phi r_{\xi}) - r_{\eta}(z_{\xi\xi} + \phi z_{\xi})] = z^2_{\eta}[2\beta(r_{\eta}/z_{\eta})_{\xi} + \gamma(r_{\eta}/z_{\eta})_{\eta}] \quad (2.64)$$

The constraint that the transverse coordinate curves $\xi = \text{constant}$ be locally straight (ie. have zero curvature) can be expressed as

$$\left(\frac{r_{\eta}}{z_{\eta\eta}}\right) = 0 \text{ on } \eta = \eta_b \quad (2.65)$$

Furthermore, the orthogonality condition with the coordinate curves and the boundary can be shown to satisfy the expression

$$r_{\xi}r_{\eta} + z_{\xi}z_{\eta} = 0 \text{ on } \eta = \eta_b \quad (2.66)$$

Evaluation of Equation (2.64) at the boundary $\eta = \eta_b$ and application of the conditions (2.65) and (2.66) yields an expression for ϕ

$$\phi = \frac{-(r_{\xi}r_{\xi\xi} + z_{\xi}z_{\xi\xi})}{(r^2_{\xi} + z^2_{\xi})} \quad (2.67)$$

that is valid along the boundary η_b . Similarly, an expression for ψ can be obtained by interchanging ϕ and ξ with ψ and η respectively in the expression above to yield

$$\psi = \frac{-(r_{\eta}r_{\eta\eta} + z_{\eta}z_{\eta\eta})}{(r^2_{\eta} + z^2_{\eta})} \quad (2.68)$$

along the boundary ξ_b . Once the parameters ϕ and ψ are defined at each grid point along the boundaries $\eta = \eta_b$ and $\xi = \xi_b$, their values at interior points can be computed by linear interpolation along the vertical grid lines $\xi = \text{constant}$ for ϕ and along the horizontal grid lines $\eta = \text{constant}$ for ψ . This procedure for evaluating ϕ and ψ insures that the grid throughout the interior of the computational domain will be governed by the grid point distribution that is assigned on the boundaries, and that the transverse grid lines will be locally orthogonal to the boundaries [72].

2.4.4 DISCRETIZATION OF EQUATIONS AND METHOD OF SOLUTION

The coupled grid generation equations (2.59) are discretized using central order finite differences to yield a system of algebraic equations. The difference relations to be used for the discretization are given in Appendix B. It should be noted that the difference between grid points in the computational domain, Δ_{ξ} and Δ_{η} are irrelevant

and can be taken to be unity. Thompson et al [73] recommend a point iterative technique such as "Successive Over Relaxation" (SOR) or line iterative scheme to solve the above system. Since the number of iterations when using a line iterative technique is reduced only by a factor of $1/\sqrt{2}$ compared to point iteration, SOR is the preferred method of solution for the grid generation equations, since it is so much simpler to apply. The procedure to solve the system is as follows:

1. Make an initial guess for the interior (r,z) grid points on the physical domain.
2. Assign the boundary values for the region for each (ξ, η) on the computational domain.
3. Calculate the parameters ϕ and ψ along the boundaries of the region and determine the interior values through linear interpolation.
4. Compute the value of the source terms P and Q for each grid point. Also, determine the values of ζ , β , γ , and J .
5. Solve Equation (2.45) using SOR to determine the refined values for the interior grid points.
6. Repeat steps 2 to 5 until the grid mesh points have converged to a specified tolerance.

The governing equations and boundary conditions are also discretized in a manner similar to the grid generation equations to yield a similar set of algebraic equations. They are then solved simultaneously with the grid generation equations. If the geometry is simple, several terms in the two sets of equations drop out leading to a simpler set of equations. Since the resulting system of equations are nonlinear, an iterative procedure must be applied. A number of iterative solution techniques

are available [30], [66], and [70], but due to the simple geometry of the disc growth problem, a point iterative scheme such as SOR is recommended. A solution algorithm for the numerical solution of the general problem (i.e. transient with curved edge interface) is shown in Figure 2.4. If the region is rectangular, the method of body fitted coordinates is much easier to apply. The transformed equations can be simplified somewhat by realizing that all cross derivative terms are zero. The terms r_{ξ} and z_{η} can also be neglected since they too are zero. A most useful feature of the BFC method for these cases is the ability to concentrate grid lines in desired regions in the real domain while the computational mesh is simple with constant nodal spacing. As a result, the finite difference discretization is also simplified since nonuniform nodal spacing need not be considered in the computational domain. Additional simplifications result since the spacing between nodes in the computational space can be taken to be unity.

The general solution procedure described above is applicable for the most complicated case (i.e. frazil ice crystal with secondary curvature at the edge). This case was not considered in this study since the main purpose was to predict crystal growth rates and not to estimate frazil crystal interface profiles. Additional difficulties such as determining an orthogonal grid; estimating the secondary curvature at a point; and employing a suitable nodal mesh distribution scheme arise when tracking the crystal profile. These additional complexities greatly complicate the already existing problems associated with the non-linear interface conditions. As a result, the edge interface was assumed to remain flat during its growth sequence and the effects of secondary curvature along the edge of the disc were neglected. The radial growth rate is calculated at each node coinciding with the edge of the crystal is calculated for each time step. Since the radial growth rate along the crystal edge varies with z , the velocity at which the edge interface grows is determined by calculating the average edge velocity (arithmetic average of the growth rate at each node) at each time step.

- Solve the grid generation equations using the algorithm listed above (step 1 through 6) to obtain the nodal mesh coordinates $r(\xi, \eta)$ and $z(\xi, \eta)$
- When a suitable grid has been computed, store the calculated values of the parameters $\zeta, \beta, \gamma, P(\xi, \eta), Q(\xi, \eta)$ which are to be used in the solution of the transformed governing equations
- Estimate the principal curvature at each node comprising the crystal edge interface. From this, the temperature depression due to the Gibbs Thompson effect can be determined
- Solve Equation (2.58) subject to the given boundary conditions iteratively with the energy balance condition and the interface kinetics relation
- At each iteration, check the phase boundary nodal velocity and the error in the temperature distribution
- Iterate until both the temperature distribution and the nodal interface velocities have converged to the desired tolerance
- Calculate the increase in the phase boundary during the current time step from the product of the nodal phase boundary velocity and the time step increment
- Advance the phase boundary nodes by the amount calculated in above step
- Continue above steps until the set time period expires
- Stop

Figure 2.4: Numerical solution procedure for general crystal growth problem

and then assuming that the entire edge interface grows at this average rate. With this added assumption, the edge interface will always remain flat and hence the solution procedure listed in Figure 2.4 can be simplified considerably. The most important simplification is that the grid generation equations (steps 1 through 6 above) do not need to be solved at each time step since the interface geometry is simple.

Chapter 3

GROWTH OF A FRAZIL ICE CRYSTAL IN A SUPERCOOLED MELT

The main objective of this chapter is to examine the applicability of the "Boundary Fitted Coordinate" method for the study of frazil ice crystal growth and verify the validity of the numerical results. The first part of this chapter compares the numerical results with an analytical solution for the case of the growth of a disc shaped crystal with no thickening effects. From this, several numerical parameters such as nodal mesh distributions, mesh resolution, convergence criteria, and solution domain dimensions are determined. The validity of the quasi-steady state growth assumption, employed by Fujioka and Sekerka [27], is also checked by examining the transient growth and temperature behaviour of a subcooled ice particle. The second portion of this chapter deals with the application of the model to the study of frazil growth in a quiescent subcooled melt. We investigate the validity of the common assumption of negligible growth in the c-axis direction made in previous studies.

3.1 GROWTH IN THE a-AXIS DIRECTION IN A QUIESCENT SUPERCOOLED MELT

Before proceeding to the more difficult and realistic frazil crystal growth models, it is first necessary to check the validity and accuracy of the computer code. Generally, this is accomplished by obtaining an analytical solution for a problem with a simplified geometry and then comparing it with the numerically obtained solution. The major difficulty associated with the numerical solution in a disc-shaped region is the development of a suitable grid mesh. This is further increased when the thickness

to diameter ratio can be as small as 0.02. Since simple geometries such as a semi-infinite slab or infinite cylinder are not as sensitive to grid spacing, the computer program cannot be tested with them. Although it may work for these simple cases, it will still yield incorrect results for the disc region. Therefore the disc geometry must be retained when checking the numerical algorithm with simplifications made to the governing equations and boundary conditions. Once an analytical solution is obtained, it can be used to verify the accuracy of the numerical results. An analytical solution for the growth of a submerged ice disc was obtained by Fujioka and Sekerka [27]. This solution presents an excellent opportunity not only to examine the validity of the computer program and to eliminate errors but also tune the computer model by enabling us to pick several important numerical parameters. We now present the solution for the simplified case as developed by Fujioka and Sekerka.

3.1.1 COMPARISON OF THE NUMERICAL AND ANALYTICAL SOLUTION

To simplify the governing partial differential Equations (2.21) and (2.22) so that an analytical solution could be obtained, Fujioka and Sekerka made the following three assumptions:

1. The disc shaped crystal grows in the radial direction only; hence, thickening effects are ignored. Also, since growth is in the a -axis direction, the interface kinetics are so rapid that they can be ignored.
2. The crystal growth process occurs in a quasi-steady state manner; therefore the governing equation describing the temperature distribution is not an explicit function of time.

3. The thermal conductivities of the solid and liquid phase region are identical and equal to that of water.

As a result of these assumptions, the temperature distribution in the solid-liquid region is satisfied by the steady state heat conduction equation

$$\frac{\partial^2 T}{\partial r^2} + \frac{1}{r} \frac{\partial T}{\partial r} + \frac{\partial^2 T}{\partial z^2} = 0 \quad (3.1)$$

and the energy balance at the disc edge may be written in the form

$$L \frac{dR(t)}{dt} H\left(\frac{h}{2} - |z|\right) = k \left(\left. \frac{\partial T}{\partial r} \right|_{r=R^-} - \left. \frac{\partial T}{\partial r} \right|_{r=R^+} \right) \quad (3.2)$$

where $H(x)$ is the Heaviside step function,

$$H(x) = \begin{cases} 1, & \text{if } x > 0 \\ 0, & \text{if } x < 0. \end{cases}$$

The temperature along the interface was specified as

$$T_e - T_\infty = \Delta T \left(1 - \frac{R_{cr}}{R}\right). \quad (3.3)$$

The general solution of (3.1) from Fujioka and Sekerka [27] was found to be

$$T(r, z) - T_\infty = \int_0^\infty A(\lambda) \cos(\lambda z) I_0(\lambda r_{<}) K_0(\lambda r_{>}) d\lambda \quad (3.4)$$

where

$$r_{<} = \begin{cases} r, & \text{for } 0 \leq r \leq R(t) \\ R(t), & \text{for } R(t) \leq r \end{cases}$$

and

$$r_{>} = \begin{cases} r, & \text{for } R(t) \leq r \\ R(t), & \text{for } 0 \leq r \leq R(t) \end{cases}$$

$I_0(x)$ and $K_0(x)$ are modified Bessel functions of order zero. $A(\lambda)$ is determined by applying the boundary conditions and is found to be

$$A(\lambda) = \frac{2L}{\pi k} R \frac{dR \sin(\lambda h/2)}{dt \lambda} \quad (3.5)$$

The radial growth rate of the disc, at its centerline $z = 0$, was determined to be

$$\frac{dR}{dt} = \frac{\pi k \Delta T}{L R q_0[h/2R]} \left(1 - \frac{R_{cr}}{R}\right) \quad (3.6)$$

where $q_0(z)$ is called the toroidal integral of order zero and is defined as

$$q_0(z) = 2 \int_0^\infty \frac{\sin(zx)}{x} I_0(x) K_0(x) dx$$

For ice discs with $R \gg h$, Equation (3.6) can be approximated as

$$\frac{dR}{dt} = \frac{\pi k \Delta T}{L R \ln(16eR/h)} \quad (3.7)$$

The numerical solution, for the simplified disc growth problem, was obtained in order to compare it with the analytical solution. As mentioned, the primary reason for doing this was to fine tune the numerical model by appropriately choosing numerical parameters such as mesh distribution and dimensions of the solution regime that normally would have to be determined from a lengthy trial and error procedure. Generally, studies in crystal growth only require an accurate determination of the temperature in the vicinity of the growing interface so that the rate of heat flow into the solid and liquid phases and hence the growth rate can be accurately computed. For the growth of a frazil crystal, an accurate estimation of the temperature distribution is required throughout the solid phase region because of the different growth mechanisms in the two coordinate directions. This is of particular importance along the basal plane of the crystal since the thickening rate of the ice disc is a function of the basal plane cooling. Therefore when comparing the analytical and numerical solutions, it is necessary not only to have an accurate determination of the crystal growth rate but also a reasonable comparison of the temperature distributions throughout the solid phase region.

The location of the outer boundary for the supercooled melt must also be approximated since it is not realistically possible to locate it at an infinite distance

from the ice water interface. For real crystals, this outer boundary would be located where the melt temperature is sufficiently uniform and constant. The distance between this boundary and the crystal interface could then be used as an approximate value for the boundary condition at infinity. Rather than employing a time consuming trial and error procedure to approximate the magnitude of this distance, it is much easier to compute the temperature values and gradients from the analytical solution (3.2), at varying distances from the ice disc. As the distance from the crystal increases in the r and z directions, the temperature will approach the constant value of T_∞ , the bulk liquid temperature. At the same time, the gradients $\partial T/\partial r$ and $\partial T/\partial z$ will approach zero. Based on this, the outer boundary is to be located at the shortest distance from the disc edge and face so that both the temperature and temperature gradients are within predefined tolerance limits of their ideal values. Table 3.1 summarizes the outer boundary locations in the radial and axial directions for discs of several aspect ratios where the aspect ratio is defined as

$$\text{Aspect Ratio} = \frac{h}{2R}$$

As a result of this analysis, it can be seen that the ratio R_∞/R of the distance R_∞ (from the disc edge to the outer boundary) and the disc radius R is relatively constant, where

$$T(R_\infty, z) \simeq T_\infty$$

and

$$\left. \frac{\partial T}{\partial r} \right|_{r=R_\infty} \simeq 0$$

However, in the axial direction, the ratio $2Z_\infty/h$ of the outer boundary distance and disc thickness varies between 20 and 200 for

$$T(r, Z_\infty) \simeq T_\infty$$

ASPECT RATIO	$R(\mu m)$	R_{∞}/R	$2Z_{\infty}/h$
0.1	50.0	20.0	100.0
0.05	100.0	20.0	150.0
0.025	200.0	20.0	250.0
0.0167	300.0	20.0	400.0
0.0125	400.0	20.0	500.0
0.010	500.0	20.0	600.0
0.0083	600.0	20.0	700.0
0.0071	700.0	20.0	800.0
0.0063	800.0	20.0	900.0
0.0056	900.0	20.0	1000.0
0.005	1000.0	20.0	1000.0

Table 3.1: Locations of the outer boundary for the disc crystal

and

$$\left. \frac{\partial T}{\partial z} \right|_{z=Z_\infty} \approx 0.$$

Thus it is evident that the location of the outer boundary depends on the disc size and thickness. Bolling and Tiller [9] have stated that for dendritic growth, the far field temperature can be assumed constant at a distance $10\alpha_l/v_n$ away from the solid interface, where v_n is the solidification rate. Applying this criterion to frazil crystal growth, we see that the smaller fast growing crystals will disturb the constant liquid temperature over a shorter distance than the larger, but slower growing crystals. Also, due to the anisotropy in radial and axial growth rates, the influence of the thermal disturbance in the axial direction will be over a much shorter distance in the axial direction compared to the radial direction of the disc. For the purposes of this study, R_∞ and Z_∞ were chosen to be $50R$ and $10R$ in the radial and axial directions respectively. For this steady state case, the characteristic length l_c was chosen to be the radius R of the ice disc.

In order to accurately predict crystal growth rates, it is essential to determine accurately the temperature distribution near the ice-water interface and then estimate precisely the temperature gradient in the solid and liquid regions at the interface. Also, since the thickening rate of the crystal is dependent on the basal plane interfacial undercooling, the temperature in the entire solid region must be computed to a fine tolerance. Although the temperature distribution in the solid region alone is not difficult to obtain, simultaneously estimating the gradients $\left. \frac{\partial T}{\partial r} \right|_{r=R^+}$ and $\left. \frac{\partial T}{\partial r} \right|_{r=R^-}$ is not a trivial task. From the form of the analytical solution, (3.3), it can be readily seen that the temperature gradient is very steep near the interface due to the terms $I_0(\lambda r)$ and $K_0(\lambda r)$, and changes signs abruptly across the interface. As a result, numerically calculating it requires a high order scheme and a suitable distribution of grid nodes. Also, since the numerical scheme is computationally

intensive, it was desired that the domain be discretized with the smallest size mesh possible.

Several types of grid meshes were tested to determine which configuration yielded and accurately calculated the crystal growth rates and basal plane undercooling. To obtain values of crystal growth rates that compared well with the analytical result, it was necessary for the grid nodes to be highly concentrated near the vicinity of the interface and for the slope of the temperature with respect to radial distance to be calculated by a third or fourth order difference scheme. An alternative method to using higher order finite difference schemes is to employ interpolating functions. For the present problem, use of an interpolating function such as a third degree polynomial or a cubic spline along with a reasonable grid mesh was found to be sufficient for accurately estimating the gradient. It should be noted that this method is $O(\delta_g^3)$, where δ_g is the magnitude of the mesh spacing, compared to forward and backward finite difference schemes which are normally $O(\delta_g^2)$ [2]. The major problem encountered was that a mesh distribution which resulted in an accurate determination of the growth rate usually resulted in a poor estimation of the basal plane supercooling. This was not an important consideration in the liquid phase since an accurate temperature profile was only required in the vicinity of the interface for the purposes of estimating the temperature gradient. Several nodal distributions were tried in order to find the right combination so that an accurate temperature profile and thermal gradients near the interface could be computed. After many combinations, a node placement scheme was arrived at which resulted in satisfying both problem requirements. Schemes that worked well consisted of nodes distributed in the radial direction in the solid phase according to the expression

$$r_i = \frac{e^{\lambda(1-i)} - 1}{e^{\lambda(1-I_{max})} - 1} \quad (3.8)$$

where i is the node number, I_s^{max} is the maximum number of nodes in the solid phase and λ is a parameter to control nodal spacing. In the liquid phase region, nodes were spaced according to the relation

$$r_i = \lambda_1 i^3 + \lambda_2 i^2 + \lambda_3 i + \lambda_4 \quad , \quad I_s^{max} \leq i \leq I_l^{max} \quad (3.9)$$

which provided more flexibility in the nodal positioning due to the choice of four spacing parameters. Figure 3.1 shows one of the grid meshes used in the numerical scheme. It is of interest to note that constant grid spacing was employed in the solid phase in the axial direction because the overall accuracy was not sensitive to nodal spacing in this direction. This is probably due to the fact that the disc face does not act as a heat source like the disc edge where latent heat is released. Even for real crystals, the latent heat release along the basal plane is very small compared to that along the edge [18]. In the liquid phase region (axial direction), grid nodes were distributed according to the Equation (3.9) so that a large number of nodes did not have to be used in the far field. In the course of evaluating various grid meshes, it was noted that sudden or abrupt changes in nodal spacing resulted in stability and convergence problems. This problem was particularly prevalent in regions of transition where the gradient increased sharply. This difficulty can be eliminated by choosing a nodal distribution which avoids abrupt changes in grid spacing and instead has a smooth transition from the coarse to fine mesh. Therefore when employing nonuniform meshes in future work, it should be kept in mind that sudden or abrupt changes in the spacing between grid nodes can seriously influence the accuracy of the solution.

Using the nodal distributions scheme just described, the solution region was discretized to a 40×36 nodal mesh. The solid region contained 14 nodes in the radial direction and 5 nodes in the axial direction while the remainder of the nodes were appropriately distributed in the liquid region. With this number of nodes, the

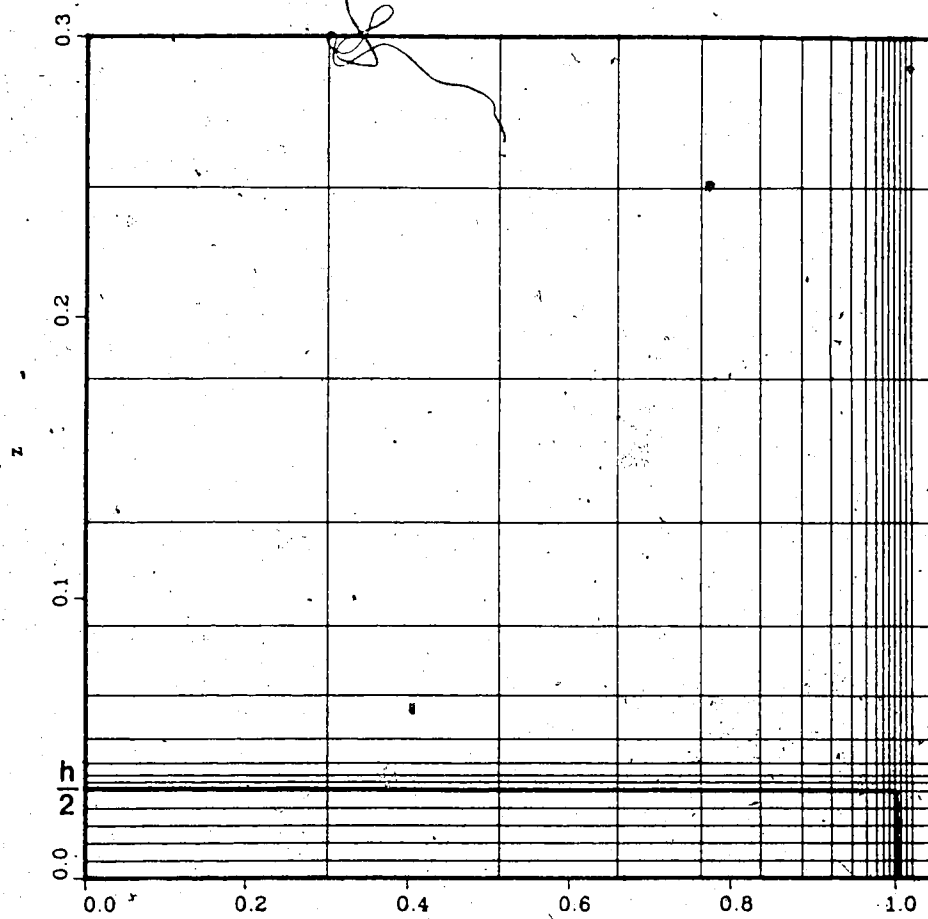


Figure 3.1: Example of a grid mesh required for the frazil growth problem. The mesh is concentrated near the location of the edge interface. The interface is located at $r = 1$ and $z = 0.033$.

number of iterations required to converge to a tolerance of

$$\sum_{i=1}^{i_{max}} \sum_{j=1}^{j_{max}} |\theta_{ij}^{\alpha} - \theta_{ij}^{\alpha-1}| \leq 1.0 \times 10^{-4}$$

(where the superscripts represent iteration number) was just under 2000 for discs with low aspect ratios. The number of iterations increased to 5000 and higher as the aspect ratio decreased or if the region was discretized by a finer mesh. As a compromise between accuracy and computer time, the 40×36 mesh was employed for all quasi-steady state calculations.

Figure 3.2 to Figure 3.4 compare the analytical and numerical solution of the temperature along the base of the disc (at $z = 0$) for three different aspect ratios. The analytical and numerical solutions are seen to be in close agreement for all values of r/R . The agreement is especially good in the solid region where the basal plane temperature is computed to within 2% and in the liquid region for values of r/R less than five. The difference between the analytical and numerical solutions increases for r/R greater than five to a maximum of 7% at the boundaries. Figures 3.5 and 3.6 show a comparison of the two solutions in the vicinity of the interface for discs of aspect ratios of 0.10 and 0.0125. The interesting point to note here is that the numerical solution is more accurate in the solid region for discs with high aspect ratios and this accuracy decreases as the aspect ratio decreases. The accuracy in the liquid portion however, increases with decreasing aspect ratios. This reversal in accuracy underlines the importance of nodal positioning in regions of high gradients. For small stubby discs, the concentration of grid nodes is higher than in the liquid region. This situation changes for larger discs as the concentration of nodes in the liquid portion increases with a corresponding decrease in the solid phase region. These apparent shifts in accuracy between the solid and liquid regions are small however, and do not significantly affect the two important quantities which are to be calculated: the

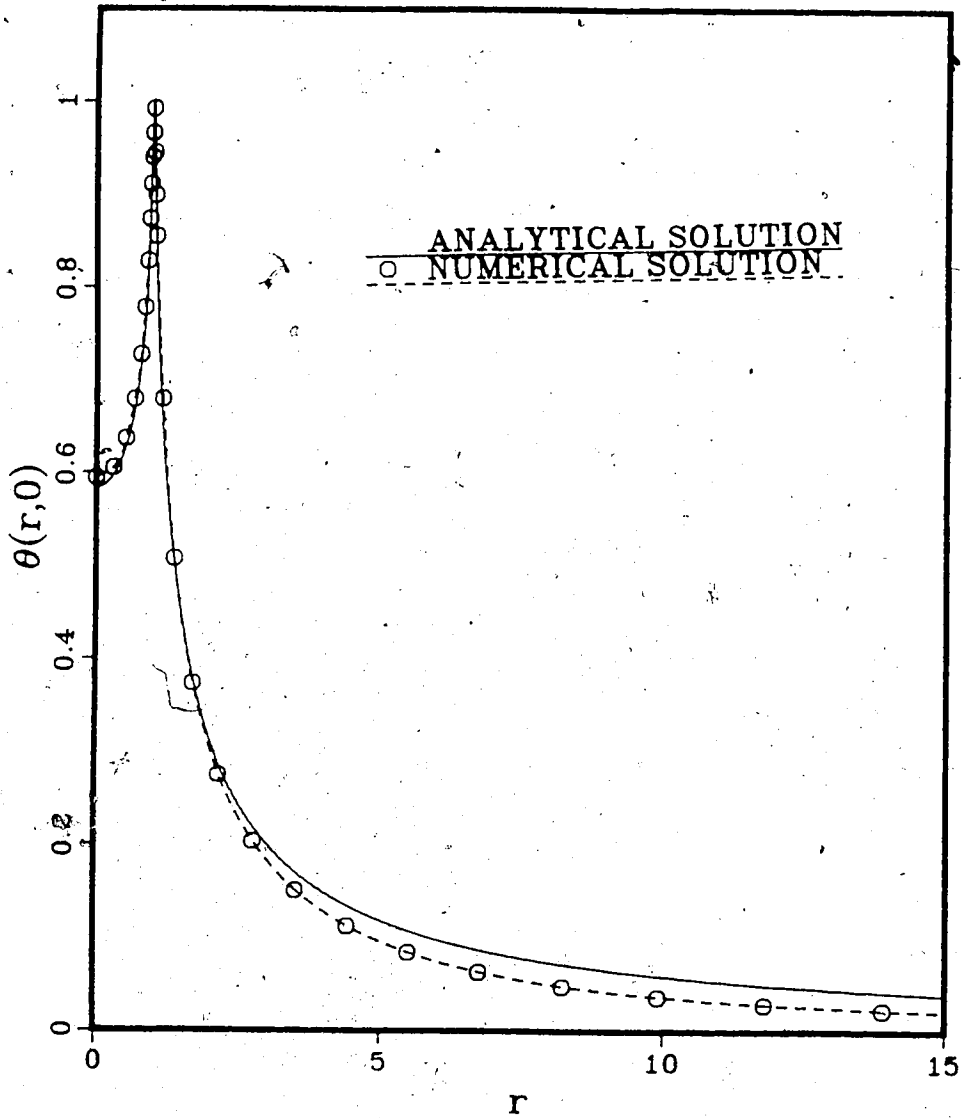


Figure 3.2: Comparison between analytical and numerical solution for $R = 50\mu m$ and $h/2 = 5\mu m$

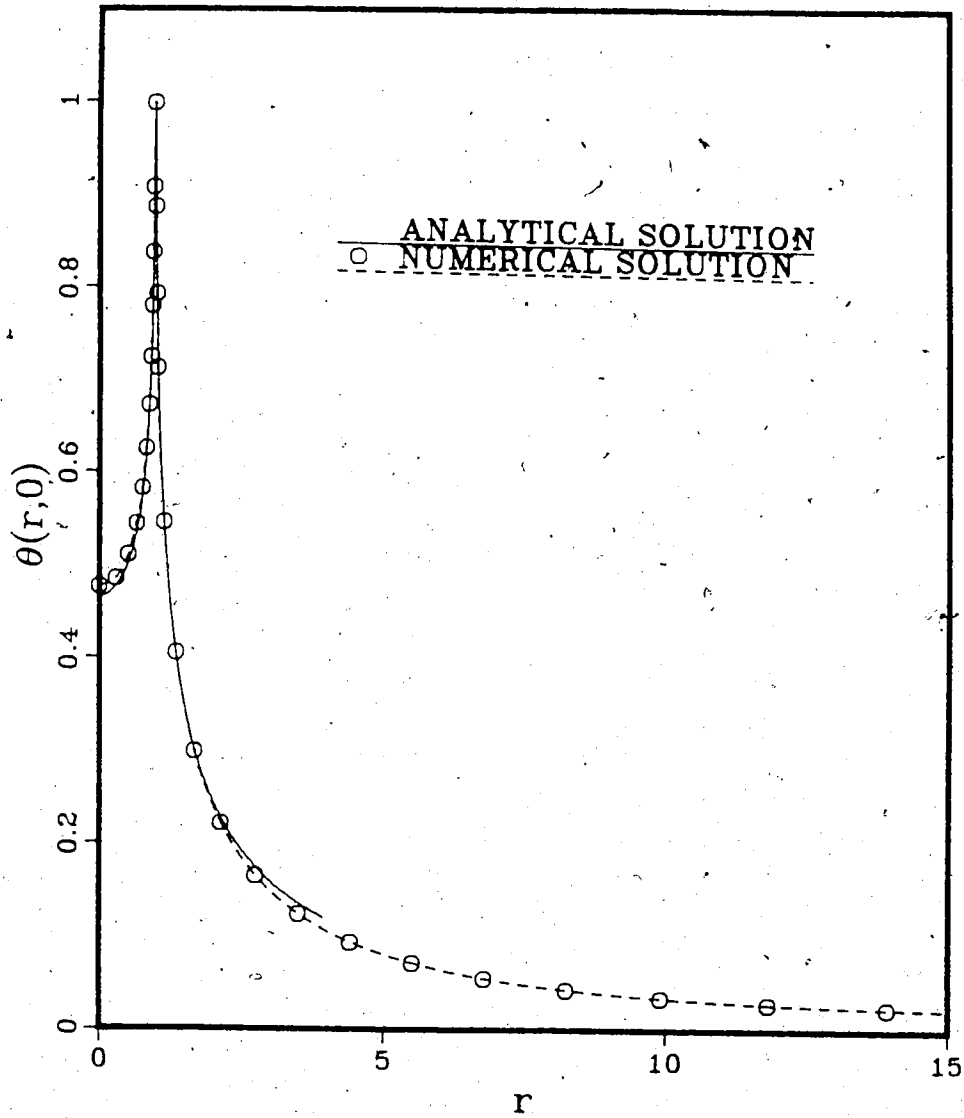


Figure 3.3: Comparison between analytical and numerical solution for $R = 200\mu m$ and $h/2 \approx 5\mu m$

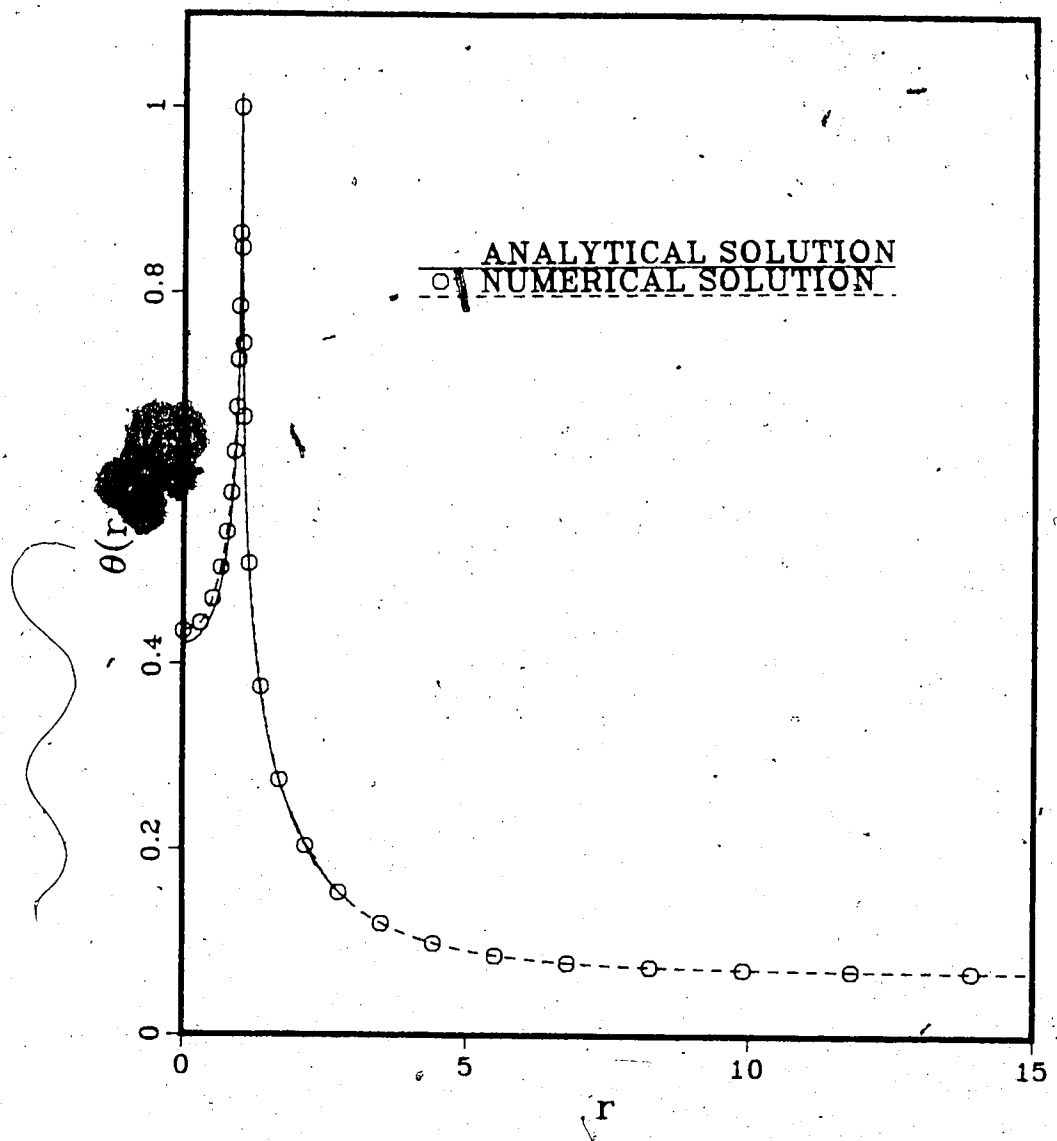


Figure 3.4: Comparison between analytical and numerical solution for $R = 400\mu m$ and $h/2 = 5\mu m$

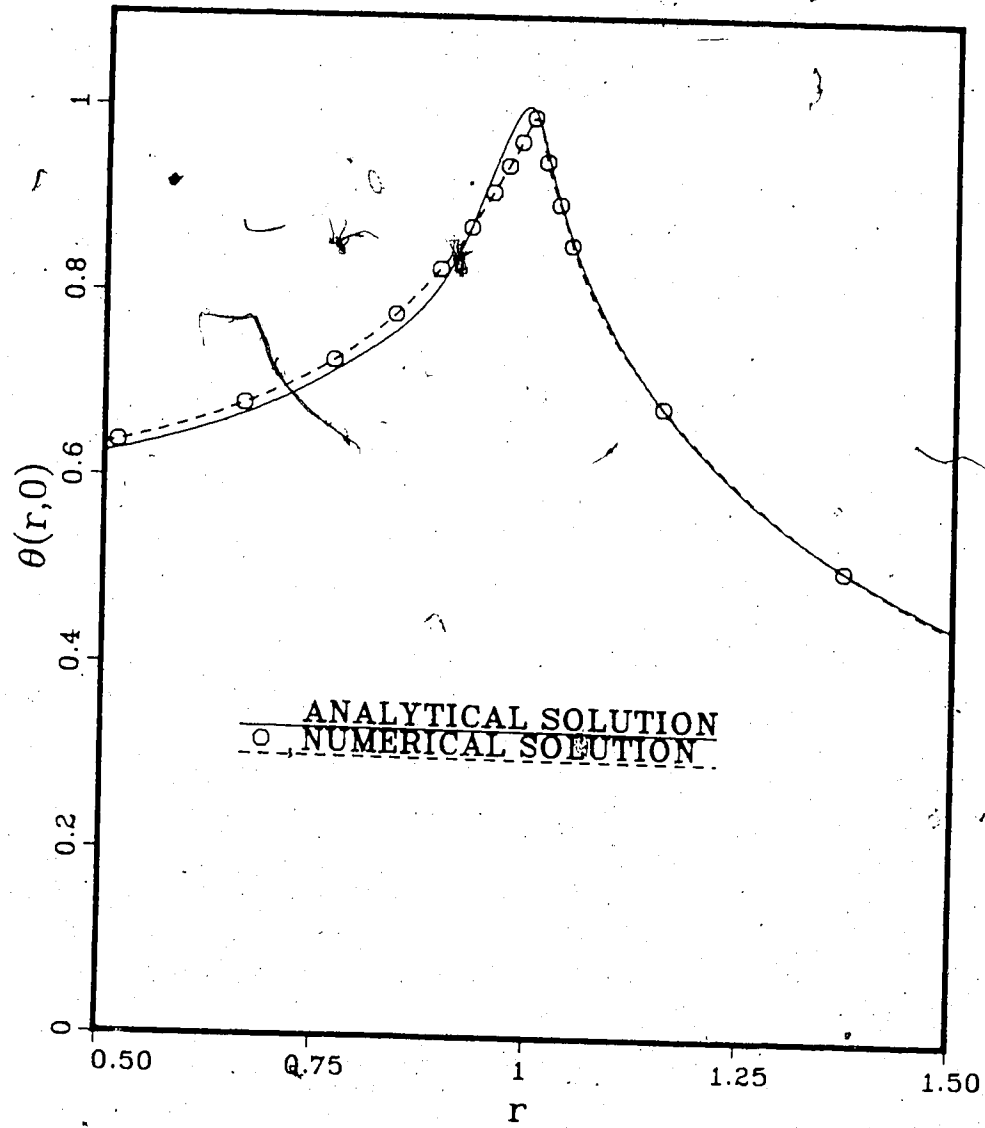


Figure 3.5: Comparison between analytical and numerical solution near the edge interface for $h/2R = 0.10$

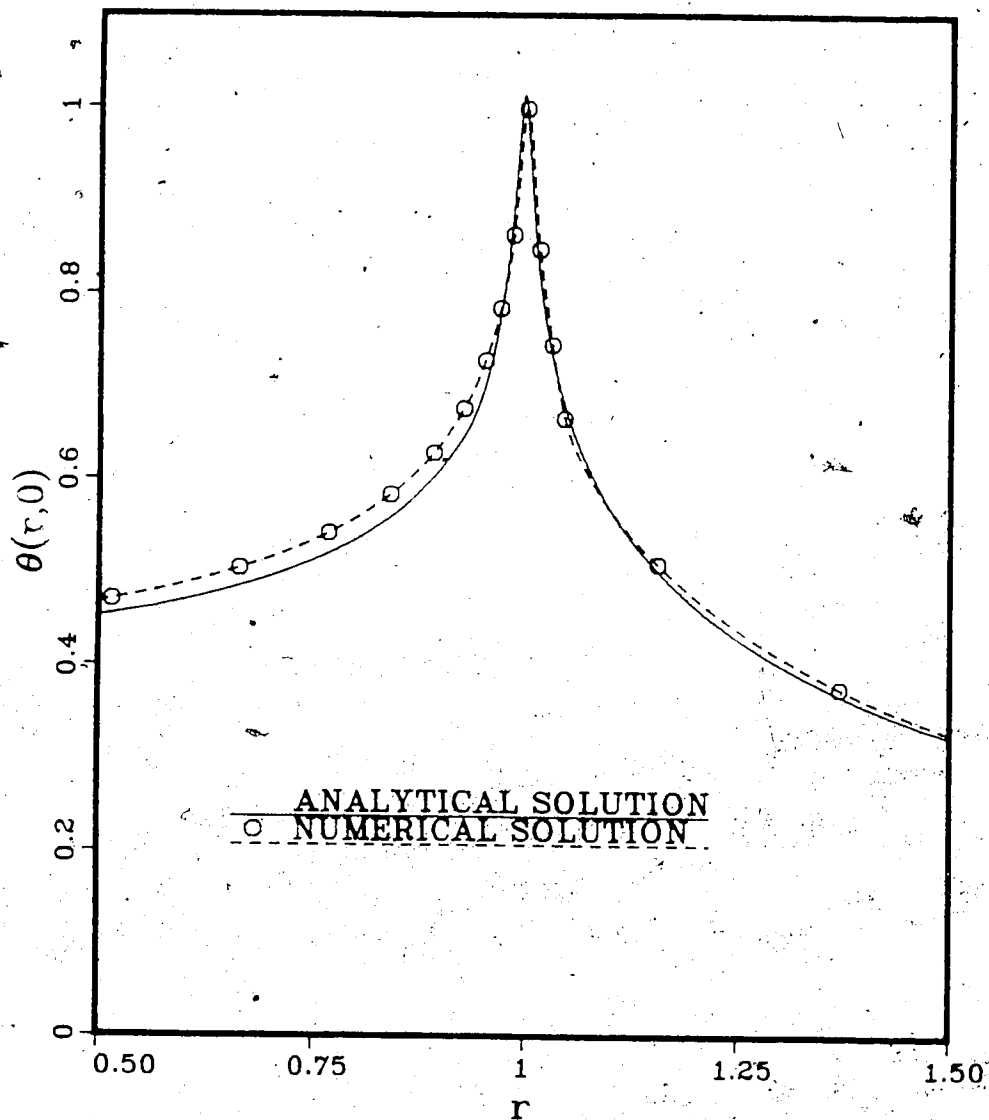


Figure 3.6: Comparison between analytical And numerical solution near the edge interface for $h/2R = 0.0125$

growth rate and the basal plane supercooling. Table 3.2 summarizes the a-axis growth rates at $z = 0$ obtained using the analytical solution and the numerical procedure for discs of several sizes and thicknesses. The temperature at the center of the disc, along the basal plane ($r = 0, z = \frac{h}{2}$) is also given in Table 3.2. A compromise had to be made between the accuracy of the temperature distribution within the solid region and the accuracy of the calculated growth rate. Since c-axis growth rates will later be computed from the basal plane undercooling, the tolerable error in this quantity is less than 5%. Although the gradients along the edge interface were computed using a method of order $O(\delta_g^3)$, the error in the calculated growth rate still varies between 12% and 18% over the range of aspect ratios and disc sizes considered. Although this may appear to be somewhat high, it should be noted that the actual difference between the analytical and numerical growth rates is a tolerable value of about $2\mu\text{m/s}$ over the range of disc sizes considered. Improvement in its accuracy can only be accomplished at the expense of the accuracy for the basal plane undercooling. Under these constraints, it is evident that the numerical procedure yields a solution which is in reasonable agreement with the analytical result for aspect ratios between 0.010 and 1.0. The solution however, becomes numerically unstable and diverges for aspect ratios less than 0.010 due to the disparity in grid spacing in the radial and axial directions.

This does not pose a problem for the present study since the diameter to thickness ratios of frazil crystals is normally in the order of 0.020 for large diameter discs and 0.10 to 1.0 for smaller size crystals [18] [75]. As a result, it is not necessary to solve these stability problems in order to calculate an accurate temperature distribution and growth rates for ice discs with aspect ratios less than 0.010. As a representative example, Figure 3.7 shows the temperature distribution for an ice disc with an aspect ratio of 0.20. With the accuracy of the numerical scheme verified and with confidence

$h/2R$	R (μm)	$dR(t)/dt$ ANALYTICAL ($\mu m/s$)	$dR(t)/dt$ NUMERICAL ($\mu m/s$)	$\theta(0, h/2)$ ANALYTICAL	$\theta(0, h/2)$ NUMERICAL
0.1	50.0	11.50	9.35	0.583	0.591
0.05	100.0	10.20	8.86	0.517	0.523
0.025	200.0	9.12	7.62	0.464	0.476
0.0167	300.0	8.60	7.53	0.438	0.477
0.0125	400.0	8.27	6.70	0.421	0.464

Table 3.2: Comparison of analytical and numerical values of centerline growth rate and basal plane temperature at $(0, h/2)$

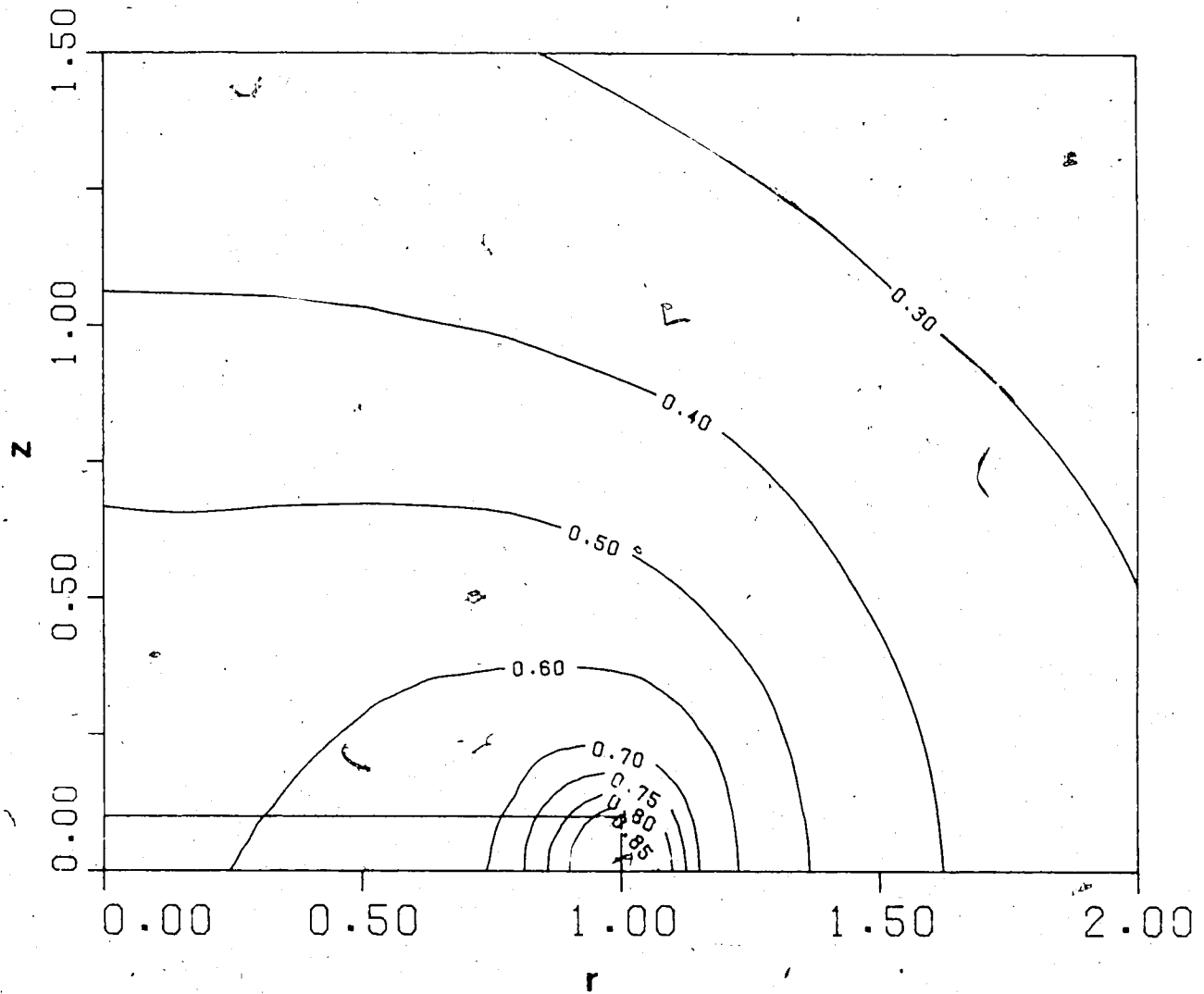


Figure 3.7: Normalized temperature contours for an ice disc of aspect ratio 0.20
($k_l = k_s$)

established in the numerical procedure, a-axis growth rates were computed for the more realistic distinct conductivity case. The temperature distribution for ice discs with aspect ratios of 0.05 and 0.20 are shown in Figures 3.8 and 3.9. Comparing these results with the single conductivity case ($k_s = k_l$) of Figure 3.7, we see that a lower thermal conductivity in the solid phase increases the basal plane supercooling and results in a temperature gradient that is steeper in the solid region but unchanged in the liquid phase. It is also noted that the isotherm $\theta = 0.3$ is located in approximately the same place for both cases.

In the recently made comparisons between the numerical and analytical growth rates, only the centerline ($z = 0$) value was compared. This was due to the difficulty in obtaining an analytical expression for the variation of growth rate along the edge. With the present numerical procedure however, there are no such restrictions since the growth rate may be computed at any point along the edge. As one would expect, the growth rate along the edge of the disc varies from a maximum at the corner ($R, h/2$), to its minimum at ($R, 0$) due to the increase in thermal resistance. Table 3.3 gives the variation in growth rate along the disc edge for crystals of different sizes. The difference between the maximum and minimum values is most significant in the early stages of growth. For larger disc diameters, the corner edge growth rate does not differ by more than 10% of the centerline value. In order to simplify the geometry, it was assumed that the edge would remain flat for all disc sizes. Consequently, the value presented as the a-axis growth rate will be the average growth velocity of the edge.

The a-axis growth rates were computed as a function of disc radius for three disc thicknesses and at two different supercoolings. Figure 3.10 shows the radial growth rate of the crystals for thicknesses of $5\mu\text{m}$, $10\mu\text{m}$ and $20\mu\text{m}$ at an overall supercooling of 0.05°C . Similar results are shown in Figure 3.11 for a supercooling of 0.10°C . The

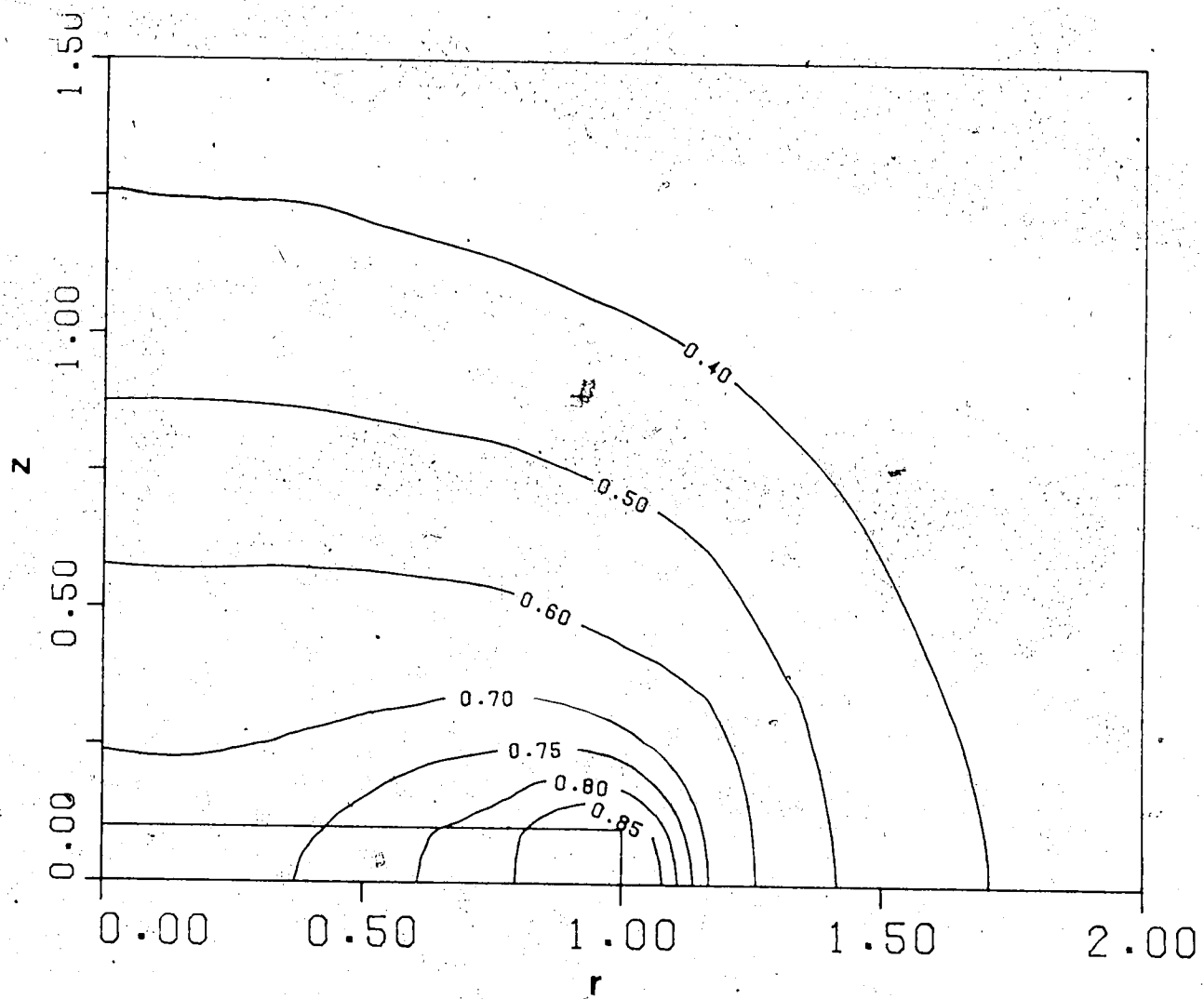


Figure 3.8: Normalized temperature contours for an ice disc of aspect ratio 0.20.
(dual conductivity case)

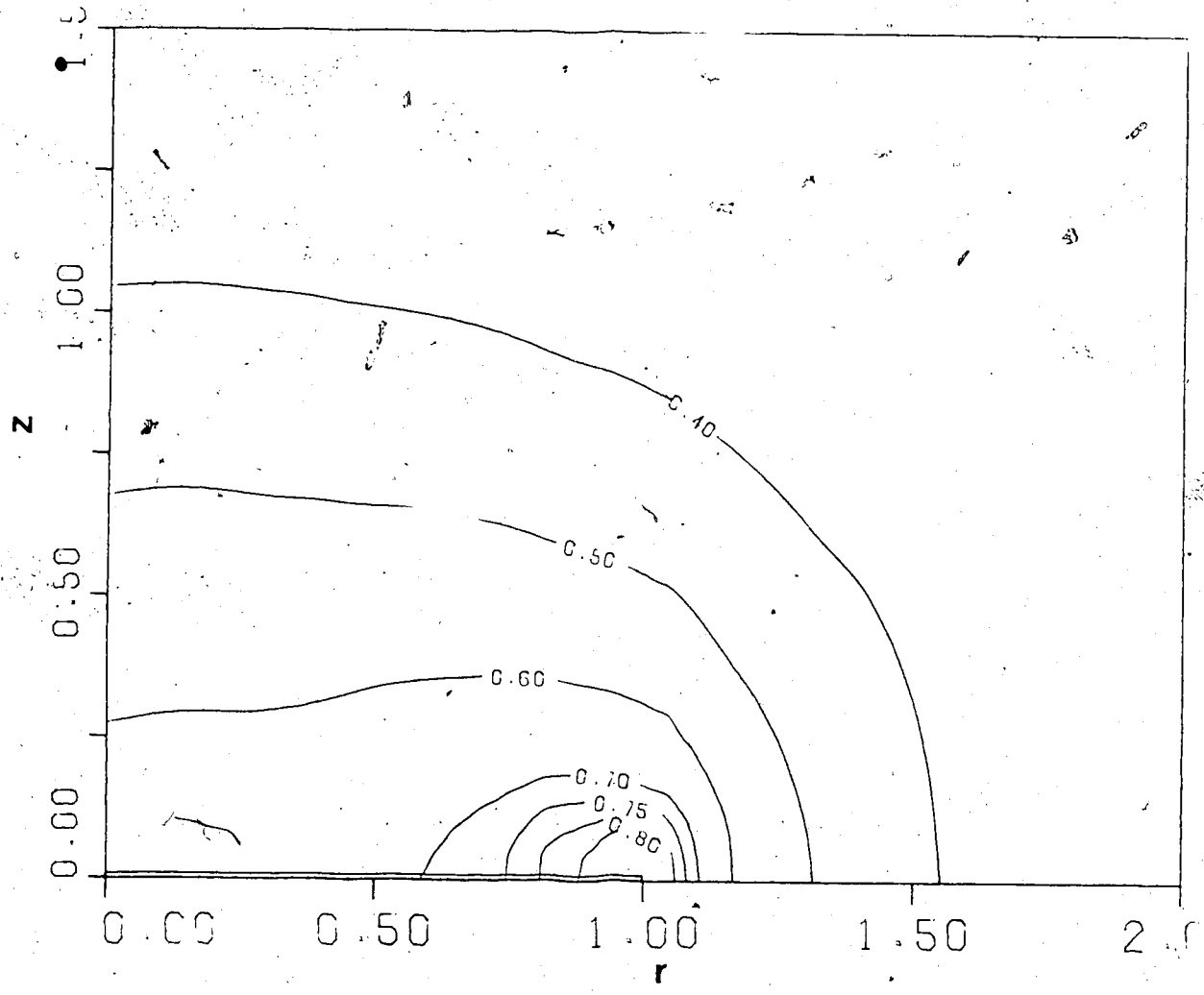


Figure 3.9: Normalized temperature contours for an ice disc of aspect ratio 0.05 (dual conductivity case)

z (μm)	RADIAL GROWTH RATE ($\mu m/s$)				
	50(μm)	100(μm)	200(μm)	300(μm)	400(μm)
0.0	9.35	8.86	7.62	7.53	6.70
1.25	9.75	9.15	7.91	7.65	6.93
2.50	10.94	9.99	8.77	8.03	7.67
3.75	14.4	12.70	11.03	8.79	9.19
5.00	42.43	26.11	17.40	12.87	12.04
AVERAGE dR/dt	17.34	13.36	10.55	8.97	8.50

Table 3.3: Variation in the growth rate along the disc edge for the identical conductivity case

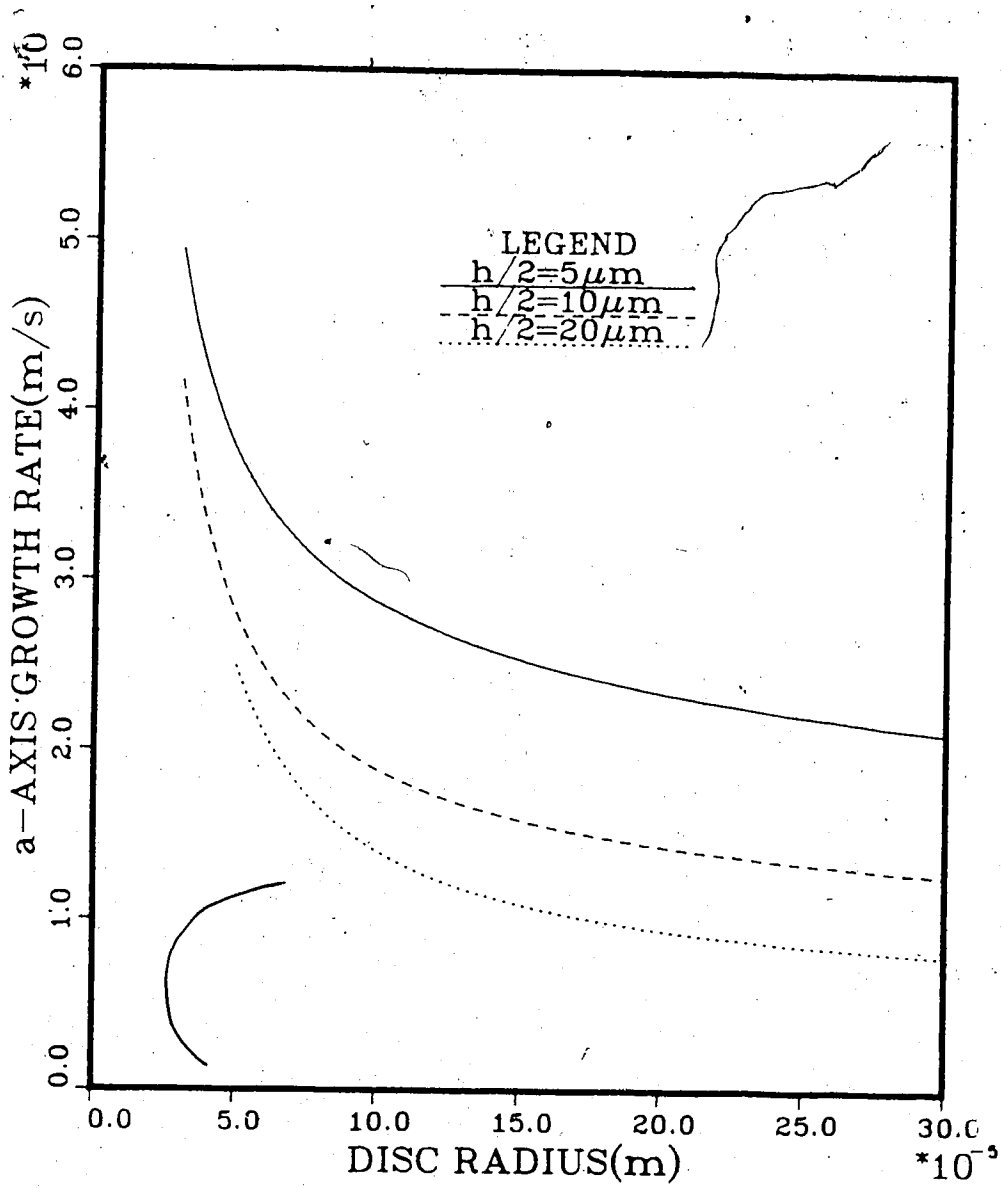


Figure 3.10: a-axis growth rates for $\Delta T = 0.05 \text{ }^\circ\text{C}$ and three constant values of disc thickness

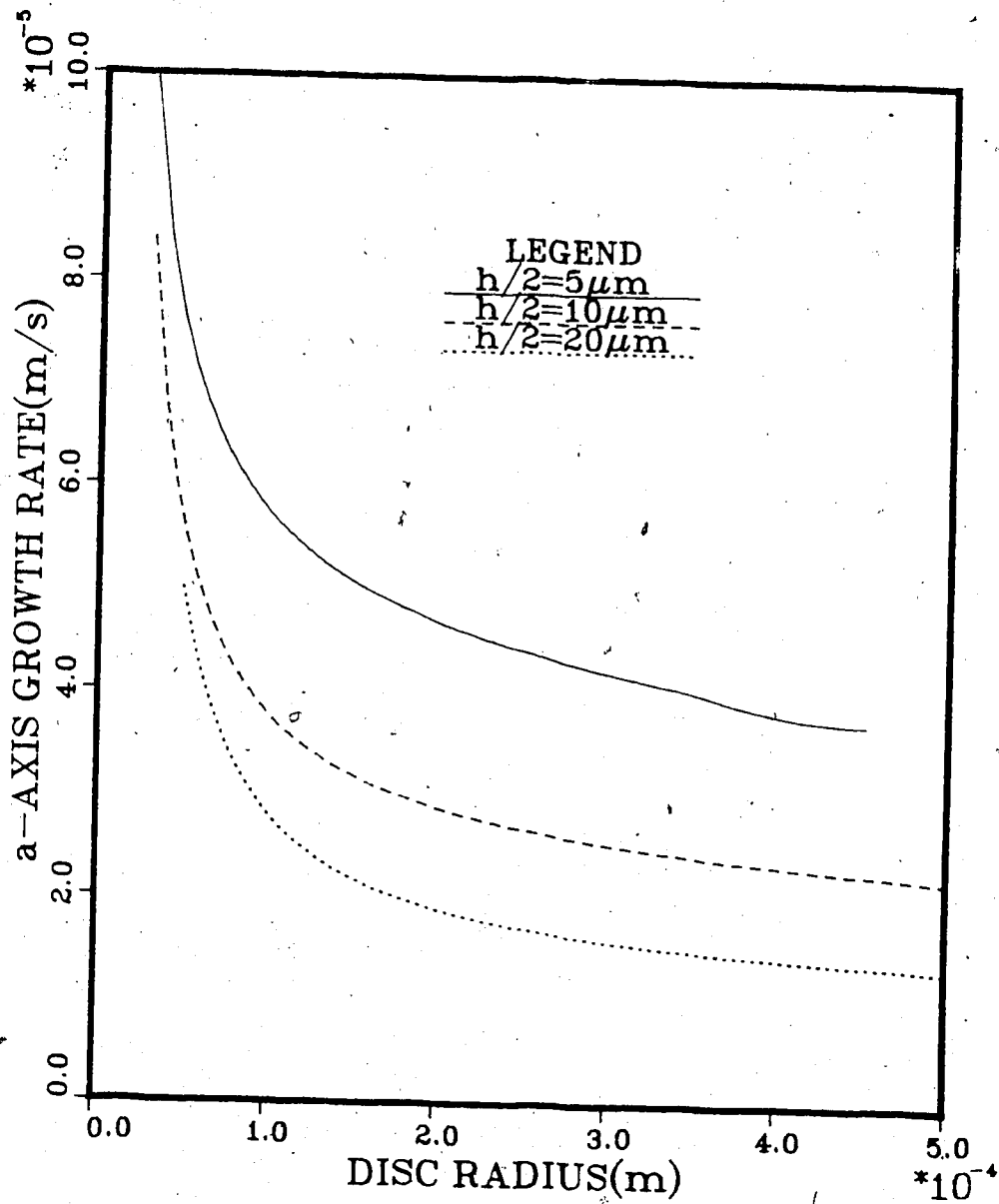



Figure 3.11: a-axis growth rates for $\Delta T = 0.10 \text{ }^\circ\text{C}$ and three constant values of disc thickness



important feature to notice is that, for a given disc radius, thinner discs tend to grow at a faster rate than the thicker ones since thinner discs are better able to dissipate latent heat from the crystal edge resulting in a higher gradient in the solid phase. This is of considerable importance particularly when considering c-axis growth because if the disc were thickening, the radial growth rate would be expected to decrease more rapidly compared to a disc growing without any thickening effects. The crystal growth rates are also observed to be higher for disc of small radii but decrease as the disc size increases. Fujioka and Sekerka [27] noted that crystal growth rates they obtained were lower than the measured values of Kumai and Itigaki [47] which they attributed to the neglect of convective heat transfer effects. From these present results, it appears that this difference is probably due to the incorrect assumption of the thermal conductivity of the ice phase equalling that of water. Another source of error in their model was that of using the growth of the centerline of the disc (which is the lowest along the edge) rather than the average growth rate.

3.1.2 TRANSIENT GROWTH OF A DISC CRYSTAL

The results for a-axis growth rates obtained so far have assumed that the crystal grows in a quasi-steady state process. By quasi-steady state, it is implied that the temperature distribution is not explicitly a function of time. Generally this assumption is employed when the solidification rate is small and approximately constant with time. In fact, this assumption has been shown to yield accurate solutions for solidification of spherical crystals and infinitely long cylindrical crystals [28]. Presently, the quasi-steady state assumption has been intuitively justified by realizing that the Stefan number for an ice water system at relatively low supercoolings was much lower than unity. In fact, for frazil ice and the typical supercoolings associated with their formation, the Stefan number is of the order

10^{-6} . In order to provide further support to the quasi-steady state assumption for frazil crystal growth and determine for which conditions it is valid, the fully transient set of equations must be solved. By a comparison of the transient and quasi-steady state solutions, we can more reasonably justify neglecting the time dependence term in Equations (2.20) and (2.21).

A transient solution is obtained for a constant thickness disc crystal immersed in a supercooled melt. The main objective of this part of the study is to determine how quickly the transient effects would dissipate. The initial crystal size is chosen to be just slightly larger than the critical radius R_{cr} and its corresponding temperature is taken as T_m , the equilibrium freezing temperature and the initial condition for the surrounding mass of water is at the uniform temperature T_∞ . These conditions can be expressed as

$$\theta(r, z, 0) = \begin{cases} 1, & \text{for } 0 \leq r < R \text{ and } 0 \leq z \leq \frac{h}{2} \\ 0, & \text{for } r > R \text{ and } z > \frac{h}{2} \end{cases} \quad (3.10)$$

This particular condition for the ice water system was chosen on the following physical grounds. Since most frazil ice crystals are initiated by the process of secondary nucleation, these secondary nuclei begin their growth phase as small fragments of ice that are broken off a larger parent crystal whose interface temperature is very close to T_m . Also, choosing the crystal size to be just slightly larger than R_{cr} would ensure that the model crystal grew.

Since the crystal is starting out at a small size, and the ratio of disc thickness to diameter is about one, a uniform nodal distribution is used in the solid region in both the radial and axial directions. A variable spaced grid is used in the liquid direction since a small number of nodes was desired. The most critical parameter found to significantly influence results was the size of the time step. Choosing too large a value results in numerical instabilities which are reflected in the smoothness

of the solution. The value for the dimensionless time step increment (used in the computer runs) ranged between $\Delta\tau = 500$ and $\Delta\tau = 2000$ which correspond to real time increments of 0.125×10^{-4} s and 0.50×10^{-3} s respectively. The smaller time step is necessary for early times in order to accurately obtain initial growth rate behaviour and is gradually increased when the growth rate approaches a quasi-steady state value. The number of nodes chosen was limited to 20 in the radial and axial directions of which 100 nodes were taken in the solid region.

Figure 3.12 and Figure 3.13 show the average growth rate and radius of disc crystals for thicknesses of $20 \mu\text{m}$, $30 \mu\text{m}$ and $50 \mu\text{m}$ and a supercooling of $0.05 \text{ }^\circ\text{C}$ as a function of time. The initial transient response of the disc results in a rapid change in growth rate which peaks at a value that is approximately of an order of magnitude larger than the quasi-steady state value. This response is due to the initial condition which sets the ice phase temperature at the melting point. As a result, the initial thermal gradients at the crystal edge interface are quite large, resulting in high growth rates. This transient effect occurs for a very short period of time of the order of 7 to 8 milliseconds at relatively small radii and as such, does not affect the subsequent radius time behaviour of the ice disc significantly. Figure 3.14 shows the radius time evolution of a $50 \mu\text{m}$ thick disc at various supercoolings. Again, the transient effects are damped quite quickly, as quasi-steady growth rates of $4.1 \mu\text{m/s}$, $8.7 \mu\text{m/s}$ and $12.5 \mu\text{m/s}$ are obtained for corresponding supercoolings of $0.01 \text{ }^\circ\text{C}$, $0.03 \text{ }^\circ\text{C}$ and $0.05 \text{ }^\circ\text{C}$ respectively. For the low supercoolings considered here, the results further indicate that the steady state growth rate is directly proportional to the supercoolings as indicated by Equation (3.7).

Before proceeding to examine c-axis growth rates for frazil ice crystals, the basis for using the quasi-steady state assumption should be recalled. Firstly, since the transient effects were observed to damp out very quickly, the long term effects of the

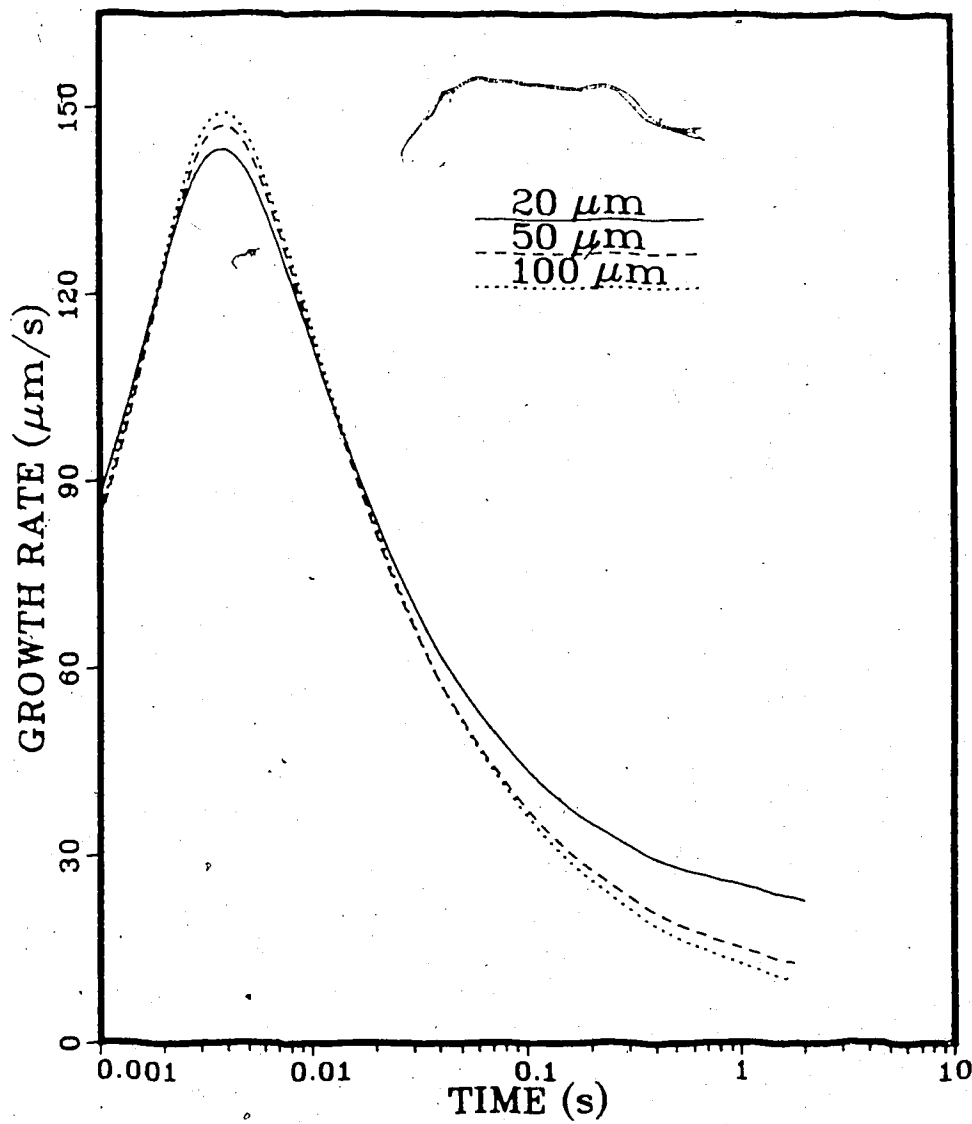


Figure 3.12: Transient growth rates for ice discs of various thicknesses exposed to water with $\Delta T = 0.05 \text{ }^\circ\text{C}$

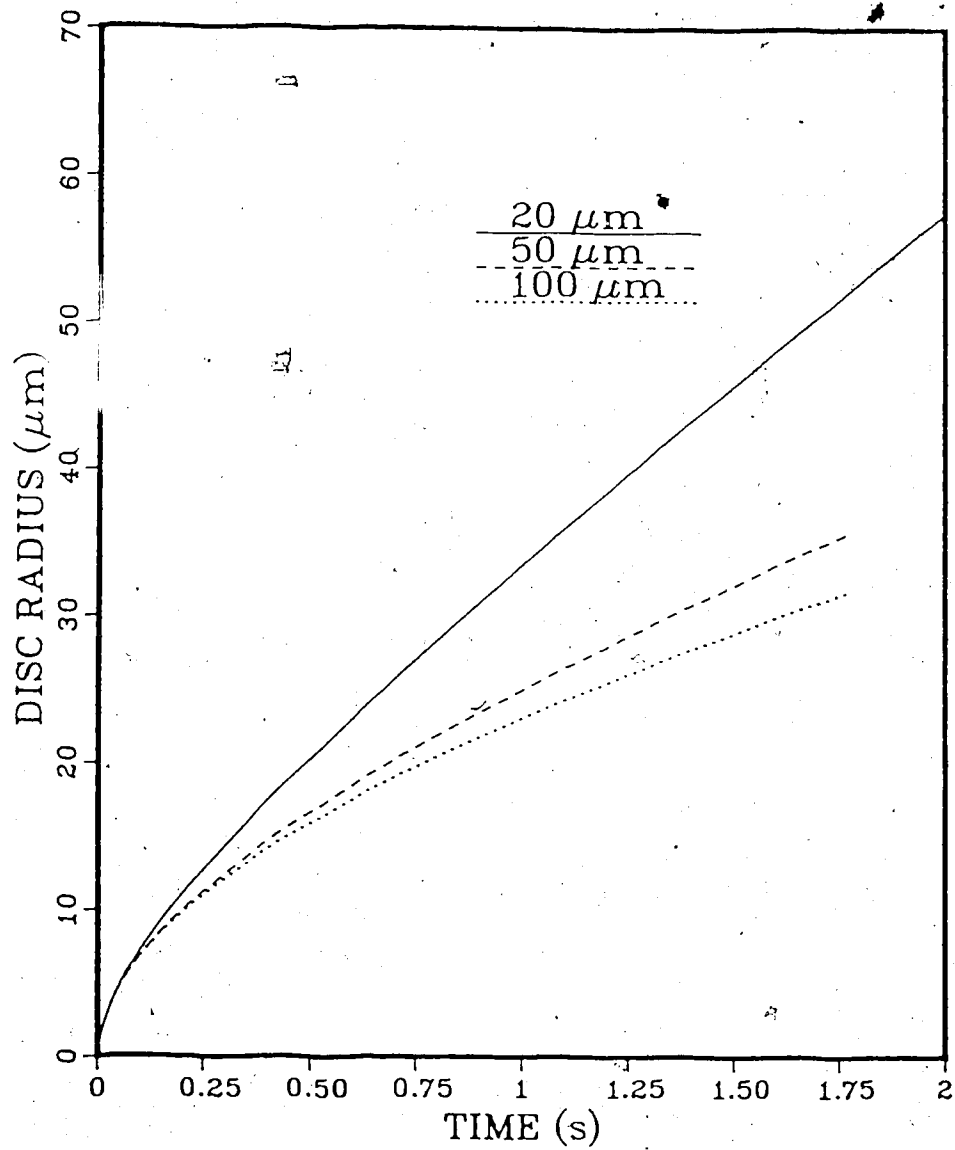


Figure 3.13: The radius-time behaviour for ice discs of various thicknesses exposed to water with $\Delta T = 0.05^\circ\text{C}$

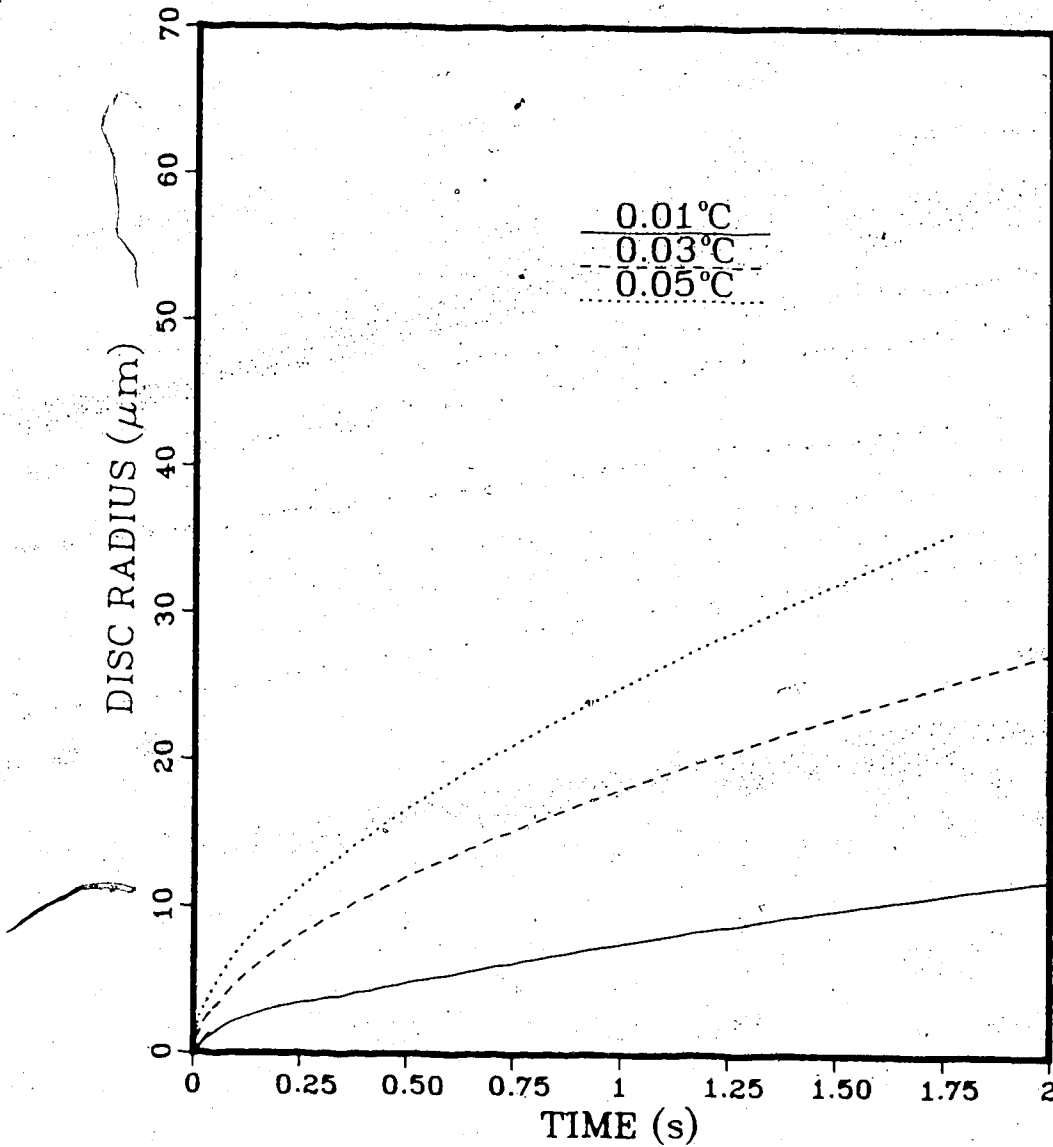


Figure 3.14: The radius-time behaviour for an ice disc 50 μm thick

initial condition on the developing temperature distribution are negligible. In fact, the initial transient effects acted over a very short time period of a few milliseconds. During this time however, the crystal can grow to a radius of 10 to 20 μm , depending on the supercooling, indicating that the quasi-steady state assumption should only be applied to crystals which have grown beyond these sizes.

3.2 GROWTH OF A DISC CRYSTAL WITH THICKENING IN A QUIESCENT SUPERCOOLED MELT

The purpose of this section is to extend the quasi-steady state model, for a-axis growth of a disc shaped crystal, to include the effects of c-axis growth perpendicular to the crystal face. It has been shown that a quasi-steady state growth assumption is applicable for frazil ice growth since the effects of the initial conditions are dissipated within the time period of a few milliseconds. Previous frazil crystal growth studies have generally ignored the thickening of frazil ice crystals assuming its rate to be very small and hence negligible when compared to the radial growth rate. At extremely low supercoolings, this is probably true but as the interfacial supercooling increases, c-axis growth also increases at a rate given by Equation (1.2). In fact, Hillig [35] has shown that for an interfacial supercooling of 0.10 $^{\circ}C$, the c-axis growth rate of an ice crystal is approximately 0.30 $\mu m/s$. Over a time frame of one minute, this can result in a thickening of 36 μm for both faces of the disc. It was shown in the previous section that the radial growth rate of a frazil ice disc decreased with increasing thickness. Therefore, even with what might appear to be insignificant thickening rates, the total increase in disc thickness over a period of time can have a significant effect. In addition, the total amount of latent heat released along the two

faces of the crystal can also be of importance.

Throughout the remaining course of this study, it will be assumed that the interfacial kinetics for growth in the c-axis direction will be due to the mechanism of surface nucleation and will progress according to Equation (1.10). The values to be used for the coefficients μ_1 and μ_2 are contained in Table 1.1. We will use the experimental values obtained by Hillig rather than his values which have been modified to incorporate the actual interface temperature. It was shown in Chapter 1 that Hillig's experimental relation yielded c-axis growth rates almost identical to those obtained using Sperry's relation for the range of supercoolings associated with frazil growth. It is not desirable to use a c-axis growth model in the form determined by Sperry because it is not well suited to iterative schemes. As mentioned earlier, it involves the use of two different correlations with each correlation only valid over a given range of supercooling. Hillig's relation, on the other hand, is in a form that is easier to apply to the numerical procedure.

Substituting Hillig's relation (1.3) for c-axis growth into the expression for the energy balance along the basal plane of the disc gives the nonlinear boundary condition

$$\rho L \mu_1 e^{\mu_2/\Delta T_k} = k_s \left. \frac{\partial T}{\partial z} \right|_{z=\frac{h}{2}^-} - k_l \left. \frac{\partial T}{\partial z} \right|_{z=\frac{h}{2}^+} \quad (3.11)$$

This equation is to be solved in conjunction with the heat conduction equation to determine the maximum interface supercooling on the basal plane surface. From this maximum basal supercooling, the rate of thickening of the crystal is computed. Again, we emphasize the importance of accurately computing the temperature distribution within the solid phase region, since the solidification rate in the c-axis direction is highly dependent on the basal plane supercooling ΔT_k .

Several numerical parameters such as the number of nodes for mesh discretization and their positioning, concentration of nodes near the interfaces and location of the

outer boundary had to be determined for the disc thickening case. Since the geometry of this problem is not significantly different from the previous case, quantities such as the number of nodes to employ need not be changed and nodal distributions in the radial and axial directions need not be re-evaluated. The major difference between this model and the a-axis growth model is the additional latent heat released along the two faces of the crystal and the slightly higher heat released along the disc edge due to its increased area. It was thought that the influence of the higher latent heat release would act in the vicinity of the crystal and generally would not affect the far field isotherms. As a result, the previously established criteria for the location of the outer boundary can be employed for the disc thickening case. It is felt that this assumption is probably valid at the relatively low supercoolings for which the crystal morphology is discoid.

3.2.1 QUASI-STEADY STATE c-AXIS GROWTH MODEL RESULTS

The influence of growth in the c-axis direction for a frazil ice crystal leads to increased latent heat release into the surrounding water. The effect this has on the temperature near the vicinity of the growing solid-liquid interfaces can best be determined by examining crystal growth rates and resulting crystal sizes. The increased latent heat release for the ice crystal arises from two sources. The first of these is the latent heat of solidification released during the thickening process of the disc and the second is due to the increase in area of the crystal edge due to the increase in disc thickness. Just as the radial growth of the crystal depends on its thickness, the thickness of the crystal is dependent on the crystal size. When the disc radius is very small, it is generally cylindrical in shape and its temperature is relatively constant throughout, equivalent to that at the edge interface. At this stage, the interfacial cooling on the basal plane is very small since the entire disc is

approximately the same temperature throughout. Furthermore, being close to the edge interface of the disc keeps the basal plane warm. As the diameter of the ice disc increases, the interfacial supercooling ΔT_k also increases. When ΔT_k reaches a threshold value, initial growth in the c-axis direction begins. Further increases in the interfacial undercooling result in thickening of the crystal at even higher rates. Prior to this though, there had been no latent heat released from the disc face but as solidification occurs in the axial direction of the disc, the surrounding fluid begins to warm up and acts to decrease the basal plane supercooling. As a result, one would expect a local maximum in the c-axis growth rate. Another important factor controlling the thickening rate of a frazil ice crystal is the overall supercooling. Since it is not physically possible to measure the interfacial supercooling ΔT_k , it is usually desirable to determine the applied supercooling ΔT which gives an appreciable c-axis growth rate.

The c-axis growth rate for an ice disc of initial size $R_o = 30\mu m$ and $h/2 = 10\mu m$ is shown in Figure 3.15 for ΔT varying between $0.05^\circ C$ and $0.25^\circ C$. Although supercoolings higher than $0.15^\circ C$ probably do not result in a disc morphology and are physically unrealistic for frazil growth conditions, they have been included here to emphasize the rather substantial effect they have on c-axis growth rates. One important observation made from Figure 3.15 is that for supercoolings less than $0.05^\circ C$, the thickening rate for the ice crystal is virtually nonexistent. For higher applied supercoolings, the solidification rate in the c-axis direction increases astoundingly to a maximum value of $1.6 \mu m/s$ with $\Delta T = 0.25^\circ C$. Another important aspect observed is that disc thickening rates increase to a maximum value which remains constant over a relatively short period of time. The crystal thickens at this maximum value until the latent heat release along the basal plane surface decreases ΔT_k , at which point, the c-axis growth rate also decreases. The length of

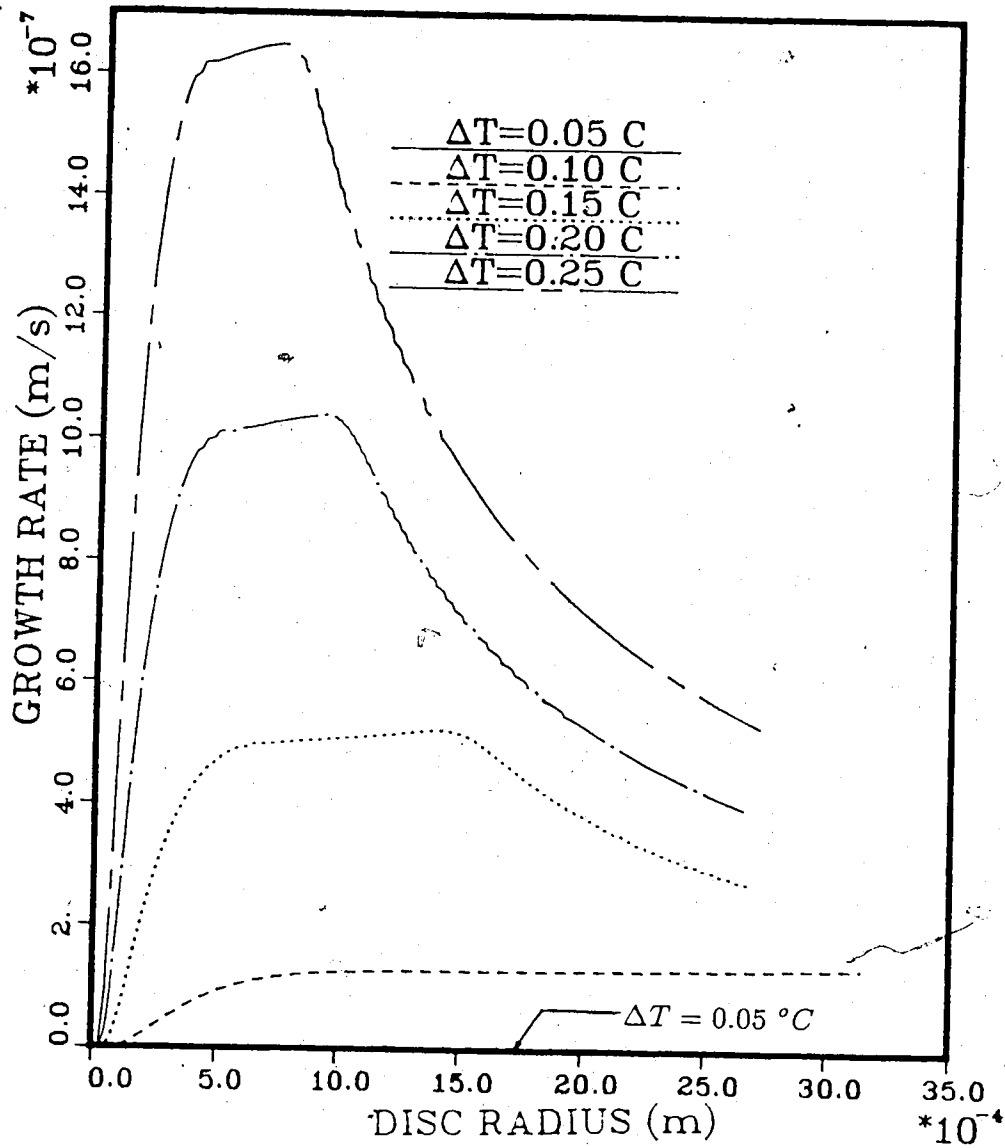


Figure 3.15: c-axis growth rates for ice discs at various supercoolings with initially $R = 30\mu\text{m}$ and $h/2 = 10\mu\text{m}$. Note that the c-axis growth rate is virtually nonexistent for $\Delta T = 0.05^\circ\text{C}$ and therefore cannot be differentiated from the horizontal axis of the graph.

time for which the disc thickens at its maximum rate is seen to be dependent on the bulk supercooling ΔT . For $\Delta T = 0.10$ °C, the c-axis growth rate reaches its maximum value and continues to grow at this constant rate without decreasing, over the range of sizes computed, indicating that the latent heat release due to thickening is not sufficient to warm the basal plane. For higher values of bulk supercooling however, the latent heat release from the disc face is of sufficient magnitude to retard the rate of thickening, as is seen from the decrease in the curves of Figure 3.15.

The corresponding basal plane undercooling is plotted in dimensionless form as a function of disc radius in Figure 3.16. For supercoolings of 0.10 °C and lower, the basal plane temperature at $r = 0$ and $z = h/2$ decreases from its initial value of $\theta = 0.88$ to a constant value of approximately $\theta = 0.60$. For higher values of ΔT , the quantity θ_B (maximum dimensionless basal plane undercooling) decreases to its minimum value, at which time its thickening rate is a maximum, and then begins to rise due to the latent heat release. The time at which this minimum occurs is earlier for increasing values of ΔT confirming the assertion that the quantity of latent heat release has a retarding effect on the thickening rate.

The corresponding growth rates in the radial direction are shown in Figure 3.17. Here the characteristic dependence of radial growth rate on crystal size is observed to be the same as for the constant thickness case. The major difference between the thickening and constant thickness cases is that the radial growth rate decreases more rapidly for a disc with thickening included. This effect is caused by the excess latent heat released from the edge due to its increased thickness. The latent heat release from the basal plane is not of sufficient magnitude to retard the edgewise growth rate significantly. For $\Delta T = 0.10$ °C, we see that the latent heat release from the basal plane is negligible but the a-axis growth rate at a disc diameter of 1 mm is reduced from 22 $\mu\text{m/s}$, for the constant thickness case, to 19 $\mu\text{m/s}$ with thickening included.

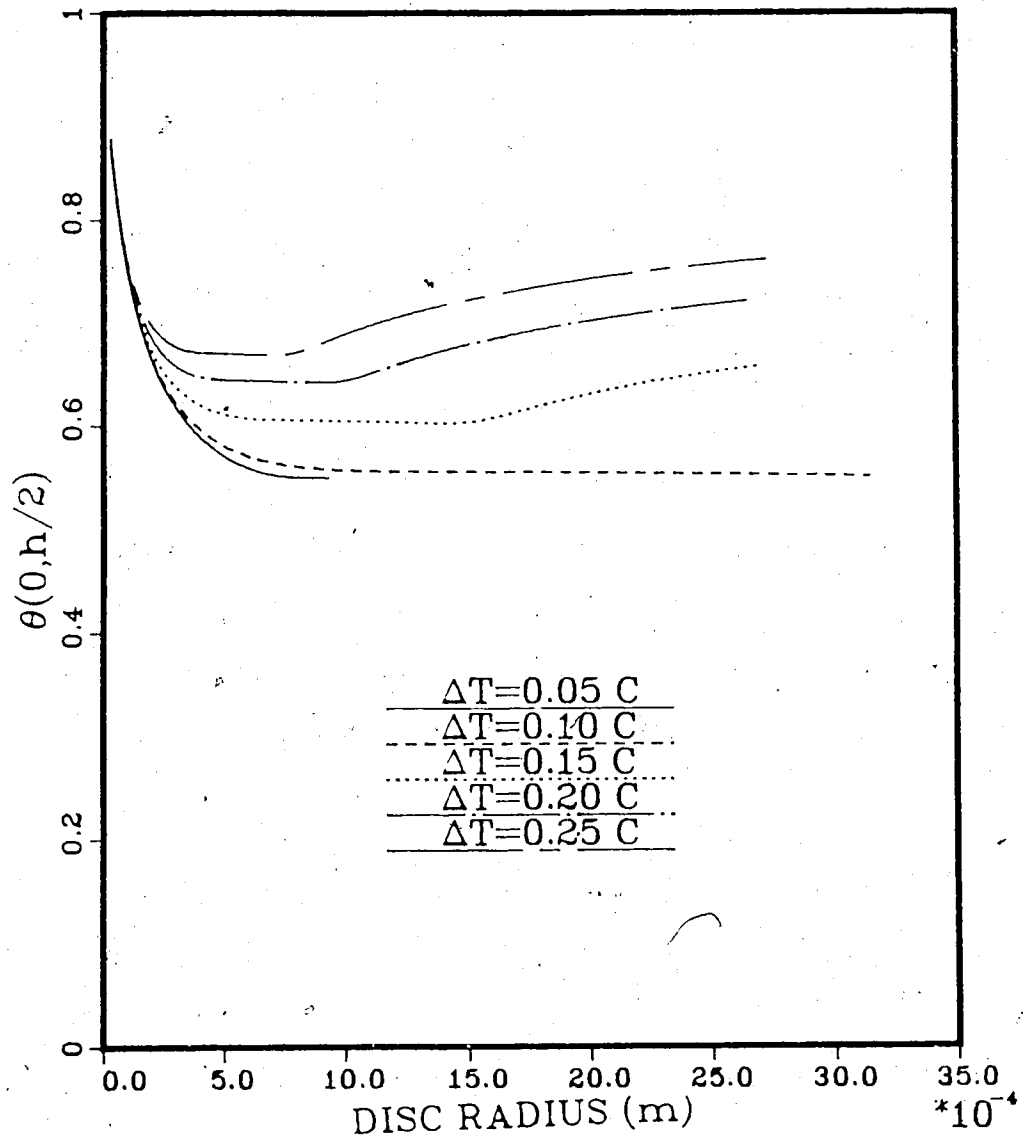


Figure 3.16: Dimensionless temperature at the center of the basal plane ($r = 0, z = h/2$) for several values of ΔT

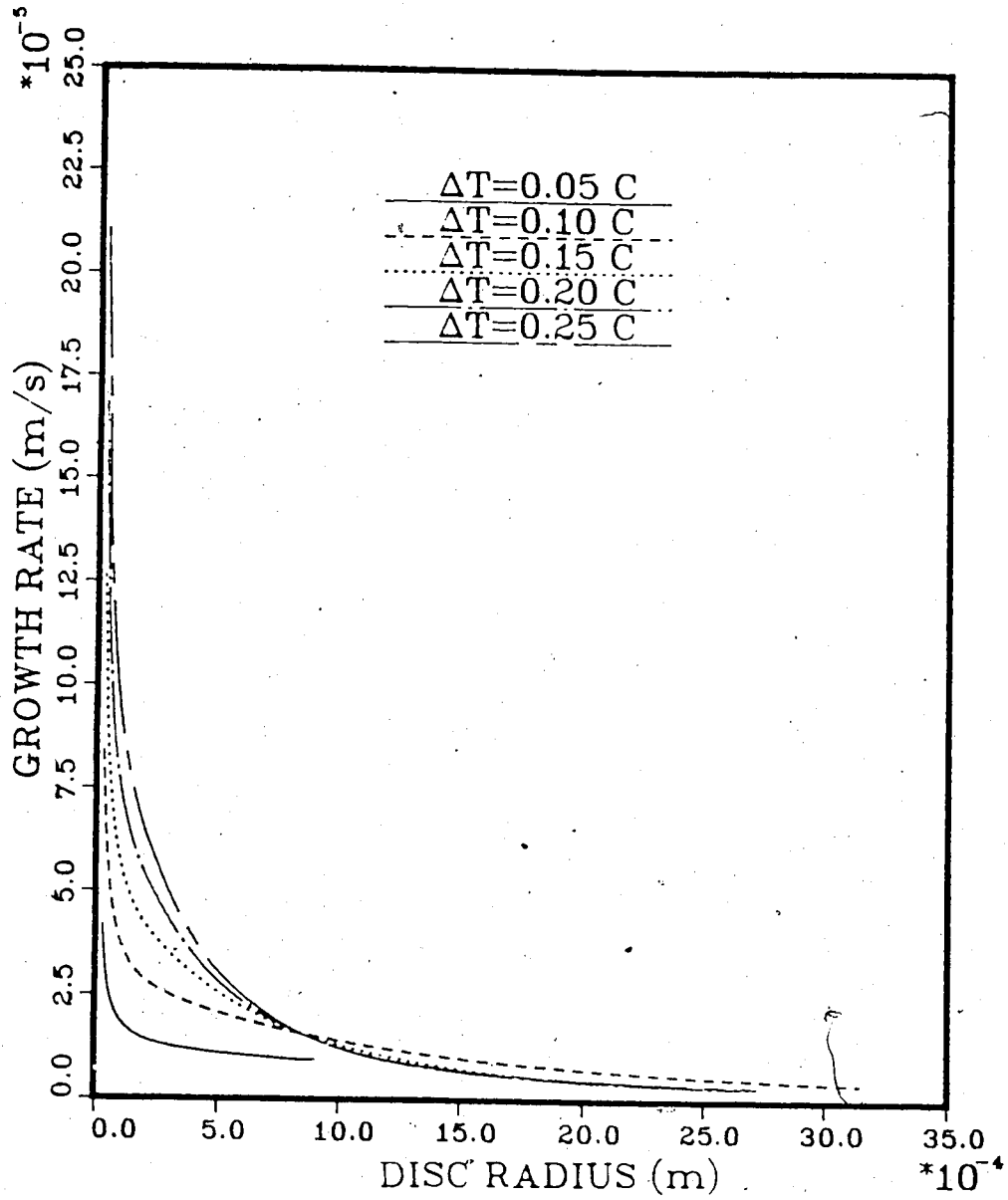


Figure 3.17: a-axis growth rates for ice discs at various supercoolings with initially $R = 30\mu\text{m}$ and $h/2 = 10\mu\text{m}$

These effects are more noticeable at the higher supercoolings although reasonable comparisons cannot be made since the crystal growth rate for the constant thickness case never reached a near steady state value due to numerical difficulties associated with disc aspect ratios falling below 0.01. For $\Delta T = 0.10\text{ }^{\circ}\text{C}$, the disc thickness has increased from $10\text{ }\mu\text{m}$ to $12\text{ }\mu\text{m}$ by the time the disc has reached 1mm in diameter. This difference in growth rates would be more significant at larger radii since the corresponding disc thickness would also have increased. The discrepancy in growth rates for supercoolings higher than $0.10\text{ }^{\circ}\text{C}$ would be even more substantial since the latent heat release would be higher.

Another point to note in Figure 3.17 is that the thickening of the crystal causes the radial growth rate to decrease as applied supercooling is increased. We see that the radial growth rate is slightly lower for $\Delta T = 0.15\text{ }^{\circ}\text{C}$ than for $\Delta T = 0.10\text{ }^{\circ}\text{C}$. This is contrary to what one would expect for ice discs with a constant thickness where, the a-axis growth rate always increases proportionately with an increase in the applied supercooling. The observed trends with thickening included are in fact consistent with what is physically expected, namely that the thicker discs have lower growth rates compared to the thinner ones. At higher supercoolings, the disc thickening rate increases resulting in a higher latent heat release. This eventually retards the radial growth rate sufficiently so that discs growing at a lower applied supercooling have higher radial growth rates than discs growing at higher levels of supercooling.

The corresponding increase in the disc radius over the same period of growth as Figure 3.17 is shown in Figure 3.18. The variation in disc thickness over this time period is plotted as a function of crystal size in Figure 3.19. From Figure 3.19, it can be seen that the increase in disc thickness can be quite large over a period of time. For example, the thickness increases from $10\text{ }\mu\text{m}$ to approximately $50\text{ }\mu\text{m}$ for a supercooling of $0.20\text{ }^{\circ}\text{C}$ and an increase in radius of 0.97 mm . This increase in

l

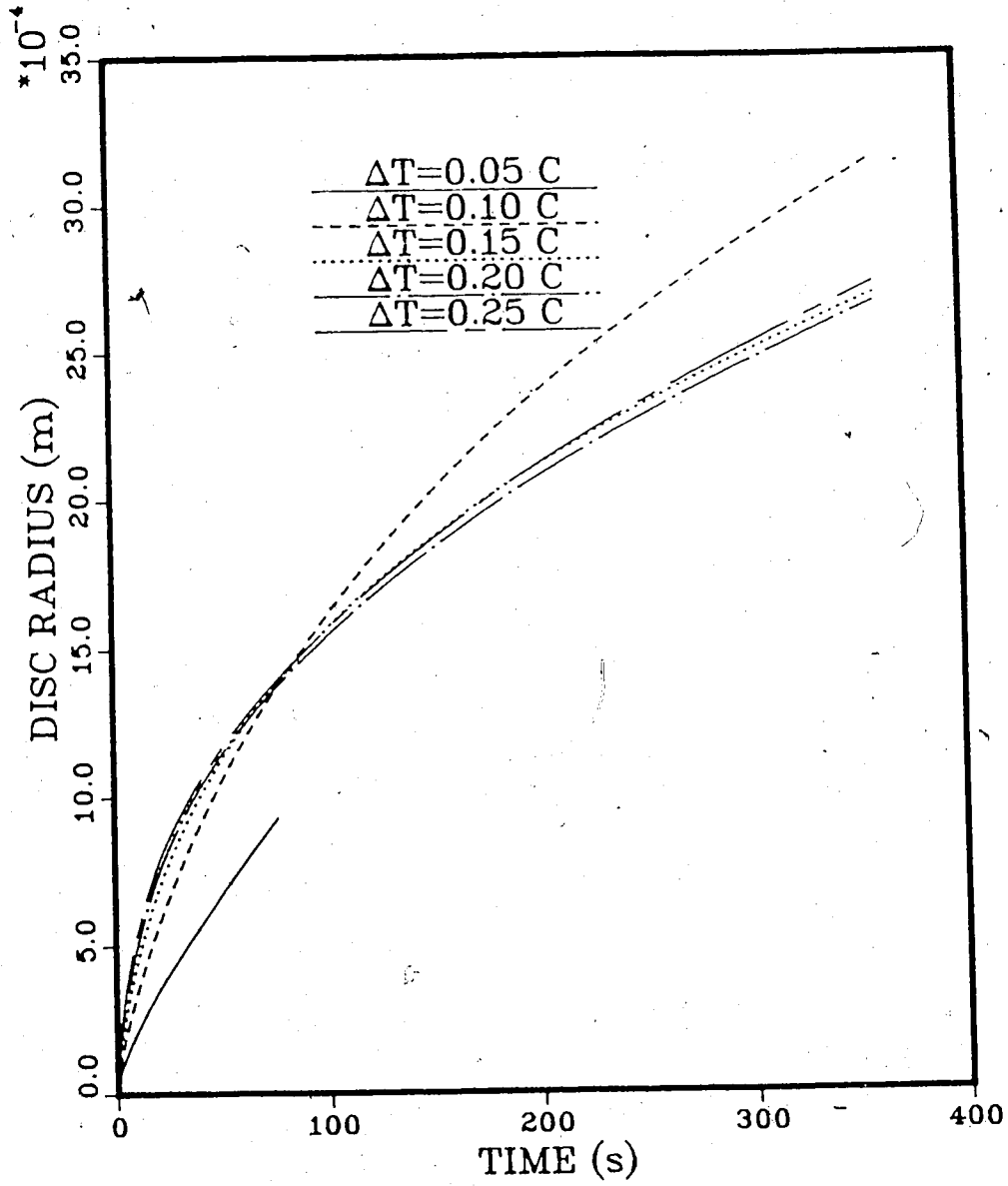


Figure 3.18: Increase in radius of a frazil ice disc for various supercoolings

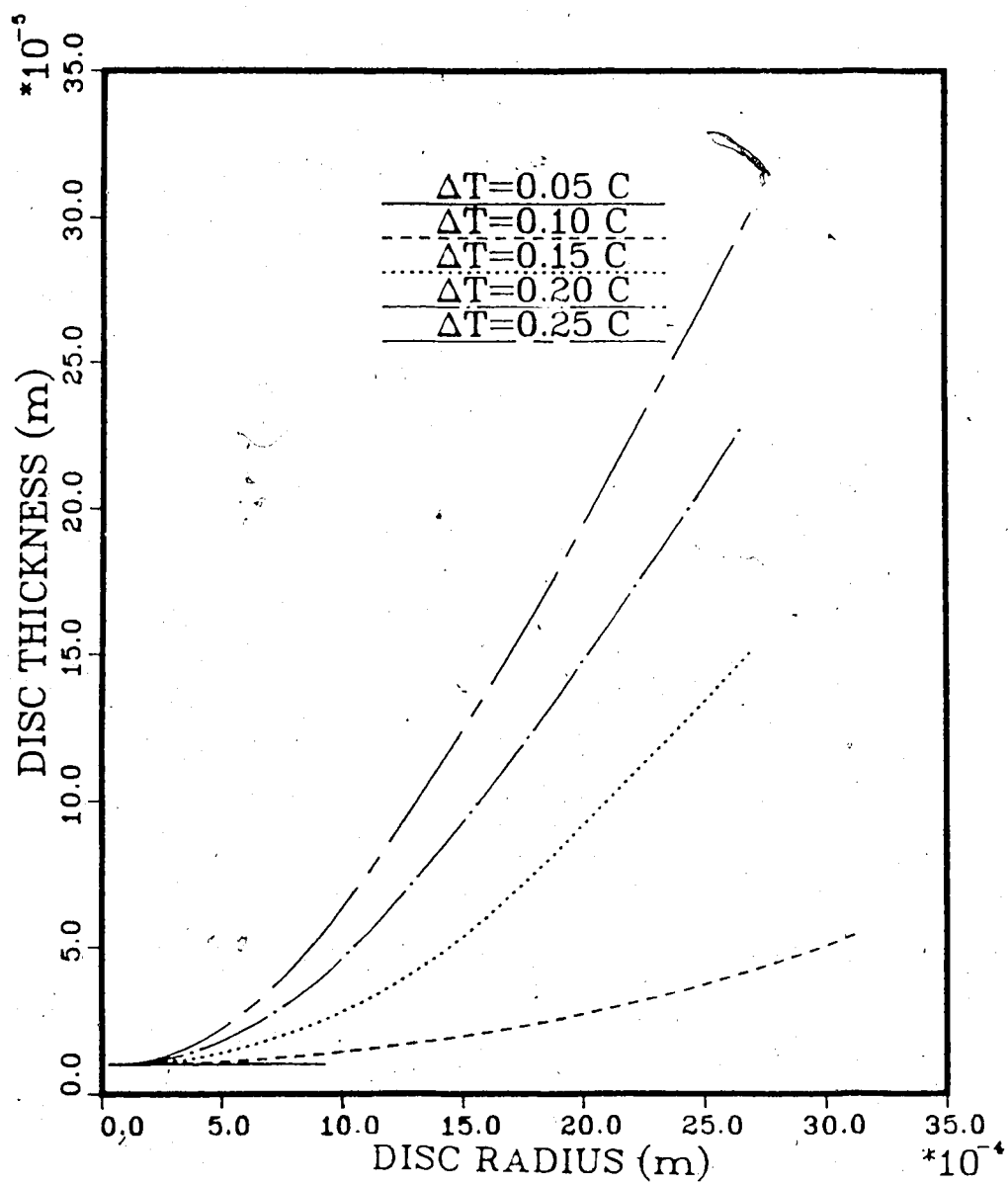


Figure 3.19: Increase in thickness of a frazil ice disc for various supercoolings

thickness was not as significant for the lower supercoolings. For $\Delta T = 0.05^\circ\text{C}$ the disc thickness remained at a constant value of $10\ \mu\text{m}$ and for $\Delta T = 0.10^\circ\text{C}$, the increase in thickness $h/2$ was approximately $2.5\ \mu\text{m}$. Since the increase in thickness is significantly larger for higher supercoolings, it is of interest to note that the increase in radius for $\Delta T = 0.10^\circ\text{C}$ is considerably higher than the other supercoolings as seen in Figure 3.18. Naturally for $\Delta T = 0.05^\circ\text{C}$, the increase in disc radius is not very high since dR/dt is considerably lower than the other supercoolings. As a result, the overall size of a frazil crystal depends not only on the applied supercooling, but also on the two competing forces of interfacial undercooling on the disc face and the latent heat release.

Figures 3.20 and 3.21 show the a-axis growth rate of ice discs with initial thicknesses of $5\ \mu\text{m}$, $10\ \mu\text{m}$, $20\ \mu\text{m}$ and $25\ \mu\text{m}$ for supercoolings of 0.08°C and 0.10°C respectively. The corresponding c-axis growth rates are shown in Figures 3.22 and 3.23. Both these sets of results indicate that the radial growth rate of ice crystals collapses to a single curve when the disc radius is approximately 1 mm regardless of the initial thickness. The basic conclusion to draw from this is that frazil crystal, if given sufficient growing time, will grow to the same thickness for a constant applied supercooling as shown in Figures 3.22 and 3.23. The reason for this is that thinner discs will have higher radial growth rates resulting in a faster reduction in the basal plane interfacial undercooling as compared to thicker discs shown in Figures 3.24 and 3.25. As a result, the thinner discs will have higher thickening rates. The increase in thickness, however will act to retard the radial growth rate. In the end, these same competing factors mentioned above will result in thicker discs although to a lesser degree. Consequently, the final result will be that discs with varying thicknesses initially will grow to a constant size and thickness. Figures 3.24 and 3.25 also indicate that the largest diameter discs are also the thickest, an argument supported from

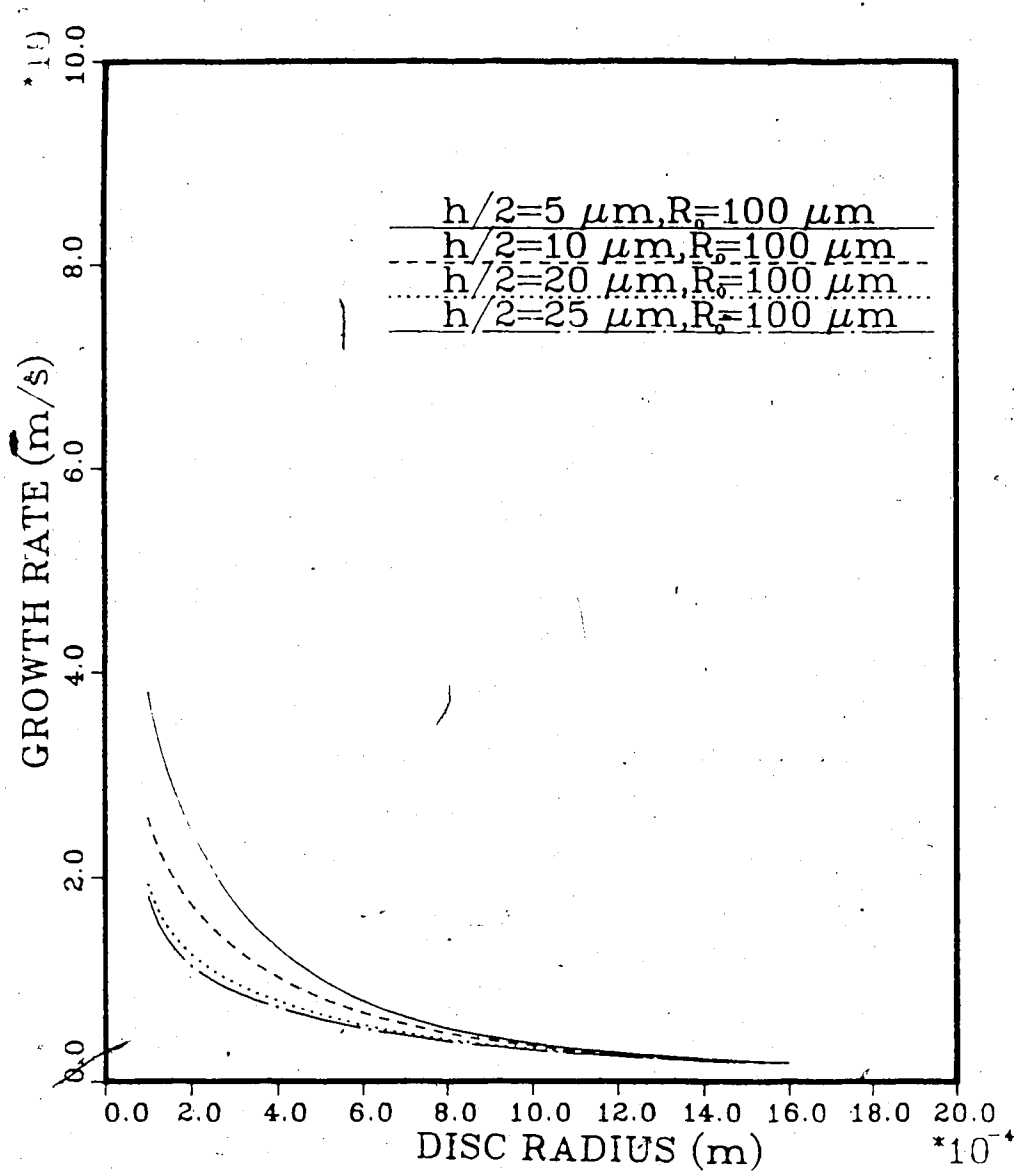


Figure 3.20: a-axis growth rates of frazil crystals of different initial thicknesses and $\Delta T = 0.08^\circ\text{C}$

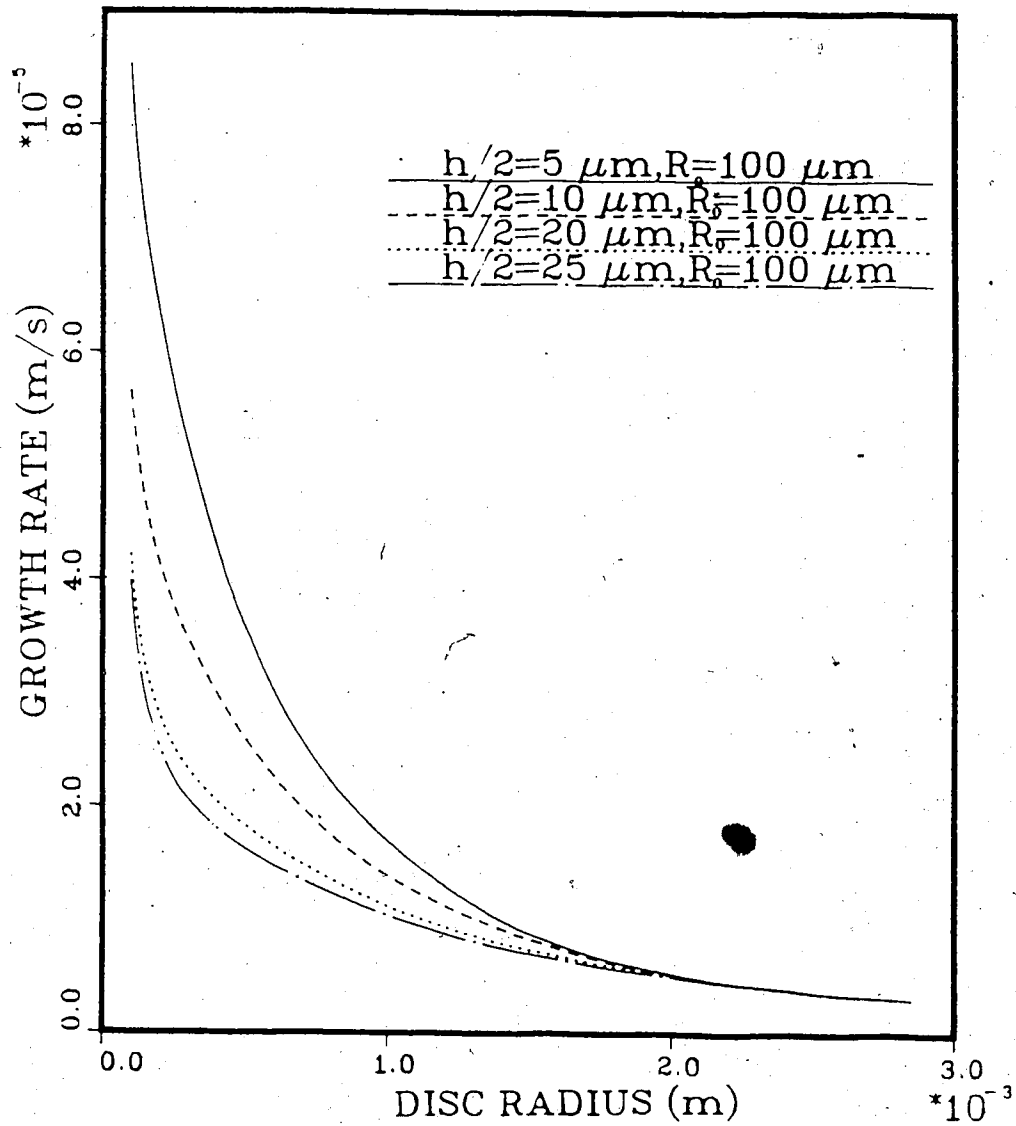


Figure 3.21: a-axis growth rates of frazil crystals of different initial thicknesses and $\Delta T = 0.10 \text{ }^\circ\text{C}$

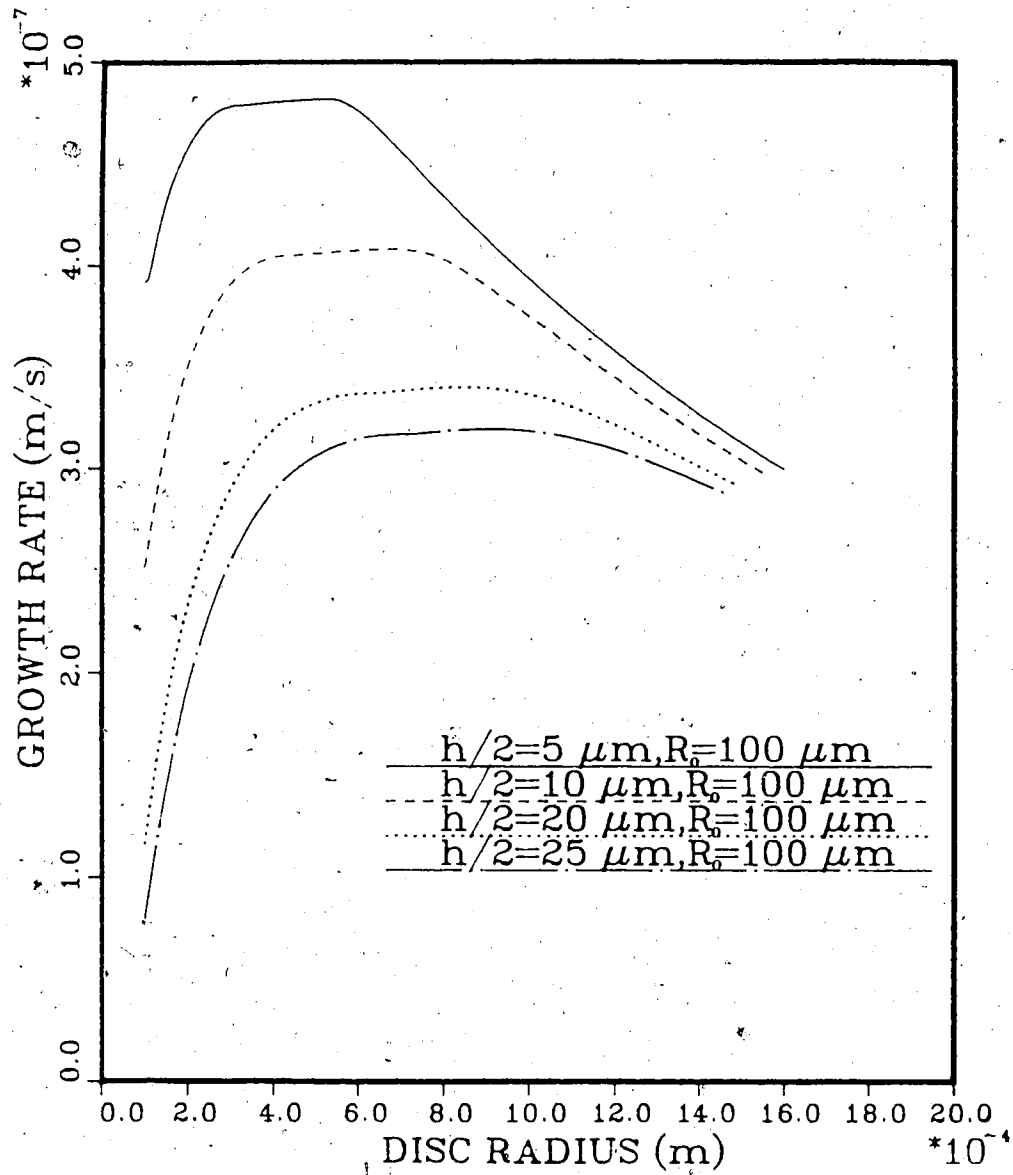


Figure 3.22: c-axis growth rates of frazil crystals for different initial thicknesses and $\Delta T = 0.08 \text{ }^\circ\text{C}$

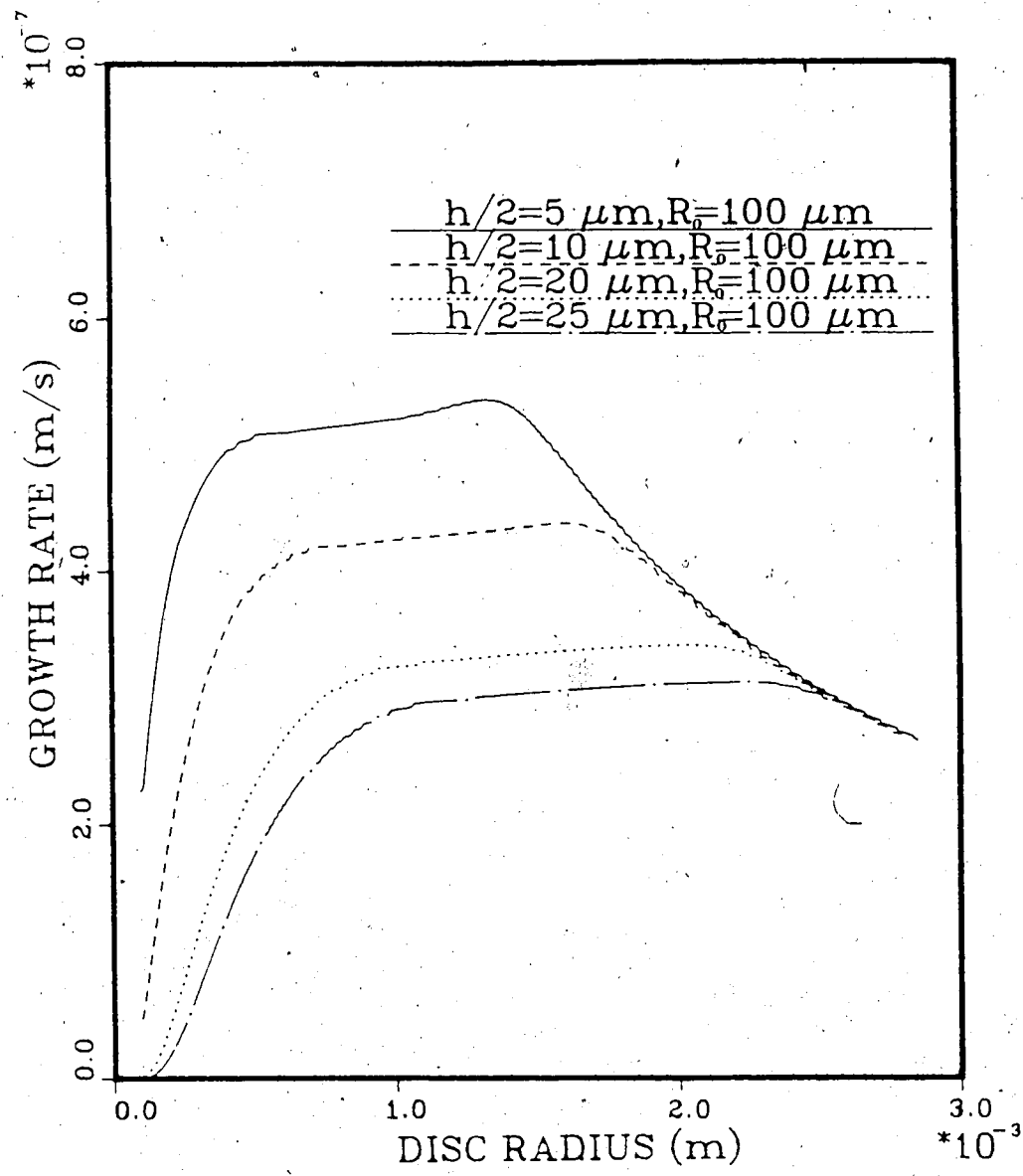


Figure 3.23: a-axis growth rates of frazil crystals for different initial thicknesses and $\Delta T = 0.10^\circ C$

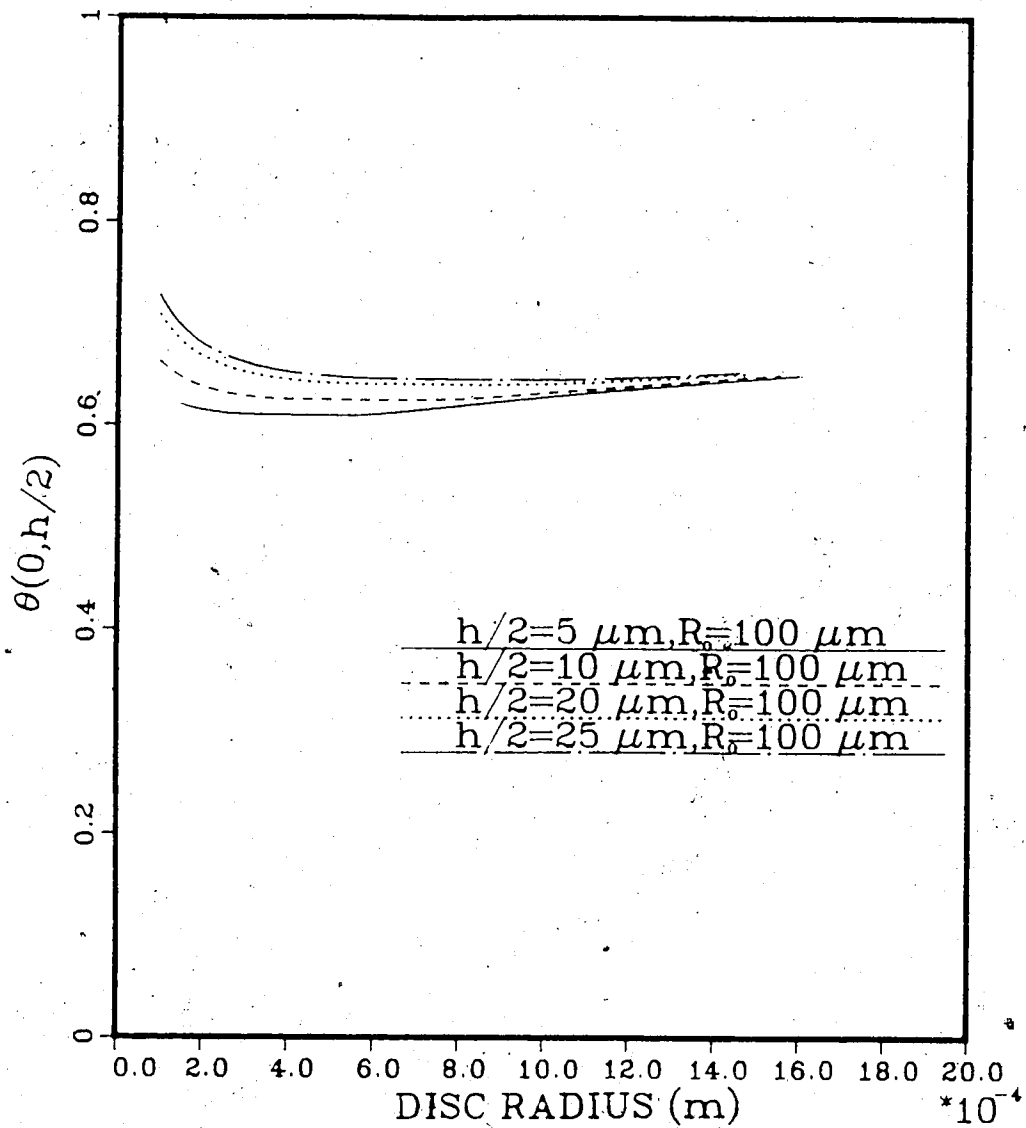


Figure 3.24: Temperature at the basal plane ($r = 0, z = h/2$) for different initial thicknesses and $\Delta T = 0.08 \text{ }^\circ\text{C}$

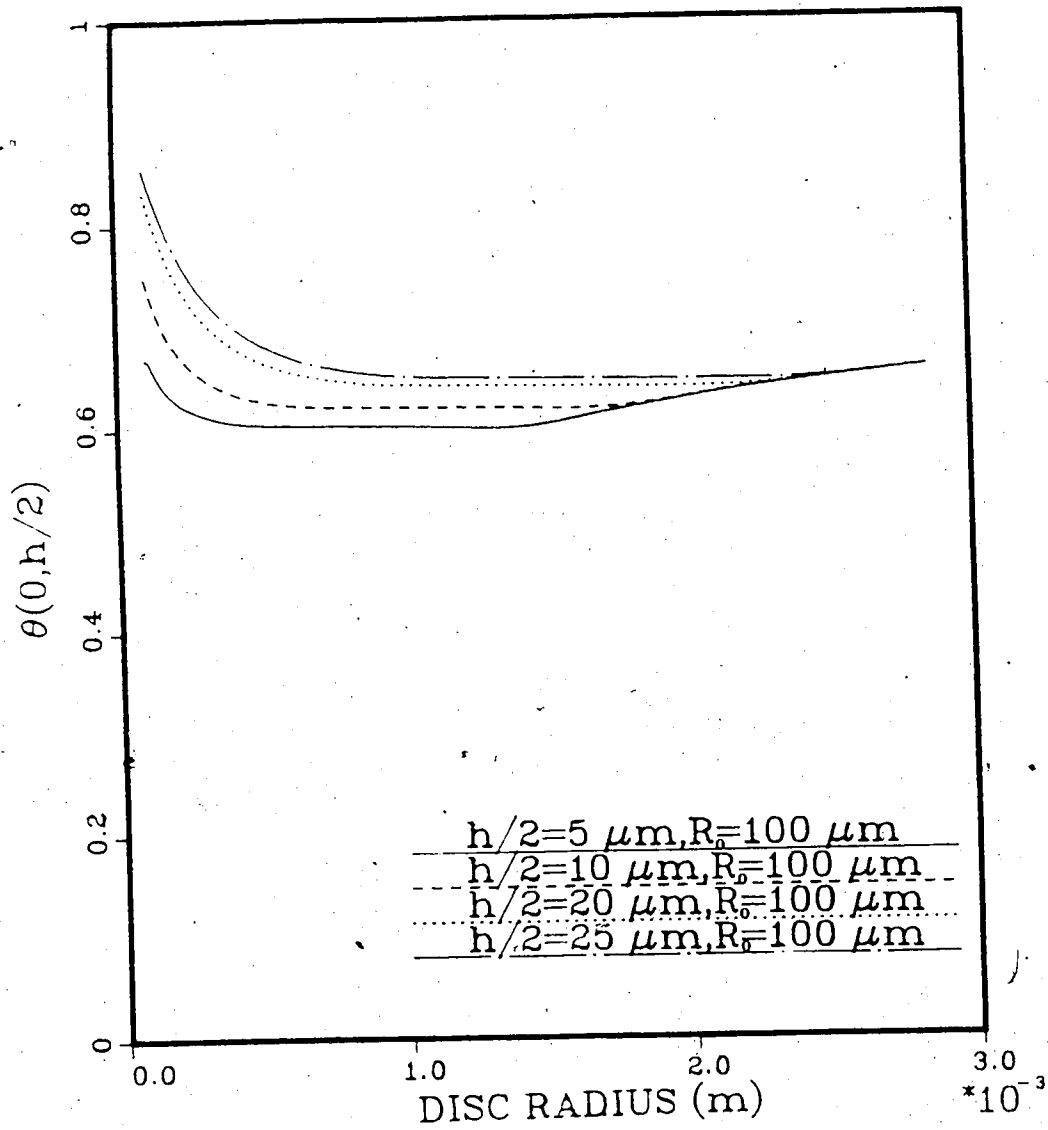


Figure 3.25: Temperature at the basal plane ($r = 0, z = h/2$) for different initial thicknesses and $\Delta T = 0.10 \text{ }^\circ\text{C}$

experimental observations by Bukina [13].

Summarizing the results of this chapter, we see that the numerical procedure employed provided a reasonably accurate solution of the frazil ice growth problem. In addition, the validity of the quasi-steady state assumption for frazil growth studies was also demonstrated. So far all the results of this chapter have resulted from assuming that relative motion between the ice and water components was negligible so that the heat transfer rates into the melt could be modelled as conduction. Although this is a reasonable assumption however in reality, frazil is generally formed in turbulent bodies of water.

Methods for including the effects of turbulence and its influence on heat transfer rates are the subject of the next chapter.

Chapter 4

GROWTH OF FRAZIL CRYSTALS IN A TURBULENT FLUID

A model considering growth of an ice disc in an infinite quiescent fluid is physically unrealistic since frazil accumulations almost always occur in turbulent bodies of water. The source of the turbulence can result from wind and flow conditions for lakes and rivers or mechanical agitation for industrial crystallizers. The turbulence intensity can depend on several factors, of which few are well researched or documented. In this section, the existing model will be further extended to include the effects of turbulence so that its influence on crystal growth rates may be assessed. The anticipated effects are increased growth rates in both the a-axis and c-axis directions due to higher rates of latent heat dissipation.

The major objective of this chapter is to evaluate some standard methods for including the effects of turbulence. Specifically, we would like to compare the stagnant layer concept for modelling turbulence intensity with other traditional turbulence representation models. In particular, we want to evaluate the feasibility of using empirical heat transfer relationships for approximating the portion of latent heat released to the surrounding turbulent liquid. The analysis of growth in a turbulent fluid is further extended to situations where the supercooling is time dependent.

4.1 EFFECT OF FLUID TURBULENCE ON CRYSTAL GROWTH

Before proceeding to describe methods for incorporating turbulence effects, a brief background on fluid turbulence characteristics is presented. Fluid turbulence can be

visualized as numerous interacting eddies or vortex tubes of various length scales. The largest sized eddies result from instabilities in the mean flow. The scale and orientation of these eddies is strongly dependent upon the geometry of the flow and its constraints. Some typical examples of large eddy length scales are as follows. In a large stirred tank, such as a crystallizer, the largest eddies are of the order of the impeller width. For river or channel flow, the large scale eddies are limited by the channel width or depth. In large, open bodies of water such as lakes, it is difficult to determine the scale of the large eddies since the turbulence is generated by some external, variable agent such as agitation of the water surface by wind generated shear forces.

The Kolmogorov Theory of Isotropic Turbulence states that "the energy contained in the large scale eddies cascades through the entire spectrum of eddy sizes to the smallest sized eddies until it is dissipated by fluid viscosity". The spectrum of eddy sizes can be classified into four main categories. The first of these consists of the largest scale eddies resulting from instabilities in the bulk flow. These large scale eddies are responsible for the generation of turbulence energy. The second category contains eddies of a slightly smaller scale which are responsible for transporting the turbulence energy down to the smallest scale eddy sizes where the energy is eventually dissipated. The third category is classified as the inertial subrange and contains eddies of length scale larger than the dissipation scale but smaller than the scale of the large energy-containing eddies. Dissipation of the turbulence energy begins at this stage by the inertial interaction of different size eddies. The final category is the viscous dissipation range and contains eddies of the smallest length scale. Fluid viscosity plays an important role in this regime by quickly damping and dissipating the remaining turbulence energy. These smallest size eddies have no memory of the mean flow orientation and are said to be locally isotropic. This energy cascade is

illustrated schematically in Figure 4.1. The fundamental assumption made in the Kolmogorov Theory is that turbulence is in local equilibrium; production from the Reynolds stress-mean shear interaction is balanced by the continuous destruction of turbulence by viscous dissipation. The kinetic energy per unit mass of fluid contained in large scale eddies is proportional to u_s^2 , where u_s is the eddy velocity. The time scale in which this energy is dissipated is proportional to u_s/l , where l is the length scale of the large eddies. From this, the rate of turbulence energy production P is estimated to be u_s^3/l , which is usually expressed in units of Watts/kg. Therefore, the rate of dissipation is defined to be

$$\epsilon \sim \frac{u_s^3}{l} \quad (4.1)$$

The scale of the smallest eddies, which are dissipated by viscosity, were estimated by Kolmogorov to be

$$\eta_k \sim \left(\frac{\nu^3}{\epsilon} \right)^{1/4} \quad (4.2)$$

where η_k is referred to as the dissipation scale or Kolmogorov scale and ν is the fluid kinematic viscosity.

The last two categories in the spectrum of eddy sizes (inertial subrange and viscous dissipation), exhibit a universal character when plotted as function of the wave number φ (reciprocal of the wavelength). This implies that the turbulence energy spectrum is shape-preserving, provided ϵ and ν remain constant. The range of eddy sizes over which this occurs is referred to as the universal equilibrium range. A typical turbulence energy spectrum is shown in Figure 4.2. It is noted that the slope of this curve is $-5/3$ in the inertial subrange region and -7 in the viscous dissipation region. These characteristic slopes have been observed for the turbulence energy spectra for a variety of turbulent flows.

Typical values for l in rivers and lakes is of the order 0.1 m and velocity fluctuations

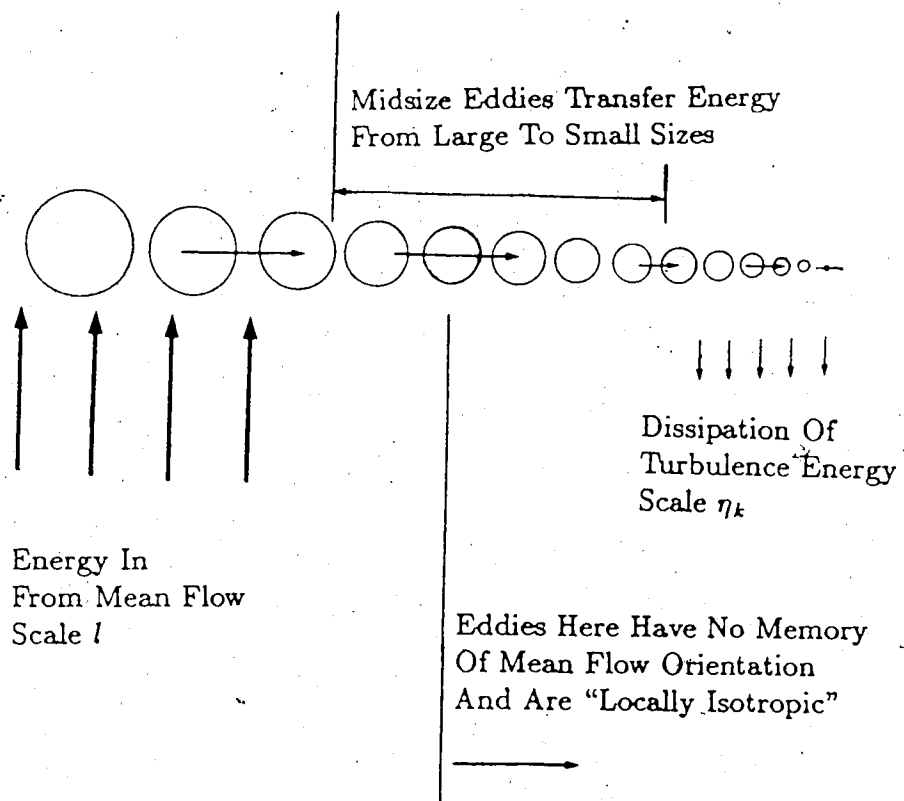


Figure 4.1: Schematic representation of the turbulence energy cascade

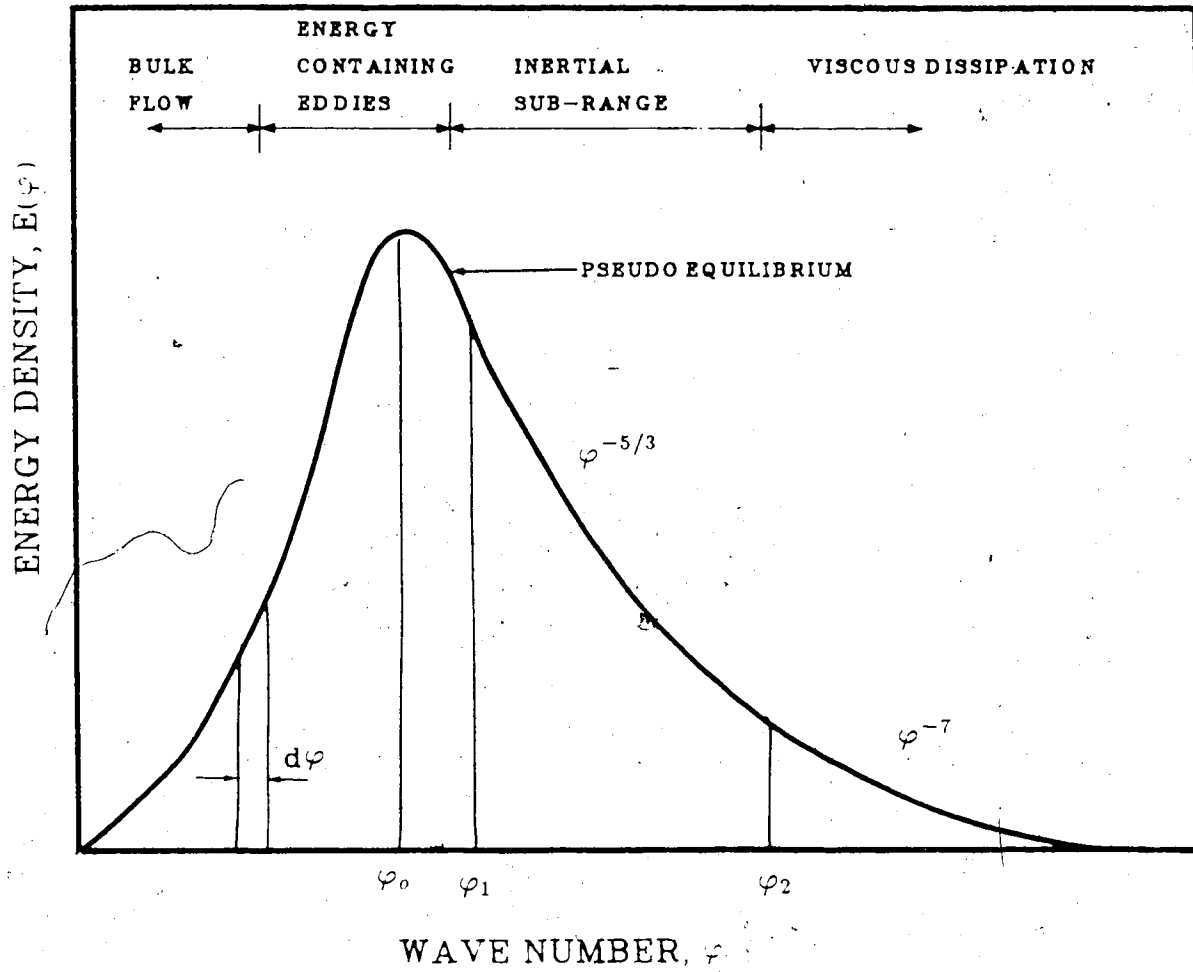


Figure 4.2: Turbulence energy spectra exhibited by many common turbulent flows

u' are between 0.2 m/s and 0.4 m/s. Thus from Equations (4.1) and (4.2), the Kolmogorov scale can be estimated to be approximately $90\mu\text{m}$. Compared to frazil crystal diameters, which range in size from a few microns to 0.80 mm, the Kolmogorov scale is of about the same order for small crystals and an order of magnitude smaller for the larger crystals. For small crystals, thermal energy dissipation is by diffusion from suspended particles of size smaller than η_k ; a quiescent layer can be assumed to surround the disc. If the crystal is much smaller than η_k , the quiescent layer can be considered to be of infinite extent since the temperature distribution in the liquid will be very close to the infinite quiescent fluid case. As the crystal radius approaches η_k , the thickness of the layer decreases resulting in a steeper temperature gradient in the liquid phase. For larger crystal sizes, the ratio of the quiescent sublayer to the disc diameter is small indicating that small crystal growth is governed by conductive heat dissipation and large crystal growth rates are more highly dependent on turbulence characteristics of the bulk flow.

The most significant effect of turbulence on frazil ice crystals, as noted previously, is that it promotes crystal collisions and in this way acts as the driving force for secondary nucleation. The presence of turbulence also acts to increase crystal growth rates by increasing the rate at which latent heat from the growing surface can be dissipated to the surrounding fluid. Neglecting it in the frazil growth model will result in significantly lower growth rates. Therefore, we are most interested in the incorporation of these effects to the frazil growth model in a straight forward manner.

There are three methods for including the effects of turbulence on frazil growth. Clearly, the most sophisticated method is to determine the velocity distribution of the fluid the crystal is immersed in, by solving the appropriate flow and turbulence energy balance equations. The major drawbacks to this approach are the computational difficulties involved when coupled with the crystal growth problem. In

addition, several assumptions must be made about the flow regime and its turbulence parameters. Omsstedt [58] attempted to model the effects of turbulence on a collection of crystals using a two equation turbulence model. He simplified the heat transfer analysis considerably by assuming a lumped capacity type heat balance relation for both the ice and liquid phases. Traditional methods for including the effects of turbulence in crystal growth problems have consisted of assuming an average turbulent heat transfer coefficient from which the rate of latent heat dissipation to the fluid can be determined. The turbulent heat transfer coefficient is determined from empirical data. The final method consists of assuming that a quiescent, conductive fluid layer surrounds the ice crystal. The thickness of the layer depends on the level of turbulence in the fluid. Since the effect of turbulence is to provide a mixing effect between fluid layers of varying temperatures. The end result is to rapidly provide a well-mixed isothermal region some distance from the disc; this distance being a function of the turbulence intensity. In the next section, the two empirical methods for including the effects of turbulence in the disc growth model will be compared. It should be noted that we cannot check the validity of one method over the other due to the lack of experimental results for the growth of frazil crystals in a turbulent fluid. Therefore, only qualitative comparisons are possible. Also, the turbulent nature of water bodies that frazil forms in has to be correlated with stagnant layer thicknesses in order to effectively use this technique.

4.2 GROWTH OF FRAZIL IN TURBULENT FLUID

4.2.1 CRYSTAL GROWTH BASED ON EMPIRICAL HEAT TRANSFER DATA

Daly [18] examined the a-axis growth rates of frazil ice crystals during the course of his work on frazil ice dynamics. The turbulent heat transfer coefficients were determined from the experimental results of Wadia [76] for mass transfer properties from suspended particles such as discs and spheres. Additional values for heat transfer coefficients of frazil crystals were determined experimentally by Bukina [13]. He correlated these heat transfer coefficients with the crystal thickness and diameter, the relative fluid velocity and the crystal growth rate. It should be noted that the magnitude of heat transfer coefficients used by Daly and those from Bukina are approximately of the same order of magnitude, although Bukina's values yield higher values for radial growth rates. The accuracy with which growth rates of frazil crystals can be determined using Daly's expressions for heat transfer coefficients depends on a prior knowledge of the fluid turbulence levels. Bukina's expression for the heat transfer coefficient is not very useful since it requires a prior knowledge of the crystal growth rate.

For disc growth in the quiescent liquid, the portion of latent heat conducted through the solid phase was found to be comparable in magnitude to the portion conducted through to the liquid phase. Since the heat transfer coefficients used by Daly are based on mass transfer data, it was necessary to assume that all the latent heat generated at the growing crystal edge be dissipated to the surrounding turbulent fluid, which is contrary to what is expected. This is because Wadia experiments measured the dissolving rates of small particles into a liquid. Since the particle dissolved into the liquid, the mass transfer coefficients determined by Wadia were for

the liquid region only. Therefore in making the mass transfer-heat transfer analogy, Daly was forced to neglect conduction through the solid phase. Daly further assumed that thickening rates of frazil ice crystals are very small in comparison to radial growth rates and hence can be ignored. As a result, the growth rate of a frazil crystal in the a-axis direction can be given as

$$\rho L \frac{dR}{dt} = \bar{h}_E (T_i - T_\infty) \quad (4.3)$$

where \bar{h}_E is the average heat transfer coefficient along the crystal edge and T_i is the edge interface temperature. Since T_i is approximately equal to T_m for crystal sizes greater than R_{cr} , the temperature difference can be replaced by ΔT .

Daly stated that heat transfer, in a turbulent fluid, is dominated by diffusion for crystals growing in the small Peclet number range, ($Pe < 1$). For these low Peclet numbers, he says that the rate of heat transfer is insensitive to the shape of the particle. The radius of these particles, for small Peclet numbers, is $R < \eta_k Pr^{1/2}$. For large crystals ($R > \eta_k$) the Peclet number is large ($Pe > 1$) and the heat transfer from the particle is determined from the Frössling equation for spherical particles. These results can be stated in a more intuitive form as follows. Firstly, the turbulent Nusselt number is defined as

$$Nu_T = \frac{\bar{h}_E \eta_k}{k_l} = \frac{\bar{h}_E}{k_l} \left(\frac{\nu^3}{\epsilon} \right)^{1/4} \quad (4.4)$$

and the radius of the ice particle is normalized by the Kolmogorov scale so that

$$m = \frac{R(t)}{\eta_k}$$

Then the following heat transfer coefficients are given as follows

for $m < 1/Pr^{1/2}$

$$Nu_T = \left(\frac{1}{m} + 0.17 Pr^{1/2} \right) \quad (4.5)$$

for $1/Pr^{1/2} < m \leq 10$

$$Nu_T = \left(\frac{1}{m} + 0.55 \frac{Pr^{1/3}}{m} \right) \beta_s \quad (4.6)$$

For $m > 1$ and low intensity ($\alpha_T m^{4/3} < 1000$)

$$Nu_T = \left(\frac{1}{m} + 0.70 \alpha_T^{0.035} \frac{Pr^{1/2}}{m} \right) \beta_s \quad (4.7)$$

where α_T is the free stream turbulence intensity and β_s is a shape factor equal to 1.1 for discs. For $m > 1$ and high intensity ($\alpha_T m^{4/3} > 1000$)

$$Nu_T = \left(\frac{1}{m} + 0.70 \alpha_T^{0.25} Pr^{1/3} \right) \beta_s \quad (4.8)$$

Figure 4.3 shows values of Nu_T plotted as a function of the parameter m for a free stream turbulence intensity of 0.20. From the experimental results of Wadia [76], Daly concluded that for large values of m , the ratio of \bar{h}_E/\bar{h}_B approaches unity, where \bar{h}_B is the average heat transfer coefficient for the frazil disc face. This result from Wadia's experiments is shown in Figure 4.4 for various aspect ratios as a function of the quantity \bar{r}/η_k , where \bar{r} is defined as the radius of a sphere with the same surface area as the disc. The plot shows that the ratio \bar{h}_E/\bar{h}_B increases rapidly for low levels of \bar{r}/η_k as the aspect ratio departs from unity. For a fixed aspect ratio, \bar{h}_E/\bar{h}_B approaches unity for increasing values of \bar{r}/η_k . From these results, Wadia speculated that the effect of turbulence intensity would be to enhance \bar{h}_B more than \bar{h}_E . For large values of \bar{r} , he felt that the effects of higher local shear at the edges of the disc increase \bar{h}_E . However, due to the simultaneous enhancement of \bar{h}_B because of the turbulence intensity, the ratio \bar{h}_E/\bar{h}_B approaches unity.

What these results indicate is that for small disc sizes, c-axis growth rates will be very small when the face heat transfer coefficient is a fraction of the edge heat transfer coefficient. With increasing crystal size, c-axis growth rates will increase since the

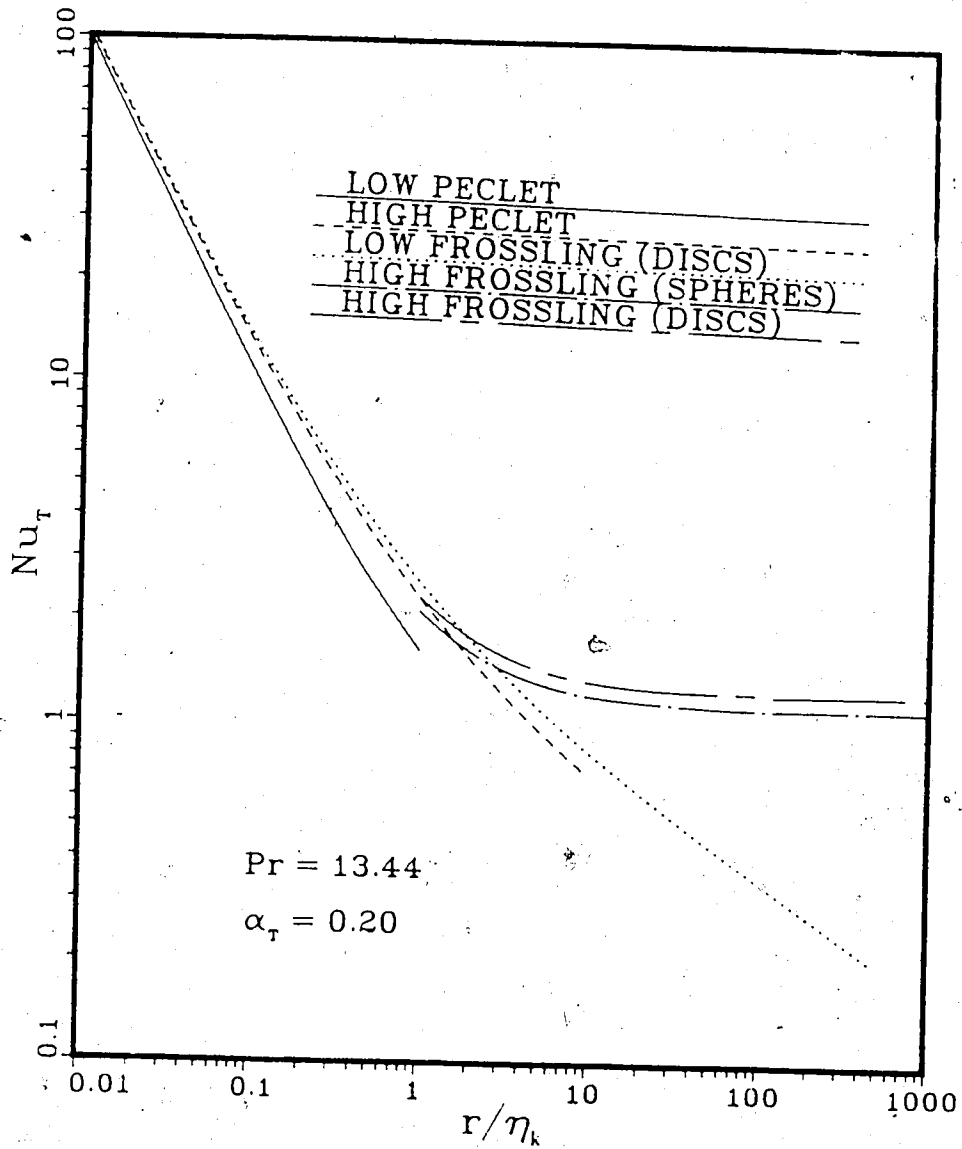


Figure 4.3: Nondimensional heat transfer correlation based on a turbulent Nusselt number (from Daly [18])

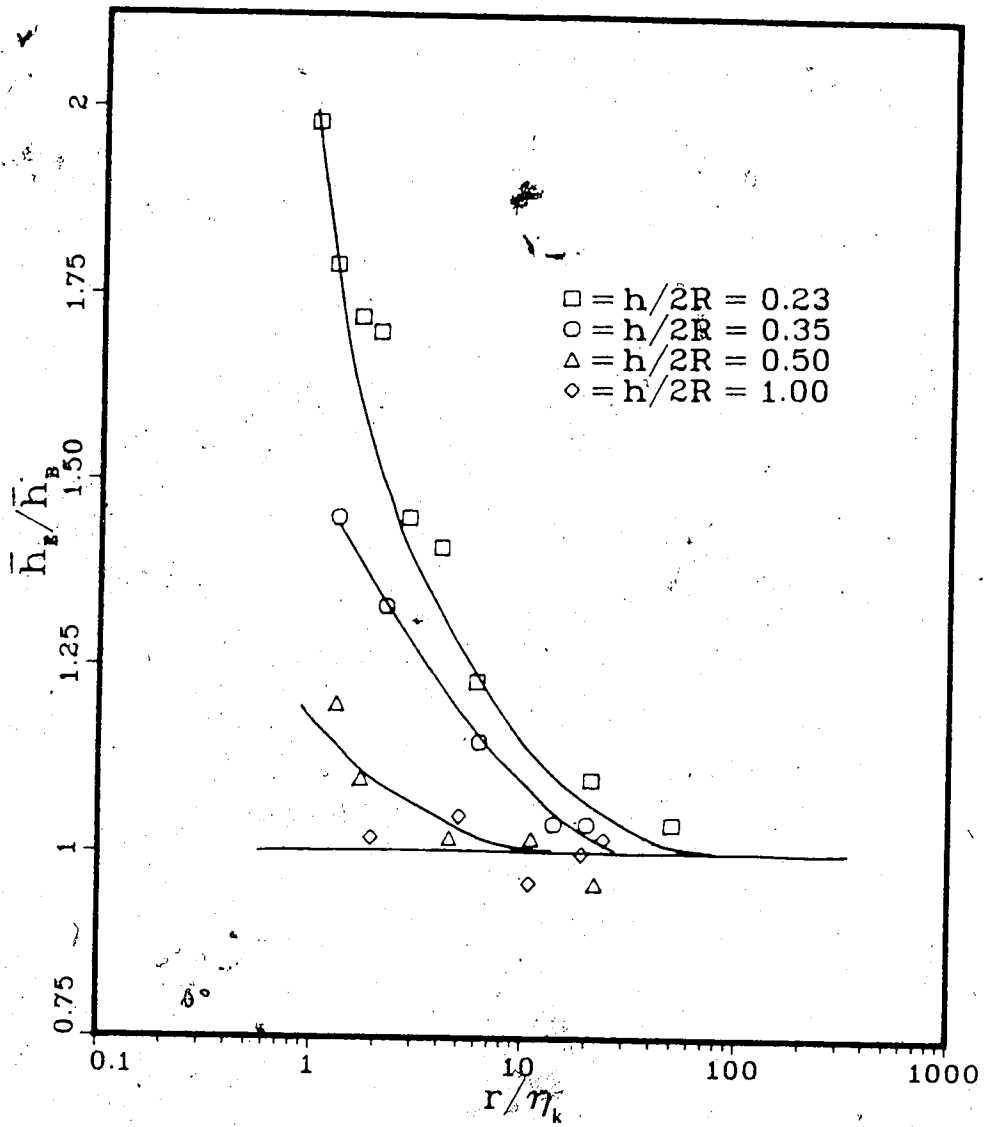


Figure 4.4: Ratio of heat transfer coefficient from the disc edge and the face (from Wadia [76])

value of the heat transfer coefficient on the basal plane will approach the value of the edge heat transfer coefficient. When the crystal has grown to a sufficiently large size, the thickening rate of the crystal will become comparable with the magnitude of the radial growth rate. Physically, this is what one would expect since the radial growth of frazil crystals decreases with increasing crystal size. This results in a reduction in the basal plane undercooling and subsequently causes an increase in the thickening rate. Although Wadia's results are only for aspect disc ratios between 0.23 and 1.0, we can still apply them to obtain c-axis growth rates for the purposes of comparing with the results of the stagnant layer model to be discussed in the next section. Therefore, we can state that the growth in the c-axis direction is given by

$$\rho L \frac{1}{2} \frac{dh}{dt} = \bar{h}_B (T_B - T_\infty), \quad (4.9)$$

where T_B is the basal plane temperature. Inclusion of the interfacial kinetics yields the additional condition

$$\frac{1}{2} \frac{dh}{dt} = \mu_1 e^{\mu_2 / \Delta T_k}$$

Using the relations (4.3) and (4.9) for a-axis and c-axis growth rates along with Equations (4.4) through (4.8), the growth behaviour of a frazil ice crystal in a turbulent body of water can be modelled. We refer to this calculation method as "Daly's model" in the remainder of this chapter for brevity. It should be noted that c-axis growth rates are computed independently of the a-axis growth rates, since equations 4.3 and 4.9 are not directly related. Growth rates in the a-axis direction however, are implicitly dependent on the thickness of the disc since the correlations (4.7) and (4.8) incorporate the disc shape of the crystal through the parameter β . For computing c-axis growth rates, it was assumed that $\bar{h}_B = \bar{h}_E/2$, which was chosen primarily because it is the maximum value within the range of Wadia's results. For our calculations, we have assumed that \bar{h}_B will always remain

as $\bar{h}_E/2$ for all disc sizes, since the correct functional dependence is not known.

Results of a-axis growth rates are summarized in Figures 4.5 to 4.6 for supercoolings of $0.05\text{ }^\circ\text{C}$ and $0.10\text{ }^\circ\text{C}$. The initial diameter and thickness of the disc were $60\text{ }\mu\text{m}$ and $20\text{ }\mu\text{m}$ respectively. Although the trends for a-axis growth rates are similar to growth trends established for the quiescent fluid model, the magnitudes are considerably lower than the previous results. A value of $\eta_k = 10\text{ }\mu\text{m}$ corresponds to a very high dissipation rate of 573 W/kg . In most lakes and rivers however, the dissipation rate ϵ is estimated to be approximately 50 mW/kg which corresponds to a Kolmogorov length scale of about $100\text{ }\mu\text{m}$. Thus, for reasonable levels of turbulence intensity, Daly's growth model predicts an edgewise growth rate of approximately $1\text{ }\mu\text{m/s}$ for a disc radius of 1 mm and a supercooling of $0.05\text{ }^\circ\text{C}$. For very high levels of turbulence, corresponding to a Kolmogorov scale of $10\text{ }\mu\text{m}$, the predicted growth rate is $6\text{ }\mu\text{m/s}$. Clearly, these values are lower than what one would expect, since the quiescent growth model predicts a radial growth rate of $10\text{ }\mu\text{m/s}$ for the same supercooling.

Thickening rates of ice crystals for the same supercoolings of $0.05\text{ }^\circ\text{C}$ and $0.10\text{ }^\circ\text{C}$ are shown in Figures 4.7 and 4.8 respectively. Unlike the calculated a-axis growth rates, the magnitude of these values appears to be consistent with those obtained from the quiescent model. For the quiescent model, the maximum c-axis growth rate is $0.19\text{ }\mu\text{m/s}$ for a supercooling of $0.10\text{ }^\circ\text{C}$ and negligibly small for a supercooling of $0.05\text{ }^\circ\text{C}$. Using Daly's heat transfer data yields c-axis growth rates of $0.10\text{ }\mu\text{m/s}$ to $0.15\text{ }\mu\text{m/s}$ for $\Delta T = 0.05\text{ }^\circ\text{C}$ and $0.45\text{ }\mu\text{m/s}$ to $1.0\text{ }\mu\text{m/s}$ for $\Delta T = 0.10\text{ }^\circ\text{C}$ for disc radii greater than 1.0 mm . The variation of the c-axis growth rates however is reversed from results obtained through the quiescent model. For the present case, the c-axis growth rate, contrary to the physics, decreases with increasing crystal size and not with increasing size as was the case with the quiescent model. This is mainly

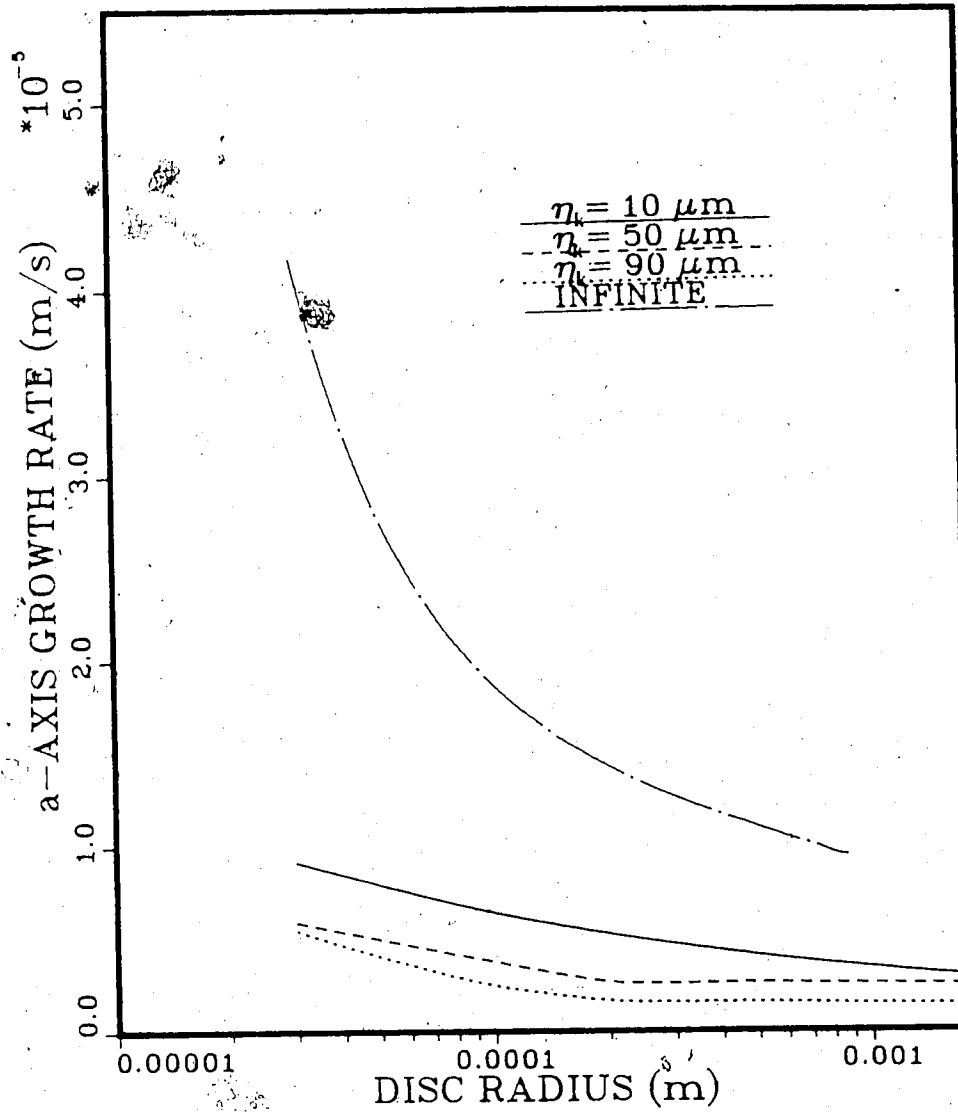


Figure 4.5: a-axis growth rate calculated from Daly's model for $\Delta T = 0.05 \text{ }^\circ\text{C}$. Initial values of R and $h/2$ are $30 \mu\text{m}$ and $10 \mu\text{m}$ respectively. The label "INFINITE" corresponds to the quiescent fluid of infinite extent.

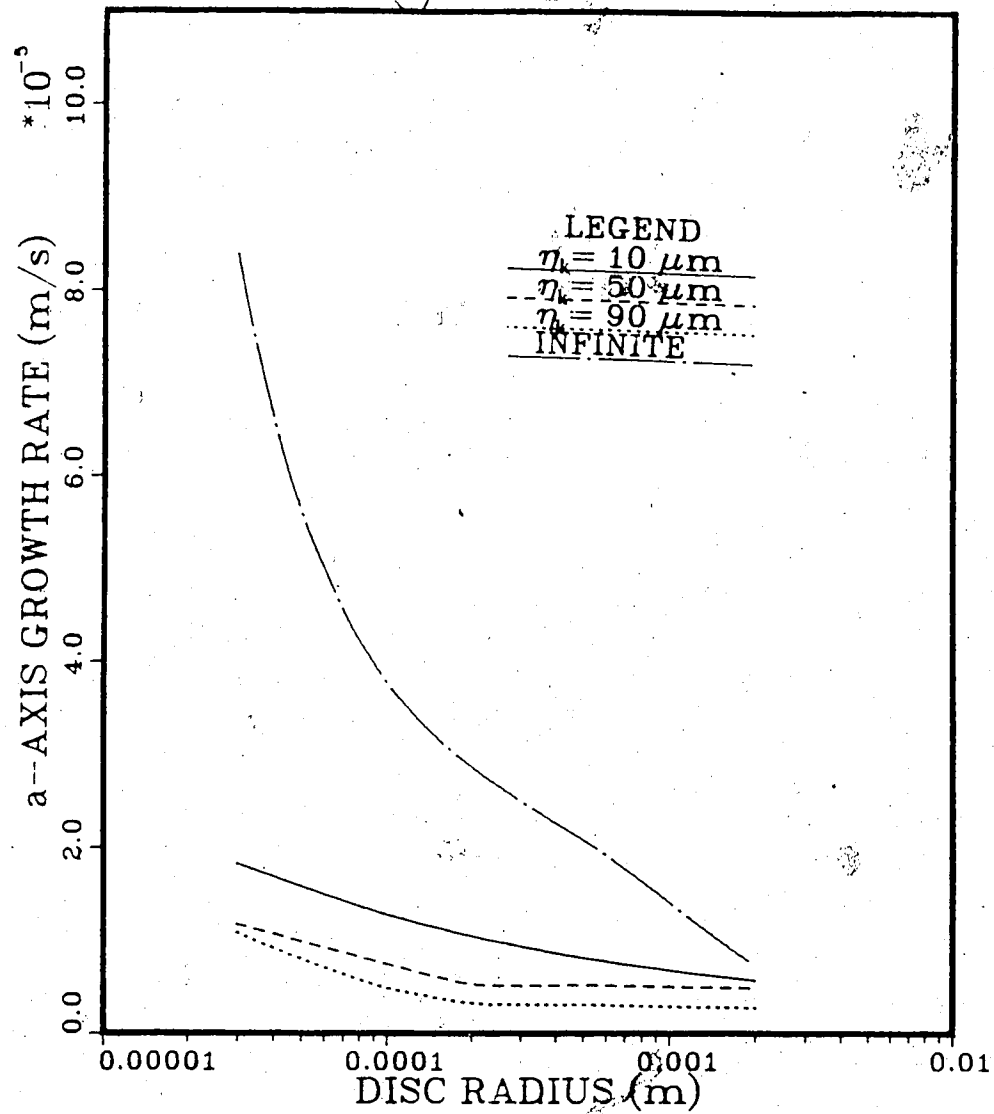


Figure 4.6: a-axis growth rate calculated from Daly's model for $\Delta T = 0.10 \text{ }^\circ\text{C}$. Initial values of R and $h/2$ are $30 \mu\text{m}$ and $10 \mu\text{m}$ respectively. The label "INFINITE" corresponds to the quiescent fluid of infinite extent.

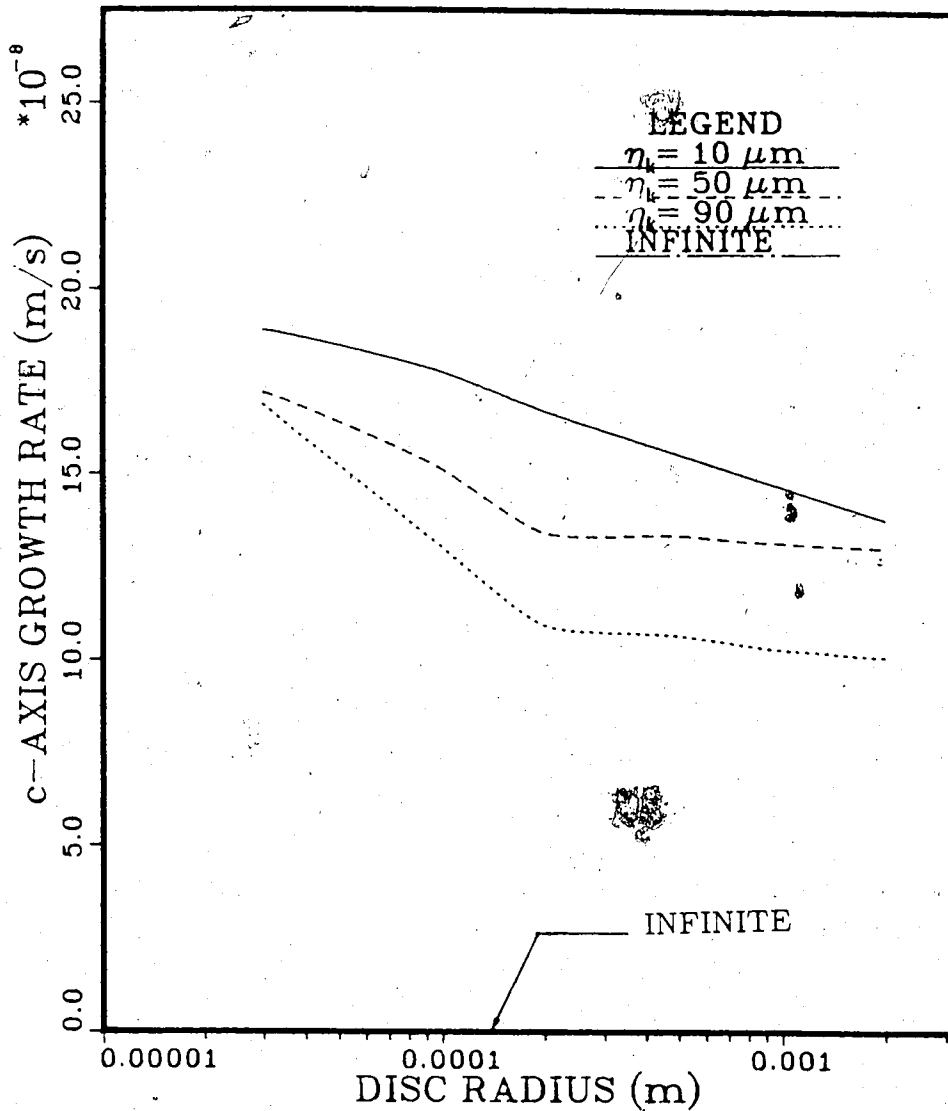


Figure 4.7: c-axis growth rate calculated from Daly's model for $\Delta T = 0.05 \text{ }^\circ\text{C}$. Initial values of R and $h/2$ are $30 \mu\text{m}$ and $10 \mu\text{m}$ respectively. The c-axis growth rate for the infinite quiescent fluid is very low and represented by the horizontal axis of the graph.

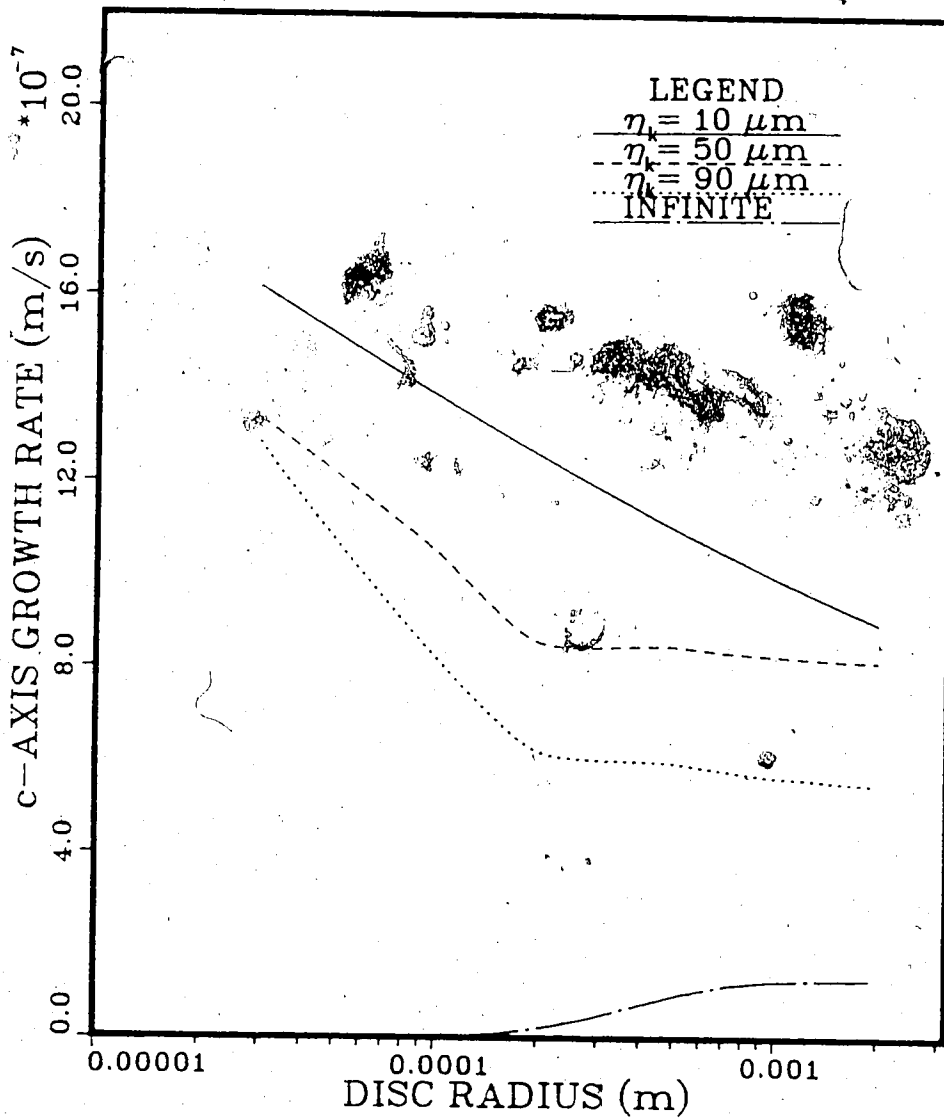


Figure 4.8: c-axis growth rate calculated from Daly's model for $\Delta T = 0.10 \text{ }^\circ\text{C}$. Initial values of R and $h/2$ are $30 \mu\text{m}$ and $10 \mu\text{m}$ respectively. The label "INFINITE" corresponds to the quiescent fluid of infinite extent.

due to the way in which c-axis growth is calculated which causes the basal plane temperature T_b to increase for increasing disc radius. The basal plane undercooling is not affected by the latent heat release from the thickening process since it is all dissipated into the liquid. The increase in T_b results from the decreasing basal plane heat transfer coefficient with increasing crystal size and consequently the incorrect behaviour of decreasing c-axis growth rates. Another major shortcoming of Daly's model is the independence of the a- and c-axis growth rates from each other. From the quiescent model, it was observed that the thickening rate of the disc indirectly reduces the radial growth rate of the crystal as a consequence of the increased latent heat released at the disc edge. In Daly's model, no such result is observed, since there is no connection between the disc radius and its thickness.

4.2.2 STAGNANT LAYER MODEL

If the fluid surrounding the crystal is assumed to be well mixed and the turbulence is homogeneous and isotropic, then it can be assumed that a thin quiescent layer of fluid is surrounding the crystal through which the mechanism of heat transfer is by conduction. Since the surrounding fluid is well mixed, it can be assumed to be at a uniform temperature. Thus, any temperature variation in the crystal occurs within the quiescent layer surrounding the crystal. This method has been employed when complicated flows are encountered in external convective heat transfer problems. The concept of a thin, stationary conductive layer of fluid surrounding the solid body is employed to calculate heat transmission rates to the fluid [34]. The thickness of this layer is usually determined from previously established experimental results. Empirical data relating the heat transfer coefficient to the conductive layer thickness are available for natural convection problems. However, there is a considerable lack of experimental work which is necessary to formulate such empirical correlations

(relating the conductivity layer thickness to levels of turbulence intensity) for a disc geometry subjected to fluid motions similar to that of frazil crystals. We will refer to this method for incorporating turbulence as the "stagnant layer" approach. This method was used by Tikuisis et al. [74] to calculate the dissolving rate of a gas bubble in a well mixed, stirred solution. They employed the concept of a thin unstirred liquid layer of thickness δ for the determination of the dissolving rate of bubbles in a stirred volume of liquid closed to mass transport. They noted that the thickness of the diffusion layer was dependent only on the level of fluid motion. The values used for the diffusion layer thickness were examined through an experimental investigation of bubble evolution in a stirred liquid. The only parameter that needs to be determined in this case, is the thickness of the stagnant liquid layer.

Clearly, for very small crystals ($R < \eta_k$) the concept of a quiescent liquid layer has physical significance. The mechanism by which heat is transferred to the liquid phase is by conduction since the crystal is smaller than the size of eddies in the viscous dissipation range. Therefore, we can consider the fluid surrounding the crystal to be quiescent and of infinite extent (It was shown in Chapter 3 that the outer boundary located at infinity can be approximated by the distances of $50R$ in the radial direction and $10R$ in the axial direction). The concept of an infinite conductive layer of fluid around the crystal weakens when the crystal grows to sizes larger than the Kolmogorov scale. Physically, the existence of a quiescent layer of fluid becomes less likely due to the relative motion created at the crystal boundary by small scale eddies. The thickness of this layer can be approximated by the length scale of the smallest size eddies (i.e. the Kolmogorov length scale). The stagnant layer approach may be employed in order to determine crystal growth rates in a turbulent fluid. The major problem is to determine values to use for the conductive layer thickness δ .

The Kolmogorov scale η_k provides some basis for the relative magnitude of the

stagnant layer thickness from which two limiting values can be estimated. The lower limiting value for the stagnant layer thickness is of the order of the Kolmogorov scale η_k and corresponds to strong levels of turbulence. The other limiting case corresponds to little or no turbulence present (i.e. infinite quiescent liquid). Intermediate values of δ can be used to vary the level of fluid turbulence. If the turbulence intensity is relatively low, the dissipative scale will be large, resulting in a thicker layer of stagnant fluid. If the turbulence intensity is high, then the dissipative scale η_k will be small (most of the fluid surrounding the ice crystal will be well mixed) and the resulting latent heat dissipation rate will be increased. Thus, the thickness of the conductive layer is strongly dependent upon the intensity of turbulence in the water.

For the results that follow, the stagnant layer thickness was varied from $\delta = 5\mu m$, corresponding to a highly turbulent fluid, to $\delta = 30\mu m$ corresponding to intermediate levels of turbulence. The infinite quiescent fluid case is also presented for the purposes of comparison. Figure 4.9 and 4.10 show the a-axis growth rates of a frazil disc for bulk supercoolings of $0.05^\circ C$ and $0.10^\circ C$. The initial size of the ice disc for both cases was taken as $R = 30\mu m$ and $h/2 = 10\mu m$. The corresponding c-axis growth rates are shown in Figures 4.11 and 4.12. The trend of the growth rate curves for all the values of δ considered is seen to decrease with increasing crystal radius. The growth rate is very high at the initial crystal size but decreases to a quasi-steady value in a manner similar to the infinite quiescent fluid case. Decreasing the stagnant layer thickness (which effectively increases the level of turbulence) is shown to increase the long term radial growth rate of the crystal. The radial growth rate is observed to be $10\mu m/s$ at a crystal size of $.1\text{ mm}$ and a supercooling of $0.05^\circ C$ for the infinite quiescent fluid case. The corresponding growth rates for values of δ equal to $5\mu m$, $10\mu m$, $15\mu m$, $20\mu m$ and $30\mu m$ are $21\mu m/s$, $29\mu m/s$, $38\mu m/s$, $44\mu m/s$ and $63\mu m/s$ respectively. The radial growth rate for the crystal would be between $10\mu m/s$ and

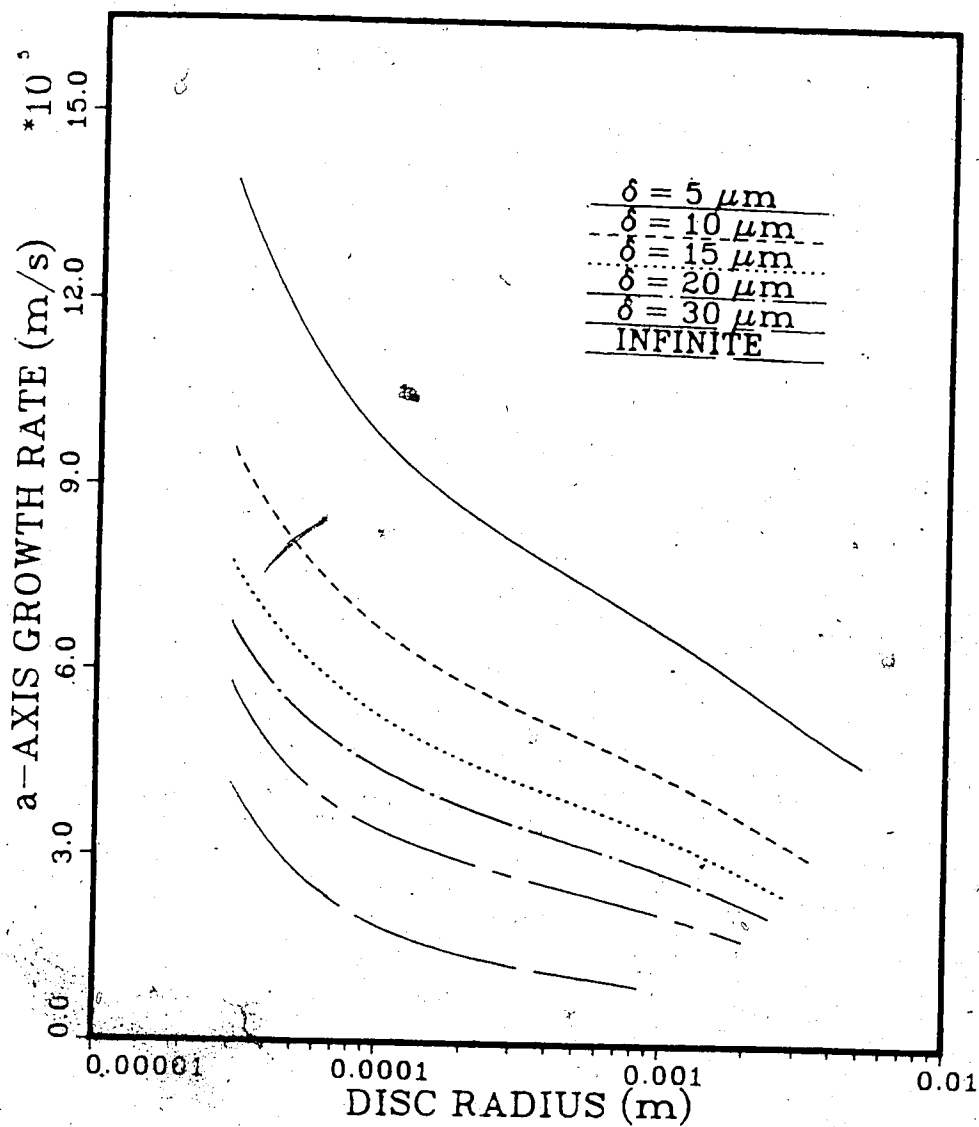


Figure 4.9: a-axis growth rates for stagnant layer model with $\Delta T = 0.05 \text{ }^\circ\text{C}$. Initial values of R and $h/2$ taken as $30 \mu\text{m}$ and $10 \mu\text{m}$ respectively. The label "INFINITE" corresponds to the quiescent fluid of infinite extent.

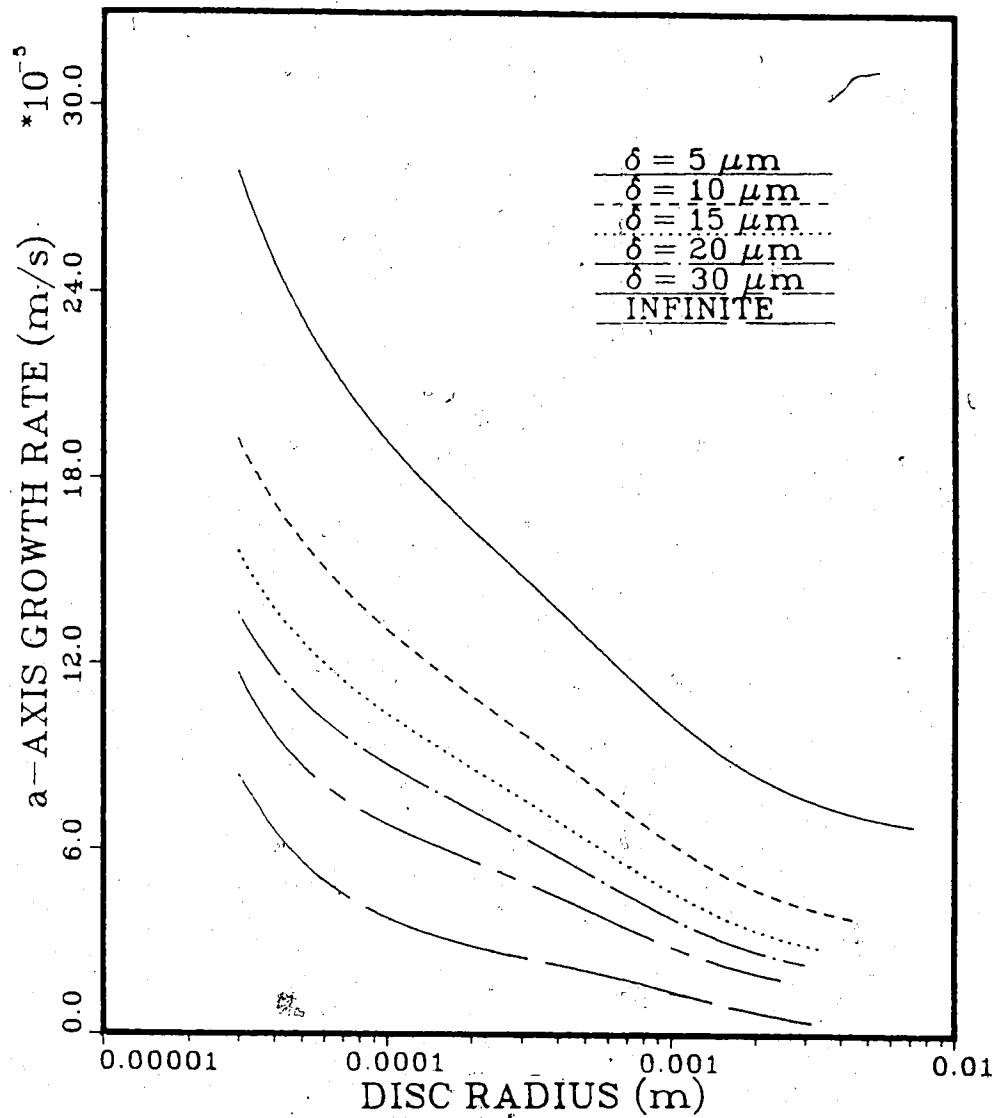


Figure 4.10: a-axis growth rates for stagnant layer model with $\Delta T = 0.10 \text{ }^\circ\text{C}$. Initial values of R and $h/2$ taken as $30 \mu\text{m}$ and $10 \mu\text{m}$ respectively. The label "INFINITE" corresponds to the quiescent fluid of infinite extent.

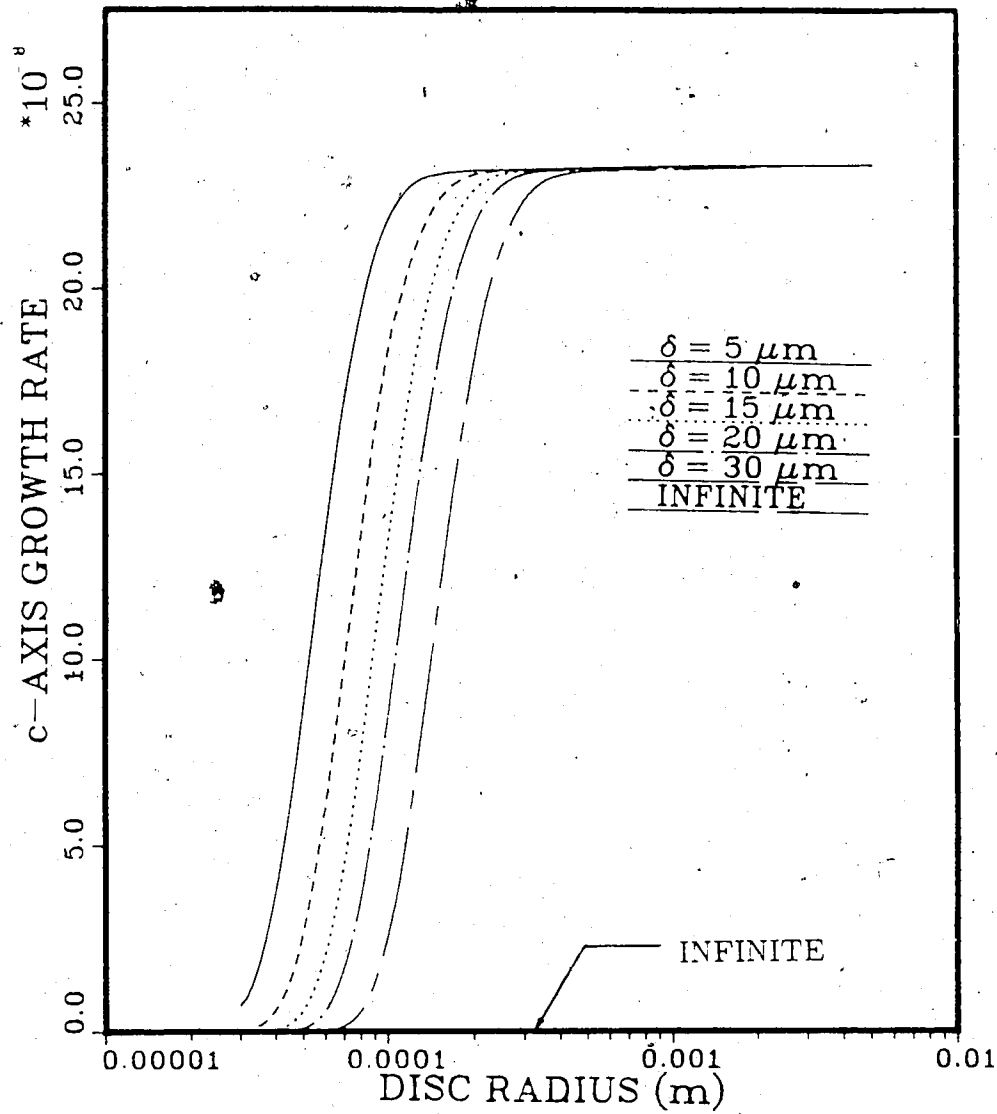


Figure 4.11: c-Axis growth rates for stagnant layer model with $\Delta T = 0.05 \text{ }^\circ\text{C}$. Initial values of R and $h/2$ taken as $30 \mu\text{m}$ and $10 \mu\text{m}$ respectively. The c-axis growth rate for the infinite quiescent fluid is very low and represented by the horizontal axis of the graph.

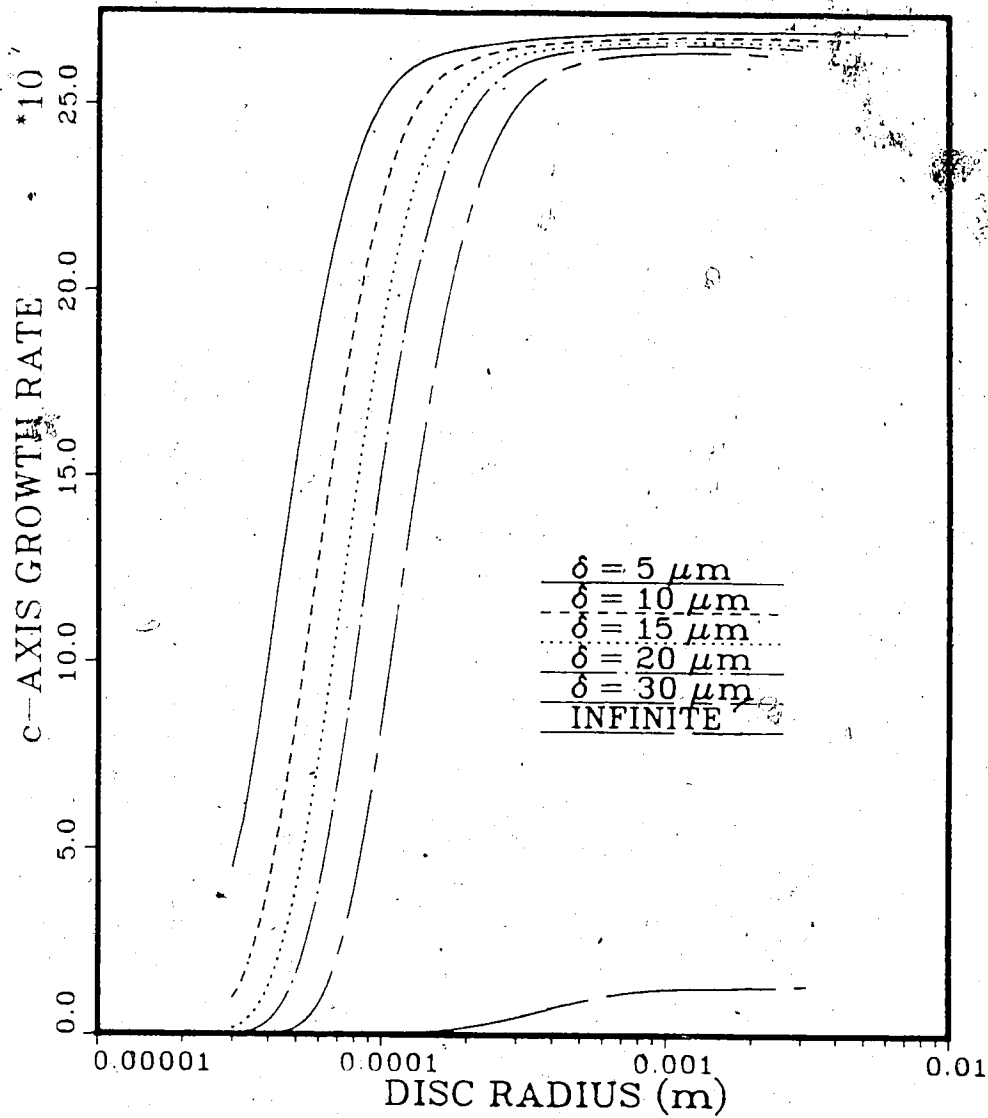


Figure 4.12: c-axis growth rates for stagnant layer model with $\Delta T = 0.10 \text{ }^\circ\text{C}$. Initial values of R and $h/2$ taken as $30\mu\text{m}$ and $10\mu\text{m}$ respectively. The label "INFINITE" corresponds to the quiescent fluid of infinite extent.

$21\mu\text{m/s}$ for a stagnant layer thickness greater than $30\mu\text{m}$. These results appear physically realistic since limited observations for radial growth rates of crystals in a quiescent fluid by Fujioka [28] and Bukina [12] also show similar trends.

There is a significant change in the c-axis growth behaviour. As the stagnant layer thickness δ decreases, the thickening rate of the crystal increases rapidly to its maximum value in contrast to the quiescent fluid cases. The maximum c-axis growth rate is observed to be independent of the stagnant layer thickness δ and the disc radius R . The thickening rate increases from almost zero, for the quiescent case, to $0.20\mu\text{m/s}$ for $\Delta T = 0.05^\circ\text{C}$. Similarly, for a supercooling of 0.10°C , it increases from a modest rate of $0.20\mu\text{m/s}$ to a substantial value of approximately $2.6\mu\text{m/s}$. These high c-axis growth rates are due to the increased basal plane supercooling as a result of increased levels of turbulence (decreasing values of δ). Recall that the growth mechanism, in the c-axis direction, is surface nucleation. Consequently, c-axis growth rates are a function of the temperature difference $\Delta T_k = T_m - T(0, h/2)$. Therefore, the thickening rate of the disc and the latent heat release along the disc face increase as the basal plane temperature ($T(0, h/2)$) decreases. The maximum basal plane undercooling (in dimensionless form) is shown in Figures 4.13 and 4.14 for the supercoolings of 0.05°C and 0.10°C respectively. The basal plane temperature decreases very rapidly to approximately $\theta = 0$, which corresponds to the bulk fluid temperature. Consequently a rapid increase in c-axis growth rates is observed. As a comparison, we see that neglecting the effects of turbulence would have yielded a dimensionless basal plane temperature of $\theta = 0.60$ for $\Delta T = 0.10^\circ\text{C}$. The radial growth rates predicted from the stagnant layer model are significantly higher in comparison to Daly's growth rates. Daly's radial growth rate predictions are unreasonable since they are even lower than those predicted from the infinite quiescent fluid model. The thickening rates obtained by using the stagnant layer model however are very

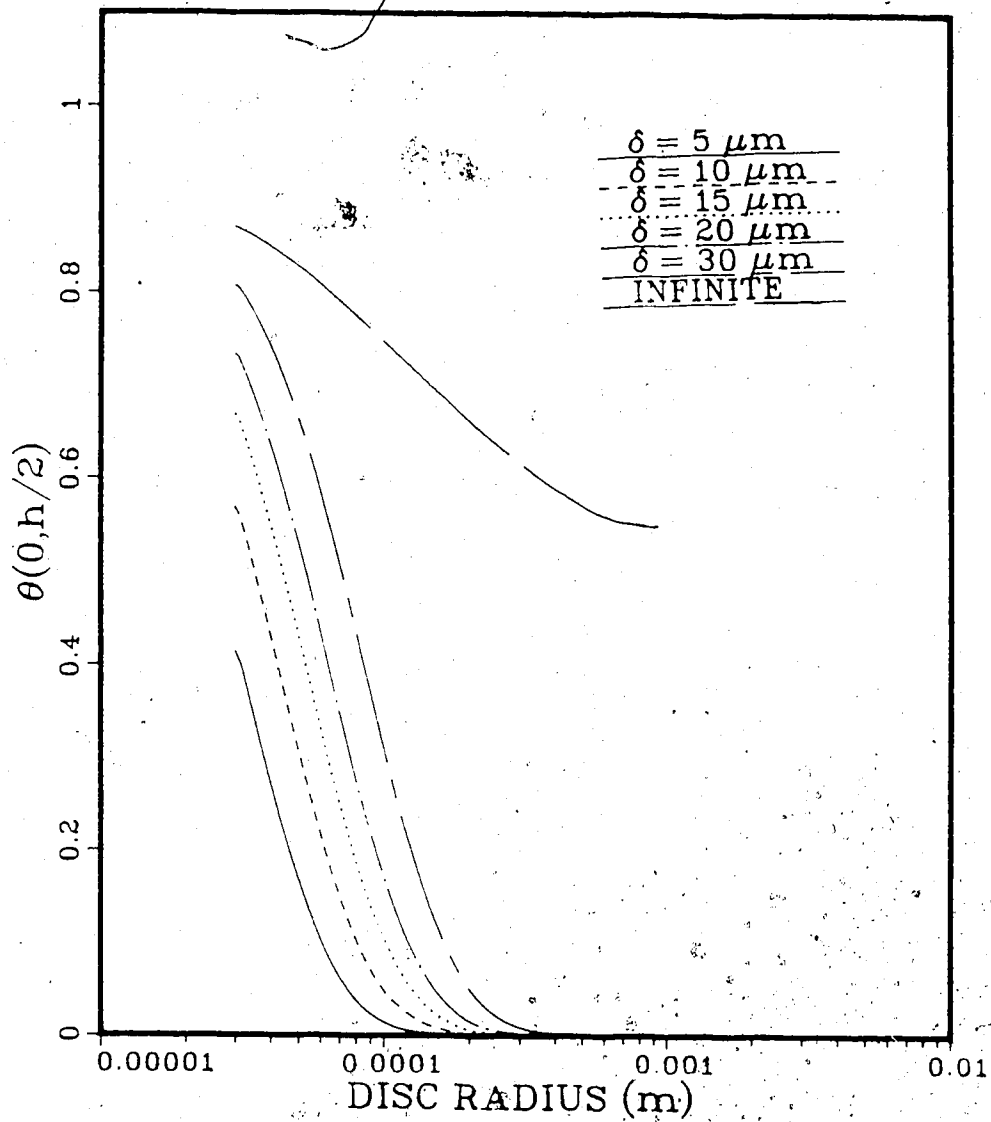


Figure 4.13: Maximum dimensionless basal plane undercooling as a function of crystal radius for $\Delta T = 0.05 \text{ }^\circ\text{C}$. The initial crystal radius is $30 \mu\text{m}$ and $h/2 = 10 \mu\text{m}$. The label "INFINITE" corresponds to the quiescent fluid of infinite extent.

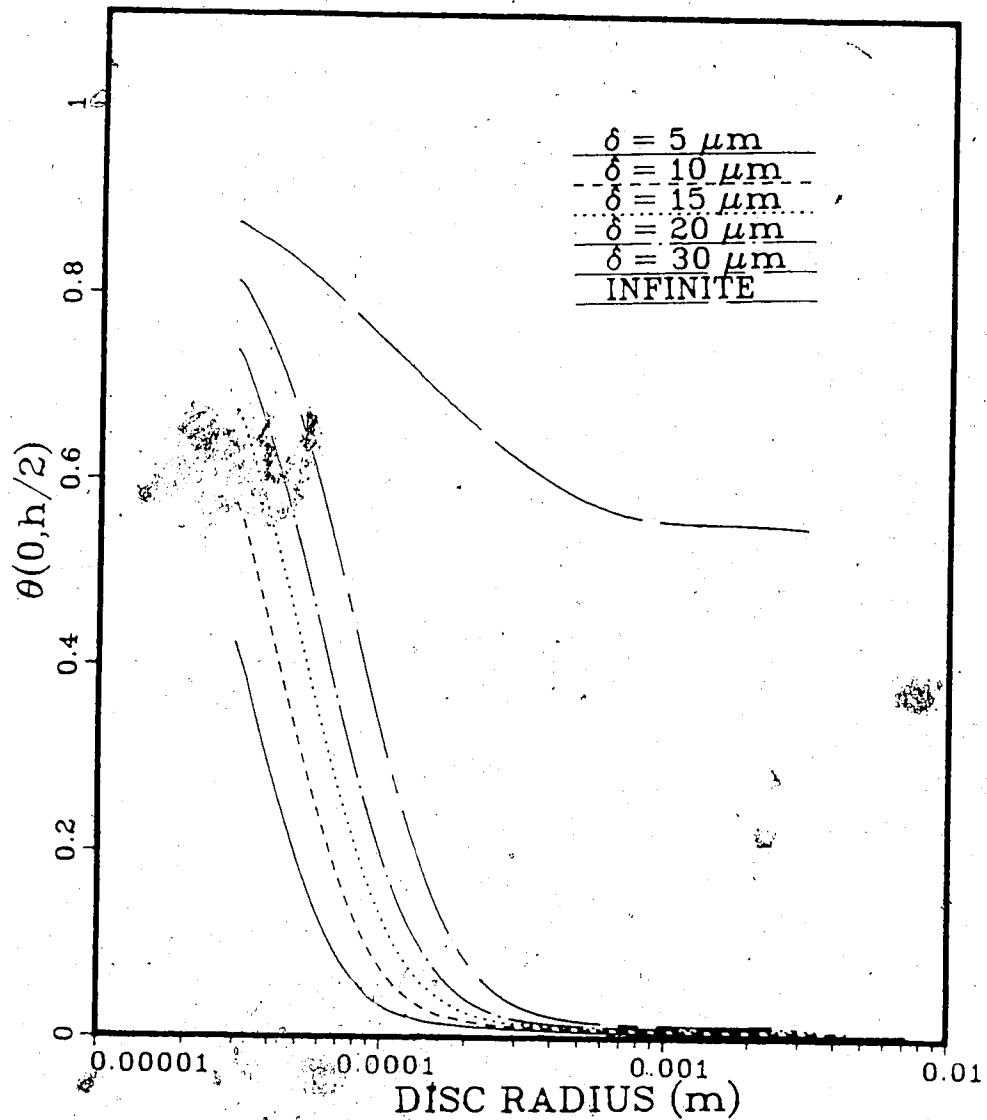


Figure 4.14: Maximum dimensionless basal plane undercooling as a function of crystal radius for $\Delta T = 0.10 \text{ }^\circ\text{C}$. The initial crystal radius is $30 \mu\text{m}$ and $h/2 = 10 \mu\text{m}$. The label "INFINITE" corresponds to the quiescent fluid of infinite extent.

similar in magnitude to those predicted on using Daly's heat transfer data. The c-axis growth rate for a supercooling of $0.05\text{ }^{\circ}\text{C}$ and high levels of turbulence ($\eta_k = 10\mu\text{m}$) is approximately $0.15\mu\text{m/s}$ for a disc radius of 1 mm. The c-axis growth rate obtained using the stagnant layer model for these same conditions is $0.23\mu\text{m/s}$. The difference in these values is somewhat larger for a supercooling of $0.10\text{ }^{\circ}\text{C}$. Daly's model yields c-axis growth rates of $1.0\mu\text{m/s}$ compared to $2.6\mu\text{m/s}$ on using the stagnant layer model. Thus, radial growth rates obtained by using Daly's model are significantly lower than those obtained from the stagnant layer model although the rate of thickening is almost the same.

The major difference in the c-axis growth rates between these two methods is the trend of the calculated values. The trend predicted by Daly's model is the reverse of what is predicted by using the stagnant layer model. Furthermore, c-axis growth rates determined from Daly's model are strongly dependent on the turbulence intensity unlike c-axis growth rates predicted using the stagnant layer model. The family of curves is seen to have a downward trend for decreasing values of η_k . Results from the stagnant layer model however are observed to be independent of the stagnant layer thickness over the range of δ 's considered. Figure 4.15 compares the aspect ratio of ice discs obtained using the stagnant layer model and Daly's model. The major conclusion that can be drawn from comparisons between these results is that Daly's model predicts small stubby disc crystals with a high aspect ratio, while the stagnant layer model predicts thin discs with a low aspect ratio.

Since radial growth rates of ice discs are highly dependent on the rate of latent heat dissipation, it is clear that Daly's model underpredicts the rate of latent heat withdrawal from the growing edge. This indicates that either the turbulent heat transfer coefficients used by Daly are incorrect, due to possible errors in measurement, or another source of heat transfer from the edge is unaccounted for. The latter

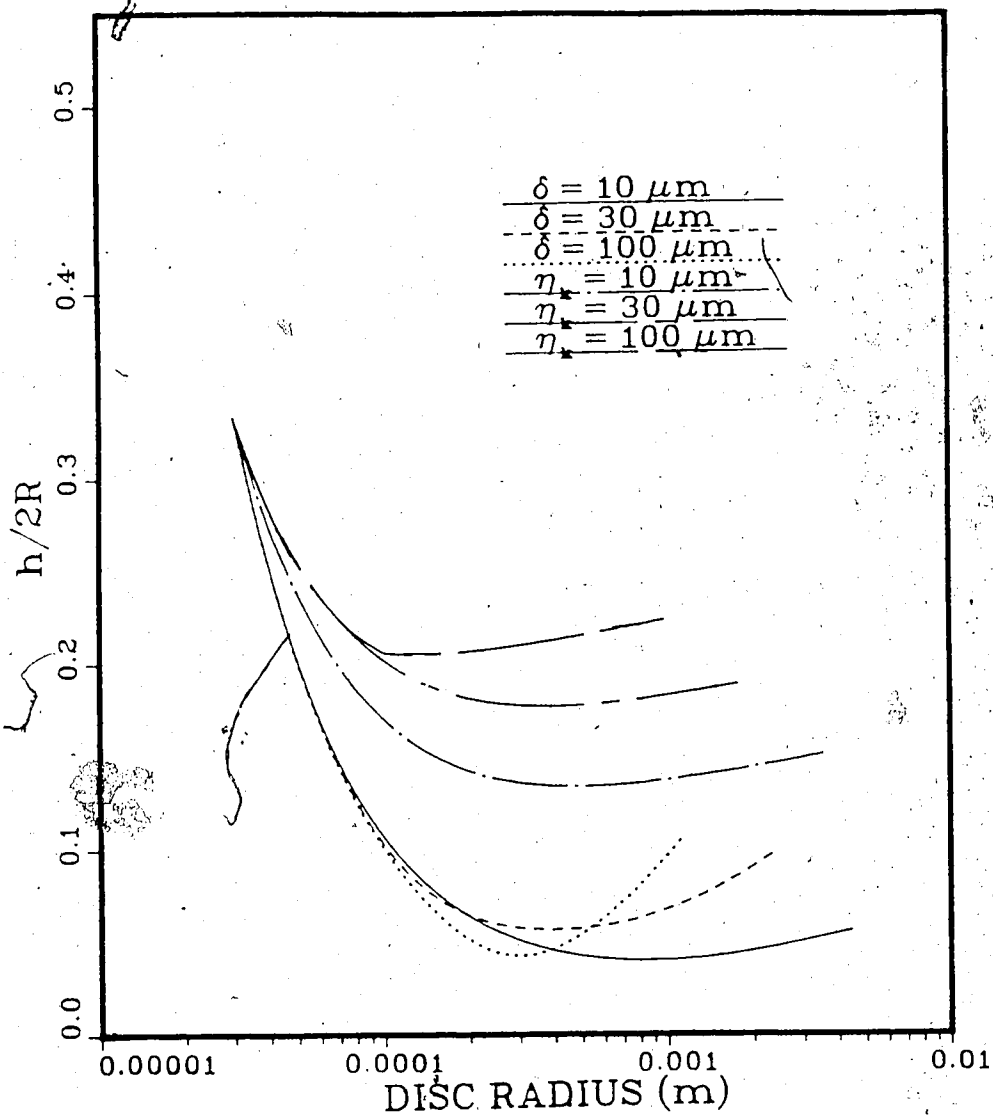


Figure 4.15: Comparison of the aspect ratios of ice discs as a function of disc radius between the stagnant layer model and Daly's model. The supercooling is $\Delta T = 0.10 \text{ }^\circ\text{C}$ with $R_o = 30 \mu\text{m}$ and $h/2 = 10 \mu\text{m}$ initially.

explanation is more plausible because Daly's model requires that all latent heat generated at the growing edge be dissipated to the surrounding liquid. The present results, including those from the infinite quiescent model, indicate that the component of the latent heat conducted through the solid phase is of comparable magnitude to the portion released into the liquid. In fact, it may be even higher than the liquid component since the thermal conductivity of ice is larger than that of water. The flux conducted through the solid is eventually dissipated to the melt through the upper and lower faces of the crystal. For the infinite quiescent model with $\Delta T = 0.05^\circ\text{C}$ and a disc of radius $300\mu\text{m}$ and aspect ratio of 0.0167, the average heat flux in the solid phase is 8248 W/m^2 compared to 660 W/m^2 in the liquid phase. The latent heat components for a disc, with radius $30\mu\text{m}$ and an aspect ratio of 0.30 are 889 W/m^2 and 1685 W/m^2 (in the solid and liquid phases) for the stagnant layer model with $\delta = 30\mu\text{m}$ and the same supercooling. As the aspect ratio of the disc decreases to 0.033, the portion conducted through the solid increases to 2609 W/m^2 and the portion transferred to the liquid increases to 1378 W/m^2 . For decreasing values of the stagnant layer thickness, the ratio of the heat fluxes in the solid and liquid phases is approximately 0.80. In fact, the portion conducted through the solid increases as the crystal face area increases and the temperature along the basal plane decreases. Therefore, the component conducted through the solid phase must be considered in a crystal growth model since it is a sizable portion of the total latent heat generated at the crystal edge.

The effective heat transfer coefficient along the crystal edge and basal plane are defined as

$$q_E = \bar{h}_E A_E \Delta T$$

and

$$q_B = \bar{h}_B A_B \Delta T$$

respectively where A_E is the area of the edge interface and A_B is the area of the basal plane. Figures 4.16 and 4.17 show the typical variations in the average edge and face heat transfer coefficients for the stagnant layer model with $\Delta T = 0.10^\circ\text{C}$.

The infinite quiescent fluid case is also shown in these plots for comparison. The plotted results are nondimensionalized in terms of the Nusselt number defined as $Nu_E = \bar{h}_E R / k_l$ for the edge and $Nu_B = \bar{h}_B R / k_l$ for the basal plane. For the infinite quiescent fluid, the Nusselt number along the basal plane is calculated to be approximately 1.3 for all disc sizes. This compares reasonably well with the theoretical value of 1.1 for a disc shaped particle suspended in a stationary fluid [18]. The effect of decreasing the stagnant layer thickness δ results in a significant increase in the disc face Nusselt number. As the radius of the disc increases the value of the Nusselt number also increases quite rapidly to a maximum value of about 7. For the same supercooling of $\Delta T = 0.10^\circ\text{C}$, the edge Nusselt number is also observed to increase to a maximum value of approximately 100. It is not possible however, to compare the calculated values of the Nusselt number obtained from the stagnant layer model with the turbulent heat transfer coefficients given in Equations (4.5) to (4.8), since those correlations are based on all latent heat generation being dissipated into the liquid phase. In order for Daly's growth rates to be equal to those for the stagnant layer model, the turbulent Nusselt number needs to be modified so that the effect of conduction into the solid phase is also included. This can be stated more precisely as

$$\bar{N}u_E^* = \bar{N}u_E + \frac{\partial\theta}{\partial r}\bigg|_{r=R^-} \quad (4.10)$$

where $\bar{N}u_E^*$ is the modified dimensionless heat transfer coefficient and $\bar{N}u_E$ is Daly's dimensionless heat transfer coefficient for the crystal edge. The second term on the righthand side of (4.10) represents the average portion of the latent heat conducted through the solid phase. The magnitude of this flux is usually 30% to 50% of the total latent heat generated along the edge.

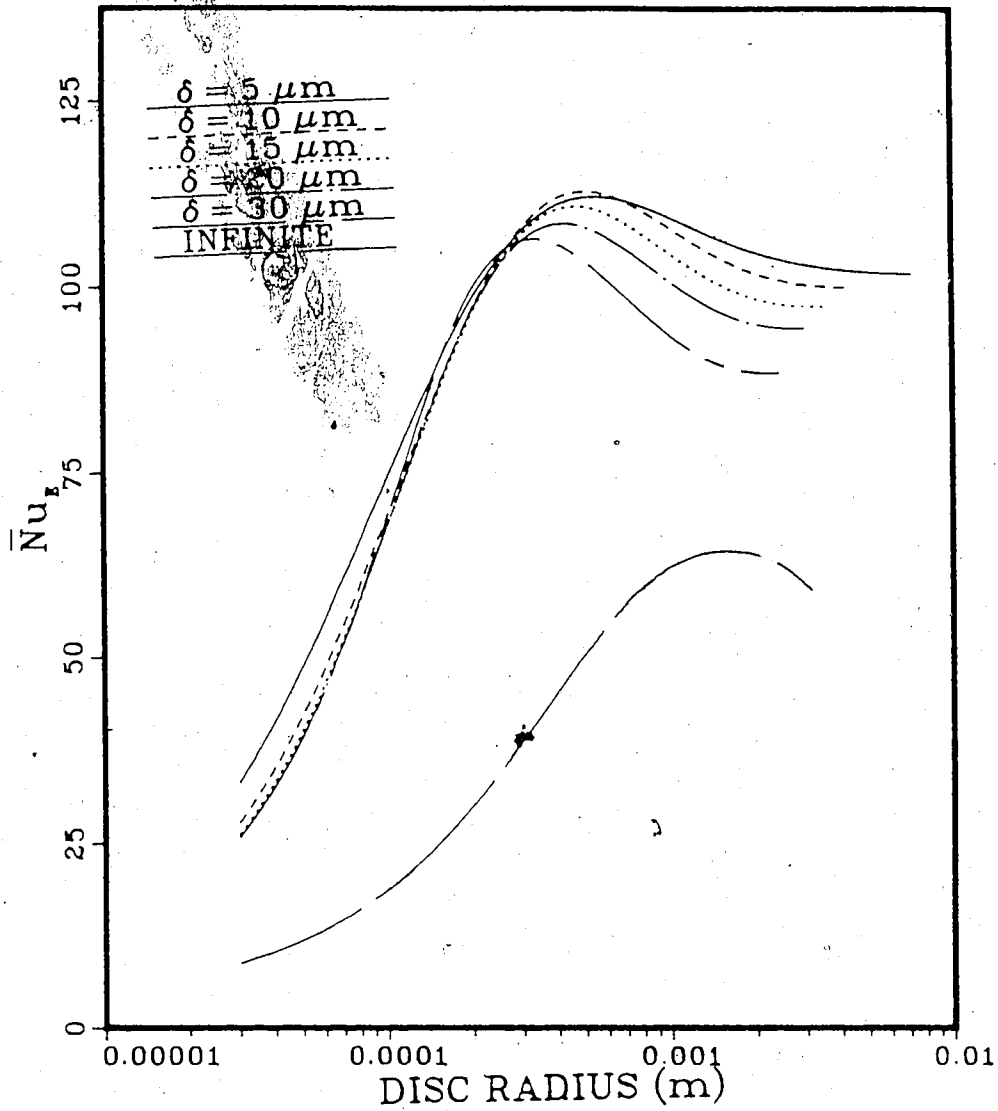


Figure 4.16: Variation of the average edge Nusselt number for an ice disc of initial radius $30\mu\text{m}$ and $h/2 = 10\mu\text{m}$ and an overall supercooling of 0.10°C . The label "INFINITE" corresponds to the quiescent fluid of infinite extent.

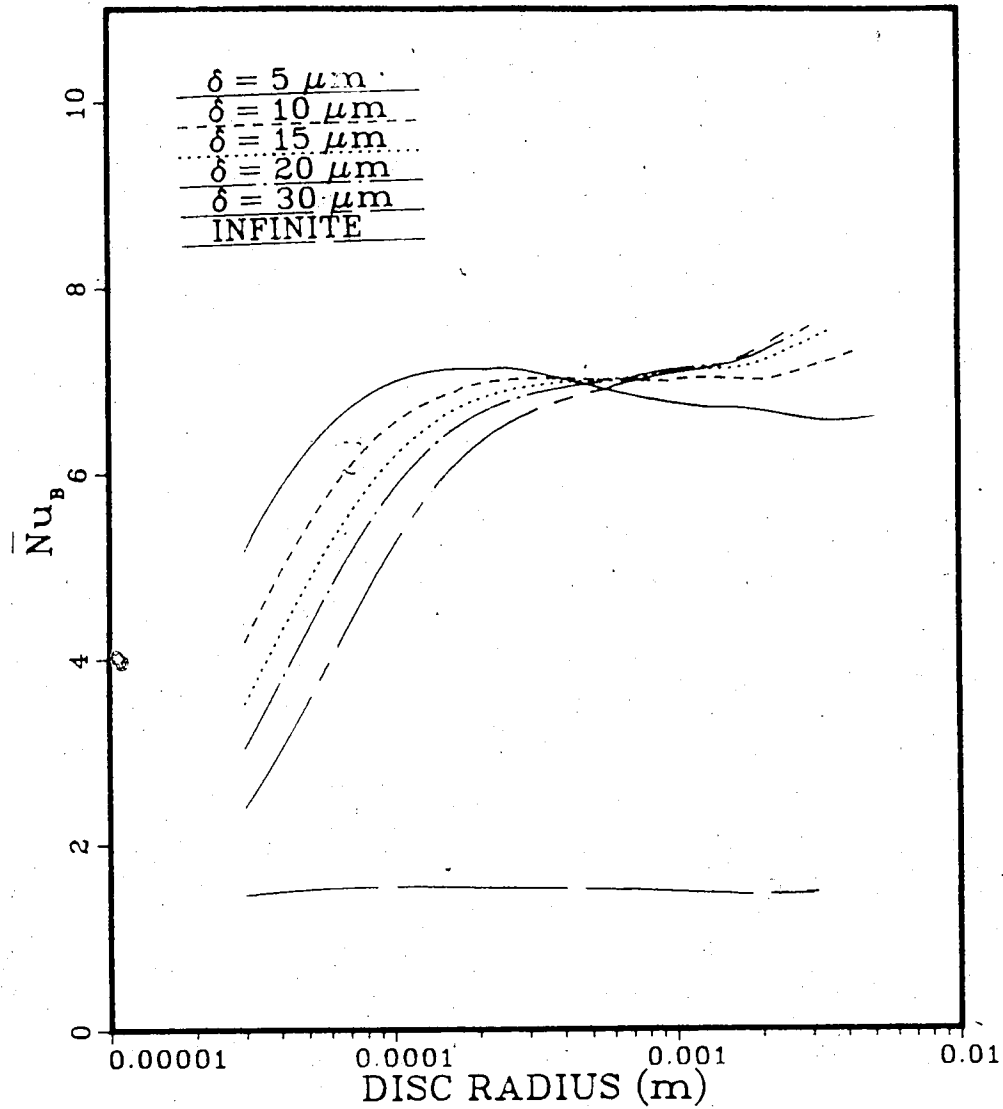


Figure 4.17: Variation of the average Nusselt number along the basal plane for an ice disc of initial radius $30\mu\text{m}$ and $h/2 = 10\mu\text{m}$ and an overall supercooling of 0.10°C . The label "INFINITE" corresponds to the quiescent fluid of infinite extent.

4.3 RESPONSE OF FRAZIL CRYSTAL GROWTH TO APPLIED COOLING RATES

In the previous sections, growth of frazil ice crystals was examined on assuming that the applied supercooling remained constant. In practice, the body of water in which the ice crystals are immersed is supercooled only for a short period of time during the initial stages of nucleation and growth. After a sufficient amount of latent heat has been absorbed by the water, its supercooling will begin to decrease resulting in a reduction in crystal growth rates. The variation in the overall supercooling results from the cooling rate of the volume of water and the growth of the crystal. In this section, emphasis will be placed on the effect of a variable applied supercooling on frazil crystal growth in a finite volume of water. The objectives of this section are to determine the nucleation temperature T_n and the maximum supercooling attainable as functions of cooling rate. These predictions can be compared with some experimental data that is available in the literature.

Consider a single frazil ice crystal submerged in a finite volume V_w of liquid. The volume of the liquid can be determined from the crystal number concentration. For relatively large bodies of water such as lakes and rivers, Schaefer [65] reports the number concentration is approximately $1/cm^3$. Daly and Colbeck [19] report number concentrations of $0.17/cm^3$ to $0.98/cm^3$ in their experiments on frazil ice generations in a flume. The slight difference is attributable to the generation of new crystals by secondary nucleation. As the supercooling of the water increases, the subsequent growth of the immersed crystal results in a warming of the surrounding water due to the latent heat release. For the case of the model, we consider this heat loss to occur over an effective area A_s . An overall heat balance of the model crystal-water system

can be described by the following

$$Q_S = Q_G - Q_L \quad (4.11)$$

where Q_L represents the heat lost to the surroundings; Q_G represents the quantity of latent heat liberated to the volume V_w of water and Q_S is the energy stored in the water. Heat losses to the surroundings are customarily expressed as

$$Q_L = h_a A_s (T_w - T_A) \quad (4.12)$$

where h_a is the convective heat loss coefficient and A_s is the effective area over which this heat loss occurs for the model system. The temperature of the water T_w is assumed to be uniform, since the water is well mixed. For natural bodies of water such as rivers, heat losses from the water usually occur by convection, evaporation and radiation due to the presence of cold air above its surface, with h_a of the order of $5W/m^2 \text{ } ^\circ C$ to $10W/m^2 \text{ } ^\circ C$. The rate of latent heat release from the crystal is given as

$$Q_G = \rho_s L \frac{dm_i}{dt} \quad (4.13)$$

where m_i is the mass of the ice phase. The quantity dm_i/dt can be related to the a- and c-axis growth rates calculated previously. Using the above two relations, the overall heat balance in Equation (4.11) can be expressed by the equation

$$\frac{dT_w}{dt} = \frac{-h_a A_s}{m_w C_{pl}} (T_w - T_A) + \frac{L}{m_w C_{pl}} \frac{dm_i}{dt} \quad (4.14)$$

where m_w is the mass of water. If we consider growth of the crystal to occur in a series of discrete time steps and take dm_i/dt to be constant over each short time interval, Equation (4.14) can be integrated to give the following variation of the overall supercooling ΔT at each time step

$$\Delta T = \left(1 - \exp\left[\frac{-h_a A_s}{m_w C_{pl}} t\right] \right) \left(\frac{L}{h_a A_s} \frac{dm_i}{dt} + T_A \right) + \Delta T_o \exp\left[\frac{-h_a A_s}{m_w C_{pl}} t\right] \quad (4.15)$$

where ΔT_o is the initial supercooling of the water. Carstens [15] in his experiments on the effect of cooling rates on frazil generation, varied the initial cooling rate between $-0.00012 \text{ }^\circ\text{C/s}$ and $-0.00106 \text{ }^\circ\text{C/s}$. In natural bodies of water such as rivers, the cooling rate of the water is documented by Carstens [15], Osterkamp [60] and others to be of the order of $-0.0001 \text{ }^\circ\text{C/s}$ to $-0.0005 \text{ }^\circ\text{C/s}$. It should be noted that these values are very rough estimates since the rate of heat loss from the water is highly dependent on the meteorological conditions.

If the initial water temperature is very close to the fusion temperature of ice, the initial cooling rate from Equation (4.14) is given by

$$\frac{dT_w}{dt} = \frac{-h_a A_s}{\rho_l V_w C_{pl}} T_a \quad (4.16)$$

since the latent heat release has a negligible effect on T_w . Assuming a crystal concentration of $1/\text{cm}^3$ and an overall heat transfer coefficient of $8 \text{ W/m}^2 \text{ }^\circ\text{C}$, it can be seen that the ratio V_w/A_s varies between 0.0182 m and 0.1603 m for the cooling rates used by Carstens in his experiments. This range of values will be used to obtain the transient ΔT curves.

Figure 4.18 shows the predicted ΔT in the water supercooling with time for several cooling rates, on using the stagnant layer model with a conductivity layer of $\delta = 100 \mu\text{m}$ and Equation (4.15). The initial nucleus size was chosen to be $R = 5.0 \mu\text{m}$ with $h/2 = 5.0 \mu\text{m}$. The initial supercooling ΔT_o was chosen to be $0.004 \text{ }^\circ\text{C}$ since the critical size for the ice particle would be just slightly lower than the disc radius chosen (for $\Delta T_o = 0.004 \text{ }^\circ\text{C}$, $R_{cr} = 4.97 \mu\text{m}$). The results of this simulation are consistent with Carstens's observations (i.e. the applied cooling rate remains constant until the latent heat release is large enough to cause the rate of cooling to decline).

Carstens conducted a series of experiments on the effect of a variable cooling rate on the overall supercooling of a volume of water. His experimental setup consisted

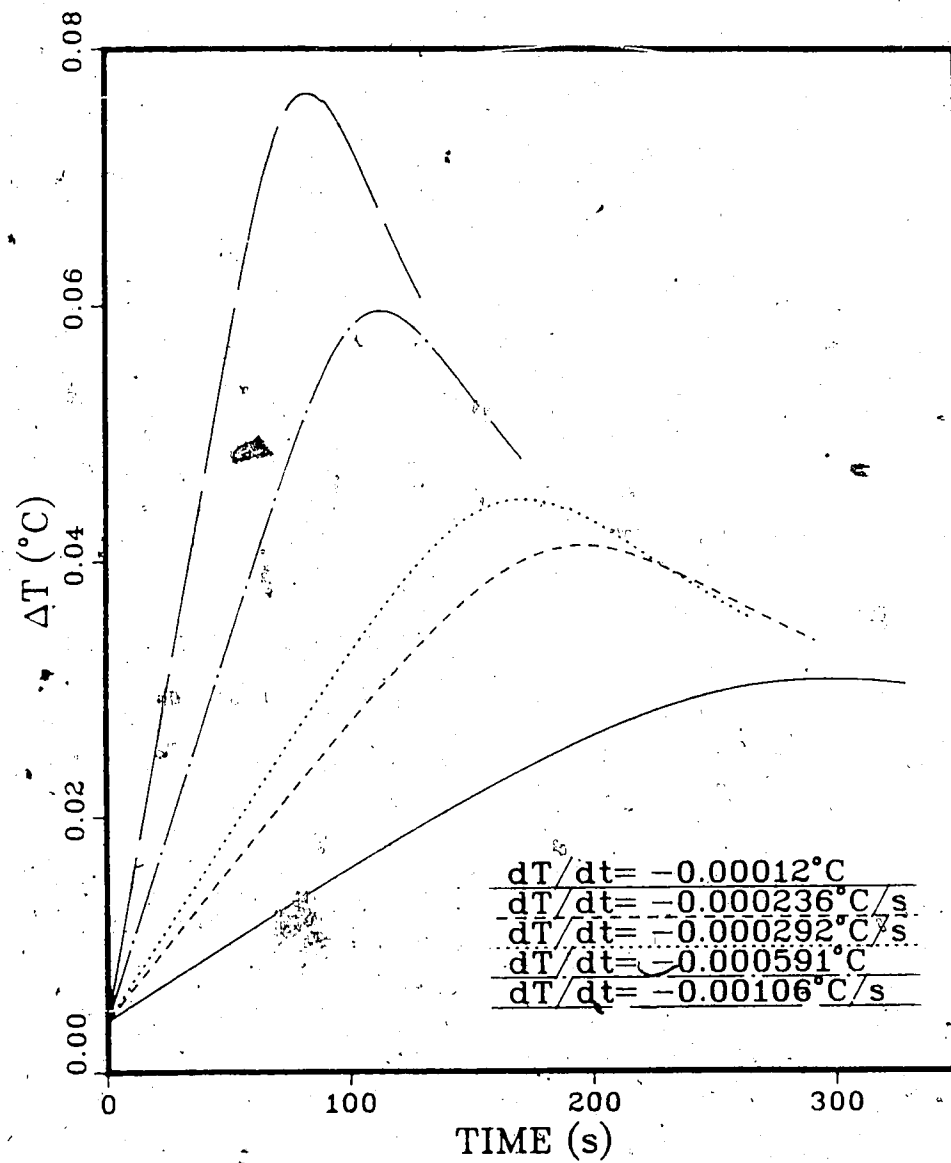


Figure 4.18: Effect of different rates of cooling on the overall supercooling ΔT for the stagnant layer model with $\delta = 100 \mu\text{m}$

of a recirculating oval-shaped flume through which supercooled water was circulated by means of a small propeller. The turbulence energy production in the flume was estimated to be 9 mW/kg from the mean water velocity generated by the propeller. Assuming turbulence dissipation rate to equal the production rate, the Kolmogorov scale η_k was determined to be approximately $160\mu m$. Figure 4.19 shows the variation in supercooling observed by Carstens for a cooling rate of $-0.00106\text{ }^\circ C/s$. The results from the stagnant layer model for values of δ equal to $50\mu m$, $100\mu m$, $150\mu m$ and $200\mu m$, and Daly's model for a dissipation scale of $\eta_k = 160\mu m$ are also shown in Figure 4.19. Carstens' observations show that the supercooling increases linearly until the rate of latent heat release is sufficient to warm the water. The cooling rate begins to decrease from $-0.00106\text{ }^\circ C/s$ and as the latent heat release becomes more dominant, the overall supercooling eventually peaks and then begins to decrease. Carstens noted that the rate at which the supercooling decreases is more rapid than the rate at which it was increasing. This is probably due to the effects of secondary nucleation which increases the crystal concentration and hence increases the latent heat release to the water. Since the effects of secondary nucleation are not included in either model, values of supercooling beyond the maximum value are not compared with Carstens' values. The trend of the transient cooling curves predicted by both Daly's model and the stagnant layer model are consistent with Carstens' observations (i.e. the supercooling increases until a maximum value is reached and then decreases). The maximum supercooling obtained from Daly's model are seen to be significantly higher than Carstens' data and the stagnant layer model results. This is due to the low growth rates predicted by Daly's model. The stagnant layer model underpredicts the maximum supercooling achieved for the values of δ used. Increasing the value of the stagnant layer thickness (δ) however, is seen to increase the value of the maximum supercooling that can be achieved. It was felt that the transient cooling curves were

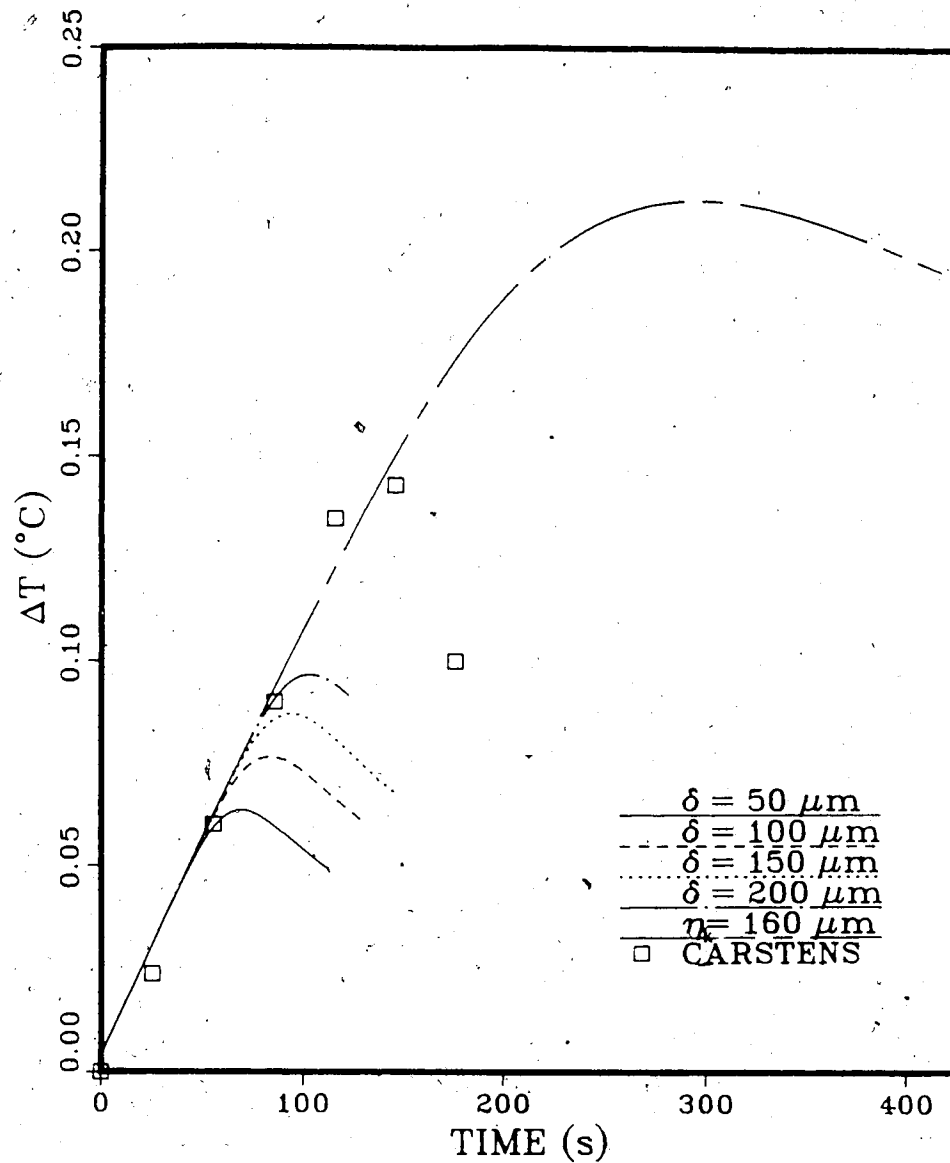


Figure 4.19: Effect of a cooling rate of $-0.00106 \text{ }^\circ\text{C}/\text{s}$ on the overall supercooling ΔT . The results for the stagnant layer model are shown for several values of δ and the result from Daly's model for $\eta_k = 160 \mu\text{m}$ is included.

dependent on the parameter h_a and decreasing its magnitude would result in a better comparison with Carsten's data. For realistic values of h_a , the stagnant layer results are insensitive to the magnitude of the heat loss coefficient h_a .

The temperature at which the first few frazil ice crystals form and begin to grow is termed the nucleation temperature. The difference between the nucleation temperature and the melting temperature is denoted by ΔT_n . This quantity is loosely defined as the temperature at which the slope of the cooling curve deviates from the initial linear cooling rate. Figure 4.20 shows the nucleation supercooling ΔT_n obtained from the stagnant layer model, Daly's model and those from Carstens' experimental results. The trends of these results are very similar to those established for the maximum supercooling results. All three sets of results indicate that the nucleation temperature increases with increased cooling rates. Daly's model predicts the nucleation supercooling to be almost double that of Carstens' measurements. The stagnant layer model predicts values for ΔT_n that are lower than Carstens' values.

Figure 4.21 shows the dependence of the maximum supercooling on the applied cooling rate for the stagnant layer model, Daly's model and Carstens' experimental data. Carstens' measurements for a cooling rate of $-0.00012 \text{ }^\circ\text{C}/\text{s}$ is seen to compare very well with the stagnant layer model results. Carstens' values however, for higher cooling rates, are seen to be consistently higher than those predicted by the stagnant layer model. Results from Daly's model consistently overpredict the maximum supercooling attainable compared to the experimental results and the stagnant layer results. The maximum supercooling is observed to decline with increasing levels of turbulence. For a cooling rate of $-0.00012 \text{ }^\circ\text{C}$ and stagnant layer thicknesses of $50 \mu\text{m}$, $100 \mu\text{m}$, $150 \mu\text{m}$ and $200 \mu\text{m}$, the maximum supercooling ΔT_{max} equals $0.023 \text{ }^\circ\text{C}$, $0.031 \text{ }^\circ\text{C}$, $0.035 \text{ }^\circ\text{C}$ and $0.039 \text{ }^\circ\text{C}$ respectively. Similar trends were also observed for Daly's model although the magnitudes of ΔT_{max} were more than twice that of

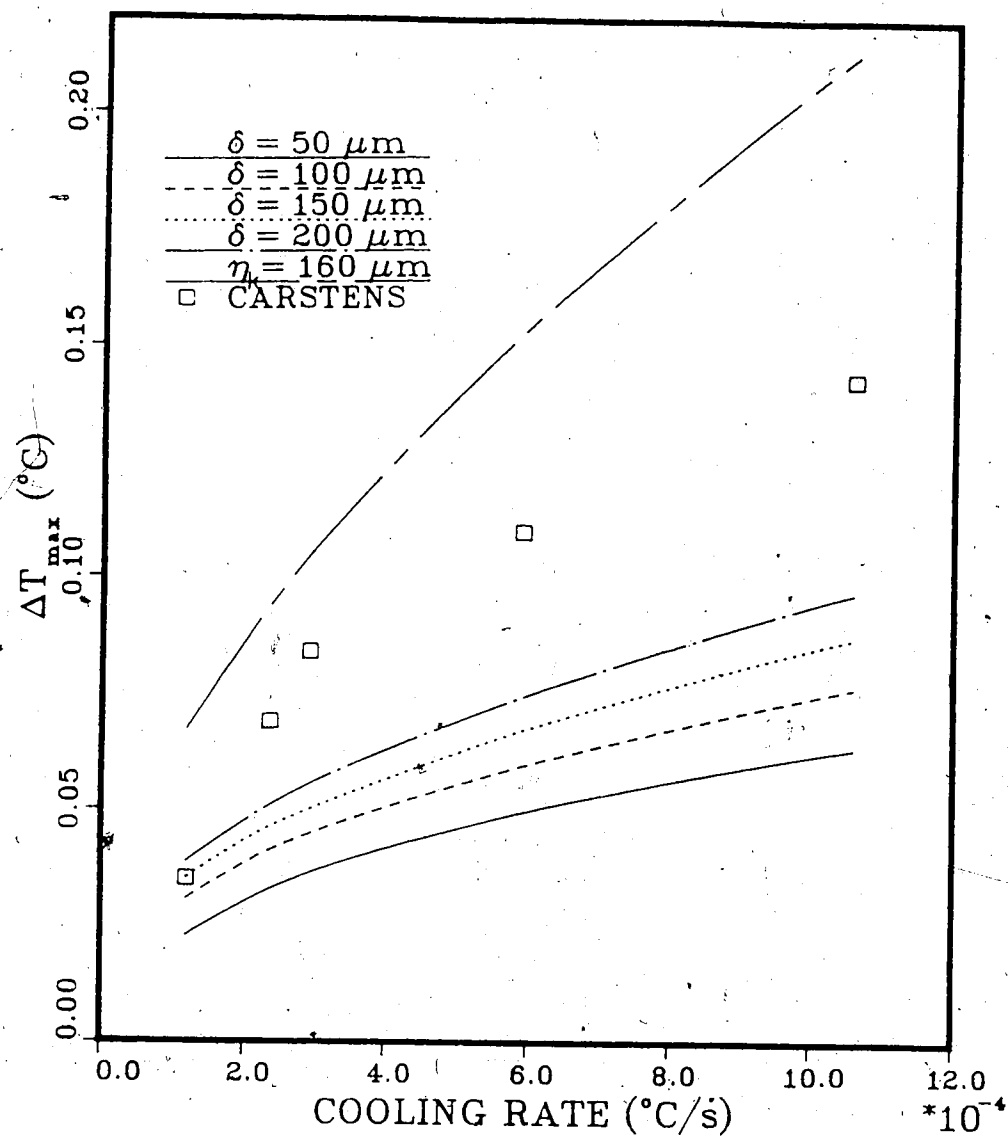


Figure 4.20: Comparison of nucleation supercooling ΔT_n attained for different rates of cooling. Stagnant layer model is shown for varying values of δ and Daly's model is for the same dissipation scale as Carstens' data

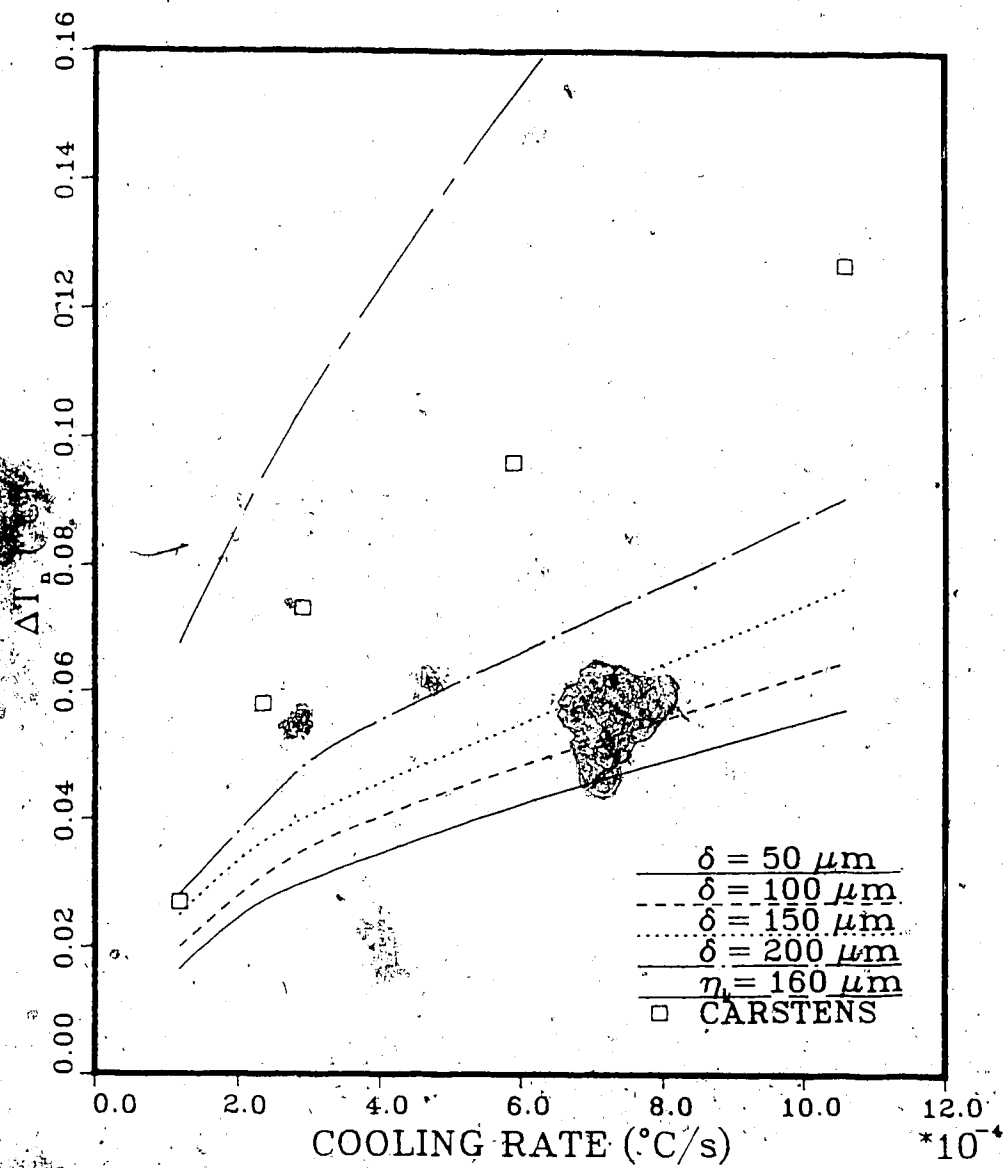


Figure 4.21: Comparison of maximum supercooling ΔT_{max} attained for different rates of cooling. Stagnant layer model is shown for varying values of δ and Daly's model is for the same dissipation scale as Carstens data.

Carstens' results and those determined by the stagnant layer model. This observation (of decreasing values of maximum supercooling for increasing levels of turbulence) was also noted by Carstens. He stated that strong levels of turbulence acted to reduce the rate of cooling of the water. This observation appears reasonable, since the rate of latent heat release to the water and hence its warming rate would increase with rising levels of turbulence. The high values of ΔT_n and ΔT_{max} predicted by Daly's model indicate that the latent heat release is not sufficient to counteract the cooling effect and substantially increase the water temperature. This is due to the low growth rates predicted by Daly's model.

Figures 4.22 and 4.23 contain plots of the frazil crystal radius at the maximum supercooling as a function of the cooling rate for the two models. Figures 4.24 and 4.25 show the corresponding aspect ratios. Osterkamp [61] reported that frazil disc diameters observed in the field are usually 2 mm to 5 mm with an aspect ratio usually between 0.02 and 0.05. Mueller [57] observed frazil disc diameters of 0.80 mm in crystallizers. Carstens [15] also observed ice crystals of 2 mm to 3 mm in diameter during his experiments on the effects of variable supercooling. Cooling rates observed in natural bodies of water, as mentioned, are reported to vary between -0.0001 °C/s and -0.0005 °C/s. The maximum cooling rate considered by Carstens was -0.001 °C/s. For cooling rates less than -0.001 °C/s, the aspect ratio predicted by the stagnant layer model is 0.03 for moderate levels of turbulence corresponding to $\delta = 100 \mu m$ and less than 0.01 for high turbulence intensities. At high turbulence intensities, the aspect ratios are relatively low since the thickening rate of crystal, which is strongly dependent on the applied supercooling, does not have the opportunity to attain significant magnitudes. Results from Daly's model also have similar trends, but due to the high supercoolings achieved, the thickening rate and hence the aspect ratio was quite large. For the range of turbulence levels considered

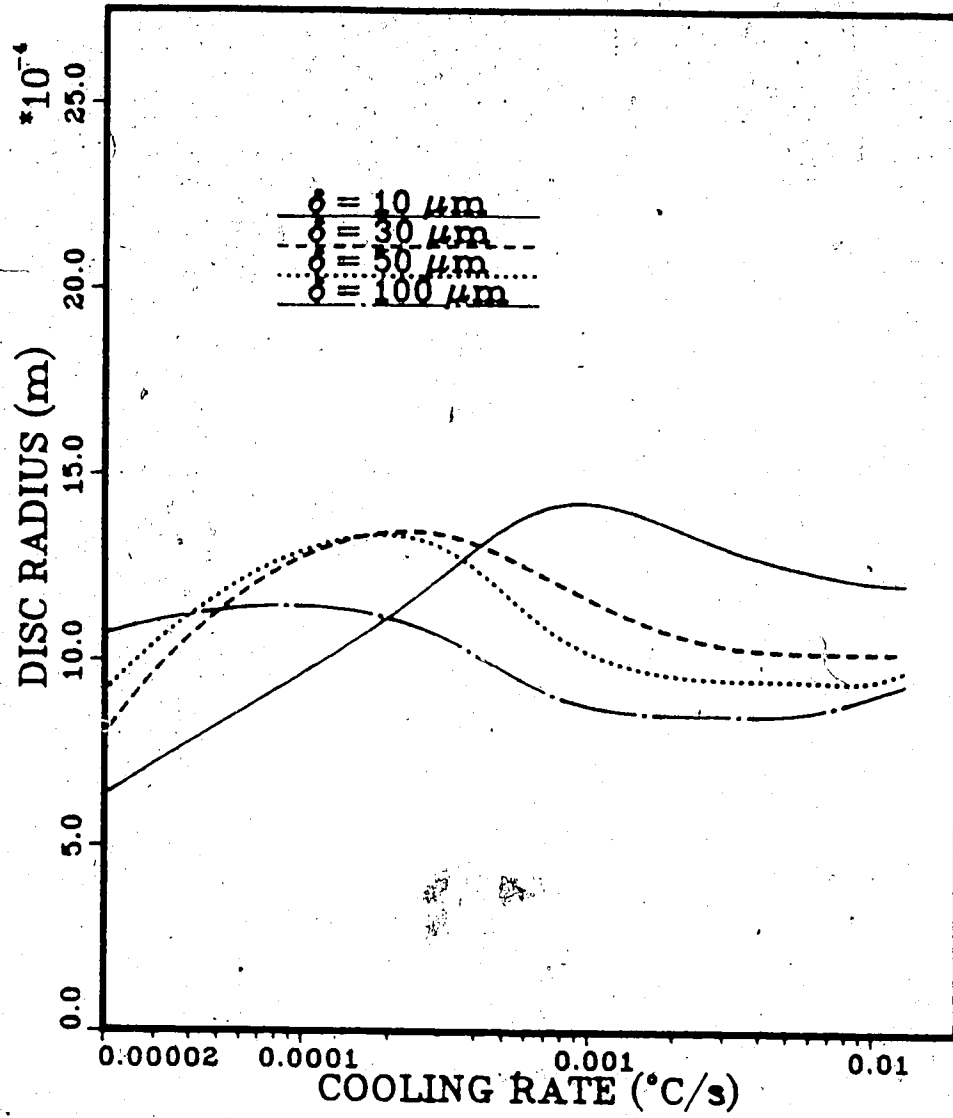


Figure 4.22: Disc radius at the maximum supercooling for several cooling rates, predicted by the stagnant layer model

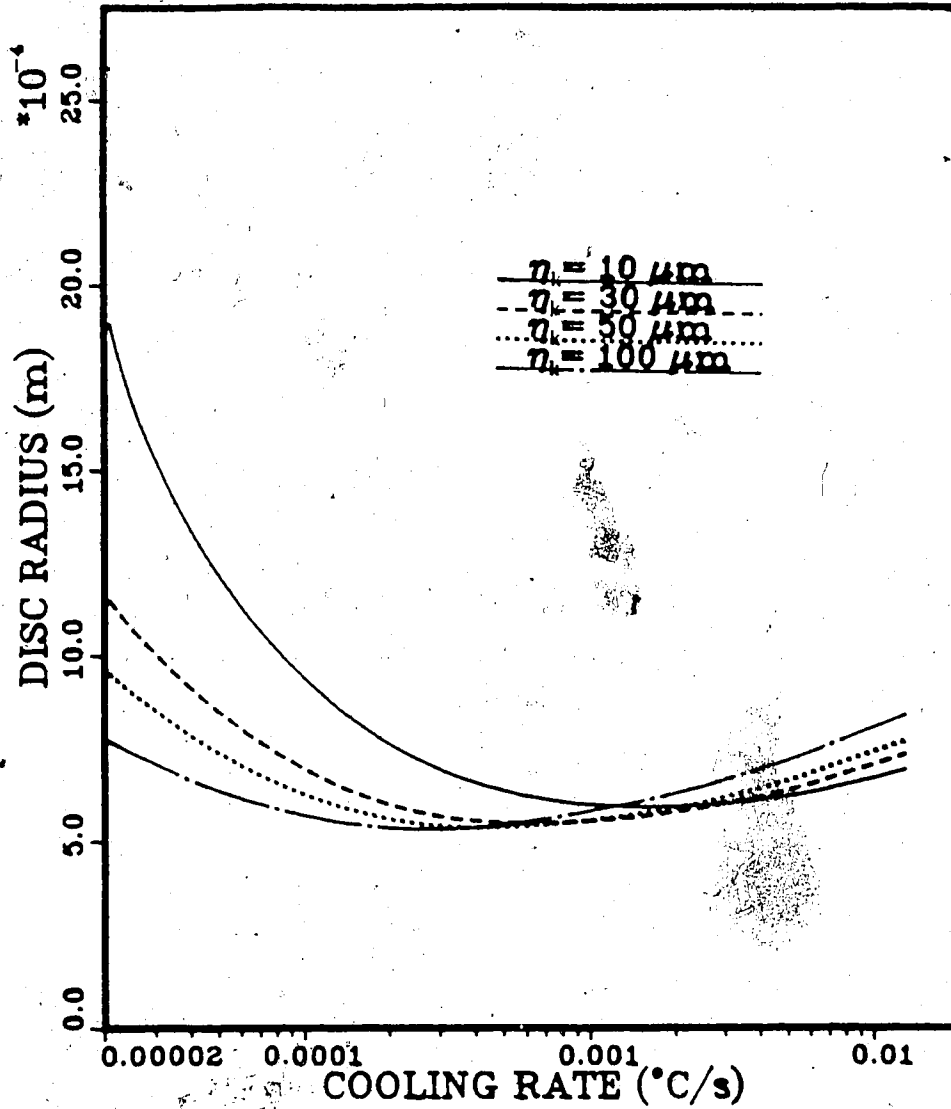


Figure 4.23: Disc radius at the maximum supercooling for several cooling rates predicted by Daly's model

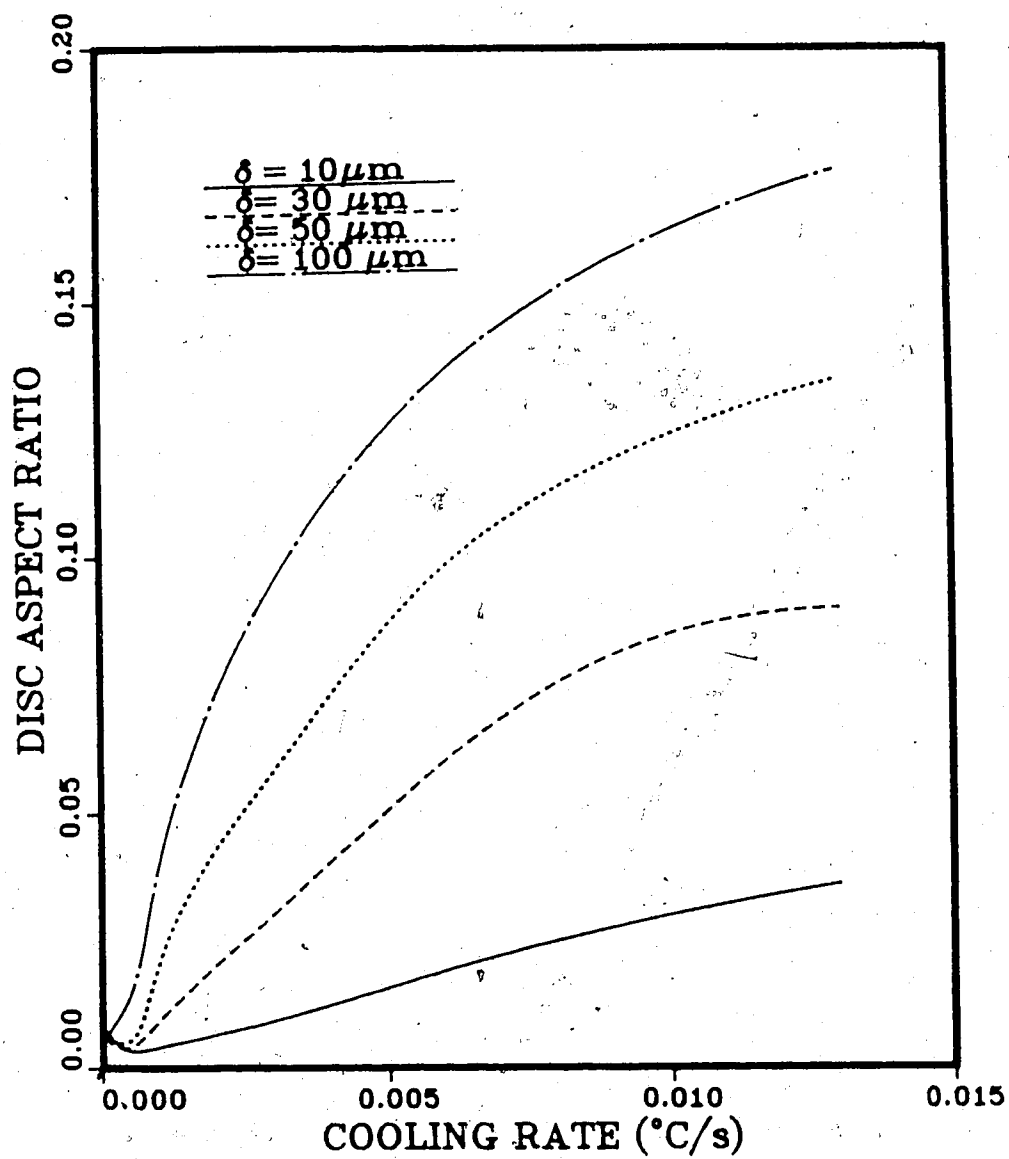


Figure 4.24: Aspect ratio of ice discs at the maximum supercooling for several cooling rates predicted by the stagnant layer model

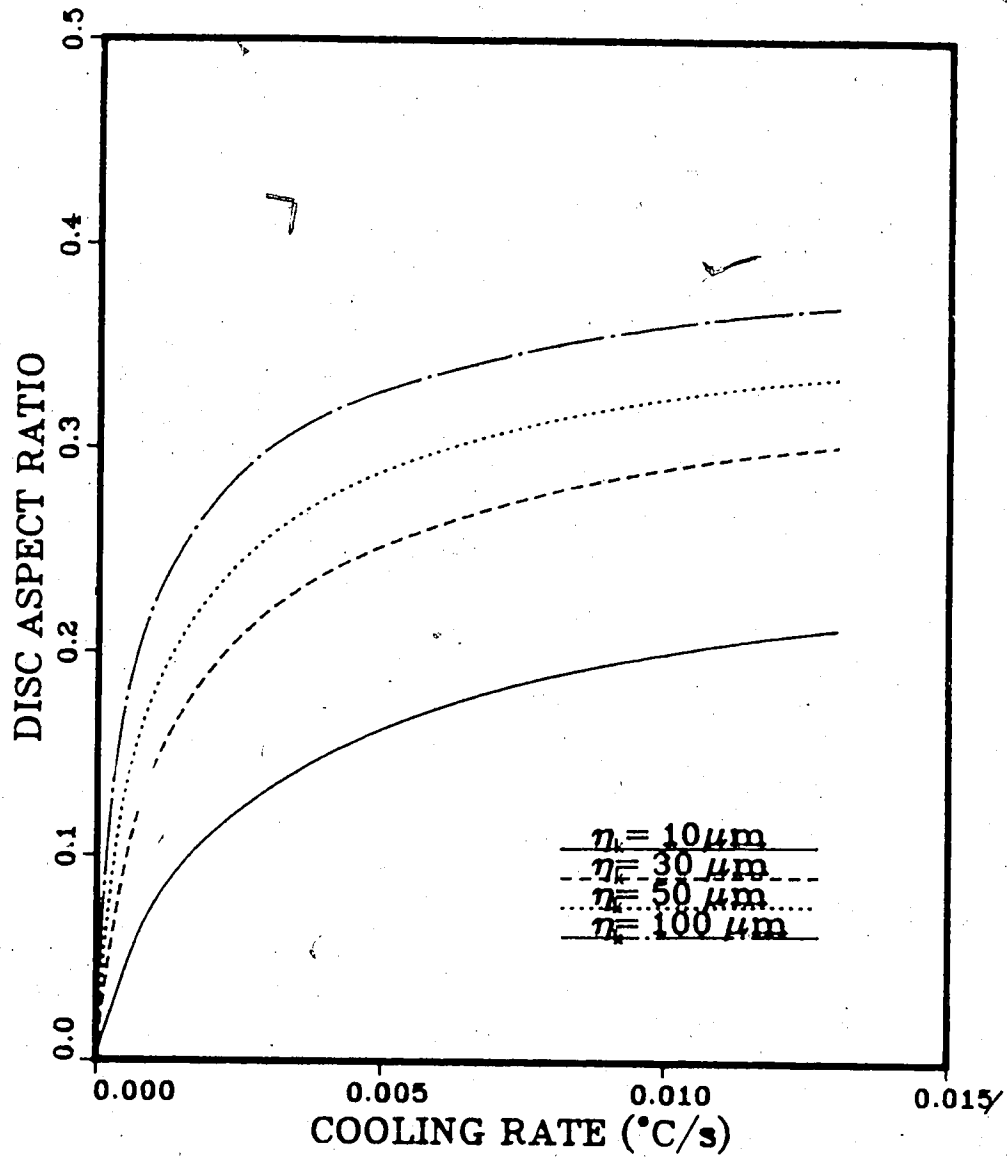


Figure 4.25: Aspect ratio of ice discs at the maximum supercooling for several cooling rates predicted by Daly's model

and realistic values of the cooling rate, Daly's model predicts aspect ratios between 0.06 and 0.1 for the range of Kolmogorov scales considered. The corresponding disc sizes obtained are just over 1 mm in diameter. For the stagnant layer model, disc diameters of 2mm were predicted. This appears to be consistent with previous field observations and some experimental results for turbulent waters, discussed in Chapter 1, where maximum disc sizes of 1.5 mm to 2mm have been reported. Both the stagnant layer model and Daly's model probably overpredict maximum disc diameters that can be reached, since the water was assumed to be free of any impurities and since interactions between existing crystals were not incorporated. This process of secondary nucleation can significantly influence frazil crystal size distributions and concentrations.

Some previous experimental studies have also predicted considerably lower values for maximum frazil sizes. A notable example was given by Daly and Colbeck [19], who conducted a series of experiments to generate frazil in a supercooled channel of water at various flow conditions and constant levels of applied supercooling. The supercoolings ranged between 0.01 °C to 0.02 °C for mean flowrates not more than 0.026 m³/s. The hydraulic conditions set in the experiments such as the slope of the channel and the bottom roughness resulted in a turbulence dissipation scale of 120µm. The maximum diameter of crystals was observed to be about 0.8 mm, which is considerably smaller than what previous studies had indicated. The mean diameter of the frazil crystal distribution was observed to be generally above 0.10 mm. Results from the stagnant layer model with $\delta = 120\mu\text{m}$ and a constant applied supercooling of 0.01 °C yield disc diameters of 0.50 mm and 1.2 mm for time intervals of 70 s and 240 s respectively. These particular time intervals were chosen because the residence time in the experiments were determined to vary from 70 s to 240 s. Similarly, results using Daly's model were also obtained for the same applied supercooling and a choice

of $\eta_k = 120\mu m$. After a time interval of 70 s after seeding, the crystal diameter was 0.15 mm and after 240 s, the disc diameter was 0.27 mm. For a supercooling of $0.02^\circ C$, the stagnant layer model yielded a crystal diameter of 0.76 mm and 1.9 mm at residence times of 70 s and 240 s respectively. Crystal diameters of 0.21 mm and 0.36 mm are obtained at these same time intervals of 70 s and 240 s using Daly's model. These values obtained using Daly's model were found to be more consistent with the experimental observations. However, it should be noted that a possible major source of error, as noted by Daly and Colbeck [19], resulted from the large production of anchor ice on the bed and sides of the flume. These anchor ice deposits were noted to act as a sink for crystals in suspension, although it was not known which particular crystal sizes were preferentially attracted for deposition as anchor ice. This affected the residence time at which crystal diameters were measured and hence the mean diameters which were reported.

4.4 SUMMARY

In order to more realistically model frazil crystal growth, it was necessary to incorporate the effects of fluid turbulence in the growth model developed in the previous chapter. Two methods for including the effects of turbulence on latent heat dissipation rates were tried and subsequently compared. The first, more traditional approach, consisted of incorporating experimentally obtained heat transfer data from suspended particles in order to determine the radial and axial growth rates of disc shaped ice crystals. The second approach involved modifying the existing conduction model by considering that the major effect of turbulence was to provide a well mixed fluid everywhere except in the immediate vicinity of the crystal. It was further assumed that a thin, stationary, conductive layer of fluid surrounded the crystal.

Levels of turbulence were then varied by varying the thickness of the conductivity layer. Qualitative comparisons between the two methods employed indicated that neglecting the latent heat generated at the edge and conducted through the solid led to significantly lower growth rates for the heat transfer coefficient model. Also, it was noticed that crystal sizes predicted by this method yielded diameters which differed by more than 50 % from previous experimental results as well as those from the stagnant layer model. The stagnant layer model indicate that the results are consistent with existing experimental and field observations. It is recommended however, that in order to further enhance the applicability of the stagnant layer model, it should be verified with more rigorous experimentation. In particular, the thickness of the stagnant layer should be correlated with the turbulence levels in the water.

Chapter 5

CONCLUSIONS

The purpose of this study has been to develop a mathematical model for the determination of frazil growth rates and verify the appropriateness of these results by comparisons with available empirical data and analytical results. The objectives of this thesis have been the following:

1. To formulate and implement the "Boundary Fitted Coordinates" procedure for a crystal growth problem.
2. To determine the effects of growth perpendicular to the basal plane on the radial growth of frazil ice.
3. To develop a simple, straight forward method for the incorporation of turbulence heat transfer effects on frazil growth.

As a result of this study, the following conclusions and recommendations are made:

1. The "Boundary Fitted Coordinate" method proved useful in the solution of the governing partial differential equations describing the temperature distribution of a frazil ice crystal. This numerical method, although developed for the solution of problems in curvilinear regions, was effectively utilized for the solution of partial differential equations on an irregular grid. Some precautions should be taken when using a variable spaced mesh. It was noticed that abrupt changes in the spacing of grid nodes, particularly in regions of high gradients, can cause stability and convergence problems in the numerical solution. Also, when the aspect ratio of the grid mesh blocks becomes too small, stability problems

can occur causing the solution to diverge. For the case of frazil crystals immersed in an infinite, quiescent melt, this occurred when the aspect ratio was less than 0.01.

2. The validity of assuming quasi-steady state crystal growth was examined. The assumption of quasi-steady state crystal growth was examined by obtaining a solution for the fully transient system of equations and then comparing these results with the quasi-steady results. It was observed that the influence of the initial condition damped out very quickly and the crystal growth rate approached values calculated from the steady state temperature distribution. As a result, the fully transient set of equations need not be solved for modelling the growth of frazil crystals over $25\mu\text{m}$ in diameter. The major advantage of this is the considerable savings in computer time.
3. Almost all previous studies reviewed have assumed that it is reasonable to neglect c-axis growth rates in the theoretical study of ice crystal growth. This has been justified by noting that c-axis growth rates are dominated by the interfacial kinetics and hence are usually an order of magnitude lower than growth rates in the a-axis direction. The results of this study indicate however that this assumption is invalid and in fact can lead to incorrect values for a-axis growth rates. The radial growth of ice discs was found to be highly dependent on the thickness of the disc, indicating that c-axis growth rates are responsible for reducing the radial growth rate of the crystal. This is due to the increased latent heat released along the edge of the crystal resulting from its increased thickness. Although c-axis growth rates are an order of magnitude lower than a-axis growth rates, the increase in thickness over the time period in which a frazil crystal grows is large enough to significantly reduce the radial growth rate. The latent heat release along the faces of the crystal caused an increase in the

basal plane temperature and consequently acted to reduce the disc thickening rate.

4. Traditional methods for the prediction of frazil ice growth rates in turbulent bodies of water are based on empirical heat transfer data. The heat transfer growth model underpredicted the quiescent growth rates. This indicated that the heat transfer coefficients cannot be used with the simple liquid phase heat balance to predict crystal growth rates. Another method for including the effects of turbulence involved using the stagnant layer approach. This method is useful to employ since heat transfer coefficients for the liquid do not have to be estimated. A direct relationship between the turbulence intensity in the melt and the thickness of the stagnant layer was not possible due to a lack of experimental data. However, the predicted trend and magnitudes of the a- and c-axis growth rates of the crystal obtained using this method was found to be consistent with what was predicted for the quiescent fluid case. Aspect ratios of the ice discs predicted by this method were also consistent with previous field observations and experimental results.
5. A more realistic simulation of frazil crystal growth behaviour requires a varying rate of supercooling. The rate at which the supercooling varies was determined from a thermal energy balance of the ice water system. The behaviour of the cooling curves determined for both Daly's model and the stagnant layer model were similar to previous experimental results. The final size of the crystals at the maximum supercooling achieved for different cooling rates using the stagnant layer model was double that determined by using Daly's model. The disc aspect ratio at final crystal sizes have been observed to be between 0.02 and 0.05. These values agree well with disc aspect ratios predicted by the stagnant layer model. Daly's model however over predicts the disc aspect ratios by an order

of magnitude compared to experimental values. The major conclusion drawn from these two sets of results is that the stagnant layer model predicts crystals sizes which are consistent with most experimental and field observations. Daly's model however, predicts frazil crystals to be small stubby discs which appears contrary to previous observations.

6. An important recommendation resulting from the course of this study is the need for more rigorous experimental work with attention paid to more precise measurement of turbulence parameters. In order to make use of the stagnant layer method, it is also necessary to correlate the conductive layer thickness with the level of turbulence in the fluid. Without experimental results, future theoretical or numerical work on frazil ice growth and the validity of its results will be difficult to ascertain.

References

- [1] Altberg, W.J., "Twenty Years Of Work In The Domain Of Underwater Ice Formation", *Int. Assoc. Of Scientific Hydrology*, Bull. No. 23, 1936, pp. 373-407.
- [2] Anderson, D.A., Tannehill and J.C., Pletcher, R.M., Computational Fluid Mechanics And Heat Transfer, Hemisphere Publishing Corp., 1984.
- [3] Arakawa, K., "Experimental Studies on Freezing of Water", *Int. Ass. of Sci. Hydrology*, Pub. No. 39, 1954, pp. 474-477.
- [4] Arakawa, K., "Studies on the Freezing of Water (II)-Formation of Disc Crystals", *J. of the Fac. of Sci., Hokaido Univ. of Japan, Ser. II, Vol: 4, No. 5, 1967*, pp. 311-319.
- [5] Arakawa, K., "The Growth of Ice Crystals in Water", *Proc. of Int. Confer. on Low Temp. Sci.*, Hakaido Univ., Sapporo, Japan, 1967, pp. 463-464.
- [6] Arden, J. and Wigle, T.E. "Dynamics of Ice Formation in the Upper Niagra River", *International Symposium on the Role of Snow and Ice in Hydrology, Banff, Alberta*, UNESCO-WHO-IAHS, Vol. 2, 1972, pp. 1296-1312.
- [7] Avignon, M., "Shape Stability of a Two-Dimensional Nucleus", *Journal of Crystal Growth*, Vol. 13-14, 1972, pp. 113-120.
- [8] Baker, A.J., Finite Element Computational Fluid Mechanics, Hemisphere Publishing Corporation, 1984.

- [9] Bolling, G.F. and Tiller, D., "Growth From The Melt", *Journal Of Applied Physics*, Vol. 32, 1961, pp. 2587-2605.
- [10] Bonnerot, R. and Jamet P., "Numerical Computation of the Free Boundary for the Two-Dimensional Stefan Problem by Space-Time Finite Elements", *Journal of Comp. Physics*, Vol. 25, 1977, pp. 163-181.
- [11] Bukina, L.A., "On the Relation Between Temperature and Ratio of Thickness Diameter of Frazil Ice Crystals of Disc Like Form", *Bull. Acad. of Science, USSR, Geophys. Ser.*, Vol. 1, 1963, pp. 112-113.
- [12] Bukina, L.A., "The Rate Of Growth Of Frazil Ice Crystals", *Bull. Acad. of Science, USSR, Geophys. Ser.*, Vol. 12, 1962, pp. 1165-1168.
- [13] Bukina, L.A., "On The Heat Emission Coefficient Of Disc Like Frazil Ice Crystals", *Bull. Acad. of Science, USSR, Geophys. Ser.*, Vol. 7, 1963, pp. 689-693.
- [14] Bukina, L.A., "A Laboratory Method Of Investigation Of The Rate Of Growth Of Frazil Ice Crystals", *Bull. Acad. of Science, USSR, Geophys. Ser.*, Vol. 6, 1961, pp. 622-625.
- [15] Carstens, T., "Experiments With Supercooling And Ice Formation", *Geofysiske Publikasjoner Geophysics Norwegica* Vol. 26, No. 9, 1966, pp. 1-18.
- [16] Chambre, P.L., "On the Dynamics of Phase Change", *Journal of Mech. and Appl. Math*, Vol. 9 No.2, 1956, pp. 24.
- [17] Chikhliwala, E.D. and Yortsos, Y.C., "Application of Orthogonal Mapping to Some Two Dimensional Domains", *J. of Comp. Phys.*, Vol. 57, 1984, pp. 402.

- [18] Daly, S.F.; Frazil Ice Dynamics, M.Sc. Thesis, MIT, 1982.
- [19] Daly, S.F. and Colbeck, S.C., "Frazil Ice Measurements In CRREL's Flume — Facility", *IAHR Ice Symposium*, Iowa, 1985, pp. 427-438.
- [20] Devik, O., "Ice Formation In Lakes And Rivers", *The Geographical Journal*, Vol. CIII No. 5, 1944, pp. 193-203.
- [21] Ettema, R, Karim, M.F. and Kennedy, J.F "Frazil Ice Formation", CRREL Report 84-18, 1984.
- [22] Fernandez, R. and Barduhn, A.J., *Desalination*, Vol. 3, 1967, pp. 330-342.
- [23] Fletcher, N.H., "The Chemical Physics of Ice", Cambridge University Press, 1970.
- [24] Forest, T.W., "Thermodynamic Stability Of Frazil Ice Crystals", *OMAE International Symposium*, Vol. 4, Tokyo, 1986, pp. 266-270.
- [25] Forest, T.W. and Sharma, R. "The Growth Rate of Ice Discs in Slightly Supercooled Water", *Int. Symp. on Cold Regions Heat Transfer*, Edmonton, 1987, pp. 107-113.
- [26] Foulds, D.M. and Wigle, T.E., "Frazil-The Invisible Strangler", *J. of Amer. Water Works Assoc.*, 1977, pp. 196-199.
- [27] Fujioka, T. and Sekerka, R.F., "Morphological Stability of Disc Crystals", *J. of Crystal Growth*, Vol. 24-25, 1974, pp. 84-93.
- [28] Fujioka, T., Study of Ice Growth in Slightly Undercooled Water, PhD. Thesis, Carnegie-Mellon University, 1978.

- [29] Garabedian, H. and Strickland-Constable, R.F., "Collision Breeding Of Ice Crystals", *J. Of Crystal Growth*, Vol. 22, 1974, pp. 188-192.
- [30] Goldman, A. and Kao, Y.C., "Numerical Solution To a Two Dimensional Conduction Problem Using Rectangular and Cylindrical Body Fitted Coordinates", *J. of Heat Transfer*, Vol. 103, 1981, pp. 753-758.
- [31] Gilpin, R.R., "The Influence of Natural Convection on Dendritic Ice Growth", *J. of Crystal Growth*, Vol. 36, 1976, pp. 101-108.
- [32] Hanley, T. O'D., "Frazil Nucleation mechanisms", *J. of Glaciology*, Vol. 21, 1978, pp. 581-587.
- [33] Haussling, H.J. and Coleman, R.M., "A Method For Generation of Orthogonal and Nearly Orthogonal Boundary-Fitted Coordinate Systems", *J. of Comp. Phys.*, Vol. 43, 1981 pp. 373-381.
- [34] Handbook of Heat Transfer Fundamentals, Second Edition, Edited by Rohsenow, W.M., Hartnett, J.P. and Ganic, E.N., McGraw Hill, 1985.
- [35] Hillig, W.B., "The Kinetics of Freezing", *Growth and Perfection of Ice Crystals*, Eds. Doremus, R.H., Roberts, B.W. and Turnbull, D. Wiley, New York, 1958, pp. 350-360.
- [36] Hobbs, P.V., Ice Physics, Oxford University Press, 1974.
- [37] Huebner, K.H., Thornton, E.A. The Finite Element Method For Engineers, John Wiley and Sons Inc., New York, 1982.
- [38] Jackson, K.A., "Interface Structure", from *Growth and Perfection of Ice Crystals*, Eds. Doremus, R.H., Roberts, B.W., Turnbull, D. Wiley, New York, 1958, pp. 319-324.

- [39] Jackson, K.A., Uhlmann, D.R., Hunt, J.D., "On The Nature Of Crystal Growth From The Melt", *J. Of Crystal Growth*, Vol. 1, 1967, pp. 1-36.
- [40] Kaischew, R. and Stranski, I.N., "Zur Theorie der Linearen Kristallisationsgeschwindigkeit" *Z. Physik. Chem.*, A170, 1934, pp. 295-301.
- [41] Kallungal, J.P., The Growth of Single Ice Crystals Parallel to the a-Axis in Subcooled Quiescent and Flowing Water, Syracuse University, 1975.
- [42] Kallungal, J.P. and Barduhn, A.J., "Growth Rate Of An Ice Crystal In Subcooled Pure Water", *AIChE Journal*, Vol. 23, No. 3, 1977, pp. 294-303.
- [43] Kivisild, H.R., "River and Lake Ice Terminology", *Proc. of IAHR Symp. on Ice and Its Action on Hydraulic Structures*, Iceland, 1970 Paper 1.0.
- [44] Knight, C.A., The Freezing of Supercooled Liquids D. Van Norstrand Company Inc., New Jersey, 1967, p. 19.
- [45] Knight, C.A., "Growth of Ice Crystals After a Method by Helmholtz", *Nature*, Vol. 220, No. 5162, 1968, pp. 62-63.
- [46] Kolman, B. and Trench, W.F., Elementary Multivariable Calculus, Academic Press, New York, 1970.
- [47] Kumai, M. and Itigaki K., "Cinematographic Study of Ice Crystal Formation In Water", *Journal of the Faculty of Science, Hokkaido University Series 2* Vol. 4, 1953, pp. 233-237.
- [48] Levinson, N. and Redheffer, R.M., Complex Variables, Holden Day, San Francisco, 1970.

- [49] Martin, S., "Frazil in Rivers and Oceans", *Ann. Rev. Fluid Mech.*, Vol 13, 1981, pp. 379-397.
- [50] Mason, B.J., "The Growth of Ice Crystals from the Vapour and the Melt", *Advances in Physics*, Vol. 7, 1958, pp. 235-253.
- [51] Mastin, C.W. and Thompson, J.F., "Elliptic Systems and Numerical Transformations", ICASE Report, NASA Langley Research Center, 1976.
- [52] Meyer, G.H., "The Numerical Solution of Multidimensional Stefan Problems—A Review", *Moving Boundary Problems, First Edition*, Academic Press, 1978, pp. 73-90.
- [53] Michaels, A.S., Brian, P.L.T. and Sperry, P.R., "Impurity Effects On the Basal Plane Solidification Kinetics Of Supercooled Water", *J. of Applied Physics*, 1966, pp. 4649-4661.
- [54] Michel, B., "Morphology of Frazil Ice", *Proc. of Int. Conf. on Low Temperature Science*, Hokkaido Univ., Sapporo Japan, 1967, pp. 119-128.
- [55] Michel, B., "Properties and Processes of River Lake Ice", *Proc. of Banff Symp. on the Role of Snow and Ice in Hydrology*, Banff, 1972, pp. 454-481.
- [56] Mobley, C.D. and Stewart, R.J., "On the Numerical Generation of Boundary Fitted Orthogonal Curvilinear Coordinate Systems", *J. of Comp. Phys.*, Vol. 34, 1980, pp. 124-135.
- [57] Mueller, A.H., "Frazil Ice Formation in Turbulent Flow", Iowa Institute of Hydraulic Research, Report No. 214, 1978.
- [58] Omstedt, A., "On Supercooling and Ice Formation in Turbulent Sea Water", *J. of Glaciology*, Vol. 31, 1985, pp. 263-271.

- [59] O'Niell, K. and Lynch, D.R., "A Finite Element Solution for Freezing Problems Using a Continuously Deforming Coordinate System", *Numerical Methods in Heat Transfer* John Wiley and Sons, 1981, pp. 215-231.
- [60] Osterkamp, T.E., "Frazil Ice Nucleation Methods", *Scientific Report, Geophysical Institute*, University Of Alaska, 1978.
- [61] Osterkamp, T.E., "Frazil Ice Formation: A Review", *J. Hydraulic Div. ASCE*, Vol. 104, 1978, pp. 1239-1255.
- [62] Pimputkar, S.M. and Ostrach, S., "Convective Effects in Crystals Grown From the Melt", *J. of Crystal Growth*, Vol. 55, 1981, pp. 614-646.
- [63] Rieger, H., Projahn, U., Bareiss, M. and Beer, H., "Heat Transfer During Melting Inside a Horizontal Tube", *J. of Heat Transfer*, Vol. 105, 1983, pp. 226-234.
- [64] Ryskin, G. and Leal, L.G., "Orthogonal Mapping", *J. of Comp. Phys.*, Vol. 50, 1982, pp. 71-100.
- [65] Schaefer, V.J., "The Formation of Frazil and Anchor Ice in Cold Water", *Trans. American Geophysical Union*, Vol. 31, No. 6, 1950.
- [66] Schneider, G.E. and Zedan, M., "A Modified Strongly Implicit Procedure For the Numerical Solution of Field Problems", *Numerical Heat Transfer*, Vol. 4, 1981, pp. 1-19.
- [67] Shih, T.M., Numerical Heat Transfer, Hemisphere Publishing Corporation, 1984.
- [68] Simpson, H.C., Beggs, G.C., Deans, J. and Nakamura, J., "The Growth of Ice Crystals", *Desalination*, Vol. 14, 1974, pp. 341-357.

- [69] Singh, B., Application of the Finite Element Method to Study Dendritic Growth, Ph.D. Thesis, University of Alberta, 1981.
- [70] Stone, H.L., "Iterative Solution of Implicit Approximations of Multidimensional Partial Differential Equations", *SIAM J. Numer. Anal.*, Vol. 5, 1965, pp. 99-110.
- [71] Sullivan, J.M., Finite Element Simulation of Solidification into an Undercooled Melt, Ph.D. Thesis, Dartmouth College, 1986.
- [72] Thomas, P.D. and Middlecoff, J.F., "Direct Control of the Grid Point Distribution in Meshes Generated by Elliptic Equations", *AIAA Journal*, Vol. 18, 1979, pp. 652-656.
- [73] Thompson, J.F., Thames, F.C. and Mastin, C.W., "Boundary-Fitted Curvilinear Coordinate Systems for Solution of Partial Differential Equations on Fields Containing Any Number of Arbitrary Two-Dimensional Bodies", *NASA Report No. CR-2729*, 1975.
- [74] Tikuisis, P., Ward, C.A. and Venter, R.D., "Bubble Evolution in a Stirred Volume of Liquid Closed to Mass Transport", *J. Appl. Phys.*, Vol. 54, 1983, pp. 1-9.
- [75] Tsang, G., Frazil And Anchor Ice: A Monograph, National Water Institute, Canada Centre For Inland Waters, Pub. Under NRC Subcommittee on Hydraulics of Ice Covered Rivers, Ottawa, Canada, 1982.
- [76] Wadia, R.B., Mass Transfer from Spheres and Discs in Turbulent Agitated Vessels, Ph.D. Thesis, MIT, 1974.
- [77] Williamson, R.B., Ph.D. Thesis, Harvard University, 1964.

- [78] Williamson, R.B. and Chalmers, B., "Morphology Of Ice Solidified In Undercooled Water", Proceedings of ICCG-1, Boston, Pergamon Press, 1967, pp. 739-743.
- [79] Winslow, A.J., "Numerical Solution of the Quasi-Linear Poisson Equation in a Non-Uniform Triangular Mesh", *Journal of Computational Physics*, 1966, p. 149.

Appendix A

DERIVATION OF THE SURFACE NUCLEATION GROWTH MODEL

Growth of a frazil ice crystal in the direction perpendicular to its basal plane was shown to proceed by the mechanism of two-dimensional nucleation in Chapter 2. It was also noted that experimental results by Hillig and others were found to match closely with theoretical surface nucleation growth models. The derivation of this growth mechanism will be discussed briefly in this appendix.

Consider a portion of the basal plane surface containing a small island of radius R and height λ_0 . The total free energy of the system is given by

$$F_T = F^1(T, A^1, N^1) + F^2(T, A^2, N^2) + F^l(T, A^l, N^l) \quad (\text{A.1})$$

where each of the terms in this expression corresponds to the regions labelled in Figure A.1. The quantities N_1 and N_2 represent the number of moles of solid and liquid and N_l is the number of moles of solid at the nucleus boundary. The critical radius, R_{cr} , of this nucleus may be obtained from the total differential of the free energy F_T , which is given as

$$dF_T = \gamma^1 dA^1 + \mu^1 dN^1 + \gamma^2 dA^2 + \mu^2 dN^2 + \gamma^l dA^l + \mu^l dN^l \quad (\text{A.2})$$

where γ^1 and γ^2 are the surface tensions corresponding to the nucleus and nucleating surface respectively and γ^l is the line tension of the monolayer boundary. Equation A.2 can be further simplified and expressed as

$$(\gamma^1 - \gamma^2) dA^1 + \gamma^l dl = 0 \quad (\text{A.3})$$

from which it can be shown that

$$(\gamma^1 - \gamma^2) = \frac{-\gamma^l}{R_{cr}} \quad (\text{A.4})$$

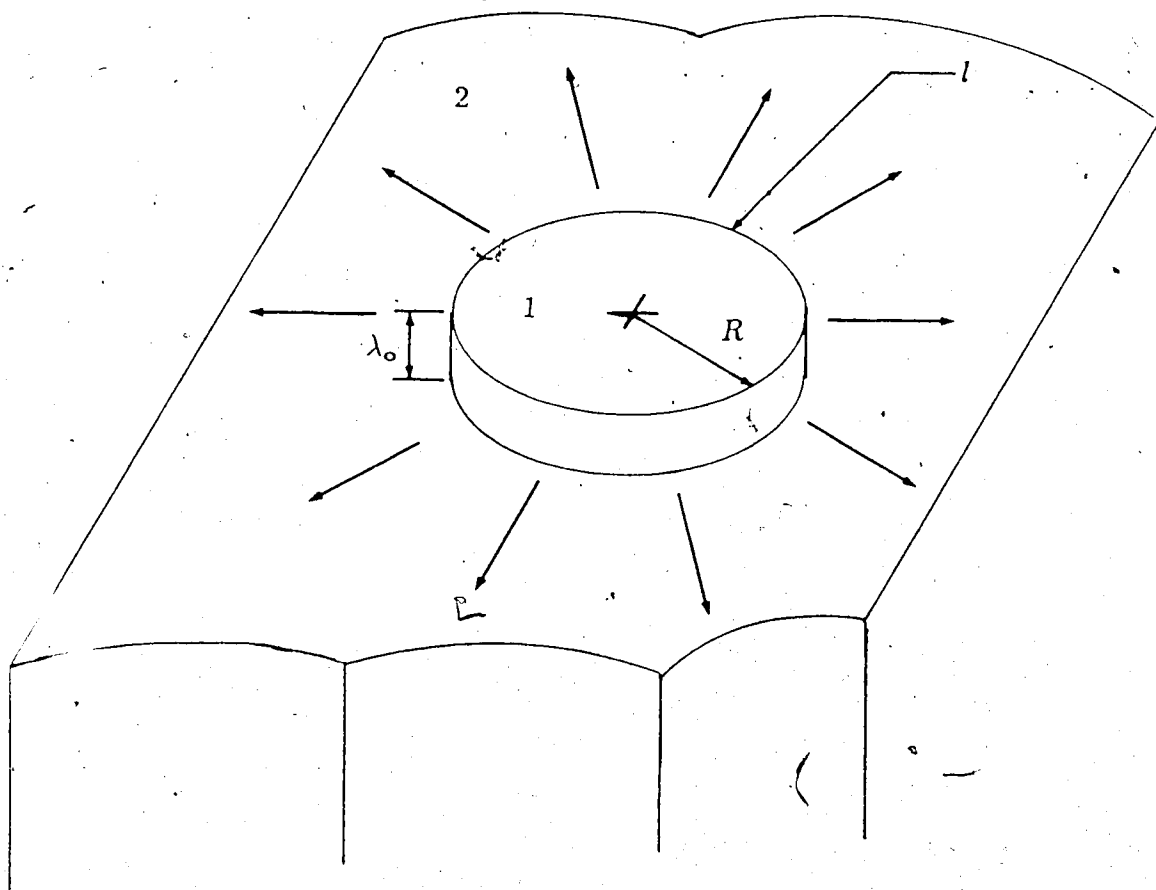


Figure A.1: Portion Of Basal Plane Surface Containing Monolayer

The left hand side of Equation A.4 may be determined in terms of more common parameters by using the Gibbs-Adsorption equations

$$d\gamma^1 = s^1 dT - \Gamma_g^1 d\mu_p^1 \quad (\text{A.5})$$

$$d\gamma^2 = s^2 dT - \Gamma_g^2 d\mu_p^2 \quad (\text{A.6})$$

where Γ_g^1 and Γ_g^2 are the surface adsorption coefficients and s^1 and s^2 represent the molar entropy. Utilizing these two relations, it can be shown that the chemical potentials μ_p^1 and μ_p^2 are equal due to equilibrium. As a result, it can be shown that by expanding the chemical potentials, μ_p^1 and μ_p^2 , about the fusion temperature T_m in a Taylor series and equating the two yields the relation

$$(s^2 - s^1)(T_i - T_m) = \frac{1}{\Gamma_g}(\gamma^1 - \gamma^2) \quad (\text{A.7})$$

Since the latent heat of fusion per atom is given by

$$L = T_m(s^2 - s^1) \quad (\text{A.8})$$

Equation A.7 may be rewritten as

$$(\gamma^1 - \gamma^2) = \frac{\Gamma_g L (T_i - T_m)}{T_m} \quad (\text{A.9})$$

Combining Equation A.9 with A.4 results in the critical size of the monolayer to be

$$R_{cr} = \frac{T_m \gamma^l}{\Gamma_g L (T_m - T_i)} \quad (\text{A.10})$$

It can be shown from classical thermodynamics that the energy required to nucleate a monolayer of size R_{cr} is a maximum and equal to

$$\Delta F_{max} = \frac{2}{3} \pi \gamma^l R_{cr}^2 \quad (\text{A.11})$$

Also, from the principles of statistical thermodynamics, it can be shown that the nucleation rate per unit area of the basal plane is given by

$$I = \kappa e^{-\Delta F_{max}/k_b T} \quad (\text{A.12})$$

where κ is an unknown parameter to be determined from the theory of molecular diffusion and k is the Boltzmann constant. The growth rate in the c-axis direction is then given as

$$V_c = IA\lambda_o \quad (\text{A.13})$$

where A is the area of the crystal face and λ_o is the step height of the nucleated monolayer. Combining Equations A.10 to A.12 with A.13 results in the following expression

$$V_c = \kappa A \lambda_o e^{-2\pi\gamma^2/3k_b\Gamma_g L T_i (T_m - T_i)} \quad (\text{A.14})$$

This expression is often expressed in the more compact form

$$V_c = \kappa A \lambda_o e^{-\Delta F_{max}/3k_b T_i} \quad (\text{A.15})$$

which is similar to the model proposed by Kaischew and Stranski [40] and Hillig [35].

Appendix B

SUMMARY OF DERIVATIVE TRANSFORMATIONS

This appendix contains a comprehensive list of the relations in the transformed (ξ, η) plane. Relations involving derivatives of the computational coordinates $\xi(r, z)$ and $\eta(r, z)$ with respect to the physical space coordinates r and z are also included. Finally, the finite difference discretization of these differential relations is presented for reference.

The following definitions are applicable throughout this section:

- $f(r, z, t)$ - a twice continuously differentiable scalar function of r , z and t .
- $r(\xi, \eta)$ - coordinate transformation function for the radial coordinate direction.
- $z(\xi, \eta)$ - coordinate transformation function for the axial coordinate direction.
- $\alpha = r_\eta^2 + z_\eta^2$
- $\beta = r_\xi r_\eta + z_\xi z_\eta$
- $\gamma = r_\xi^2 + z_\xi^2$
- $J = r_\xi z_\eta - r_\eta z_\xi$

The general transformation from the physical region to the transformed region is defined by the vector valued function:

$$\begin{bmatrix} \xi \\ \eta \end{bmatrix} = \begin{bmatrix} \xi(r, z) \\ \eta(r, z) \end{bmatrix} \quad (\text{B.1})$$

The inverse function of the above transform is:

$$\begin{bmatrix} r \\ z \end{bmatrix} = \begin{bmatrix} r(\xi, \eta) \\ z(\xi, \eta) \end{bmatrix} \quad (\text{B.2})$$

Derivatives of $\xi(r, z)$ and $\eta(r, z)$

$$\begin{aligned}\xi_r &= z_\eta/J \\ \xi_z &= -r_\eta/J\end{aligned}\tag{B.3}$$

$$\eta_r = -z_\xi/J$$

$$\eta_z = r_\xi/J$$

$$\xi_{rr} = \frac{(\xi_r z_{\xi\eta} + \eta_r z_{\eta\eta})}{J} - \frac{(\xi_r^2 J_\xi + \xi_r \eta_r J_\eta)}{J}\tag{B.4}$$

$$\xi_{zz} = \frac{-(\xi_z r_{\xi\eta} + \eta_z r_{\eta\eta})}{J} - \frac{(\xi_z^2 J_\xi + \xi_z \eta_z J_\eta)}{J}\tag{B.5}$$

$$\xi_{rz} = \frac{(\xi_z z_{\xi\eta} + \eta_z z_{\eta\eta})}{J} - \frac{(\xi_r \xi_z J_\xi + \xi_r \eta_r J_\eta)}{J}\tag{B.6}$$

$$\eta_{rr} = \frac{-(\eta_r z_{\xi\eta} + \xi_r z_{\xi\xi})}{J} - \frac{(\eta_r^2 J_\eta + \xi_r \eta_r J_\xi)}{J}\tag{B.7}$$

$$\eta_{zz} = \frac{(\eta_z r_{\xi\eta} + \xi_z r_{\xi\xi})}{J} - \frac{(\eta_z^2 J_\eta + \xi_z \eta_z J_\xi)}{J}\tag{B.8}$$

$$\eta_{rz} = \frac{-(\eta_z z_{\xi\eta} + \xi_z z_{\xi\xi})}{J} - \frac{(\eta_r \eta_z J_\eta + \xi_z \eta_r J_\xi)}{J}\tag{B.9}$$

Partial derivatives of a function $f(x, y)$, which is some sufficiently differentiable function of x and y , are transformed using the relations:

Derivative Transformations

$$f_r = \frac{\partial f}{\partial r} \Big|_{z,t} = \frac{(z_\eta f_\xi - z_\xi f_\eta)}{J}\tag{B.10}$$

$$f_z = \frac{\partial f}{\partial z} \Big|_{r,t} = \frac{(r_\xi f_\eta - r_\eta f_\xi)}{J}\tag{B.11}$$

$$\begin{aligned}f_t = \frac{\partial f}{\partial t} \Big|_{r,z} &= \frac{\partial f}{\partial t} \Big|_{\xi,\eta} - \frac{(z_\eta f_\xi - z_\xi f_\eta)}{J} \left(\frac{\partial r}{\partial t} \right)_{\xi,\eta} \\ &\quad - \frac{(r_\xi f_\eta - r_\eta f_\xi)}{J} \left(\frac{\partial z}{\partial t} \right)_{\xi,\eta}\end{aligned}\tag{B.12}$$

$$f_{rr} = \frac{\partial^2 f}{\partial r^2} = \frac{(z_\eta^2 f_{\xi\xi} - 2z_\xi z_\eta f_{\xi\eta} + z_\xi^2 f_{\eta\eta})}{J^2} + \frac{(z_\eta^2 z_{\xi\xi} - 2z_\xi z_\eta z_{\xi\eta} + z_\xi^2 z_{\eta\eta})(r_\eta f_\xi - r_\xi f_\eta)}{J^3} + \frac{(z_\eta^2 r_{\xi\xi} - 2z_\xi z_\eta r_{\xi\eta} + z_\xi^2 r_{\eta\eta})(z_\xi f_\eta - z_\eta f_\xi)}{J^3}$$

$$f_{zz} = \frac{\partial^2 f}{\partial z^2} = \frac{(r_\eta^2 f_{\xi\xi} - 2r_\xi r_\eta f_{\xi\eta} + r_\xi^2 f_{\eta\eta})}{J^2} + \frac{(r_\eta^2 r_{\xi\xi} - 2r_\xi r_\eta r_{\xi\eta} + r_\xi^2 r_{\eta\eta})(z_\xi f_\eta - z_\eta f_\xi)}{J^3} + \frac{(r_\eta^2 z_{\xi\xi} - 2r_\xi r_\eta z_{\xi\eta} + r_\xi^2 z_{\eta\eta})(r_\eta f_\xi - r_\xi f_\eta)}{J^3}$$

$$f_{rz} = \frac{\partial^2 f}{\partial r \partial z} = \frac{(r_\xi z_\eta + r_\eta z_\xi) f_{\xi\eta} - r_\xi z_\xi f_{\eta\eta} - r_\eta z_\eta f_{\xi\xi}}{J^2} + \frac{(r_\eta z_\eta r_{\xi\xi} - (r_\xi z_\eta + r_\eta z_\xi) r_{\xi\eta} + r_\xi z_\xi r_{\eta\eta})(z_\eta f_\xi - z_\xi f_\eta)}{J^3} + \frac{(r_\eta z_\eta z_{\xi\xi} - (r_\xi z_\eta + r_\eta z_\xi) z_{\xi\eta} + r_\xi z_\xi z_{\eta\eta})(r_\xi f_\eta - r_\eta f_\xi)}{J^3}$$

Laplacian in axisymmetric coordinates:

$$\nabla^2 f = \frac{(\zeta f_{\xi\xi} + 2\beta f_{\xi\eta} + \gamma f_{\eta\eta})}{J^2} + \frac{(\zeta r_{\xi\xi} + 2\beta r_{\xi\eta} + \gamma r_{\eta\eta})(z_\xi f_\eta - z_\eta f_\xi)}{J^3} + \frac{(\zeta z_{\xi\xi} + 2\beta z_{\xi\eta} + \gamma z_{\eta\eta})(r_\eta f_\xi - r_\xi f_\eta)}{J^3} + \frac{1}{r} \left(\frac{z_\eta f_\xi - z_\xi f_\eta}{J} \right) \quad (\text{B.13})$$

or this can be expressed more simply as

$$\nabla^2 f = \frac{(\zeta f_{\xi\xi} + 2\beta f_{\xi\eta} + \gamma f_{\eta\eta} \zeta f_\eta + \vartheta f_\xi)}{J^2} \quad (\text{B.14})$$

Gradient:

$$\vec{\nabla} f = \frac{(z_\eta f_\xi - z_\xi f_\eta)}{J} \vec{i} + \frac{(r_\xi f_\eta - r_\eta f_\xi)}{J} \vec{j} \quad (\text{B.15})$$

B.1 FINITE DIFFERENCE APPROXIMATIONS IN THE TRANSFORMED PLANE

A compilation of second order finite difference expressions used to approximate partial derivatives in the transformed plane are given below. The field step sizes $\Delta\xi$

and $\Delta\eta$ are both taken to be unity since due to cancellation after substitution in the transformed equations results in the actual values of ξ and η to be immaterial. All functions and their derivatives are evaluated at the discrete locations (ξ_i, η_j) on the computational plane.

First Derivative, Central Differences

$$(f_\xi)_{i,j} \simeq \frac{f_{i+1,j} - f_{i-1,j}}{2} \quad (\text{B.16})$$

$$(f_\eta)_{i,j} \simeq \frac{f_{i,j+1} - f_{i,j-1}}{2} \quad (\text{B.17})$$

First Derivative, Forward Differences

$$(f_\xi)_{i,j} \simeq \frac{-f_{i+2,j} + 4f_{i+1,j} - 3f_{i,j}}{2} \quad (\text{B.18})$$

$$(f_\eta)_{i,j} \simeq \frac{-f_{i,j+2} + 4f_{i,j+1} - 3f_{i,j}}{2} \quad (\text{B.19})$$

First Derivative, Backward Differences

$$(f_\xi)_{i,j} \simeq \frac{f_{i-2,j} - 4f_{i-1,j} + 3f_{i,j}}{2} \quad (\text{B.20})$$

$$(f_\eta)_{i,j} \simeq \frac{-f_{i,j-2} + 4f_{i,j-1} - 3f_{i,j}}{2} \quad (\text{B.21})$$

Second Derivative, Central Differences

$$(f_{\xi\xi})_{i,j} \simeq \frac{f_{i+1,j} - 2f_{i,j} + f_{i-1,j}}{4} \quad (\text{B.22})$$

$$(f_{\eta\eta})_{i,j} \simeq \frac{f_{i,j+1} - 2f_{i,j} + f_{i,j-1}}{4} \quad (\text{B.23})$$

$$(f_{\xi\eta})_{i,j} \simeq \frac{(f_{i+1,j+1} - f_{i+1,j-1} - f_{i-1,j+1} + f_{i-1,j-1})}{4} \quad (\text{B.24})$$

Transformation Parameters

$$\zeta_{i,j} \simeq \frac{(r_{\eta})_{i,j}^2 + (z_{\eta})_{i,j}^2}{4} \quad (\text{B.25})$$

$$\beta_{i,j} \simeq \frac{(r_{\xi})_{i,j}(r_{\eta})_{i,j} + (z_{\xi})_{i,j}(z_{\eta})_{i,j}}{4} \quad (\text{B.26})$$

$$\gamma_{i,j} \simeq \frac{(r_{\xi})_{i,j}^2 + (z_{\xi})_{i,j}^2}{4} \quad (\text{B.27})$$

$$J_{i,j} \simeq \frac{(r_{\xi})_{i,j}(z_{\eta})_{i,j} - (r_{\eta})_{i,j}(z_{\xi})_{i,j}}{4} \quad (\text{B.28})$$

$$s_{i,j} \simeq \frac{(r_{\eta})_{i,j}^2 + (z_{\eta})_{i,j}^2}{4} \quad (\text{B.29})$$

$$\vartheta_{i,j} \simeq \frac{(r_{\eta})_{i,j}^2 + (z_{\eta})_{i,j}^2}{4} \quad (\text{B.30})$$

Appendix C

PROPERTIES OF WATER AND ICE

The thermal properties of water and ice used throughout the course of this study are given below:

SYMBOL	PHYSICAL PROPERTY	VALUE USED
T_m	Freezing Point Of Water	273.15K
L	Latent Heat Of Fusion	333600 J/kg
γ_{sl}	Surface Free Energy Of Ice-Water Interface	0.022 J/m ²
k_s	Thermal Conductivity Of Water	0.601 W/m °C
α_s	Thermal Diffusivity Of Water	$0.1338 \times 10^{-6} \text{ m}^2/\text{s}$
ρ_s	Density Of Water	997 kg/m ³
ν_w	Kinematic Viscosity Of Water	$1.798 \times 10^{-6} \text{ m}^2/\text{s}$
C_{p1}	Specific Heat Of Water	4170 J/gm °C
Pr	Prandtl Number For Water	13.44
k_i	Thermal Conductivity Of Ice	2.25 W/m °C
α_i	Thermal Diffusivity Of Ice	$0.1778 \times 10^{-5} \text{ m}^2/\text{s}$
$C_{p,i}$	Specific Heat Of Ice	2250 J/gm °C
R_g	Universal Gas Constant	8.31434 J/mol K
M	Molecular Weight Of H ₂ O	18.015